UNIVERSITY OF LIVERPOOL

THE UNIVERSITY *of* LIVERPOOL

Perturbation Observer based Adaptive Passive Control and Applications for VSC-HVDC Systems and FACTS Devices

Thesis submitted in accordance with the
requirements of the University of Liverpool
for the degree of Doctor of Philosophy

in

Electrical Engineering and Electronics

by

Bo Yang, B.Sc.(Eng.)

August 2015

Perturbation Observer based Adaptive Passive Control and Applications for VSC-HVDC Systems and FACTS Devices

by

Bo Yang

Acknowledgements

I would like to give my heartfelt thanks to my primary supervisor, Dr. L. Jiang, whose encouragement, guidance and support enabled me to develop a deep understanding of my work. Without his consistent and illuminating instructions, my research work and my life could not proceed to this stage. The research skill, writing skill and presenting skill he taught me will benefit me throughout my life.

I would like to show my gratitude to my secondary supervisor, Professor Q. H. Wu, for his kind guidance with his knowledge of control and power systems, and his inspiring insight into life philosophy, piano, and poetry.

I offer my regards and blessings to all of the members of Smart Grid Control and Renewable Energy Group, the University of Liverpool, especially to Dr. W. Yao for his kind and helpful discussion on power system modelling and operation, Dr. C. K. Zhang for his expert control knowledge, and Mr. S. Kai for his excellent hardware experiment skill. Special thanks also go to my friends, Mr. Nick Liu, Mr. Z. H. Fang, and Dr. Simon for their consistent support and friendship, which made my life in U. K. so wonderful.

I am grateful to the Department of Electrical Engineering and Electronics at the University of Liverpool, for providing the research facilities that made it possible for me to carry out this research. I am indebted to the University of Liverpool for the studentship (2011-2015), and China Scholarship Council (CSC) (2011-2015) for the financial support.

Finally, I am greatly thankful to my father Z. H. Yang and my mother P. L. Yang, for their encouragement and love for my whole life.

Abstract

The technology of voltage source converter based high voltage direct current (VSC-HVDC) system and devices used in flexible AC transmission systems (FACTS) has evolved significantly over the past two decades. It is used to effectively enhance power system stability. One of the important issues is how to design an applicable nonlinear adaptive controller for these devices to effectively handle the system nonlinearities and uncertainties.

Passive control (PC) has been proposed for the control of nonlinear systems based on Lyapunov theory, which has the potential to improve the system damping as the beneficial system nonlinearities are remained instead of being fully cancelled. However, PC is not applicable in practice as it requires an accurate system model. Adaptive passive control (APC) and robust passive control (RPC) have been developed to handle some specific type of system uncertainties based on strict assumptions on system structure and uncertainty. However, their applications are limited as various system uncertainties exist.

This thesis aims to develop a perturbation observer based adaptive passive control (POAPC) to make PC applicable in practice. The combinatorial effect of system nonlinearities, parameter uncertainties, unmodelled dynamics and time-varying external disturbances is aggregated into a perturbation, which is estimated by a perturbation observer (PO). The proposed approach does not require an accurate system model and can handle various system uncertainties.

POAPC is applied to two-terminal VSC-HVDC systems to handle various system uncertainties. The VSC-HVDC system model is firstly developed, the proposed controller can inject an extra system damping and only the measurement of direct current (DC) voltage, active and reactive power is needed. The effectiveness of

POAPC is verified by simulation in comparison with that of passive control (PC) and proportional-integral (PI) control. Moreover, a hardware experiment is carried out to verify its implementation feasibility and applicability.

A passive controller is designed for multi-terminal VSC-HVDC (VSC-MTDC) systems via energy shaping, in which the dynamics related to the active power, reactive power, and DC cable voltage is transformed into an output strictly passive form. Then the remained internal dynamics related to DC cable current and common DC voltage is proved to be asymptotically stable in the context of Lyapunov criterion. PC is applied on a four-terminal VSC-MTDC system under eight cases to evaluate its control performance.

POAPC is developed on the VSC-MTDC system to maintain a consistent control performance under different operating points and provide a significant robustness to parameter uncertainties, together with other unmodelled dynamics and time-varying external disturbances. Simulation results are provided to evaluate the control performance of POAPC in comparison to that of PI control and PC.

Perturbation observer based coordinated adaptive passive control (POCAPC) is proposed for excitation controller (EC) and FACTS controller on both single machine infinite bus (SMIB) systems and multi-machine power systems. Only the range of control Lyapunov function (CLF) is needed and the dependence of an accurate system model can be partially reduced, thus POCAPC can be easily applied to multi-machine power systems. Its control performance is compared with that of conventional proportional-integral-derivative and lead-lag (PID+LL) control, coordinated passive control (CPC) and coordinated adaptive passive control (CAPC) on both an SMIB system and a three-machine power system by simulation. Then a hardware-in-the-loop (HIL) test is undertaken to verify the implementation feasibility of the proposed controller.

Declaration

The author hereby declares that this thesis is a record of work carried out in the Department of Electrical Engineering and Electronics at the University of Liverpool during the period from October 2011 to September 2015. The thesis is original in content except where otherwise indicated.

Contents

List of Figures **x**

List of Tables **xiii**

1 Introduction **1**
1.1 Background . . . 1
1.1.1 VSC-HVDC systems . . . 1
1.1.2 FACTS devices . . . 11
1.1.3 Passive control . . . 14
1.2 Motivation and Methodology . . . 16
1.3 Main Contributions . . . 17
1.4 Publication List . . . 19
1.5 Thesis Outline . . . 20

2 Perturbation Observer based Adaptive Passive Control **23**
2.1 Introduction . . . 23
2.2 Problem Formulation . . . 26
2.3 Design and Stability Analysis of POAPC . . . 27
2.4 Case Studies . . . 35
2.4.1 Magnetic levitator system . . . 35
2.4.2 Interconnected inverted pendulum system . . . 41
2.5 Conclusion . . . 43

3 Perturbation Observer based Adaptive Passive Control for Two-terminal VSC-HVDC Systems **47**
3.1 Introduction . . . 47
3.2 Problem Formulation . . . 48
3.3 Two-terminal VSC-HVDC System Modelling . . . 53
3.4 POAPC Design for Two-terminal VSC-HVDC System . . . 55
3.4.1 Rectifier controller design . . . 55
3.4.2 Inverter controller design . . . 57
3.5 Simulation Results for Two-terminal VSC-HVDC System . . . 59
3.6 Experiment Results for Rectifier Controller and Inverter Controller . 66

3.6.1 Experiment platform 67
3.6.2 Case studies 70
3.7 Conclusion 74

4 Passive Control Design for VSC-MTDC Systems via Energy Shaping 75
4.1 Introduction 75
4.2 N-terminal VSC-MTDC System Modelling 77
4.3 PC Design for N-terminal VSC-MTDC System 80
4.3.1 Rectifier controller design 80
4.3.2 Inverter controller design 82
4.3.3 Internal dynamics stability 84
4.4 Case Studies 86
4.5 Conclusion 96

5 Perturbation Observer based Adaptive Passive Control for VSC-MTDC Systems 98
5.1 Introduction 98
5.2 POAPC Design for N-terminal VSC-MTDC System 99
5.2.1 Rectifier controller design 99
5.2.2 Inverter controller design 102
5.3 Case Studies 104
5.4 Conclusion 114

6 Perturbation Observer based Coordinated Adaptive Passive Control for Multi-machine Power Systems with FACTS Devices 116
6.1 Introduction 116
6.2 Problem Formulation 118
6.2.1 Design of HGSPO and HGPO 119
6.2.2 Design of stabilizing controller and coordinated controller . 122
6.2.3 The closed-loop system stability 125
6.3 Power System Modelling 128
6.3.1 An SMIB system with a TCSC device 128
6.3.2 A multi-machine power system with a TCSC device 129
6.4 POCAPC Design for Generator Excitor and TCSC Device 130
6.4.1 Controller design for an SMIB system 130
6.4.2 Controller design for a multi-machine power system 132
6.5 Case Studies 136
6.5.1 The SMIB system 136
6.5.2 The three-machine power system 143
6.6 Hardware-in-the-loop Test 153
6.7 Discussion 157
6.8 Conclusion 157

7 Conclusions and Future Works **159**
7.1 Summary 159
7.2 Future Studies 161

A Basic Concepts of Passive Systems **163**

References **168**

List of Figures

1.1 HVDC system based on CSC technology built with thyristors. . . . 3
1.2 HVDC system based on VSC technology built with IGBTs. 3
1.3 Conventional three-phase two-level VSC topology. 5
1.4 Two-level sinusoidal PWM method: reference (sinusoidal) and carrier (triangular) signals and line-to-neutral voltage waveform. 6
1.5 Active-reactive locus diagram of VSC-based power transmission system with limitations. 6

2.1 Structure of the POAPC 33
2.2 The magnetic levitator system. 36
2.3 System responses obtained under the nominal model. 37
2.4 System responses obtained under the unmodelled dynamics. 38
2.5 System responses obtained under the time-varying external disturbance. 39
2.6 Two inverted pendulums on two carts. 40
2.7 System responses obtained under the nominal model. 44
2.8 System responses obtained under the unmodelled dynamics. 45

3.1 The two-terminal VSC-HVDC system 54
3.2 Structure of the rectifier controller in two-terminal VSC-HVDC systems. 57
3.3 Structure of the inverter controller in two-terminal VSC-HVDC systems. 59
3.4 System responses obtained in an active and reactive power tracking. 62
3.5 System responses obtained in the voltage drop of AC grids. 63
3.6 System responses obtained under a 20% increase of system resistances and inductances. 64
3.7 Control efforts obtained under a 20% increase of system resistances and inductances. 65
3.8 Overall hardware platform. 66
3.9 Experiment configuration of Case I. 68
3.10 Experiment configuration of Case II. 69
3.11 The structure of an IGBT converter. 69

3.12 Experiment results obtained in case I. 71
3.13 Experiment results obtained in case II. 72

4.1 One terminal in an N-terminal VSC-MTDC system. 78
4.2 The topology of an N-terminal VSC-MTDC system. 79
4.3 Structure of PC for the VSC-MTDC system. 83
4.4 A four-terminal VSC-MTDC system. 87
4.5 System responses obtained in active and reactive power tracking. . . 88
4.6 System responses obtained under a 10-cycle LLLG fault at bus 1. . . 89
4.7 System responses obtained under a 10-cycle LLLG fault at bus 4. . . 90
4.8 The overall storage function obtained under a 10-cycle LLLG fault at bus 1 and bus 4. 91
4.9 System responses obtained under a transmission line disconnection of AC network$_1$ and AC network$_4$. 91
4.10 System responses obtained in a temporary DC cable$_1$ fault. 92
4.11 System responses obtained when a modulated change occurs in the angular frequency. 93
4.12 System responses obtained under a 20% decrease of the system resistances and inductances. 94
4.13 System responses obtained when weak AC networks are connected. 95
4.14 System responses obtained with DC voltage measurement noises. . 96

5.1 Structure of the rectifier controller in VSC-MTDC systems. 100
5.2 Structure of the inverter controller in VSC-MTDC systems. 103
5.3 System responses obtained in active and reactive power tracking. . . 106
5.4 System responses obtained under a 10-cycle LLLG fault at bus 1. . . 107
5.5 System responses obtained under a 10-cycle LLLG fault at bus 4. . . 107
5.6 Estimation errors of HGSPO$_1$ and HGPO$_1$ obtained under a 10-cycle LLLG fault at bus 1. 108
5.7 System responses obtained under a transmission line disconnection of AC network$_1$ and AC network$_4$. 109
5.8 System responses obtained in a temporary DC cable$_1$ fault. 110
5.9 System responses obtained when a modulated change occurs in the angular frequency. 111
5.10 System responses obtained under a 20% decrease of the system resistances and inductances. 112
5.11 System responses obtained when weak AC networks are connected. 113
5.12 System responses obtained with DC voltage measurement noises. . 114

6.1 Structure of the stabilizing controller u_2. 123
6.2 Structure of the coordinated controller u_1. 124
6.3 The SMIB system equipped with a TCSC device. 129
6.4 Structure of conventional PID+LL controller. 137

6.5 System responses obtained with the EC alone, coordinated EC and TCSC controller, and approximated EC and TCSC controller in the SMIB system. 138
6.6 System responses obtained under the nominal model in the SMIB system. 139
6.7 System responses obtained under an unmodelled TCSC dynamics in the SMIB system. 141
6.8 System responses obtained under an inter-area type disturbance in the SMIB system. 142
6.9 The three-machine power system equipped with a TCSC device. . . 143
6.10 System responses obtained under operation Type I and the nominal model in the three-machine power system. 144
6.11 Estimation errors of HGSPO_1 for G_1 obtained under operation Type I and the nominal model in the three-machine power system. 146
6.12 Estimation errors of HGPO for TCSC obtained under operation Type I and the nominal model in the three-machine power system. 146
6.13 The effect of a 50% parameter increase on the dynamic response of proposed controller without perturbation compensation obtained in the three-machine power system. 148
6.14 The effect of a 50% parameter increase on the dynamic response of proposed controller with perturbation estimation obtained in the three-machine power system. 149
6.15 System responses obtained under operation Type I and the parameter uncertainties in the three-machine power system. 150
6.16 System responses obtained under operation Type II and the parameter uncertainties in the three-machine power system. 151
6.17 The configuration of the HIL test. 154
6.18 The experiment platform of the HIL test. 154
6.19 System responses obtained in the HIL test with large observer poles $\lambda = \lambda' = 15$ ($f_{\text{s}} = 50$ kHz, $f_{\text{c}} = 500$ Hz and $\tau = 2$ ms). 155
6.20 System responses obtained in the HIL test with proper observer poles $\lambda = \lambda' = 5$ ($f_{\text{s}} = 50$ kHz, $f_{\text{c}} = 500$ Hz and $\tau = 2$ ms). 156

List of Tables

1.1 Summary of fully controlled high power semiconductors [4] 2
1.2 Summary of worldwide VSC-HVDC projects and their basic parameters 9
1.3 Estimated number of worldwide installed FACTS devices and their estimated total installed power 13

3.1 System parameters used in the two-terminal VSC-HVDC system. . 60
3.2 Control parameters in the two-terminal VSC-HVDC systems. 60
3.3 System parameters used in Case I. 68
3.4 System parameters used in Case II. 68
3.5 Control parameters used in the experiment. 73

4.1 System parameters used in the four-terminal VSC-MTDC system. . 87

5.1 Control parameters used in the four-terminal VSC-MTDC system. . 105

6.1 PID+LL control parameters of the SMIB system. 136
6.2 POCAPC parameters of the SMIB system. 140
6.3 SMIB system parameters (in p.u.). [56] 140
6.4 PID+LL control parameters of the three-machine power system. . . 144
6.5 POCAPC parameters of the three-machine power system. 145
6.6 Three-machine power system transmission line parameters (in p.u.). [56] 145
6.7 Three-machine power system operation Type I. 147
6.8 Three-machine power system operation Type II. 147
6.9 IAE index of different control schemes 152

List of Abbreviations and Notations

Abbreviations in Control Systems

PC	Passive control.
PO	Perturbation observer.
HGO	High-gain observer.
HGPO	High-gain perturbation observer.
HGSPO	High-gain state and perturbation observer.
FLC	Feedback linearization control.
APC	Adaptive passive control.
POAPC	Perturbation observer based adaptive passive control.
RPC	Robust passive control.
CPC	Coordinated passive control.
CAPC	Coordinated adaptive passive control.
POCAPC	Perturbation observer based coordinated adaptive passive control.
PID	Proportional-integral-derivative.
VC	Vector control.
PI	Proportional-integral.
SMO	Sliding-mode observer.
SMC	Sliding-mode control.
TDC	Time delay control.
ADP	Adaptive dynamic programming.
ADRC	Adaptive disturbance rejection controller.
CLF	Control Lyapunov function.
SISO	Single-input single-output.
MIMO	Multi-input multi-output.

Abbreviations in VSC-HVDC Systems

VSC	Voltage source converter.
LCC	Line-commutated converter.
HVDC	High voltage direct current.
VSC-HVDC	Voltage source converter based high voltage direct current.
VSC-MTDC	Voltage source converter based multi-terminal high voltage direct current.
HIL	Hardware-in-the-loop.
IGBT	Insulated gate bipolar transistor.
PWM	Pulse width modulation.
SPWM	Sinusoidal pulse width modulation.
SVM	Space vector modulation.
PLL	Phase-locked loop.
AC	Alternating current.
DC	Direct current.
I/O	Input/output.
A/D	Analogue/digital.
SVPWM	Space vector pulse width modulation.

Abbreviations in Power Systems

EC	Excitation controller.
TCSC	Thyristor controlled series capacitor.
FACTS	Flexible alternating current transmission systems.
SMIB	Single machine infinite bus.
LL	Lead-lag.
PSS	Power system stabilizer.
AVR	Automatic voltage regulator.
SVC	Static VAR compensator.
STATCOM	Static synchronous compensator.
p.u.	Per unit.

Symbols

$\forall$	for all.
$\exists$	exist.

$\Rightarrow$	implies.
$\rightarrow$	tends to.
$\mapsto$	maps to.
∂	partial derivative.
$\sum$	sum.
$\in$	in.
∞	infinity.
$\angle$	angle.
$\lim$	limit.
$\max$	maximum.
$\min$	minimum.
$\sup$	supremum, the least upper bound.
$\inf$	infimum, the greatest lower bound.
$\min$	designation the end of proofs.
$\mathbb{R}^n$	the n-dimensional Euclidean space.

Vectors and Matrices

$\|a\|$	the absolute value of a scalar a.
$\|x\|_p$	the induced p-norm of vector x, i.e. $\|x\|_p = (\|x_1\|^p + \cdots + \|x_n\|^p)^{1/p}$, $1 \leq p < \infty$; $\|x\|_\infty = \max_i \|x_i\|$.
$\|x\|$	the Euclidean norm of a vector x, i.e. $\|x\| = (x^{\mathrm{T}}x)^{1/2}$.
$\|A\|_p$	the induced p-norm of a matrix A, i.e. $\|A\|_p = \sup_{x \neq 0} \frac{\|Ax\|_p}{\|x\|_p}$.
$\|A\|$	the induced 2-norm of a matrix A, i.e. $\|A\| = [\lambda_{\max}(A^{\mathrm{T}}A)]^{1/2}$.
diag$[a_1, \cdots, a_n]$	a diagonal matrix with diagonal elements a_1 to a_n.
$A^{\mathrm{T}}(x^{\mathrm{T}})$	the transpose of a matrix A (a vector x).
$\lambda_{\max}(P)(\lambda_{\min}(P))$	the maximum and (minimum) eigenvalues of a symmetric matrix P.
$P > 0 (P \geq 0)$	a positive definite (semi-definite) matrix P.

Chapter 1

Introduction

1.1 Background

1.1.1 VSC-HVDC systems

The need for more secure power grids and increasing environmental concerns continue to drive the worldwide deployment of high voltage direct current (HVDC) transmission technology. HVDC systems use power electronic devices to convert alternative current (AC) into direct current (DC), and it is an economical way of transmitting bulk electrical power in DC over long-distance overhead lines or short submarine cables [1]. An HVDC system allows power transmission between unsynchronized AC transmission systems. Since the power flow through an HVDC link can be controlled independently of the phase angle between sources and loads, it can effectively stabilize a power network against disturbances due to rapid changes in power transmission [2]. The HVDC system also allows transfer of power between power grids running at different frequencies, such as 50 Hz and 60 Hz. This improves the stability and energy efficiency of each power grid, by allowing exchange of power between incompatible networks [3]. It is characterized by a number of advantages: lower overall costs, smaller environmental footprints, easier integration with renewable energy sources, and above all, higher transmission stability and power quality. HVDC systems can resolve many practical issues, including the voltage stability of connected AC networks, reduction of fault currents and optimal

Table 1.1: Summary of fully controlled high power semiconductors [4]

Acronym	Type	Full Name
IGBT	Transistor	Insulated Gate Bipolar Transistor
IEGT	Transistor	Injection Enhanced Gate Transistor
GTO	Thyristor	Gate Turn-off Thyristor
IGCT	Thyristor	Integrated Gate Commutated Thyristor
GCT	Thyristor	Gate Commutated Turn-off Thyristor

management of electrical power, which ensures the technology has a remarkably important role in the modern electrical power industry [4].

The ever increasing penetration of power electronics technologies into power systems mainly results from the continuous development of high voltage high power fully controlled semiconductors [5], which adopts different types of fully controlled semiconductor devices, such as thyristor or transistor based electronics shown in Table 1.1 [4]. These devices can be employed for a voltage source converter (VSC) with pulse width modulation (PWM) operating at a frequency higher than the line frequency. These devices are all self-commuted via a gate pulse [6]. Typically, it is desirable that a VSC generates PWM waveforms of higher frequency when compared to the thyristor-based systems. However, the operating frequency of these devices is also determined by the switching losses and the design of the heat sink, both of which are closely related to the power through the components. Switching losses, which are directly linked to high-frequency PWM operation, are one of the most serious and challenging issues that must be resolved by VSC-based high power applications [7]. Other obvious disadvantages are the electromagnetic compatibility or electromagnetic interference (EMC/EMI) and transformer insulation stresses [8, 9].

Currently, there are over 100 HVDC installations worldwide (in operation or planned for the very near future) transmitting more than 80 GW of power employing two distinct technologies as follows:

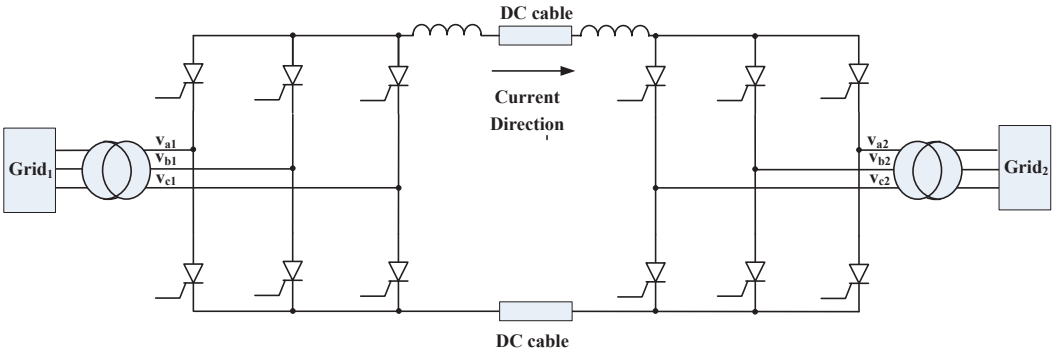

Figure 1.1: HVDC system based on CSC technology built with thyristors.

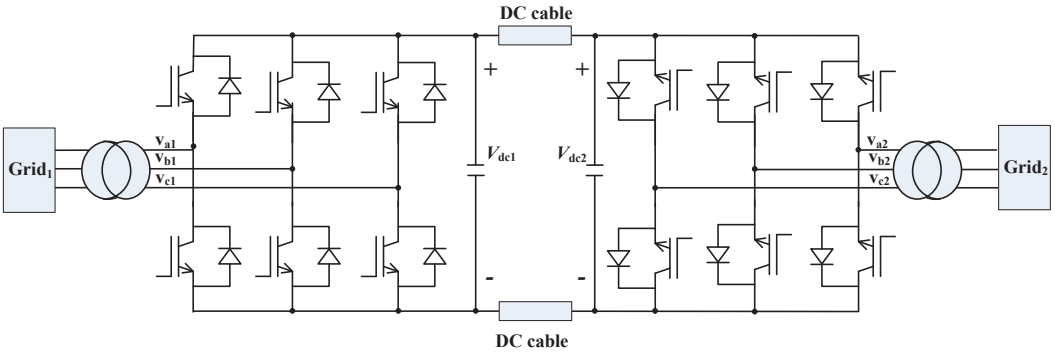

Figure 1.2: HVDC system based on VSC technology built with IGBTs.

- Line-commutated current source converters (CSCs) that use thyristors shown in Fig. 1.1. This technology is well established for high power, typically around 1000 MW, with the largest project being the Itaipu system in Brazil at 6300 MW power level. The longest power transmission in the world transmits 6400 MW power from the Xiangjiaba hydropower plant to Shanghai, which line length is 2071 km and will use 800 kV HVDC and 1000 kV ultrahigh-voltage AC transmission technology [10].

- Forced-commutated VSCs that use gate turn-off thyristors (GTOs) or in most industrial cases insulated gate bipolar transistors (IGBTs) illustrated in Fig. 1.2. It is a well-established technology for medium power levels with recent projects ranging around 300-400 MW power level [11].

On one hand, the CSC-HVDC systems represent mature technology today (i.e.,

also referred to as the 'classical' HVDC system), and recently, a large number of significant advances have been achieved [12]. On the other hand, the VSC-HVDC systems represent latest developments in the area of DC power transmission technology [11]. The operation experience with VSC-HVDC system at commercial level scatters over the last two decades [11, 12]. The breakthrough was made when the world's first VSC-based PWM-controlled HVDC system using IGBTs was installed in March 1997 (Hellsjön project, Sweden, 3 MW, 10 km distance, $\pm$10 kV) [13]. Since then, more VSC-HVDC systems have been installed worldwide [14].

The CSCs have the natural ability to withstand short-circuit fault because the DC inductors can limit the currents when faults occur. In contrast, the VSCs are more vulnerable to line faults, hence cables are more attractive for VSC-HVDC applications. It is worth mentioning that relevant developments, such as the advanced extruded DC cable technologies [15], can lead to the success of VSC-HVDC system. Furthermore, faults on the DC side of VSC-HVDC systems can also be addressed by using the DC circuit breakers (CBs) [16, 17]. In the event of the loss of a VSC in a multi-terminal HVDC (MTDC) system, the excess of power can be restricted by the advanced DC voltage controller [18].

A basic VSC-HVDC system comprising of two converters built with VSC topology is demonstrated by Fig. 1.2. The simplest VSC topology is the conventional two-level three-phase bridge shown in Fig. 1.3. Typically, many series-connected IGBTs are used for each semiconductor as illustrated by Fig. 1.3, such that a higher blocking voltage capability for the converter can be delivered, and therefore increase the DC bus voltage level of the VSC-HVDC system. Note that an antiparallel diode is also required for the purpose of ensuring the four-quadrant operation of the converter. The DC bus capacitor provides the required storage of the energy so that the active and reactive power can be controlled and offers filtering for the DC harmonics.

The converter is generally controlled by sinusoidal PWM (SPWM), and the harmonics are directly associated with the switching frequency of each converter leg. Fig. 1.4 presents the basic waveforms associated with SPWM and the line-to-neutral voltage waveform of the two-level converter given in Fig. 1.3. Each phase leg of the

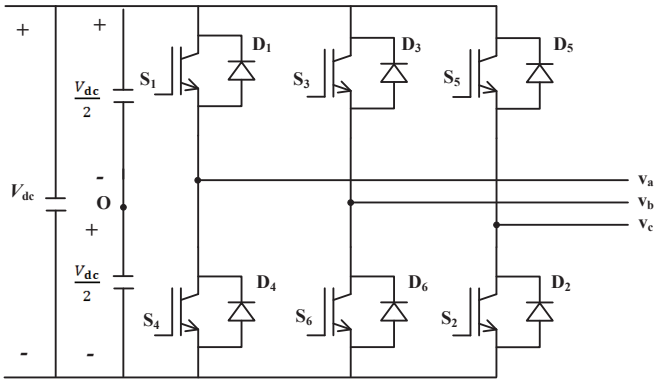

Figure 1.3: Conventional three-phase two-level VSC topology.

converter is connected through a reactor to the AC system. Filters are also included on the AC side to further reduce the harmonics flowing into the AC system.

Fig. 1.5 shows the entire active-reactive power area where the VSC can be operated with 1.0 per unit (p.u.) value being the megavolt amperes rating of each converter with limitations. The use of VSC as opposed to a line-commutated CSC offers the following advantages [4]:

- Avoidance of commutation failures due to disturbances in the AC network.
- Independent control of the active and reactive power consumed or generated by the converter.
- Possibility to connect the VSC-HVDC system to a weak AC network or even to one where no generation source is available, and naturally, the short-circuit level is very low.
- Faster dynamic response due to higher PWM than the fundamental switching frequency (phase-controlled) operation, which further results in reduced need for filtering, and hence smaller filter size.
- No need of transformers to assist the commutation process of the converter's fully controlled semiconductors.

In the past decade, studies on the VSC-HVDC system have been growing due to the interconnection between the mainland and offshore wind farms [19], power

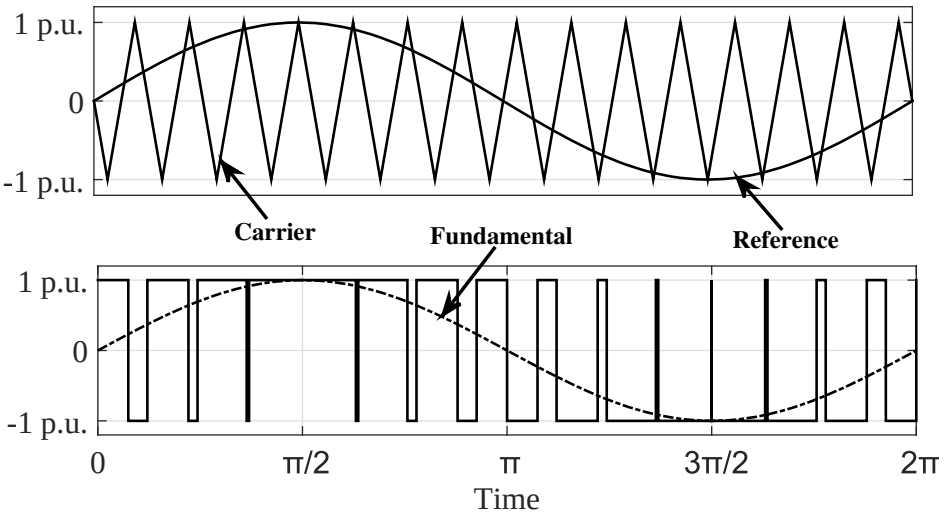

Figure 1.4: Two-level sinusoidal PWM method: reference (sinusoidal) and carrier (triangular) signals and line-to-neutral voltage waveform.

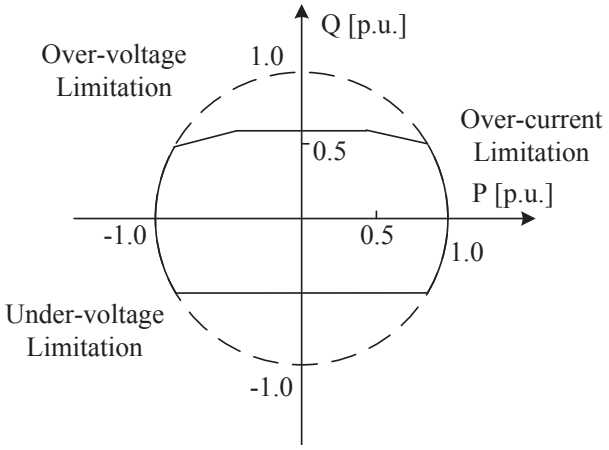

Figure 1.5: Active-reactive locus diagram of VSC-based power transmission system with limitations.

flow regulation in AC power systems, long-distance transmission, and introduction of the supergrid, which is a large-scale power grid interconnected between national power grids [20]. The VSC-HVDC system has been proposed for integration of long-distance large onshore wind farms via overhead line and offshore wind farms via submarine cable [18, 21].

One important issue that needs to be addressed carefully before the implementation is the protection design of VSC-HVDC systems. Currently, many studies have been carried out to investigate the VSC-HVDC system protection as the whole system has to be isolated from the power system when the DC cable fault occurs. A transient harmonic current protection scheme is proposed in [22], in which the discrete Fourier transform was used to extract transient harmonic currents at both terminals of the DC transmission line and the type of fault can be identified by the transient harmonic currents. Based on the zero- and positive-sequence backward traveling waves, an integrated traveling wave-based protection scheme was developed [23], which can detect faults rapidly, determine the fault type effectively, and select the faulty pole correctly. In addition, a transient energy protective scheme was developed [24] based on the distributed parameter line model, in which the transient energy distribution over the line can be obtained from the voltage and current measurements at both terminals and the fault can be recognized from the calculated value simply. Recently, an apparent impedance calculation method was proposed [25], which utilizes the bus impedance matrix to calculate the impedances viewed by distance relays during a three-phase SC fault. [26] proposed a whole-line quick-action protection principle for HVDC transmission lines, which is based on the boundary characteristics of the line, can distinguish internal faults from external ones using single-terminal current measurements only.

As the conventional two-terminal VSC-HVDC system can only carry out point-to-point power transfer, recently the economic development and construction of power grids require DC grids to achieve power exchanges among multiple power suppliers and multiple power consumers, thus multi-terminal VSC-HVDC (VSC-MTDC) systems draw more and more attention. As a DC transmission network connecting more than two converters, the VSC-MTDC system offers a larger transmis-

sion capacity than that of AC networks and provides a more flexible, efficient transmission method. The main applications of VSC-MTDC systems include power exchange among multi-points, connection between multiple asynchronous networks, and integration of scattered power plants like offshore renewable energy sources such as wind farms and solar plants [27]. Other application can be found in urban sub-transmission [28], oil and gas platforms [29], premium quality power parks [30], wind power transmission in Norway [21], and European supergrid [31]. Recently, the world's first MTDC system employing VSC technology called Nanao's VSC-MTDC project has been built in China [32]. Table 1.2 summarizes some worldwide VSC-HVDC projects [4, 33].

VSC-HVDC systems have also been used to improve the power system stability, a standard VSC-HVDC dynamic model has been proposed in [34] to study the power system stability. By having embedded VSC-HVDC systems in AC grids it is possible to enhance the power system stability and have a higher control of power flow [35]. Both linear and nonlinear supplementary control are employed to enhance the stability of the power system by modulating the active power in [36]. The Hopf stability margin of an AC grid can be increased through the VSC-HVDC operating-point adjustment [37], and adaptive fuzzy controllers have been designed in [38] to enhance the system stability when an offshore wind farm is connected to weak AC grids.

Table 1.2: Summary of worldwide VSC-HVDC projects and their basic parameters

Project Name	Year of Commission	Power Rating	AC Voltage	DC Voltage	Length of DC Cables	Topology
Hellsjön, Sweden	1997	3 MW ± 3 MVar	10 kV (both ends)	± 10 kV	10 km Overhead lines	2-level
Gotland HVDC Light, Sweden	1999	50 MW - 55 to +50 MVar	80 kV (both ends)	± 80 kV	2 × 70 km Submarine cables	2-level
Eagle Pass, USA	2000	36 MW ± 36 MVar	138 kV (both sides)	± 15.9 kV	Back-to-Back HVDC light	3-level NPC
Tjæreborg, Denmark	2000	8 MVA 7.2 MW - 3 to +4 MVar	10.5 kV (both sides)	± 9 kV	2 × 4.3 km Submarine cables	2-level
MurrayLink, Australia	2002	220 MW - 150 to +140 MVar	132 kV- Berri 220 kV- Red Cliffs	± 150 kV	2 × 180 km Underground cables	3-level ANPC
Troll A offshore, Norway	2005	84 MW - 20 to +24 MVar	132 kV- Kollsnes 56 kV- Troll	± 60 kV	4 × 70 km Submarine cables	2-level
Estlink,Estonia-Finland	2006	350 MW ± 125 MVar	330 kV- Estonia 400kV- Finland	± 150 kV	2 × 31 km Underground cables 2 × 74 km Submarine cables	2-level
NORD E,ON 1, Germany	2009	400 MW	380 kV-Diele 170kV- Borkum 2	± 150 kV	2 × 75 km Underground cables 2 × 128 km Submarine cables	- - - -
Caprivi Link, Namibia	2009	300 MW	330 kV- Zambezi 300kV- Gerus	± 350 kV	970 km Overhead lines	- - - -
Valhall offshore, Norway	2009	78 MW	300 kV- Lista 11kV- Valhall	± 150 kV	292 km Submarine coaxial cables	2-level
Trans Bay Cable, USA	2010	400 MW	115 kV- Potrero 230kV- Pittsburg	± 200 kV	88 km Submarine cables	Modular Multi-Level Converter (MMC)
Naoao Multi-terminal VSC HVDC, China	2013	200/100 /50 MW	220 kV- Chenghai Sucheng 110kV- Jinniu 110kV- Qingao	± 160 kV	40.7 km Mixture of submarine cables, overhead lines and underground cables	Modular Multi-Level Converter (MMC)
BorWin1, Germany	2015	400 MW	170 kV- BorWin Alpha platform 380kV-Diele	± 150 kV	2 × 125 km Submarine cables 2 × 75 km Underground cables	2-level

A proper control system design is crucial for the operation of VSC-HVDC systems. Conventional vector control (VC) [39] using proportional-integral (PI) loop is widely used. However its control performance will be degraded under different operating conditions as its control parameters are obtained from the local linearization. Since VSC-HVDC systems are highly nonlinear resulted from the converters, several nonlinear approaches are proposed, such as feedback linearization control (FLC) [40], power-synchronization control [41], and interconnection and damping assignment passivity-based (IDA-PB) control [42]. However, these approaches need an accurate system model, which cannot maintain their control performance in the presence of parameter uncertainties, unmodelled dynamics, and time-varying external disturbances. In order to tackle the above issue, several adaptive and robust control schemes have been developed, such as linear matrix inequality (LMI)-based robust control [43], adaptive backstepping [44], adaptive control [45], and feedback linearization sliding-mode control (FLSMC) [46].

Several adaptive control schemes have been developed for VSC-MTDC systems, such as adaptive droop control [47], which can share the burden according to the available headroom of each converter. An adaptive backstepping droop controller is proposed in [48], which can adaptively tune the droop gains to enhance the control performance of traditional droop controllers by considering DC cable dynamics. In order to improve the PI control performance, fuzzy logic-based PI controllers have been designed [49, 50], which can provide an optimal operating range to handle parameter uncertainties of VSC-MTDC systems by auto-tuning the PI gains. However, the tuning burden will be significantly increased when the number of terminal grows as four interacted PI gains need to be simultaneously tuned in each terminal. A generalized control algorithm is proposed to solve the power flow problems with various nonlinear voltage droops [51]. In [52], a distributed DC voltage control method was investigated where a PI control on the main slack bus is combined with a droop control on the other buses. In order to achieve a rapid power control performance, a hierarchical voltage control was developed which acts in a way similar to the primary control action of generators in AC systems, while the secondary control action is performed by an outer power control loop in [53]. The covariance matrix

adaptation was employed to obtain optimal power flows inside the offshore network with VSC-MTDC networks in [54]. [55] proposed a control scheme based on communications between the different converters. If a communication fault occurred, the control system would rapidly switch to droop control and the system could be safely operated without communications.

1.1.2 FACTS devices

In the late 1980s, the Electric Power Research Institute (EPRI) formulated the vision of flexible AC transmission systems (FACTS), in which various power electronics based controllers regulate power flow and transmission voltage and mitigate dynamic disturbances [56]. In general, the main objectives of FACTS are to increase the useable transmission line capacity and control power flow over designated transmission routes. The concept of FACTS is proposed in [57] while the terms and definitions for different FACTS controllers are given by [58]. FACTS devices have gained a great interest during the last few years, due to recent advances in power electronics. They have been mainly used for solving various power system steady-state control problems, such as voltage regulation, power flow control, transfer capability enhancement, inter-area modes damping, and power system stability enhancement [59].

For FACTS the taxonomy in terms of ‘dynamic’ and ‘static’ needs some explanation. The term ‘dynamic’ is used to express the fast controllability of FACTS devices provided by the power electronics. This is one of the main differentiation factors from the conventional devices. The term ‘static’ means that the devices have no moving parts like mechanical switches to perform the dynamic controllability. Therefore most of the FACTS devices can equally be static and dynamic [60].

FACTS devices can be connected in series, in parallel, or in a combination of both. The benefits they offer to power grids are widely referenced [57, 59, 61, 62]. These benefits include improvement of the power system stability, control of the active and reactive power, loss minimization, and increased power efficiency. FACTS devices can be divided into four categories:

- The series controllers such as thyristor controlled series capacitor (TCSC),

which consists of a series capacitor bank shunted by a thyristor controlled reactor to provide a smoothly variable series capacitive reactance. And static synchronous series compensator (SSSC), which injects a voltage in series with the transmission line where it is connected.

- The shunt controllers such as static VAR compensator (SVC), whose output is variable so as to maintain or control specific parameters (e.g. voltage or reactive power of buses) of power systems. And static synchronous compensator (STATCOM), which operates as a shunt connected SVC whose capacitive or inductive output current can be controlled independently from the AC system voltage.

- The combined series-series controllers such as interline power flow controller (IPFC), which is a combination of two or more independently controllable SSSCs to inject an almost sinusoidal voltage at variable magnitude via a common DC link.

- The combined series-shunt controllers such as unified power flow controller (UPFC), which is a combination of STATCOM and SSSC via a common DC link to allow bidirectional flow of active power between the series output terminals of SSSC and the shunt output terminals of STATCOM, and is controlled to provide concurrent active and reactive series line compensation without an external electrical energy source.

FACTS devices are usually perceived as new technologies, but hundreds of installations worldwide, especially of SVC since early 1970s with a total installed power of 90,000 MVar, show the acceptance of this kind of technology. Table 1.3 [60] presents the estimated number of worldwide installed FACTS devices and the estimated total installed power. Even the newer developments like STATCOM or TCSC show a quick growth rate in their specific application areas.

Table 1.3: Estimated number of worldwide installed FACTS devices and their estimated total installed power

Type	Number	Total Installed Power in MVA
SVC	600	90,000
STATCOM	15	1,200
Series Compensation	700	350,000
TCSC	10	2,000
UPFC	2-3	250

FACTS controller can effectively enhance the power system stability, a robust FACTS controller was developed through the H_∞ loop shaping to handle parameter uncertainties in [61]. [63] employs the neural network for the FACTS controller to provide a good system damping under a wide range of operating conditions and contingencies. A nonlinear FACTS controller was designed in [64] to damp the inter-area oscillations in power systems. A decentralized optimal FACTS controller using the overlapping decomposition technique was proposed in [65] to reduce the transient frequency deviation in a deregulated power system. Both the genetic algorithms and particle swarm optimization have been employed for the design of an optimal FACTS controller, which aims to enhance the power system stability subjected to different disturbances over a wide range of loading conditions and parameter variations [66]. A fuzzy logic based FACTS controller was designed to damp local modes and inter-area modes of oscillations in a multi-machine power system in [67]. A normalized H_∞ loop-shaping technique for design and simplification of damping controllers in the liner matrix inequalities (LMI) framework is illustrated in [68], which control performance was verified by the real-time based platform. In [69], a new linear programming based optimal power flow algorithm for corrective FACTS control was proposed to relieve overloads and voltage violations caused by system contingencies. In particular, a phase-to-phase open and close control scheme

for industrial SVC is proposed in [70], in which the forward loop was based on instantaneous reactive power theory, while a fuzzy proportional-integral-differential (PID) control was applied to the close loop. Reference [71] proposed adopted the shunt converter to make the DC-link voltage constant and output the reactive power for reactive power-flow control, while the series converter is controlled to maintain the UPFC bus voltage constant and adjust the real power flow in the transmission line, which performs better than the conventional control framework. Multivariable feedback linearization was employed to control the STATCOM, which control performance was evaluated under various types of loads and/or disturbances [72].

1.1.3 Passive control

Lyapunov function techniques have received much interest in applied mathematics and in particular in systems and control theory over the last one hundred years. A Lyapunov function is a scalar function $V(x)$ defined on a region D that is continuous, positive definite, $V(x) > 0$ for all $x \neq 0$, and has continuous first-order partial derivatives at every point of D. Suppose x_{e} is the equilibrium point, one can construct a positive definite continuously differentiable function $V(x) : \mathbb{R}^n \mapsto \mathbb{R}$. Then the Lyapunov stability criterion can be illustrated as follows: if $\dot{V}(x) \leq 0$, then x_{e} is stable; if $\dot{V}(x) < 0$, then x_{e} is asymptotically stable [74]. The main reasons for this interest are the simplicity, intuitive appeal, and universality of the Lyapunov function techniques [73]. Today, there is no doubt that they have become the main tools to tackle a stability or stabilization problem for both linear and nonlinear systems, and provide systematical analysis and design tools of modern control systems [74]. However, there are usually other important requirements besides stability which have to be taken into account. Therefore, It is natural to ask the following question: Is it possible to generalize the ideas of Lyapunov function techniques to address robustness and performance issues in control systems? Such a generalization is indeed possible and has lead to the important concept of passive system.

The concept of passive system originally arose in the context of electrical circuit theory, a passive system is characterized by the property that at any time the

amount of energy which the system can conceivably supply to its environment cannot exceed the amount of energy that has been supplied to it. When time evolves, a passive system absorbs a fraction of its supplied energy and transforms it into heat, an increase of entropy, mass, electro-magnetic radiation, or other kinds of energy 'losses'. Alternatively, one can say that the basic idea behind passive system is to generalize the concept of Lyapunov function techniques to systems with inputs and outputs [75]. Over the past two decades, the notion of passive system is a most important concept in control systems theory both for theoretical considerations as well as from a practical point of view, particularly in the physical sciences, which is closely related to the notion of energy. In many applications, the question whether a system is passive or not can be answered from physical considerations on the way the system interacts with its environment.

The property of passive system motivates the idea of passivity-based control or passive control (PC) [76], which views dynamic systems as energy-transformation devices. This perspective is notably useful in studying complex nonlinear systems by decomposing complex nonlinear systems into simpler subsystems that, upon interconnection, add up their local energies to determine the full system's behaviour [76, 77, 78]. The action of a controller connected to a dynamic system may also be regarded, in terms of energy, as another separate dynamic system. Thus the control problem can then be treated as finding an interconnection pattern between the controller and the dynamic system, such that the changes of the overall energy function can take a desired form. This 'energy shaping' approach is the essence of PC, which takes into account the energy of the system and gives a clear physical meaning [79, 80, 81, 82].

PC requires the relative degree must exist and be zero or one, in which the zero-dynamics must be stable (weakly minimum-phase) [73]. When the relative degree fails to exist, stabilization may still be possible under a weaker input-output invertibility condition. This motivates the coordinated passive control (CPC) [83, 84] design which is pursued for systems with two (or more) inputs. The design procedure can be divided into the following three steps: (a) An input-output pair is chosen for which the relative degree is one (or zero); (b) The stabilization of its zero-dynamics

by the remaining input (or inputs). This task is crucial not only in the case of unstable zero-dynamics, but also when the behaviour of stable zero-dynamics is not acceptable and must be modified by feedback; (c) When satisfactory zero-dynamics behaviour is achieved, the design proceeds with feedback passivation of the chosen input-output pair.

1.2 Motivation and Methodology

PC is not applicable in practice due to the following four reasons:

- PC requires an accurate system model for controller design with a vector relative degree of one, which restricts its application for general uncertain nonlinear systems.
- Adaptive passive control (APC) was proposed in [85, 87, 90] to handle parameter uncertainties, in which an uncertain nonlinear system is assumed to have explicit linearly parametric uncertainties, then a linearly parametric estimation based adaption law is developed to approximate the unknown parameters. However, these laws might not be trivial and the resulting adaptive system is highly nonlinear, with slow system responses to parameter uncertainties.
- Robust passive control (RPC) is developed by [88, 89, 91], in which the structural uncertainty is assumed to be a nonlinear function of the state and bounded by a known function. In general, such a function may not be easily found, and it would give an over-conservative result as well.
- Coordinated adaptive passive control (CAPC) requires an explicit control Lyapunov function (CLF), which is difficult to find for complex nonlinear systems [92, 93].

In order to resolve the above issues such that the PC can be applicable in practice, this thesis proposes a perturbation observer based adaptive passive control (POAPC). The combinatorial effect of system nonlinearities, parameter uncertainties, unmodelled dynamics, and time-varying external disturbances is aggregated

into a perturbation, and estimated by a perturbation observer (PO) [94, 95, 96, 97, 98]. Moreover, POAPC does not require an accurate system model and can be easily extended into general uncertain nonlinear systems. It can effectively handle various system uncertainties with only one state measurement, which releases the strict assumptions made by APC or RPC. Finally, only the range of CLF is needed by perturbation observer based adaptive coordinated passive control (POCAPC), which can then be readily applied on complex nonlinear systems. Based on the above merits, the proposed approach has been applied to the following two practical applications to verify its effectiveness and applicability:

- The POAPC design for VSC-HVDC systems, which are highly nonlinear resulted from converters. As there exists parameter uncertainties, together with unmodelled dynamics and time-varying external disturbances, the accurate modelling for VSC-HVDC systems is very difficult. POAPC provides a powerful way to design adaptive controllers with only the measurement of DC voltage, active and reactive power. It is applied on both the two-terminal VSC-HVDC systems and N-terminal VSC-MTDC systems, which can effectively handle various system uncertainties and maintain a consistent control performance without any control parameter tuning.

- The POCAPC design of EC and TCSC controller for power systems. A decentralized stabilizing EC is firstly designed with one PO, in which no explicit CLF is needed. Then a coordinated controller is designed for TCSC device to passivize the whole system via another PO. POCAPC provides a systematic control design for both single machine infinite bus (SMIB) systems and multi-machine power systems, which can partially release the dependence of an accurate system model.

1.3 Main Contributions

The contribution of this thesis can be grouped as two parts: (a) A novel POAPC has been proposed to handle various system uncertainties using the PO; and (b)

The POAPC has been applied on both VSC-HVDC systems and FACTS devices to improve the system stability. Main contributions are summarized as follows:

- This thesis proposes a novel adaptive passive control scheme called POAPC. The combinatorial effect of system nonlinearities, parameter uncertainties, unmodelled dynamics and time-varying external disturbances can be estimated online via a PO, which is then compensated by the controller. Hence POAPC does not require an accurate system model and only one state measurement is needed. Moreover, the proposed approach can be applied for general canonical systems, such that the strict requirement of a vector relative degree of one used in PC can be released. In addition, the assumptions made by APC or RPC for system uncertainties and structure can be avoided. These merits of POAPC make PC applicable in practice.

- POAPC is applied for two-terminal VSC-HVDC systems, which can handle various system uncertainties and provide a great robustness. The majority of studies for the advanced controller design for VSC-HVDC systems is only based on simulation, while the implementation feasibility remains undiscussed. This thesis undertakes a simulation for the VSC-HVDC system at first, then a hardware experiment is carried out for rectifier controller and inverter controller to verify the implementation feasibility of the proposed controller.

- PC has only been applied on two-terminal VSC-HVDC systems, this thesis extends the PC design into N-terminal VSC-MTDC systems. It partially cancels the system nonlinearities and keeps the beneficial parts, which can improve the system damping. The remained internal dynamics related to the DC cable current and common DC voltage is proved to be asymptotically stable in the context of Lyapunov criterion.

- POAPC is designed for the N-terminal VSC-MTDC system, which does not require an accurate system model thus a significant robustness can be provided. Moreover, the control scheme only requires the measurement of DC

voltage, active and reactive power. Once it is set up for the VSC-MTDC system within a predetermined range of variation in system variables, no tuning is needed for start-up or compensation of changes in the system dynamics and disturbance.

- POCAPC is developed for EC and FACTS controller on both SMIB systems and multi-machine power systems. It does not need an explicit CLF and the dependence of an accurate system model can be partially reduced, thus POCAPC can be easily applied for multi-machine power systems. The control performance of POCAPC is evaluated by simulation, then its implementation feasibility is verified through the hardware-in-the-loop (HIL) test.

1.4 Publication List

The following publications linked to this thesis closely are listed as follows:

[1] **B. Yang**, L. Jiang, Wei Yao, and Q. H. Wu, "Perturbation estimation based adaptive coordinated passive control for multi-machine power systems," *Control Engineering Practice*, vol. 44, pp. 172-192, 2015.

[2] **B. Yang**, L. Jiang, and Q. H. Wu, "Perturbation observer based adaptive passive control for uncertain nonlinear systems," *IET Control Theory Applications*, 2015, under the second round of review.

[3] **B. Yang**, L. Jiang, Chuan-Ke Zhang, and Q. H. Wu, "Passive control design for multi-terminal VSC-HVDC systems via energy shaping," *IET Generation, Transmission, Distribution*, 2015, under review.

[4] **B. Yang**, L. Jiang, Wei Yao, and Q. H. Wu, "Perturbation observer based adaptive passive control for damping improvement of VSC-MTDC systems," *Electric Power Systems Research*, 2015, under review.

[5] **B. Yang**, Q. H. Wu, L. Jiang and J. S. Smith, "Adaptive passivity-based control of a TCSC for the power system damping improvement of a PMSG based offshore wind farm," *ICRERA*, Madrid, Spain, Oct. 20-23, 2013.

[6] Y. Y. Sang, **B. Yang**, and L. Jiang, "Nonlinear adaptive control design for the VSC-HVDC light transmission system," *UPEC 2015*, Staffordshire, UK, Sep. 1-4, 2015.

The related publications during the PhD study are listed as below:

[1] **B. Yang**, L. Jiang, L. Wang, Wei Yao, and Q. H. Wu, "Nonlinear maximum power point tracking control and modal analysis of DFIG based wind turbine," *International Journal of Electrical Power and Energy Systems*, vol. 74, pp. 429-436, 2016.

[2] T. Yu, L. Xi, **B. Yang**, Z. Xu, and L. Jiang, "Multiagent stochastic dynamic game for smart generation control," *Journal of Energy Engineering*, DOI:10.1061/(ASCE)EY.1943-7897.0000275, 2015.

[3] L. Xi, T. Yu, **B. Yang**, X. S. Zhang, "A novel multi-agent decentralized win or learn fast policy hill-climbing(λ) algorithm for smart generation control of interconnected complex power grids," *Energy Conversion and Management*, vol. 103, pp. 82-93, 2015.

1.5 Thesis Outline

This thesis is organized as follows:

Chapter 2: Perturbation Observer based Adaptive Passive Control

In Chapter 2, we propose the adaptive passive control of normal uncertain nonlinear systems via high-gain perturbation observers. The estimate of the perturbation is used to realize the adaptive passivation of the original nonlinear system without requiring an accurate system model. The closed-loop system stability is proved in the context of Lyapunov criterion. Simulation results of two examples are given.

Chapter 3: Perturbation Observer based Adaptive Passive Control for Two-terminal VSC-HVDC Systems

In this chapter, POAPC is firstly extended into general canonical systems, then its application for two-terminal VSC-HVDC systems is investigated. Discussion be-

gins with the modelling of VSC-HVDC system, in which one converter is chosen as the rectifier to regulate the DC voltage and reactive power, while the other is chosen as the inverter to regulate the active and reactive power. The rectifier controller only requires the measurement of DC voltage and reactive power, while the inverter controller only requires the measurement of active and reactive power. Both simulation and hardware experiment are carried out.

Chapter 4: Passive Control Design for VSC-MTDC Systems via Energy Shaping

In this chapter, PC is developed for an N-terminal VSC-MTDC system via energy shaping. It reshapes the storage function into an output strictly passive form of three controlled states: active power, reactive power, and DC voltage. The proposed control partially cancels the system nonlinearities and keeps the beneficial parts, which improves the system damping. Considering zero-dynamics of the active power, reactive power, and DC voltage, the remained internal dynamics related to the DC cable current and common DC voltage is proved to be asymptotically stable in the context of Lyapunov criterion. Simulation results obtained in a four-terminal VSC-MTDC system is provided.

Chapter 5: Perturbation Observer based Adaptive Passive Control for VSC-MTDC Systems

This chapter develops POAPC design for the same VSC-MTDC systems used in Chapter 4. It only requires the measurement of active and reactive power in each terminal, and the DC voltage of rectifier. It can effectively handle the parameter uncertainties, unmodelled dynamics, and time-varying external disturbances through the fast compensation of perturbation. Simulation results are given with the comparison to those of PC designed in Chapter 4.

Chapter 6: Perturbation Observer based Coordinated Adaptive Passive Control for Multi-machine Power Systems with FACTS Devices

This chapter applies perturbation observer for the coordinated control of EC and TCSC controller for both SMIB systems and multi-machine power systems. Controller design starts with decomposing the original power system into several

subsystems, in which the TCSC reactance and its modulated input are chosen as the output and input, respectively, such that the relative degree is one. A decentralized stabilizing EC for each generator is designed and a coordinated TCSC controller is developed via passivation, which ensures the whole system stability. Both simulation and HIL test are undertaken.

Chapter 7: Conclusions

We conclude this thesis with a summary of the obtained results and several suggestions for future work, which are mostly unsolved problems that remain in this thesis. Several basic concepts and results of passive system can be found in Appendix.

Chapter 2

Perturbation Observer based Adaptive Passive Control

2.1 Introduction

Nonlinear systems are ubiquitous in nature and the concept of passivity has played a crucial role in the nonlinear system control based on the Lyapunov stability. Passivity is the state or condition of being passive, it views a dynamic system as an energy-transformation device, which decomposes complex nonlinear systems into simpler subsystems that, upon interconnection, add up their local energies to determine the full system's behaviour. The action of a controller connected to the dynamic system may also be regarded, in terms of energy, as another separate dynamic system. Thus the control problem can then be treated as finding an interconnection pattern between the controller and the dynamic system, such that the changes of the overall energy function can take a desired form. This 'energy shaping' approach is the essence of PC, which takes into account the energy of the system and gives a clear physical meaning [77, 79, 80, 81]. The application of passivity can be found in mechanical system control [99], power system control [100, 101], and power converter control [102, 103, 104]. However, PC requires an accurate system model for controller design, which restricts its application for uncertain and complex nonlinear systems.

In order to handle the parameter uncertainties, APC was proposed by [85, 87, 90]. In which an uncertain nonlinear system is assumed to have explicit linearly parametric uncertainties, then a linearly parametric estimation based adaption law is developed to approximate the constant or slow varying unknown parameters. However, these laws might not be trivial and the resulting adaptive system is highly nonlinear, with slow system responses to parameter uncertainties. RPC is another effective method [88, 89, 91], in which the structural uncertainty was assumed to be a nonlinear function of the state and bounded by a known function. In general, such a function may not be easily found, and it would give an over-conservative result as well.

Recently, functional approximators have been proposed to estimate uncertain fast time-varying nonlinear dynamics, such as adaptive neural network (ANN) [105, 106, 107], which has the capability of nonlinear function approximation, learning, and fault tolerance. Moreover, adaptive dynamic programming (ADP) [108, 109] can directly approximate, through learning and online measurement, the optimal controllers with guaranteed stability for dynamic systems with the unmodelled dynamics. Robust ADP [110] extends it into uncertain systems with unmeasured states and unknown system order. A Fradkov theorem based passification approach has been developed to stabilize a nonlinear system with functional and parametric uncertainties [111], which is extended to apply on the nonlinear delay systems with an unmodelled dynamics [112].

So far, functional estimation for system nonlinearities, parameter uncertainties, unmodelled dynamics, and time-varying external disturbances existing in passive systems has not been fully investigated. This problem is crucial and challenging in both theory and practice. For the robust performance of passive systems, if a reliable model for a part of the modelling uncertainties is available, it can be readily compensated using a model-based technique. However, most of the modelling uncertainties are arbitrary and cannot be readily identified. So a robust compensation method is needed to cope with it in real-time without depending on a direct perturbation model. The original idea of the perturbation estimation stems from time delay controller (TDC), in which the time-delayed values of derivatives of states

and control inputs are used to cancel the uncertain nonlinear dynamics [164]. Recently, PO has been widely used which can rapidly estimate the lumped uncertainty not considered in the nominal plant model based on an extended state. It can be regarded as a model regulator which drives the physical plant with uncertainties to the nominal model [163].

There are typically three types of PO as follows: (a) The sliding-mode control with perturbation estimation (SMCPE), which uses PO to reduce the conservativeness of the sliding-mode control (SMC) [163]; (b) The active disturbance rejection controller (ADRC) [165], which designs nonlinear disturbance observers; and (c) The high-gain perturbation observer (HGPO) [94, 95]. In fact, HGPO can provide similar performance as other types of PO but it provides merits of easy design and implementation, compared with the sliding-mode observer (SMO) [163] which suffers the discontinuity of high-speed switching, and the nonlinear observer [165] which is too complex for stability analysis.

This chapter develops the design and stability analysis of POAPC. The combinatorial effect of system nonlinearities, parameter uncertainties, unmodelled dynamics and time-varying external disturbances is aggregated into a perturbation, which is estimated online by an HGPO. The original high-gain observer (HGO) gain must be chosen to be large enough to suppress the upper bound of perturbation, which will produce an undesirable peaking phenomenon [166]. In contrast, the proposed method introduces the perturbation estimation and compensation, such that the HGO gain only needs to be chosen to suppress the perturbation estimation error. As the perturbation estimation error is usually smaller than the upper bound of perturbation, thus a relatively small gain value is needed and the malignant effect of the peaking phenomenon can be reduced [94, 95]. POAPC does not require an accurate system model and is inherently robust against plant variations. Once it is set up for the problem within a predetermined range of variation in system variables, no tuning is needed for start-up or for compensation for changes in the system dynamics and disturbance. Both the convergence of the observer estimation error and the stability of the closed-loop system are analyzed. It is evaluated in two examples, a magnetic levitator system and an interconnected inverted pendulums system, respectively.

2.2 Problem Formulation

Consider a normal passive system as follows

$$\begin{cases} \dot{y} = a(y,z) + \bar{B}u + \zeta(t) \\ \dot{z} = f_0(z) + p(y,z)y \end{cases} \tag{2.2.1}$$

where the output $y \in \mathbb{R}^m$ and control input $u \in \mathbb{R}^m$, such that system (2.2.1) is of the vector relative degree of one. $a(y,z) \in \mathbb{R}^m$ is nonlinear which includes the structure and parameter uncertainties, $\zeta(t) \in \mathbb{R}^m$ is the time-varying external disturbance. $z \in \mathbb{R}^{n-m}$ is the internal dynamics, with $f_0(z) \in \mathbb{R}^{n-m}$ represents the zero-dynamics and $p(y,z)$ is a known smooth function of dimension $(n-m) \times m$. The unknown control gain $\bar{B} \in \mathbb{R}^{m \times m}$ is written as

$$\bar{B} = \begin{bmatrix} b_{11}(y,z) & \cdots & b_{1m}(y,z) \\ \vdots & \vdots & \vdots \\ b_{m1}(y,z) & \cdots & b_{mm}(y,z) \end{bmatrix} \tag{2.2.2}$$

Remark 2.1. A known $p(y,z)$ and the vector relative degree of one are two basic assumptions for a passive system [85]. Note that several work has been done to relax such fundamental assumptions by [87, 111, 112].

Assume system (2.2.1) is zero-state detectable and locally weakly minimum-phase, and the known part of function $a(y,z)$ and $\bar{B}$ be zero for the simplification of formulations. In fact, one can assume the nominal part is known, and only use the perturbation to represent the uncertain part. Define a fictitious state as

$$\Psi(y,z,u,t) = a(y,z) + (\bar{B} - B_0)u + \zeta(t) \tag{2.2.3}$$

where $\Psi(\cdot) \in \mathbb{R}^m$ is called the perturbation. $B_0 = \text{diag}[b_{10}, b_{20}, \cdots, b_{m0}]$ with b_{i0} the nominal control gain. Extend the output dynamics of system (2.2.1), yields

$$\begin{cases} \dot{y}_i = \Psi_i(\cdot) + b_{i0}u_i \\ \dot{y}_{ei}(\cdot) = \dot{\Psi}_i(\cdot) \qquad\qquad , \ i = 1, \ldots, m \\ \dot{z} = f_0(z) + p(y,z)y \end{cases} \tag{2.2.4}$$

where $y_{ei} = \Psi_i(\cdot)$ is the extended state to represent the perturbation.

Assumption 2.1. [94, 95] b_{i0} is chosen to satisfy:

$$\left| \frac{\|\bar{B}\|}{|b_{i0}|} - 1 \right| \leq \theta_i < 1 \tag{2.2.5}$$

where θ_i is a positive constant, and $\|\cdot\|$ is the Euclidean norm.

Assumption 2.2. [94, 95] The function $\Psi_i(y, z, u, t) : \mathbb{R}^m \times \mathbb{R}^{n-m} \times \mathbb{R}^m \times \mathbb{R}^+ \mapsto \mathbb{R}$ and $\dot{\Psi}_i(y, z, u, t) : \mathbb{R}^m \times \mathbb{R}^{n-m} \times \mathbb{R}^m \times \mathbb{R}^+ \mapsto \mathbb{R}$ are locally Lipschitz in their arguments over the domain of interest and are globally bounded:

$$| \Psi_i(y, z, u, t) | \leq \gamma_{i1}, \quad | \dot{\Psi}_i(y, z, u, t) | \leq \gamma_{i2} \tag{2.2.6}$$

where γ_{i1} and γ_{i2} are positive constants. In addition, $\Psi_i(0, 0, 0, 0) = 0$ and $\dot{\Psi}_i(0, 0, 0, 0) = 0$, such that the origin is an equilibrium point of the open-loop system.

A second-order HGPO [94, 95] is designed for extended system (2.2.4) as

$$\begin{cases} \dot{\hat{y}}_i = \hat{\Psi}_i(\cdot) + h_{i1}(y_i - \hat{y}_i) + b_{i0}u_i \\ \dot{\hat{\Psi}}_i(\cdot) = h_{i2}(y_i - \hat{y}_i) \end{cases}, \ i = 1, \ldots, m \tag{2.2.7}$$

where $\hat{y}_i$ and $\hat{\Psi}_i(\cdot)$ are the estimates of y_i and $\Psi_i(\cdot)$. Positive constants h_{i1} and h_{i2} are the observer gains.

Remark 2.2. The HGPO is used in this thesis for its relatively easy design and implementation. Note that other types of observer, i.e., SMO [163] and nonlinear observer [165] can also be used for PO. They can provide almost similar performance.

2.3 Design and Stability Analysis of POAPC

Define the estimation error as $\tilde{y}_{\mathrm{po}_i} = [\tilde{y}_i, \tilde{y}_{\mathrm{e}i}]^{\mathrm{T}}$, where $\tilde{y}_i = y_i - \hat{y}_i$ and $\tilde{y}_{\mathrm{e}i} = y_{\mathrm{e}i} - \hat{y}_{\mathrm{e}i}$ symbolize the estimation error of y_i and $y_{\mathrm{e}i}$. The system dynamics (2.2.4) can be written as follows

$$\begin{bmatrix} \dot{y}_i \\ \dot{y}_{\mathrm{e}i} \end{bmatrix} = \begin{bmatrix} 0 & 1 \\ 0 & 0 \end{bmatrix} \begin{bmatrix} y_i \\ y_{\mathrm{e}i} \end{bmatrix} + \begin{bmatrix} 0 \\ 1 \end{bmatrix} \dot{\Psi}_i(\cdot) + \begin{bmatrix} b_{i0} \\ 0 \end{bmatrix} u_i \tag{2.3.1}$$

The HGPO dynamics (2.2.7) can be written as

$$\begin{bmatrix} \dot{\hat{y}}_i \\ \dot{\hat{y}}_{ei} \end{bmatrix} = \begin{bmatrix} 0 & 1 \\ 0 & 0 \end{bmatrix} \begin{bmatrix} \hat{y}_i \\ \hat{y}_{ei} \end{bmatrix} + \begin{bmatrix} h_{i1} \\ h_{i2} \end{bmatrix} \tilde{y}_i + \begin{bmatrix} b_{i0} \\ 0 \end{bmatrix} u_i \tag{2.3.2}$$

The estimation error dynamics can be obtained by subtracting (2.3.2) from (2.3.1) as

$$\begin{bmatrix} \dot{\tilde{y}}_i \\ \dot{\tilde{y}}_{ei} \end{bmatrix} = \begin{bmatrix} -h_{i1} & 1 \\ -h_{i2} & 0 \end{bmatrix} \begin{bmatrix} \tilde{y}_i \\ \tilde{y}_{ei} \end{bmatrix} + \begin{bmatrix} 0 \\ 1 \end{bmatrix} \dot{\Psi}_i(\cdot) \tag{2.3.3}$$

HGPO estimation error (2.3.3) can be rewritten in the following compact form

$$\dot{\tilde{y}}_{\mathrm{po}_i} = A_{\mathrm{po}_i} \tilde{y}_{\mathrm{po}_i} + B_{\mathrm{po}_i} \dot{\Psi}_i(\cdot) \tag{2.3.4}$$

Which shows that the estimation error $\tilde{y}_{\mathrm{po}_i}$ is driven by $\dot{\Psi}_i(\cdot)$. Matrices A_{po_i} and B_{po_i} are given as

$$A_{\mathrm{po}_i} = \begin{bmatrix} -h_{i1} & 1 \\ -h_{i2} & 0 \end{bmatrix}, B_{\mathrm{po}_i} = \begin{bmatrix} 0 \\ 1 \end{bmatrix} \tag{2.3.5}$$

where A_{po_i} is a Hurwitz matrix.

As in any asymptotic observer, the observer gain $H_{\mathrm{po}_i} = [h_{i1}, h_{i2}]^{\mathrm{T}}$ should be chosen to achieve the asymptotic error convergence, that is

$$\lim_{t \to \infty} \tilde{y}_{\mathrm{po}_i}(t) = 0 \tag{2.3.6}$$

In the absence of $\dot{\Psi}_i(\cdot)$, the estimation error will asymptotically convergence to the origin as A_{po_i} is Hurwitzian for any positive constants h_{i1} and h_{i2}.

In the presence of $\dot{\Psi}_i(\cdot)$, one needs to determine the observer gain with an additional goal of rejecting the effect of $\dot{\Psi}_i(\cdot)$ on the estimation error $\tilde{y}_{\mathrm{po}_i}$. This can be ideally achieved, for any $\dot{\Psi}_i(\cdot)$, if the transfer function from $\dot{\Psi}_i(\cdot)$ to $\tilde{y}_{\mathrm{po}_i}$

$$H_{\mathrm{po}_i}(s) = \frac{1}{s^2 + h_{i1}s + h_{i2}} \begin{bmatrix} 1 \\ s + h_{i1} \end{bmatrix} \tag{2.3.7}$$

is identically zero.

By calculating the $\|H_{\mathrm{po}_i}\|_\infty$, it can be seen that the norm can be arbitrarily small by choosing $h_{i2} \gg h_{i1} \gg 1$. Define $h_{i1} = \alpha_{i1}/\epsilon_i$ and $h_{i2} = \alpha_{i2}/\epsilon_i^2$, where $\alpha_{i1} =$

$2\lambda_i$, $\alpha_{i2} = \lambda_i^2$ such that the pole of HGPO (2.2.7) can be placed at $-\lambda_i$, where $\lambda_i > 0$ and $\epsilon_i \ll 1$ are some positive constants. It can be shown that

$$H_{\mathrm{po}_i}(s) = \frac{\epsilon_i}{(\epsilon_i s)^2 + \alpha_{i1}\epsilon_i s + \alpha_{i2}} \begin{bmatrix} \epsilon_i \\ \epsilon_i s + \alpha_{i1} \end{bmatrix} \tag{2.3.8}$$

Hence, $\lim_{\epsilon_i \to 0} H_{\mathrm{po}_i}(s) = 0$. As an infinite observer gain is impossible in practice, one can determine the observer gain such that the estimation error $\tilde{y}_{\mathrm{po}_i}$ will exponentially converge to a small neighbourhood which is arbitrarily close to the origin. The result is summarized as the following Proposition 2.1.

Proposition 2.1. [94, 95] *Consider system (2.2.4), and design a second-order HGPO (2.2.7). If Assumptions 2.1-2.2 hold for some values γ_{i1}, γ_{i2}, and b_{i0}. Then given any positive constant δ_{po_i}, from the initial estimation error $\tilde{y}_{po_i}(0)$, the observer gain H_{po_i} can be chosen such that the estimation error will exponentially converge into the neighbourhood*

$$\|\tilde{y}_{\mathrm{po}_i}(t)\| \leq \delta_{\mathrm{po}_i} \tag{2.3.9}$$

HGPO (2.2.7) is basically an approximate differentiator. This can be readily seen in the special case when the perturbation $\Psi_i(\cdot)$ and control u_i are chosen to be zero and thus the observer becomes linear. The transfer function from y_i to $\hat{y}_{\mathrm{po}_i}$ for system (2.3.4) is given by

$$\frac{\alpha_{i2}}{(\epsilon_i s)^2 + \alpha_{i1}\epsilon_i s + \alpha_{i2}} \begin{bmatrix} 1 + (\epsilon_i \alpha_{i1}/\alpha_{i2})s \\ s \end{bmatrix} \to \begin{bmatrix} 1 \\ s \end{bmatrix} \quad \text{as} \quad \epsilon_i \to 0 \tag{2.3.10}$$

As a consequence, on a compact frequency interval, the HGPO approximates $\Psi_i(\cdot) = \dot{y}_i$ for a sufficiently small ϵ_i.

The estimate of perturbation $\Psi(\cdot)$ is used to realize the adaptive feedback passivation of the uncertain nonlinear system (2.2.1). After the lumped system uncertainties are estimated by the HGPO, an output feedback passive controller can be designed for the equivalent linear system. The POAPC is designed as follows

$$\begin{cases} u = B_0^{-1}\left(-\hat{\Psi}(\cdot) - Ky - \left(\frac{\partial W_0(z)}{\partial z^{\mathrm{T}}} p(y,z)\right)^{\mathrm{T}} + \nu\right) \\ \nu^{\mathrm{T}} = -\phi(y) \end{cases} \tag{2.3.11}$$

where $K = \text{diag}[k_1, \ldots, k_m]$, with $k_i \geq 1$, is the feedback control gain, $\nu \in \mathbb{R}^m$ is the additional input, where $\phi : \mathbb{R}^m \to \mathbb{R}^m$ is any smooth function such that $\phi(0) = 0$ and $y^{\mathrm{T}}\phi(y) > 0$ for all $y \neq 0$.

Rewrite system (2.3.4) into the singularly perturbed form by defining the scaled estimation error $\eta_i = [\eta_{i1}, \eta_{i2}]^{\mathrm{T}} = [\tilde{y}_i/\epsilon_i, \tilde{\Psi}_i(\cdot)]^{\mathrm{T}}$, which satisfies

$$\epsilon_i \dot{\eta}_i = A_{i1}\eta_i + \epsilon_i B_{i1}\dot{\Psi}_i(\cdot), \quad i = 1, \ldots, m \tag{2.3.12}$$

with

$$A_{i1} = \begin{bmatrix} -\alpha_{i1} & 1 \\ -\alpha_{i2} & 0 \end{bmatrix}, B_{i1} = \begin{bmatrix} 0 \\ 1 \end{bmatrix} \tag{2.3.13}$$

where positive constants α_{i1} and α_{i2} are chosen such that A_{i1} is a Hurwitz matrix.

The closed-loop system dynamics obtained under HGPO (2.2.7) and passive controller (2.3.11) is represented in the following form

$$\begin{cases} \dot{y} = -Ky + \eta_{i2} - \left(\frac{\partial W_0(z)}{\partial z^{\mathrm{T}}} p(y,z)\right)^{\mathrm{T}} + \nu \\ \dot{z} = f_0(z) + p(y,z)y \\ \epsilon_i \dot{\eta}_i = A_{i1}\eta_i + \epsilon_i B_{i1}\dot{\Psi}_i(\cdot) \end{cases}, \ i = 1, \ldots, m \tag{2.3.14}$$

The reduced system, obtained by substituting $\eta_i = 0$ and $z = 0$ in system (2.3.14), is calculated as

$$\dot{y}_i = -k_i y_i + \nu_i, \quad i = 1, \ldots, m \tag{2.3.15}$$

The boundary-layer system, obtained by applying the change $\tau_i = t/\epsilon_i$ to system (2.3.14) and setting $\epsilon_i = 0$, is given by

$$\frac{d\eta_i}{d\tau_i} = A_{i1}\eta_i, \quad i = 1, \ldots, m \tag{2.3.16}$$

Theorem 2.1. *Let Assumptions 2.1-2.2 hold, design HGPO (2.2.7) and passive controller (2.3.11); then there exists ϵ_{i1}^*, with $i = 1, \ldots, m$, $\epsilon_{i1}^* > 0$ such that, $\forall \epsilon_i, 0 < \epsilon_i < \epsilon_{i1}^*$, the closed-loop system (2.3.14) is output strictly passive and the origin is stable.*

Proof. For the proof of Theorem 2.1, the following corollary which is a special case of Young's inequality will be used

Corollary 2.1. $\forall a, b \in \mathbb{R}^+$, $\forall p > 1$, $\epsilon_0 > 0$ *it has*

$$ab \leq \frac{1}{\epsilon_0} a^p + (\epsilon_0)^{1/(p-1)} b^{p/(p-1)} \tag{2.3.17}$$

For the reduced system (2.3.15), define a Lyapunov function $V(y_i) = (1/2)y_i^2$ over a ball $B(0, r_i)$, for some $r_i > 0$. $\forall y_i \in B(0, r_i)$, one can have

$$\dot{V}(y_i) = -k_i y_i^2 - y_i \phi(y_i) \leq -y_i^2 \tag{2.3.18}$$

Hence the origin of reduced system (2.3.15) is stable in a region $\mathcal{R}_i$ which includes the origin.

The boundary-layer system (2.3.16) is exponentially stable in a region Ω_i which includes the origin as A_{i1} is Hurwitzian. Define a Lyapunov function $W(\eta_i) = \eta_i^{\mathrm{T}} P_{i1} \eta_i$, where $P_{i1} \in \mathbb{R}^{2\times 2}$ is the positive definite solution of the Lyapunov equation $P_{i1} A_{i1} + A_{i1}^{\mathrm{T}} P_{i1} = -I$. This function satisfies

$$\lambda_{\min}(P_{i1}) \|\eta_i\|^2 \leq W(\eta_i) \leq \lambda_{\max}(P_{i1}) \|\eta_i\|^2 \tag{2.3.19}$$

$$\frac{\partial W(\eta_i)}{\partial \eta_i} A_{i1} \eta_i \leq -\|\eta_i\|^2 \tag{2.3.20}$$

$$\|\frac{\partial W(\eta_i)}{\partial \eta_i}\| \leq 2\lambda_{\max}(P_{i1}) \|\eta_i\| \tag{2.3.21}$$

Consider a storage function for the closed-loop system (2.3.14) as follows

$$H(y, \eta, z) = \frac{1}{2} y^{\mathrm{T}} y + \sum_{i=1}^{m} \beta_i W(\eta_i) + W_0(z) \tag{2.3.22}$$

where $\beta_i > 0$ is to be determined. Choose $\xi_i < r_i$, given Assumptions 2.1 and 2.2, for all $(y_i, \eta_i) \in B(0, \xi_i) \times \{\|\eta_i\| \leq \xi_i\} = \Lambda_i$, where $B(\|\eta_i\|, \xi_i) \in \Omega_i$, ξ_i is a positive constant. Moreover, assume

$$|\dot{\Psi}_i(\cdot)| \leq L_{i1} \|y_i\| + L_{i2} \|\eta_i\| \tag{2.3.23}$$

where L_{i1} and L_{i2} are Lipschitz constants.

Differentiate $H(y, \eta, z)$ along system (2.3.14), use inequalities (2.3.18) to (2.3.21),

(2.3.23) and Corollary 2.1, with $p = 2$, $a = \|y_i\|$ and $b = \|\eta_i\|$, yields

$$\begin{aligned}
\dot{H} &= y^{\mathrm{T}}\left(-Ky + \eta_{i2} - \left(\frac{\partial W_0(z)}{\partial z^{\mathrm{T}}}p(y,z)\right)^{\mathrm{T}} + \nu\right) \\
&+ \sum_{i=1}^{m}\beta_i\frac{\partial W(\eta_i)}{\partial \eta_i}\left(\frac{A_{i1}\eta_i}{\epsilon_i} + B_{i1}\dot{\Psi}_i(\cdot)\right) + \frac{\partial W_0(z)}{\partial z^{\mathrm{T}}}(f_0(z) + p(y,z)y) \\
&\leq \sum_{i=1}^{m}\Big(-k_i\|y_i\|^2 - \frac{\beta_i}{\epsilon_i}\|\eta_i\|^2 + 2\beta_i L_{i2}\|P_{i1}\|\|\eta_i\|^2 + (1 + 2\beta_i L_{i1}\|P_{i1}\|)\|y_i\|\|\eta_i\|\Big) \\
&+ \frac{\partial W_0(z)}{\partial z^{\mathrm{T}}}f_0(z) + \nu^{\mathrm{T}}y \\
&\leq \sum_{i=1}^{m}\Big(-\|y_i\|^2 - \frac{\beta_i}{\epsilon_i}\|\eta_i\|^2 + 2\beta_i L_{i2}\|P_{i1}\|\|\eta_i\|^2 + (1 + 2\beta_i L_{i1}\|P_{i1}\|) \\
&\times (\frac{1}{\epsilon_{i0}}\|y_i\|^2 + \epsilon_{i0}\|\eta_i\|^2)\Big) + \nu^{\mathrm{T}}y \\
&\leq \sum_{i=1}^{m}\Big(-\frac{1}{2}\|y_i\|^2 - \frac{\beta_i}{2\epsilon_i}\|\eta_i\|^2 - b_{i1}\|y_i\|^2 - b_{i2}\|\eta_i\|^2\Big) + \nu^{\mathrm{T}}y
\end{aligned} \tag{2.3.24}$$

where $\epsilon_{i0} > 0$, and

$$b_{i1} = \frac{1}{2} - \frac{2}{\epsilon_{i0}}(\frac{1}{2} + \beta_i L_{i1}\|P_{i1}\|) \tag{2.3.25}$$

$$b_{i2} = \frac{\beta_i}{2\epsilon_i} - 2\beta_i(\epsilon_{i0}L_{i1} + L_{i2})\|P_{i1}\| - \epsilon_{i0} \tag{2.3.26}$$

Now choose β_i small enough and $\epsilon_{i0} \geq \epsilon_{i0}^* = 2 + 4\beta_i L_{i1}\|P_{i1}\|$ such that $b_{i1} > 0$, and then choose $\epsilon_{i1}^* = \beta_i/(\epsilon_{i0}^{*2} + 4\beta_i L_{i2}\|P_{i1}\|)$, $\forall \epsilon_i, \epsilon_i \leq \epsilon_{i1}^*$, and choose an additional input $\omega^{\mathrm{T}} = -\phi(y)$, where $\phi(y)$ is a sector-nonlinearity defined by (A.0.11). It can be shown that

$$\dot{H} \leq \nu^{\mathrm{T}}y - \sum_{i=1}^{m}\big(\min(1/2, \beta_i/(2\epsilon_i))(\|y_i\|^2 + \|\eta_i\|^2)\big) \leq \nu^{\mathrm{T}}y \leq -\phi(y)y \leq 0 \tag{2.3.27}$$

Hence one can conclude that the closed-loop system (2.3.14) is output strictly passive and the origin is stable. □

Controller (2.3.11) does not require an accurate system model which structure is illustrated in Fig. 2.1. The nominal plant is disturbed by the perturbation, the adaptive feedback passivation law u can be separated as $u = B_0^{-1}(u_1 + u_2 + u_3 + u_4)$,

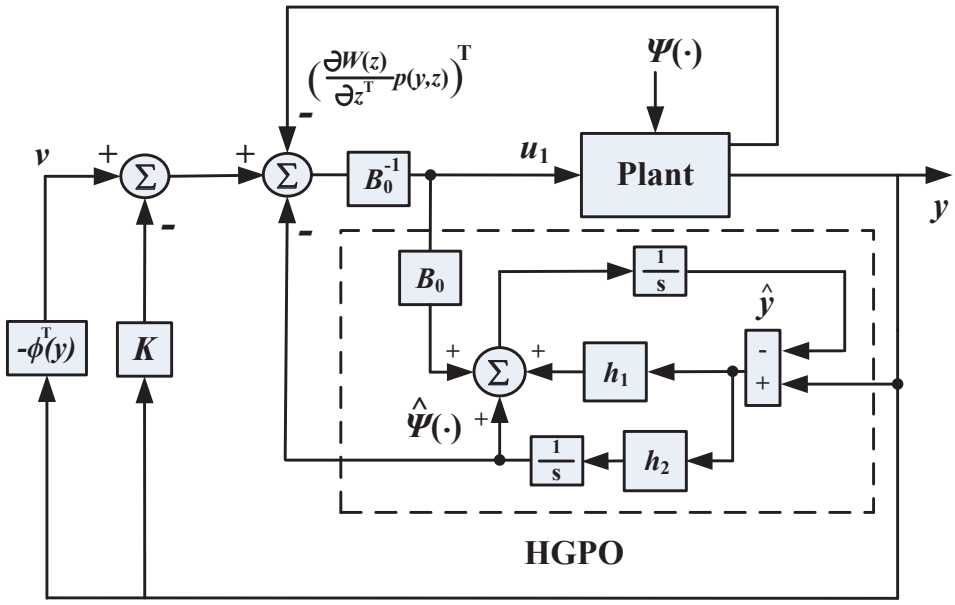

Figure 2.1: Structure of the POAPC

where $u_1 = -\hat{\Psi}(\cdot)$ is the distinctive adaption mechanism based on fast nonlinearly functional estimations, which provides significant robustness for lumped system uncertainties; $u_2 = -Ky$ is the output feedback; $u_3 = \left(\frac{\partial W_0(z)}{\partial z^{\mathrm{T}}}p(y,z)\right)^{\mathrm{T}}$ compensates the internal dynamics and reshapes the changes of stored energy; and $u_4 = \omega$ helps to construct a passive system by introducing an additional input with the form of a sector-nonlinearity $\phi(y)$.

Remark 2.3. It should be mentioned that during the design procedure, ϵ_i is only required to be some relatively small positive constant and the PO's performance is not sensitive to the observer gain, as it is determined based on the bound of the perturbation estimation error. Moreover, the bound of estimates used in the PO can be obtained through the analysis of the system within a predetermined range of variation in system variables.

Remark 2.4. Note that for the closed-loop system (2.3.14), control gain K should be designed to suppress the perturbation estimation error $\tilde{\Psi}_i(\cdot)$. Compared to the approach without perturbation compensation, in which K should be chosen to suppress the perturbation $\Psi_i(\cdot)$. As $|\tilde{\Psi}_i(\cdot)|$ is usually smaller than $|\Psi_i(\cdot)|$, a relatively

small K could be resulted in due to the compensation of perturbation by POAPC.

Remark 2.5. The PO can be regarded as a nonlinearly functional estimation method, contrast to the linearly parametric estimation based adaptive passive approaches. It can deal with the fast varying unmodelled dynamics and time-varying external disturbances. If there does not exist parameter uncertainties and time-varying external disturbances, and if the accurate system model is available, it can provide the same performance as the exact passive controller. Otherwise, it will perform much better than the exact passive controller. The use of the PO results in a less concern of measurements and identification of the fast varying unmodelled dynamics and time-varying external disturbances. This tends to require less control efforts as the perturbation has already included all of this information. It can also avoid the issues of control parameter initialization, learning coefficient optimization, and slow system response to the parameter uncertainties existed in the conventional APC.

Remark 2.6. The adaptive tracking can be easily achieved by choosing the tracking error $e = y - y_{\rm d}$ as the output, where $y_{\rm d}$ is the reference signal. Note that, in this case, the zero-dynamics must be locally bounded reference weakly minimum-phase, i.e., $\frac{\partial W_0(z)}{\partial z^{\rm T}} f_0(y_{\rm d}, z) \leq 0$.

To this end, the POAPC design procedure for system (2.2.1) can be summarized as follows:

Step 1: Define perturbation (2.2.3) for the original system (2.2.1);

Step 2: Define a fictitious state $y_{ei} = \Psi_i(\cdot)$ to represent perturbation (2.2.3);

Step 3: Extend the original system (2.2.1) into the extended system (2.2.4);

Step 4: Design the second-order HGPO (2.2.7) for the extended system (2.2.4) to obtain the state estimate $\hat{y}_i$ and the perturbation estimate $\hat{\Psi}_i(\cdot)$ by only the measurement of y_i;

Step 5: Design controller (2.3.11) for the original system (2.2.1).

2.4 Case Studies

This section will illustrate various features of the proposed POAPC and show its advantages over the existing results. In the first example, the control performance of the nonlinearly functional estimation based POAPC is compared with that of the linearly parametric estimation based adaptive passive control (APC) for a magnetic levitator system. In the second example, POAPC is applied on an interconnected inverted pendulum system to verify its robustness against passive control (PC) in the presence of unmodelled dynamics.

2.4.1 Magnetic levitator system

Consider a single-input single-output (SISO) magnetic levitator system used in [85], which is illustrated in Fig. 2.2. The levitation object is a ping-pong ball with a small permanent magnetic attached to it, by which an attraction force could be induced. The attraction force is generated by the electromagnet and controlled by an amplifier circuit. The height of the ball is determined by a photo emitter-detector. The system dynamics is presented in the following second-order differential equation

$$m\ddot{d} = F_{\mathrm{c}} - mg + \zeta \tag{2.4.1}$$

where m is the mass of the ball, d is the distance of the ball from the reference line, g is the standard gravity and F_{c} is the magnetic control force, ζ includes the parameter uncertainties and unmodelled dynamics.

The magnetic force characteristics is described as a function of voltage applied to the amplifier circuit and height of the ball, leading to the expression

$$F_{\mathrm{c}} = V_{\mathrm{c}}\hat{b}(d) = V_{\mathrm{c}}\frac{1}{a_1 d^2 + a_2 d + a_3} \tag{2.4.2}$$

where V_{c} is the input control voltage applied to the amplifier, and $\hat{b}(d) = 1/(a_1 d^2 + a_2 d + a_3)$. a_1, a_2 and a_3 are real constant coefficients.

The equilibrium points d_0 and $\dot{d}_0$ of system (2.4.1) without disturbances for a given nominal command voltage V_{c0} are obtained as

$$d_0 = \frac{-a_2 \pm \sqrt{a_2^2 - 4a_1(a_3 - V_{\mathrm{c0}}/mg)}}{2a_1}, \quad \dot{d}_0 = 0 \tag{2.4.3}$$

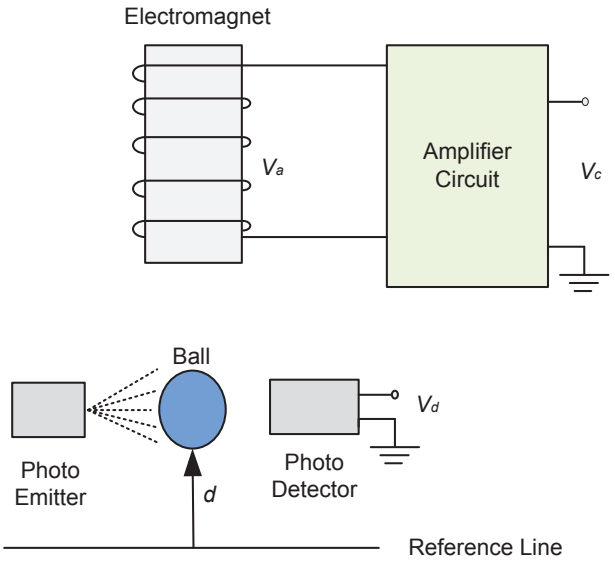

Figure 2.2: The magnetic levitator system.

Define the output $y = \dot{d} - \dot{d}_0$ and internal dynamics $z = d - d_0$, together with the control input $u = V_{\rm c} - V_{\rm c0}$. In addition, define the perturbation as follows

$$\Psi(\cdot) = \frac{\hat{b}(z)V_{\rm c0}}{m} - g + (\frac{\hat{b}(z)}{m} - b_0)u + \zeta \tag{2.4.4}$$

System (2.4.1) can be obtained as

$$\begin{cases} \dot{y} = \Psi(\cdot) + b_0 u \\ \dot{z} = f_0(z) + p(y,z)y \end{cases} \tag{2.4.5}$$

where

$$b_0 = \frac{9}{10ma_3}, \qquad f_0(z) = 0, \qquad p(y,z) = 1. \tag{2.4.6}$$

A second-order HGPO is designed to estimate the perturbation by only the measurement of y as

$$\begin{cases} \dot{\hat{y}} = \hat{\Psi}(\cdot) + h_1(y - \hat{y}) + b_0 u \\ \dot{\hat{\Psi}}(\cdot) = h_2(y - \hat{y}) \end{cases} \tag{2.4.7}$$

where h_1 and h_2 are the observer gains. During the most severe disturbance, the voltage of the amplifier circuit will reduce from its initial value to around zero within a short period of time, Δ. Thus the boundary values of the perturbation can be

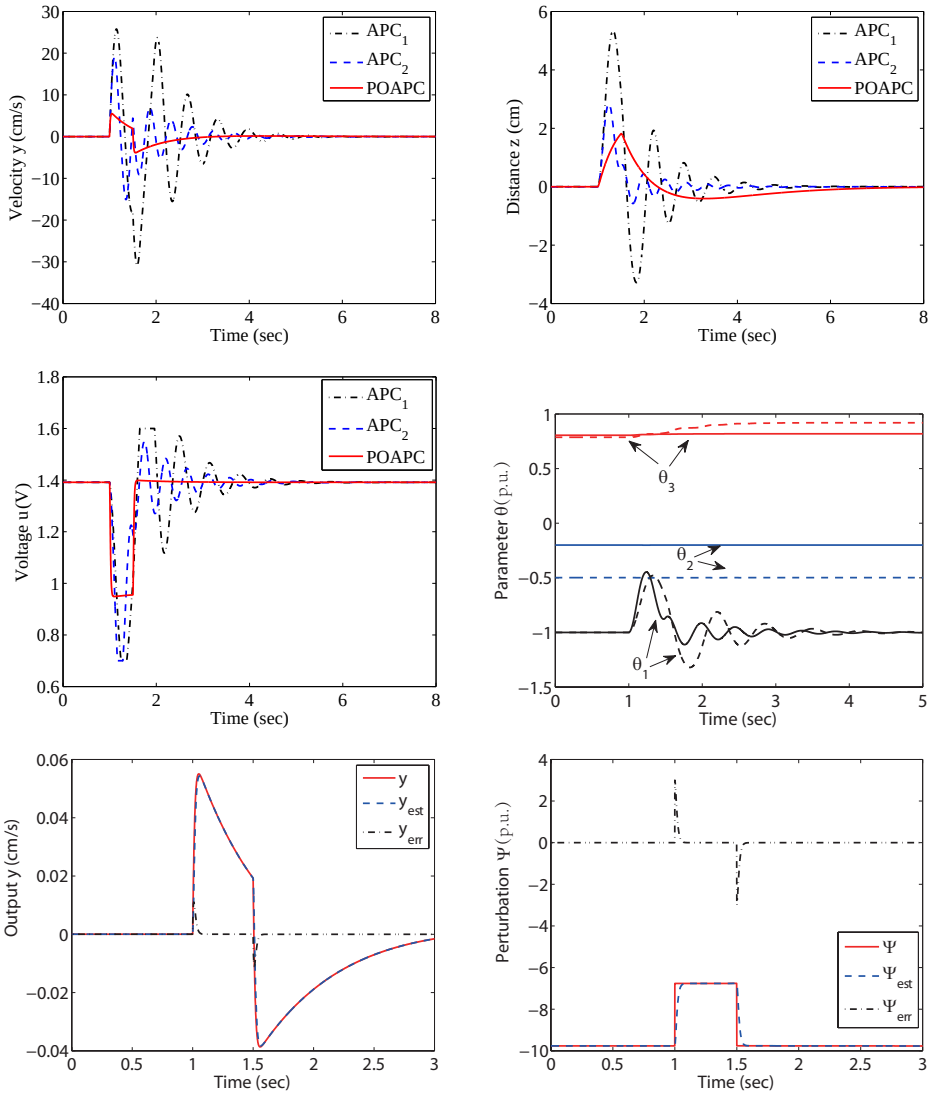

Figure 2.3: System responses obtained under the nominal model.

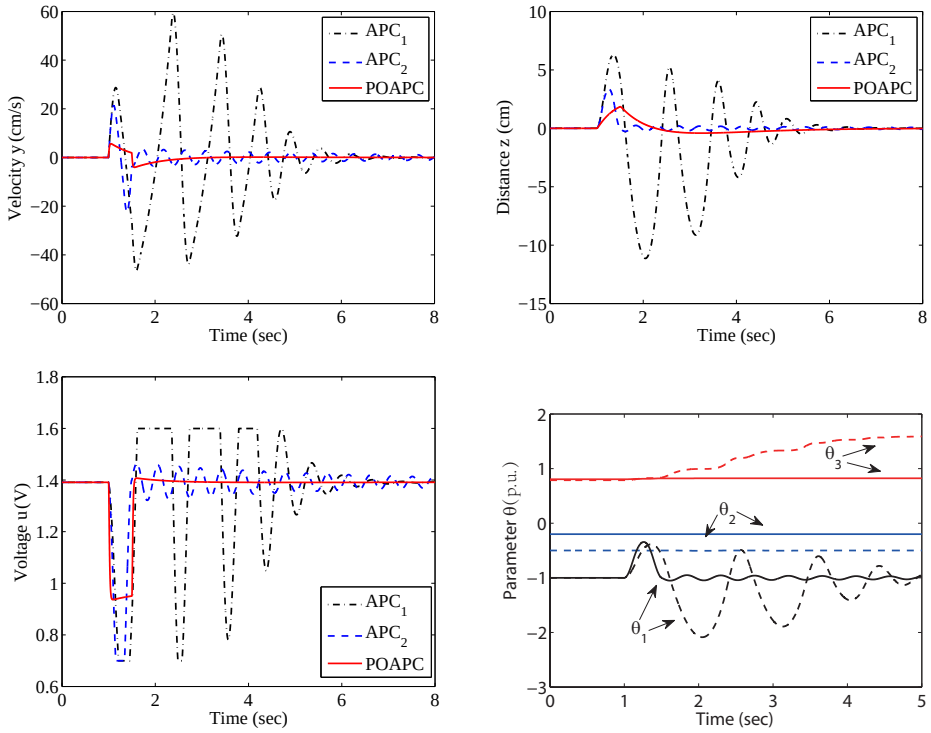

Figure 2.4: System responses obtained under the unmodelled dynamics.

obtained as

$$|\hat{\Psi}(\cdot)| \leq (\frac{\hat{b}(z)V_{\text{c0}}}{m} - g + \max|\zeta|) \tag{2.4.8}$$

$$|\dot{\hat{\Psi}}(\cdot)| \leq (\frac{\hat{b}(z)V_{\text{c0}}}{m} - g + \max|\zeta|)/\Delta \tag{2.4.9}$$

The POAPC is designed as

$$\begin{cases} u = b_0^{-1}(-\hat{\Psi}(\cdot) - Ky - z + \omega) \\ \omega^{\text{T}} = -Dy \end{cases} \tag{2.4.10}$$

where a linear damping function $\phi(y) = Dy$, $D > 0$, is chosen to construct a passive system. The zero-dynamics of system are described by $\dot{z} = 0$ which are Lyapunov stable. Choose $H(y, \eta, z) = (1/2)y^2 + \beta W(\eta) + W_0(z)$ with $W_0(z) = (1/2)z^2$, it is easy to find that the output y and state z are locally zero-state detectable.

The conventional APC used in [85] is

$$\begin{cases} u = (m/\hat{b}(d))\Theta^{\text{T}} u_{\text{p}} \\ \dot{\Theta} = -\Lambda y u_{\text{p}} \end{cases} \tag{2.4.11}$$

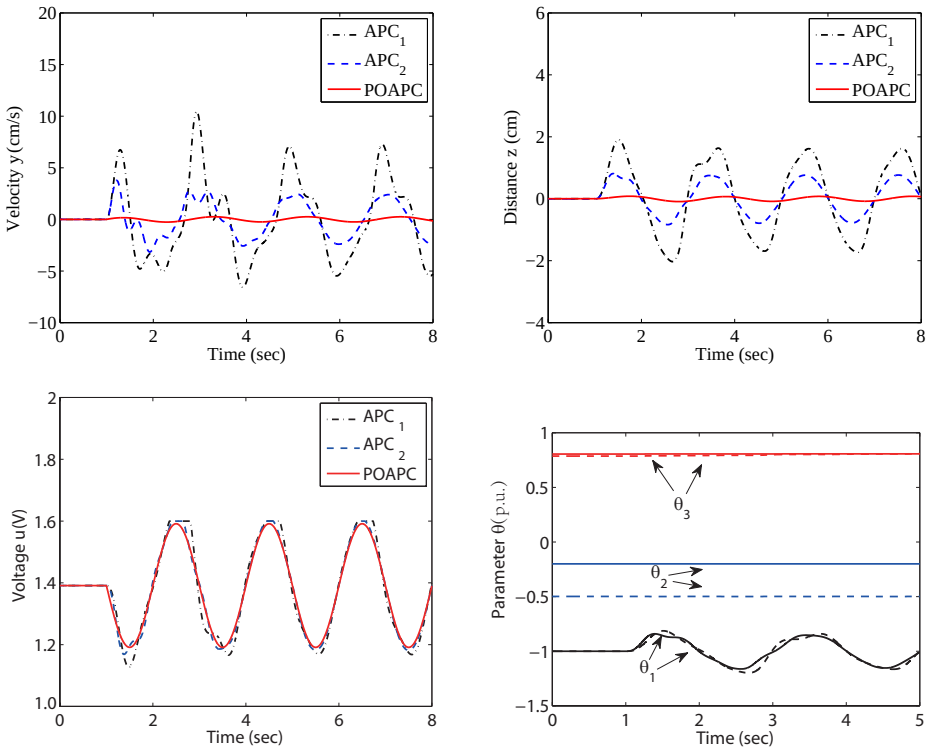

Figure 2.5: System responses obtained under the time-varying external disturbance.

where $\Theta = [\theta_1, \theta_2, \theta_3]^{\mathrm{T}}$ and $u_{\mathrm{p}} = [\omega_1, z, \omega_2]^{\mathrm{T}}$, $\omega_1 = \hat{b}(d)V_{\mathrm{c0}}/m - g$, $\omega_2 = -\beta y$ with $\beta = 2.9$, $\Lambda = \mathrm{diag}[\lambda_1, \lambda_2, \lambda_3]$ is the learning coefficient. Two sets of control parameters are used, i.e., APC_1: $\Lambda_1 = [-1, -1, -1]^{\mathrm{T}}$, $\Theta_1(0) = [-1, -0.5, 0.8]^{\mathrm{T}}$ (dashed line) and APC_2: $\Lambda_2 = [-2, -1.5, -0.5]^{\mathrm{T}}$, $\Theta_2(0) = [-1, -0.2, 0.8]^{\mathrm{T}}$ (solid line). Observer (2.4.7) parameters are chosen as $h_1 = 300$, $h_2 = 22500$, and $\Delta = 0.05$ s. Controller (2.4.10) parameters are selected as $K = 1.5$ and $D = 0.5$.

The parameters for the plant are as follows [85]: $m = 2.206$ g, $a_1 = 0.0231$ mg, $a_2 = -2.4455$ mg, $a_3 = 64.58$ mg, and $g = 9.8$ m/s^2, $V_{\mathrm{c0}} = 4.87$ V. While control input is bounded as 0 V$\leq u \leq$ 1.6 V.

Fig. 2.3 shows the system responses obtained when an equivalent 3 N force applied at $t = 1$ s and removed at $t = 1.5$ s under the nominal model. One can find that APC consumes longer time for control parameter learning and requires larger control efforts, its control performance is sensitive to control parameters which can only be optimized locally at a particular operating point. In contrast, POAPC can

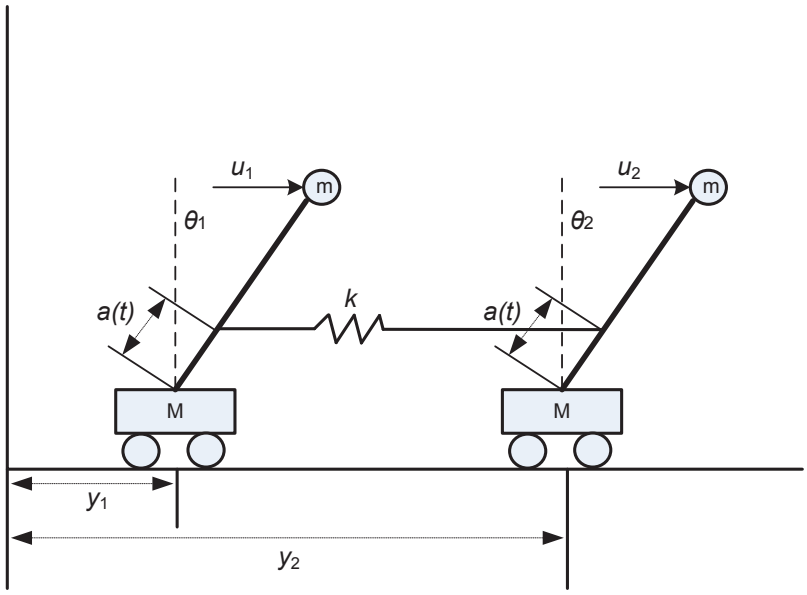

Figure 2.6: Two inverted pendulums on two carts.

effectively stabilize the disturbed system with less control efforts as the system nonlinearities are globally removed. Moreover, a fast tracking of the state and perturbation can be obtained by the observer, the relatively large estimation error at the instant of $t = 1$ s and $t = 1.5$ s is due to the discontinuity when the magnetic control force F_c is applied and removed.

System responses obtained under an unmodelled dynamics $\zeta = 1.5\sin(y)$ are given by Fig. 2.4. It shows that POAPC can maintain satisfactory control performance as the unmodelled dynamics can be estimated and compensated online. In contrast, APC control performance degrades dramatically with a destabilizing effect as the system uncertainty is not in the assumed linearly parametric form. Fig. 2.5 illustrates the system responses obtained when a time-varying external disturbance $\zeta = 1.4\sin(\pi t)$ occurs, in which POAPC can rapidly attenuate the disturbance thus provide significant robustness. In contrast, APC cannot find the optimal control parameters which results in an unsuppressed time-varying oscillation.

2.4.2 Interconnected inverted pendulum system

Consider a multi-input multi-output (MIMO) system composed of two inverted pendulums on two carts, interconnected by a moving spring [168], which is shown in Fig. 2.6. Assume that the pivot position of the moving spring is a function of time and it can change along the full length of the pendulums. In this example the motion of the carts is specified as a sinusoidal trajectory. The input to each pendulum is the torque u_i, $i = 1, 2$, applied to the pivot point. It is desired to control each pendulum with mass independently, so that each pendulum tracks its own desired reference trajectory while the connected spring and carts are moving. The system dynamics can be described as

$$\begin{cases} \dot{\theta}_1 &= \omega_1 \\ \dot{\omega}_1 &= \left(\frac{g}{cl} - \frac{ka(t)(a(t)-cl)}{cml^2}\right)\theta_1 + \frac{ka(t)(a(t)-cl)}{cml^2}\theta_2 - \beta_1\omega_1^2 - \frac{k(a(t)-cl)}{cml^2}(s_1(t) - s_2(t)) \\ &\quad + \frac{u_1}{cml^2} + \zeta_1 \\ \dot{\theta}_2 &= \omega_2 \\ \dot{\omega}_2 &= \left(\frac{g}{cl} - \frac{ka(t)(a(t)-cl)}{cml^2}\right)\theta_2 + \frac{ka(t)(a(t)-cl)}{cml^2}\theta_1 - \beta_2\omega_2^2 - \frac{k(a(t)-cl)}{cml^2}(s_2(t) - s_1(t)) \\ &\quad + \frac{u_2}{cml^2} + \zeta_2 \end{cases} \tag{2.4.12}$$

where $\beta_1 = (m/M)\sin\theta_1$, $\beta_2 = (m/M)\sin\theta_2$, l is the length of the pendulum, $c = m/(M+m)$, k and g are the spring and gravity constants, respectively. The definition of the symbols can be referred to [95]. Choose $g = l = k = 1$, $m = M = 10$, then $c = 0.5$. $s_1(t) = \sin(2t)$ and $s_2(t) = L + \sin(3t)$, L is the natural length of the spring. $L = 2$, $a = \sin(5t)$, the input to each pendulum is the torque $|u_i| \leq 50$. ζ_1 and ζ_2 are the unmodelled dynamics.

Define the output $y = [\omega_1, \omega_2]^{\mathrm{T}}$ and internal dynamics $z = [\theta_1, \theta_2]^{\mathrm{T}}$, together with the control input $u = [u_1, u_2]^{\mathrm{T}}$. The desired trajectories are chosen as $\theta_{\mathrm{r}1} = \sin(2t)$ and $\theta_{\mathrm{r}2} = \sin(t)$. System initial states are $z(0) = [1, -1]^{\mathrm{T}}$ and $y(0) =$

$[0,0]^{\mathrm{T}}$. Define the perturbation as follows

$$\Psi(\cdot) = \begin{bmatrix} \left(\frac{g}{cl} - \frac{ka(t)(a(t)-cl)}{cml^2}\right) z_1 + \frac{ka(t)(a(t)-cl)}{cml^2} z_2 - \beta_1 y_1^2 - \frac{k(a(t)-cl)}{cml^2}(s_1(t) - s_2(t)) + \zeta_1 \\ \left(\frac{g}{cl} - \frac{ka(t)(a(t)-cl)}{cml^2}\right) z_2 + \frac{ka(t)(a(t)-cl)}{cml^2} z_1 - \beta_2 y_2^2 - \frac{k(a(t)-cl)}{cml^2}(s_2(t) - s_1(t)) + \zeta_2 \end{bmatrix} \tag{2.4.13}$$

System (2.4.12) can be rewritten as

$$\begin{cases} \dot{y} = \Psi(\cdot) + B_0 u \\ \dot{z} = f_0(z) + p(y,z) y \end{cases} \tag{2.4.14}$$

where

$$B_0 = \begin{bmatrix} b_{10} & 0 \\ 0 & b_{20} \end{bmatrix}, \quad f_0(z) = \begin{bmatrix} 0 \\ 0 \end{bmatrix}, \quad p(y,z) = \begin{bmatrix} 1 & 0 \\ 0 & 1 \end{bmatrix}. \tag{2.4.15}$$

During the most severe disturbance, both the angle and angular speed of the pendulum will reduce from their initial values to around zero within a short period of time, Δ. Thus the boundary values of the perturbation can be obtained as

$$\begin{aligned} |\hat{\Psi}_1(\cdot)| &= |(2 - 0.2\sin(5t)(\sin(5t) - 0.5))z_1 + 0.2\sin(5t)(\sin(5t) - 0.5)z_2 \\ &\quad - \sin(z_1)y_1^2 - 0.2(\sin(5t) - 0.5)(\sin(2t) - \sin(3t) - 2) + \zeta_1| \\ &\leq 2.1|z_1| + 0.3|z_2| + y_1^2 + 1.2 + \max|\zeta_1| \end{aligned} \tag{2.4.16}$$

$$|\dot{\hat{\Psi}}_1(\cdot)| \leq (2.1|z_1| + 0.3|z_2| + y_1^2 + 1.2 + \max|\zeta_1|)/\Delta \tag{2.4.17}$$

$$\begin{aligned} |\hat{\Psi}_2(\cdot)| &= |(2 - 0.2\sin(5t)(\sin(5t) - 0.5))z_2 + 0.2\sin(5t)(\sin(5t) - 0.5)z_1 \\ &\quad - \sin(z_2)y_2^2 - 0.2(\sin(5t) - 0.5)(2 + \sin(3t) - \sin(2t)) + \zeta_2| \\ &\leq 2.1|z_2| + 0.3|z_1| + y_2^2 + 1.2 + \max|\zeta_2| \end{aligned} \tag{2.4.18}$$

$$|\dot{\hat{\Psi}}_2(\cdot)| \leq (2.1|z_2| + 0.3|z_1| + y_2^2 + 1.2 + \max|\zeta_2|)/\Delta \tag{2.4.19}$$

Two identical second-order HGPOs are designed to estimate the perturbation by only the measurement of y_i as follows

$$\begin{cases} \dot{\hat{y}}_i = \hat{\Psi}_i(\cdot) + h_{i1}(y_i - \hat{y}_i) + b_{i0}u_i \\ \dot{\hat{\Psi}}_i(\cdot) = h_{i2}(y_i - \hat{y}_i) \end{cases} \quad i = 1, 2. \tag{2.4.20}$$

The POAPC is designed as

$$\begin{cases} u = B_0^{-1}(-\hat{\Psi}(\cdot) - Ky - z + \omega) \\ \omega^{\mathrm{T}} = -Dy \end{cases} \tag{2.4.21}$$

HGPOs (2.4.20) parameters are chosen as $h_{i1} = 200$, $h_{i2} = 10000$, $b_{i0} = \frac{1}{cml^2} = 0.2$. Controller (2.4.21) parameters are chosen as follows

$$K = \begin{bmatrix} 1 & 1 \\ 1 & 1 \end{bmatrix}, \quad D = \begin{bmatrix} 3 & 0 \\ 0 & 3 \end{bmatrix} \tag{2.4.22}$$

In order to verify the effectiveness of POAPC, PC is used which assumes the accurate system model is completely known for comparison. Fig. 2.7 gives the tracking performance of PC and POAPC obtained under the nominal model, one can find that POAPC can achieve as satisfactory tracking performance as that of PC, their tiny differences are resulted from the estimation error. Fig. 2.8 demonstrates that POAPC can perform much better in the presence of the unmodelled dynamics ($\zeta_1 = 5\sin(\omega_1)$ and $\zeta_2 = 5\cos(\omega_2)$), as the real-time estimate of perturbation is used to compensate the perturbation. Hence, it provides a significant robustness in the presence of unmodelled dynamics with only one state measurement.

2.5 Conclusion

A nonlinearly functional estimation based POAPC approach has been developed for the normal passive system in this chapter, which does not require an accurate system model. It can effectively resolve the weakness of conventional APC or RPC design occurred in the presence of parameter uncertainties, unmodelled dynamics, and time-varying external disturbances. A proposition is given at first, which shows that for any given constant δ_{po_i}, from the initial estimation error $\tilde{y}_{\mathrm{po}_i}(0)$, the estimation error will exponentially converge into the neighbourhood $\|\tilde{y}_{\mathrm{po}_i}(t)\| \leq \delta_{\mathrm{po}_i}$. Then a theorem has been proved by the Lyapunov criterion, which shows that there exists ϵ_{i1}^*, with $i = 1, \ldots, m$, $\epsilon_{i1}^* > 0$ such that, $\forall \epsilon_i, 0 < \epsilon_i < \epsilon_{i1}^*$, the closed-loop system is output strictly passive and the origin is stable. Two case studies have been

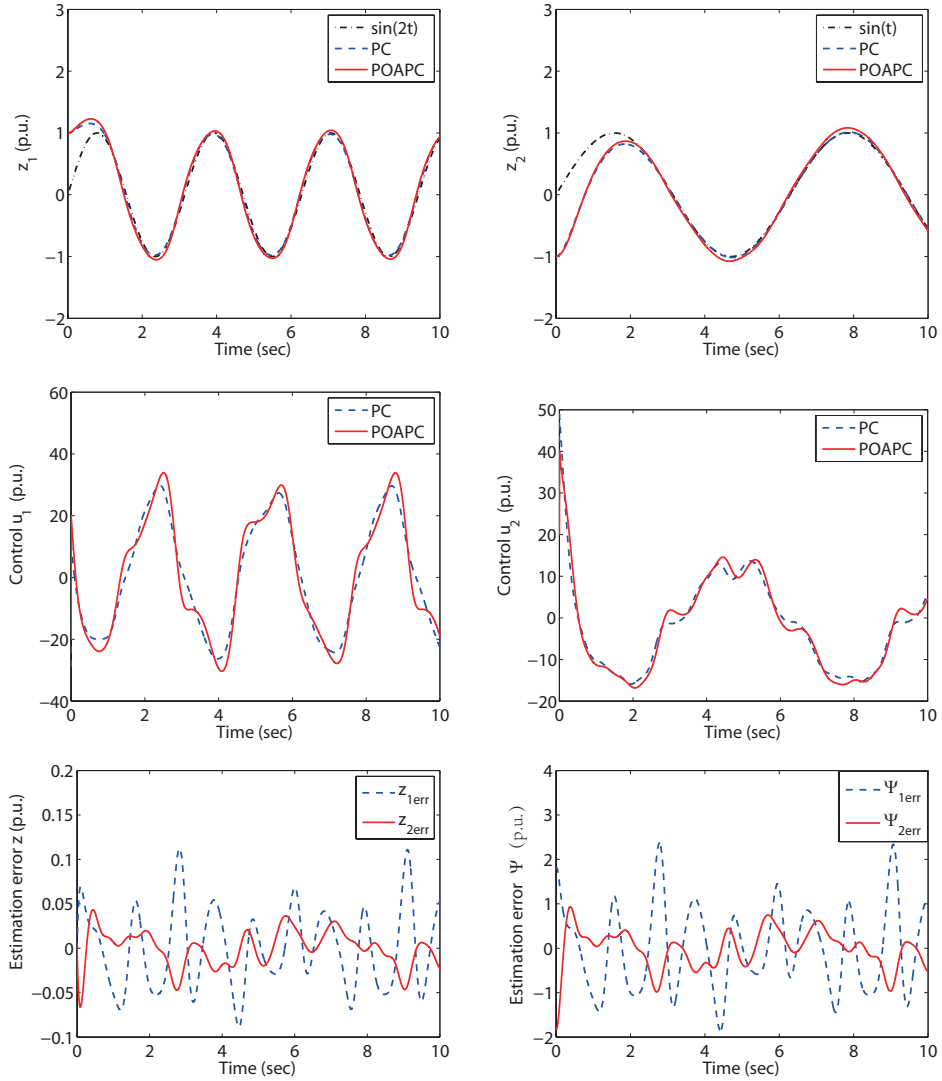

Figure 2.7: System responses obtained under the nominal model.

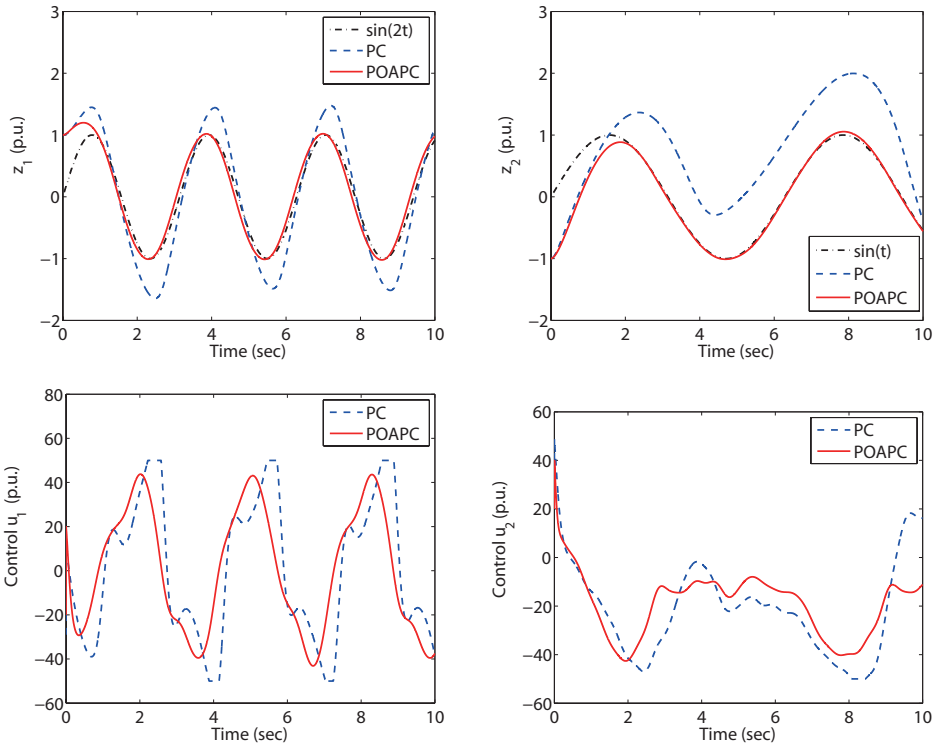

Figure 2.8: System responses obtained under the unmodelled dynamics.

carried out, the simulation results verify that POAPC can provide significant robustness without the requirement of further assumptions/conditions made on system, and also achieve as satisfactory control performance as that of PC when an accurate system model is available.

Chapter 3

Perturbation Observer based Adaptive Passive Control for Two-terminal VSC-HVDC Systems

3.1 Introduction

The past three decades have witnessed a significant development in HVDC electrical power transmission systems, which are continuously innovated by utilizing state-of-the-art power electronic devices [8, 9]. Currently, most of these transmission systems are based on CSC utilizing thyristor technology [14]. The shortcoming of this transmission technology is that the thyristor valve cannot be turned off with gate signal directly, which limits the range of its application [169].

Recently, rapid advancement is achieved in the field of power electronic devices which can not only switch on but also switch off immediately, such as IGBT [6]. This motivates the development of VSC-HVDC systems using IGBT technology. The principal characteristics of VSC-HVDC systems are that they do not need any external voltage source for commutation, and they can independently control active and reactive power at each AC grid and supply to a passive network. The reverse of the power flow can be easily implemented by reversing the direction of DC current without changing the polarity of DC voltage [4]. These features make the VSC-

HVDC systems attractive for connection of weak AC systems, island networks, and renewable sources to the main power grid [19, 20, 21, 31].

Recently, rigorous tests have been employed in order to validate advanced controllers' performance for the VSC-HVDC system before their implementation in real systems, such as special software which adopted a mathematically exact equivalent system model, and can drastically reduce the computational time without sacrificing any accuracy [133], real-time digital simulator (RTDS) which can operate in the real-time for fast, reliable, accurate and cost-effective study of modular multilevel converter (MMC)-based HVDC systems [134]. Moreover, an HIL simulation was carried out to emulate the behaviour of the PI controller in VSC-HVDC systems using a low power and safe hardware [135]. Hardware experiments based on a small test system have been undertaken in [136, 27] to evaluate the control performance of VSC-MTDC systems for offshore wind farms consisting of doubly-fed induction generators (DFIGs) or permanent-magnetic synchronous generators (PMSGs).

This chapter extends POAPC into general canonical systems, which is then applied for the two-terminal VSC-HVDC system. Based on the functional perturbation estimation using an HGPO, it only requires the measurement of active and reactive power and DC voltage, while no accurate system model is required. The control performance of POAPC is firstly evaluated by the simulation, in which the active and reactive power tracking, AC grid voltage drop and robustness to parameter uncertainties are carried out. Then the hardware experiment is undertaken, in which the rectifier controller and inverter controller are implemented and tested separately.

3.2 Problem Formulation

Consider an SISO system as

$$\begin{cases} \dot{x} = Ax + B(a(x) + b(x)u + \xi(t)) \\ y = x_n \end{cases} \tag{3.2.1}$$

where $y \in \mathbb{R}$ is the output and $u \in \mathbb{R}$ is the control input; $x = [x_1, x_2, \cdots, x_n]^{\mathrm{T}} \in \mathbb{R}^n$ is the state vector; $a(x) : \mathbb{R}^n \mapsto \mathbb{R}$ and $b(x) : \mathbb{R}^n \mapsto \mathbb{R}$ are C^∞ unknown smooth

functions; $\xi(t) \in \mathbb{R}$ is the time-varying external disturbance; Matrices A and B are given by

$$A = \begin{bmatrix} 0 & 1 & 0 & \cdots & 0 \\ 0 & 0 & 1 & \cdots & 0 \\ \vdots & \vdots & \vdots & \ddots & \vdots \\ 0 & 0 & 0 & \cdots & 1 \\ 0 & 0 & 0 & \cdots & 0 \end{bmatrix}_{n\times n}, \quad B = \begin{bmatrix} 0 \\ 0 \\ \vdots \\ 0 \\ 1 \end{bmatrix}_{n\times 1} \tag{3.2.2}$$

The perturbation of system (3.2.1) is defined as

$$\Psi(x, u, t) = a(x) + (b(x) - b_0)u + \xi(t) \tag{3.2.3}$$

where b_0 is the constant control gain.

Define a fictitious state to represent the perturbation, that is, $x_{n+1} = \Psi(\cdot)$. System (3.2.1) can be rewritten into

$$\dot{x}_{\mathrm{e}} = A_0 x_{\mathrm{e}} + B_1 u + B_2 \dot{\Psi}(\cdot) \tag{3.2.4}$$

where $x_{\mathrm{e}} = [x_1, x_2, \cdots, x_n, x_{n+1}]^{\mathrm{T}} \in \mathbb{R}^{n+1}$. $B_1 = [0, 0, \ldots, b_0, 0]^{\mathrm{T}} \in \mathbb{R}^{n+1}$ and $B_2 = [0, 0, \ldots, 1]^{\mathrm{T}} \in \mathbb{R}^{n+1}$. Matrix A_0 is

$$A_0 = \begin{bmatrix} 0 & 1 & \cdots & \cdots & 0 \\ 0 & 0 & 1 & \cdots & 0 \\ \vdots & \vdots & \vdots & \ddots & \vdots \\ 0 & 0 & 0 & \cdots & 1 \\ 0 & 0 & 0 & \cdots & 0 \end{bmatrix}_{(n+1)\times(n+1)} \tag{3.2.5}$$

An $(n+1)$th-order HGSPO is used to estimate $\hat{x}_{\mathrm{e}}$ for system (3.2.4) as

$$\dot{\hat{x}}_{\mathrm{e}} = A_0 \hat{x}_{\mathrm{e}} + B_1 u + H(x_1 - \hat{x}_1) \tag{3.2.6}$$

where $H = [\alpha_1/\epsilon, \alpha_2/\epsilon^2, \cdots, \alpha_n/\epsilon^n, \alpha_{n+1}/\epsilon^{n+1}]^{\mathrm{T}}$ is the observer gain with $0 < \epsilon \ll 1$, $\alpha_i = C_{n+1}^i \lambda^i$ such that the pole of HGSPO (3.2.6) can be placed at $-\lambda$, where $i = 1, 2, \cdots, n+1$ and $\lambda > 0$.

The following assumptions are made on system (3.2.4).

Assumption 3.1. b_0 is chosen to satisfy:

$$0 < |b(x)/b_0 - 1| \leq \theta \tag{3.2.7}$$

where $\theta < 1$ is a positive constant.

Assumption 3.2. The function $\Psi(x, u, t) : \mathbb{R}^n \times \mathbb{R} \times \mathbb{R}^+ \mapsto \mathbb{R}$ and $\dot{\Psi}(x, u, t) : \mathbb{R}^n \times \mathbb{R} \times \mathbb{R}^+ \mapsto \mathbb{R}$ are locally Lipschitz in their arguments over the domain of interest and are globally bounded:

$$|\Psi(x, u, t)| \leq \gamma_1, \quad |\dot{\Psi}(x, u, t)| \leq \gamma_2 \tag{3.2.8}$$

where γ_1 and γ_2 are positive constants. In addition, $\Psi(0, 0, 0) = 0$ and $\dot{\Psi}(0, 0, 0) = 0$, such that the origin is an equilibrium point of the open-loop system.

Use the estimate of perturbation, we design POAPC for system (3.2.1) as

$$\begin{cases} u = b_0^{-1}\left(-\hat{\Psi}(\cdot) - K\hat{x} + \nu\right) \\ \nu = -\phi(y) \end{cases} \tag{3.2.9}$$

where ν is the additional input; ϕ is any smooth function such that $\phi(0) = 0$ and $y\phi(y) > 0$ for all $y \neq 0$; $K = [k_1, k_2, \cdots, k_n]$ is the feedback control gain, and choose $k_j = C_n^j \xi^j$ to place the pole of equivalent linear system of (3.2.1) at $-\xi$, where $j = 1, \cdots, n$ and $\xi > 0$, which makes matrix $A_1 = A - BK$ Hurwitzian.

Define the scaled estimation error as $\eta = [\eta_1, \eta_2, \cdots, \eta_{n+1}]^{\mathrm{T}}$, where $\eta_i = \tilde{x}_i/\epsilon^{n+1-i}$, and $D(\epsilon) = \mathrm{diag}[\epsilon^n, \cdots, 1]_{(n+1)\times(n+1)}$. It gives $\hat{x} = x - D'(\epsilon)\eta'$, $\hat{x}_{n+1} = x_{n+1} - \eta_{n+1}$, where $D'(\epsilon) = \mathrm{diag}[\epsilon^n, \cdots, \epsilon]_{n\times n}$ and $\eta' = [\eta_1, \eta_2, \cdots, \eta_n]^{\mathrm{T}}$. Control (3.2.9) can be represented as

$$u = \frac{1}{b_0}(-x_{n+1} - Kx + K_1 D(\epsilon)\eta + \nu) \tag{3.2.10}$$

where $K_1 = [K, 1]$.

Apply control (3.2.10) to system (3.2.1), the closed-loop system can be represented by

$$\dot{x} = A_1 x + BK_1 D(\epsilon)\eta + V \tag{3.2.11}$$

$$\epsilon\dot{\eta} = A_{10}\eta + \epsilon B_1 \dot{\Psi}(\cdot) \tag{3.2.12}$$

where $V = [0, \cdots, 0, \nu]^{\mathrm{T}} \in \mathbb{R}^n$, and

$$A_{10} = \begin{bmatrix} -\alpha_1 & 1 & \cdots & \cdots & 0 \\ -\alpha_2 & 0 & 1 & \cdots & 0 \\ \vdots & \vdots & \vdots & \ddots & \vdots \\ -\alpha_n & 0 & 0 & \cdots & 1 \\ -\alpha_{n+1} & 0 & 0 & \cdots & 0 \end{bmatrix}_{(n+1)\times(n+1)}$$

Systems (3.2.11) and (3.2.12) are standard singularly perturbed systems, and $\eta = 0$ is the unique solution of system (3.2.12) when $\epsilon = 0$. The reduced system is obtained by substituting $\eta = 0$ into system (3.2.11), while the boundary-layer system is obtained by applying the change of time variable $\tau = t/\epsilon$ and then setting $\epsilon = 0$, which are given as follows

$$\dot{x} = A_1 x \tag{3.2.13}$$

$$\frac{\mathrm{d}\eta}{\mathrm{d}\tau} = A_{10}\eta \tag{3.2.14}$$

Theorem 3.1. *Let Assumptions 3.1-3.2 hold, design HGSPO (3.2.6) and passive controller (3.2.9); then there exists $\epsilon_1^* > 0$ such that, $\forall \epsilon, 0 < \epsilon < \epsilon_1^*$, the closed-loop systems (3.2.11) and (3.2.12) are output strictly passive and the origin is stable.*

Proof. For the reduced system (3.2.13), define a Lyapunov function as $V_0(x) = x^{\mathrm{T}} P_0 x$, where $P_0 \in \mathbb{R}^{n\times n}$ is the positive definite solution of the Lyapunov equation $P_0 A_1 + A_1^{\mathrm{T}} P_0 = -I$. This function satisfies

$$\lambda_{\min}(P_0)\|x\|^2 \leq V_0(x) \leq \lambda_{\max}(P_0)\|x\|^2 \tag{3.2.15}$$

$$\frac{\partial V_0(x)}{\partial x} A_1 x \leq -\|x\|^2 \tag{3.2.16}$$

$$\|\frac{\partial V_0(x)}{\partial x}\| \leq 2\lambda_{\max}(P_0)\|x\| \tag{3.2.17}$$

For the boundary-layer system (3.2.14), define a Lyapunov function as $W_{10}(\eta) = \eta^{\mathrm{T}} P_{10} \eta$, where $P_{10} \in \mathbb{R}^{(n+1)\times(n+1)}$ is the positive definite solution of the Lyapunov

equation $P_{10}A_{10} + A_{10}^{\mathrm{T}}P_{10} = -I$. This function satisfies

$$\lambda_{\min}(P_{10})\|\eta\|^2 \leq W_{10}(\eta) \leq \lambda_{\max}(P_{10})\|\eta\|^2 \tag{3.2.18}$$

$$\frac{\partial W_{10}(\eta)}{\partial \eta} A_{10}\eta \leq -\|\eta\|^2 \tag{3.2.19}$$

$$\|\frac{\partial W_{10}(\eta)}{\partial \eta}\| \leq 2\lambda_{\max}(P_{10})\|\eta\| \tag{3.2.20}$$

Consider a storage function of the closed-loop systems (3.2.11) and (3.2.12) as follows

$$H(x,\eta) = V_0(x) + \beta W_{10}(\eta) \tag{3.2.21}$$

where $\beta > 0$ is to be determined and assume $y = x_n = \frac{\partial V_0(x)}{\partial x_n}$. Note that this is always possible as $V_0(x)$ can be arbitrarily chosen. Moreover, assume

$$\|\dot{\Psi}(\cdot)\| \leq L_1\|x\| + L_2\|\eta\| \tag{3.2.22}$$

where L_1 and L_2 are Lipschitz constants.

Differentiate $H(x,\eta)$ along systems (3.2.11) and (3.2.12), use inequalities (3.2.15) to (3.2.20), (3.2.22), with Corollary 2.1, yields

$$\begin{aligned}
\dot{H} &= \frac{\partial V_0(x)}{\partial x^{\mathrm{T}}}(A_1 x + BK_1 D(\epsilon)\eta + V) + \beta \frac{\partial W_{10}(\eta)}{\partial \eta^{\mathrm{T}}}\left(\frac{A_{10}\eta}{\epsilon} + B_1\dot{\Psi}(\cdot)\right) \\
&\leq y\nu - \|x\|^2 - \frac{\beta}{\epsilon}\|\eta\|^2 + 2\beta L_2\|P_{10}\|\|\eta\|^2 + (2\|P_0\|\|K_1\|\|D(\epsilon)\| \\
&+ 2\beta L_1\|P_{10}\|)\|x\|\|\eta\| \\
&\leq y\nu - \|x\|^2 - \frac{\beta}{\epsilon}\|\eta\|^2 + 2\beta L_2\|P_{10}\|\|\eta\|^2 + (2\|P_0\|\|K_1\| + 2\beta L_1\|P_{10}\|) \\
&\times \left(\frac{1}{\epsilon_0}\|x\|^2 + \epsilon_0|\eta\|^2\right) \\
&\leq y\nu - \frac{1}{2}\|x\|^2 - \frac{\beta}{2\epsilon}\|\eta\|^2 - b_1\|x\|^2 - b_2\|\eta\|^2
\end{aligned} \tag{3.2.23}$$

where

$$b_1 = \frac{1}{2} - \frac{2}{\epsilon_0}\left(\|P_0\|\|K_1\| + \beta L_1\|P_{10}\|\right) \tag{3.2.24}$$

$$b_2 = \frac{\beta}{2\epsilon} - 2\beta(\epsilon_0 L_1 + L_2)\|P_{10}\| - 2\epsilon_0\|P_0\|\|K_1\| \tag{3.2.25}$$

with $\epsilon_0 > 0$. One can choose β small enough and $\epsilon_0 \geq \epsilon_0^* = 4\|P_0\|\|K_1\| + 4\beta L_1\|P_{10}\|$ such that $b_1 > 0$, and then choose $\epsilon_1^* = \beta/(\epsilon_0^{*2}+4\beta L_2\|P_{10}\|)$, $\forall \epsilon, \epsilon \leq \epsilon_1^*$, such that $b_2 > 0$. It can be shown that

$$\dot{H} \leq y\nu - \min(1/2, \beta/(2\epsilon))(\|x\|^2 + \|\eta\|^2) \leq -y\phi(y) \leq 0 \tag{3.2.26}$$

Thus it can conclude that the closed-loop systems (3.2.11) and (3.2.12) are output strictly passive and the origin is stable. □

To this end, the POAPC design procedure for system (3.2.1) can be summarized as follows:

Step 1: Define perturbation (3.2.3) for the original nth-order system (3.2.1);

Step 2: Define a fictitious state $x_{n+1} = \Psi(\cdot)$ to represent perturbation (3.2.3);

Step 3: Extend the original nth-order system (3.2.1) into the extended $(n+1)$th-order system (3.2.4);

Step 4: Design the $(n+1)$th-order HGSPO (3.2.6) for the extended $(n+1)$th-order system (3.2.4) to obtain the state estimate $\hat{x}$ and the perturbation estimate $\hat{\Psi}(\cdot)$ by only the measurement of x_1;

Step 5: Design controller (3.2.9) for the original nth-order system (3.2.1).

3.3 Two-terminal VSC-HVDC System Modelling

There are two VSCs in the VSC-HVDC system shown in Fig. 3.1, in which the rectifier regulates DC voltage and reactive power, while the inverter regulates the active and reactive power. Only the balanced condition is considered, e.g., the three phases have identical parameters and their voltages and currents have the same amplitude while each phase shifts 120° between themselves. The rectifier dynamics can be written at the angular frequency ω as [40]

$$\begin{cases} \frac{\mathrm{d}i_{\mathrm{d1}}}{\mathrm{d}t} = -\frac{R_1}{L_1}i_{\mathrm{d1}} + \omega i_{\mathrm{q1}} + u_{\mathrm{d1}} \\ \frac{\mathrm{d}i_{\mathrm{q1}}}{\mathrm{d}t} = -\frac{R_1}{L_1}i_{\mathrm{q1}} - \omega i_{\mathrm{d1}} + u_{\mathrm{q1}} \\ \frac{\mathrm{d}V_{\mathrm{dc1}}}{\mathrm{d}t} = \frac{3u_{\mathrm{sq1}}i_{\mathrm{q1}}}{2C_1V_{\mathrm{dc1}}} - \frac{i_{\mathrm{L}}}{C_1} \end{cases} \tag{3.3.1}$$

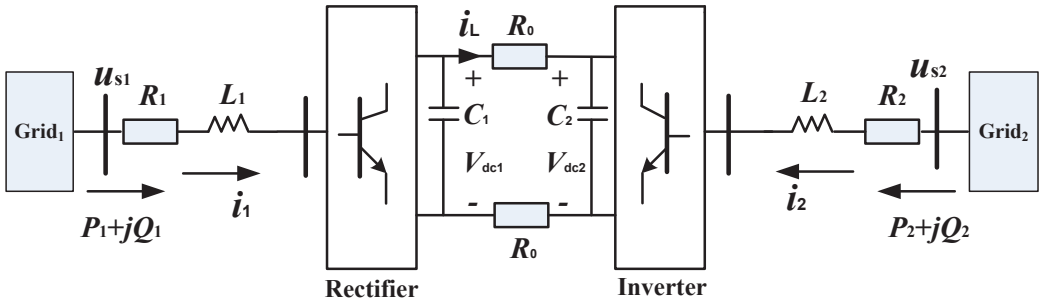

Figure 3.1: The two-terminal VSC-HVDC system

where the rectifier is connected with the AC grid via the equivalent resistance and inductance R_1 and L_1, respectively; C_1 is the DC bus capacitor; $u_{\mathrm{q1}} = \frac{u_{\mathrm{sq1}} - u_{\mathrm{rq1}}}{L_1}$ and $u_{\mathrm{d1}} = \frac{u_{\mathrm{sd1}} - u_{\mathrm{rd1}}}{L_1}$.

The inverter dynamics is written as

$$\begin{cases} \frac{\mathrm{d}i_{\mathrm{d2}}}{\mathrm{d}t} = -\frac{R_2}{L_2} i_{\mathrm{d2}} + \omega i_{\mathrm{q2}} + u_{\mathrm{d2}} \\ \frac{\mathrm{d}i_{\mathrm{q2}}}{\mathrm{d}t} = -\frac{R_2}{L_2} i_{\mathrm{q2}} - \omega i_{\mathrm{d2}} + u_{\mathrm{q2}} \\ \frac{\mathrm{d}V_{\mathrm{dc2}}}{\mathrm{d}t} = \frac{3 u_{\mathrm{sq2}} i_{\mathrm{q2}}}{2 C_2 V_{\mathrm{dc2}}} + \frac{i_{\mathrm{L}}}{C_2} \end{cases} \tag{3.3.2}$$

where the inverter is connected with the AC grid via the equivalent resistance and inductance R_2 and L_2, respectively; C_2 is the DC bus capacitor; $u_{\mathrm{q2}} = \frac{u_{\mathrm{sq2}} - u_{\mathrm{rq2}}}{L_2}$ and $u_{\mathrm{d2}} = \frac{u_{\mathrm{sd2}} - u_{\mathrm{rd2}}}{L_2}$.

The interconnection between the rectifier and inverter through DC cable is given as

$$V_{\mathrm{dc1}} i_{\mathrm{L}} = V_{\mathrm{dc2}} i_{\mathrm{L}} + 2 R_0 i_{\mathrm{L}}^2 \tag{3.3.3}$$

where R_0 represents the equivalent DC cable resistance.

The phase-locked loop (PLL) is used during the transformation of the *abc* frame to the *dq* frame [137, 148]. In the synchronous frame, u_{sd1}, u_{sd2}, u_{sq1}, and u_{sq2} are the d, q axes components of the respective AC grid voltages; i_{d1}, i_{d2}, i_{q1}, and i_{q2} are that of the line currents; u_{rd1}, u_{rd2}, u_{rq1}, and u_{rq2} are that of the converter input voltages; P_1, P_2, Q_1, and Q_2 are the active and reactive power transferred from the AC grid to the VSC; V_{dc1} and V_{dc2} are DC voltages; and i_{L} is DC cable current.

At the rectifier side, the *q*-axis is set to be in phase with the AC grid voltage u_{s1}. Correspondingly, the *q*-axis is set to be in phase with the AC grid voltage u_{s2} at the

inverter side. Hence, u_{sd1} and u_{sd2} are equal to 0 while u_{sq1} and u_{sq2} are equal to the magnitude of u_{s1} and u_{s2}. Then the power flows from the AC grid can be given as

$$\begin{cases} P_1 = \frac{3}{2}\left(u_{\mathrm{sq1}} i_{\mathrm{q1}} + u_{\mathrm{sd1}} i_{\mathrm{d1}}\right) = \frac{3}{2} u_{\mathrm{sq1}} i_{\mathrm{q1}} \\ Q_1 = \frac{3}{2}\left(u_{\mathrm{sq1}} i_{\mathrm{d1}} - u_{\mathrm{sd1}} i_{\mathrm{q1}}\right) = \frac{3}{2} u_{\mathrm{sq1}} i_{\mathrm{d1}} \\ P_2 = \frac{3}{2}\left(u_{\mathrm{sq2}} i_{\mathrm{q2}} + u_{\mathrm{sd2}} i_{\mathrm{d2}}\right) = \frac{3}{2} u_{\mathrm{sq2}} i_{\mathrm{q2}} \\ Q_2 = \frac{3}{2}\left(u_{\mathrm{sq2}} i_{\mathrm{d2}} - u_{\mathrm{sd2}} i_{\mathrm{q2}}\right) = \frac{3}{2} u_{\mathrm{sq2}} i_{\mathrm{d2}} \end{cases} \tag{3.3.4}$$

3.4 POAPC Design for Two-terminal VSC-HVDC System

3.4.1 Rectifier controller design

Define the tracking error $e_{\mathrm{r}} = [e_{\mathrm{r1}}, e_{\mathrm{r2}}]^{\mathrm{T}} = [V_{\mathrm{dc1}} - V_{\mathrm{dc1}}^*, Q_1 - Q_1^*]^{\mathrm{T}}$, and differentiate e_{r} until control inputs u_{q1} and u_{d1} appear explicitly as

$$\begin{cases} \ddot{e}_{\mathrm{r1}} & = \frac{3u_{\mathrm{sq1}}}{2C_1V_{\mathrm{dc1}}}\left[-\omega i_{\mathrm{d1}} - \frac{R_1}{L_1} i_{\mathrm{q1}} - \frac{i_{\mathrm{q1}}}{V_{\mathrm{dc1}}}\left(\frac{3u_{\mathrm{sq1}} i_{\mathrm{q1}}}{2C_1V_{\mathrm{dc1}}} - \frac{i_{\mathrm{L}}}{C_1}\right)\right] \\ & \quad - \frac{1}{2R_0C_1}\left(\frac{3u_{\mathrm{sq1}} i_{\mathrm{q1}}}{2C_1V_{\mathrm{dc1}}} - \frac{i_{\mathrm{L}}}{C_1} - \frac{3u_{\mathrm{sq2}} i_{\mathrm{q2}}}{2C_2V_{\mathrm{dc2}}} - \frac{i_{\mathrm{L}}}{C_2}\right) - \ddot{V}_{\mathrm{dc1}}^* + \frac{3u_{\mathrm{sq1}}}{2C_1L_1V_{\mathrm{dc1}}} u_{\mathrm{q1}} \\ \dot{e}_{\mathrm{r2}} & = \frac{3u_{\mathrm{sq1}}}{2}\left(-\frac{R_1}{L_1} i_{\mathrm{d1}} + \omega i_{\mathrm{q1}}\right) - \dot{Q}_1^* + \frac{3u_{\mathrm{sq1}}}{2L_1} u_{\mathrm{d1}} \end{cases} \tag{3.4.1}$$

The perturbations of system (3.4.1) are defined as

$$\begin{aligned} \Psi_{\mathrm{r1}}(\cdot) = & \frac{3u_{\mathrm{sq1}}}{2C_1V_{\mathrm{dc1}}}\left[-\omega i_{\mathrm{d1}} - \frac{R_1}{L_1} i_{\mathrm{q1}} - \frac{i_{\mathrm{q1}}}{V_{\mathrm{dc1}}}\left(\frac{3u_{\mathrm{sq1}} i_{\mathrm{q1}}}{2C_1V_{\mathrm{dc1}}} - \frac{i_{\mathrm{L}}}{C_1}\right)\right] - \frac{1}{2R_0C_1} \\ & \times \left(\frac{3u_{\mathrm{sq1}} i_{\mathrm{q1}}}{2C_1V_{\mathrm{dc1}}} - \frac{i_{\mathrm{L}}}{C_1} - \frac{3u_{\mathrm{sq2}} i_{\mathrm{q2}}}{2C_2V_{\mathrm{dc2}}} - \frac{i_{\mathrm{L}}}{C_2}\right) + \left(\frac{3u_{\mathrm{sq1}}}{2C_1L_1V_{\mathrm{dc1}}} - b_{\mathrm{r1}}\right) u_{\mathrm{q1}} \end{aligned} \tag{3.4.2}$$

$$\Psi_{\mathrm{r2}}(\cdot) = \frac{3u_{\mathrm{sq1}}}{2}\left(-\frac{R_1}{L_1} i_{\mathrm{d1}} + \omega i_{\mathrm{q1}}\right) + \left(\frac{3u_{\mathrm{sq1}}}{2L_1} - b_{\mathrm{r2}}\right) u_{\mathrm{d1}} \tag{3.4.3}$$

And system (3.4.1) can be expressed by

$$\begin{cases} \ddot{e}_{\mathrm{r1}} = \Psi_{\mathrm{r1}}(\cdot) + b_{\mathrm{r1}} u_{\mathrm{q1}} - \ddot{V}_{\mathrm{dc1}}^* \\ \dot{e}_{\mathrm{r2}} = \Psi_{\mathrm{r2}}(\cdot) + b_{\mathrm{r2}} u_{\mathrm{d1}} - \dot{Q}_1^* \end{cases} \tag{3.4.4}$$

where b_{r1} and b_{r2} are constant control gains.

Define $z_{11} = V_{\mathrm{dc1}}$ and $z_{12} = \dot{z}_{11}$, a third-order HGSPO is designed as

$$\begin{cases} \dot{\hat{z}}_{11} = \hat{z}_{12} + \frac{\alpha_{\mathrm{r1}}}{\epsilon}(z_{11} - \hat{z}_{11}) \\ \dot{\hat{z}}_{12} = \hat{\Psi}_{\mathrm{r1}}(\cdot) + \frac{\alpha_{\mathrm{r2}}}{\epsilon^2}(z_{11} - \hat{z}_{11}) + b_{\mathrm{r1}} u_{\mathrm{q1}} \\ \dot{\hat{\Psi}}_{\mathrm{r1}}(\cdot) = \frac{\alpha_{\mathrm{r3}}}{\epsilon^3}(z_{11} - \hat{z}_{11}) \end{cases} \tag{3.4.5}$$

where $\alpha_{\mathrm{r}1}$, $\alpha_{\mathrm{r}2}$, and $\alpha_{\mathrm{r}3}$ are positive observer gains, with $0 < \epsilon \ll 1$.

Define $z'_{11} = Q_1$, a second-order HGPO is designed as

$$\begin{cases} \dot{\hat{z}}'_{11} = \hat{\Psi}_{\mathrm{r}2}(\cdot) + \frac{\alpha'_{\mathrm{r}1}}{\epsilon}(z'_{11} - \hat{z}'_{11}) + b_{\mathrm{r}2}u_{\mathrm{d}1} \\ \dot{\hat{\Psi}}_{\mathrm{r}2}(\cdot) = \frac{\alpha'_{\mathrm{r}2}}{\epsilon^2}(z'_{11} - \hat{z}'_{11}) \end{cases} \tag{3.4.6}$$

where $\alpha'_{\mathrm{r}1}$ and $\alpha'_{\mathrm{r}2}$ are positive observer gains.

The POAPC for system (3.4.1) using the estimates of state and perturbation is designed as

$$\begin{cases} u_{\mathrm{q}1} & = b_{\mathrm{r}1}^{-1}[-\hat{\Psi}_{\mathrm{r}1}(\cdot) - k_{\mathrm{r}1}(\hat{z}_{11} - V^*_{\mathrm{dc}1}) - k_{\mathrm{r}2}(\hat{z}_{12} - \dot{V}^*_{\mathrm{dc}1}) + \ddot{V}^*_{\mathrm{dc}1} + \nu_{\mathrm{r}1}] \\ u_{\mathrm{d}1} & = b_{\mathrm{r}2}^{-1}(-\hat{\Psi}_{\mathrm{r}2}(\cdot) - k'_{\mathrm{r}1}(\hat{z}'_{11} - Q^*_1) + \dot{Q}^*_1 + \nu_{\mathrm{r}2}) \end{cases} \tag{3.4.7}$$

where $k_{\mathrm{r}1}$, $k_{\mathrm{r}2}$ and $k'_{\mathrm{r}1}$ are the feedback control gains; $V_{\mathrm{r}} = [\nu_{\mathrm{r}1}, \nu_{\mathrm{r}2}]^{\mathrm{T}}$ is the additional input.

Choose the output of system (3.4.1) as $Y_{\mathrm{r}} = [Y_{\mathrm{r}1}, Y_{\mathrm{r}2}]^{\mathrm{T}} = [\dot{V}_{\mathrm{dc}1} - \dot{V}^*_{\mathrm{dc}1}, Q_1 - Q^*_1]^{\mathrm{T}}$. Then let $V_{\mathrm{r}} = [-\lambda_{\mathrm{r}1}Y_{\mathrm{r}1}, -\lambda_{\mathrm{r}2}Y_{\mathrm{r}2}]^{\mathrm{T}}$, where $\lambda_{\mathrm{r}1}$ and $\lambda_{\mathrm{r}2}$ are some positive constants to inject an extra system damping into system (3.4.1). Hence the closed-loop system is output strictly passive from output Y_j to input V_j.

Constants $b_{\mathrm{r}1}$ and $b_{\mathrm{r}2}$ are chosen to satisfy following inequalities when the rectifier operates within its normal region:

$$3u_{\mathrm{sq}1}/[2C_1L_1V_{\mathrm{dc}1}(1-\theta_{\mathrm{r}1})] \geq b_{\mathrm{r}1} \geq 3u_{\mathrm{sq}1}/[2C_1L_1V_{\mathrm{dc}1}(1+\theta_{\mathrm{r}1})] \tag{3.4.8}$$

$$3u_{\mathrm{sq}1}/[2L_1(1-\theta_{\mathrm{r}2})] \geq b_{\mathrm{r}2} \geq 3u_{\mathrm{sq}1}/[2L_1(1+\theta_{\mathrm{r}2})] \tag{3.4.9}$$

where $\theta_{\mathrm{r}1} < 1$ and $\theta_{\mathrm{r}2} < 1$ are positive constants. During the most severe disturbance, both the reactive power and DC voltage reduce from their initial value to around zero within a short period of time Δ. Thus the boundary values of the state and perturbation estimates can be obtained as $|\hat{z}_{11}| \leq |V^*_{\mathrm{dc}1}|$, $|\hat{z}_{12}| \leq |V^*_{\mathrm{dc}1}|/\Delta$, $|\hat{\Psi}_{\mathrm{r}1}(\cdot)| \leq |V^*_{\mathrm{dc}1}|/\Delta^2$, $|\hat{z}'_{11}| \leq |Q^*_1|$, and $|\hat{\Psi}_{\mathrm{r}2}(\cdot)| \leq |Q^*_1/\Delta|$, respectively.

The structure of rectifier controller is illustrated by Fig. 3.2, in which only DC voltage $V_{\mathrm{dc}1}$ and reactive power Q_1 need to be measured.

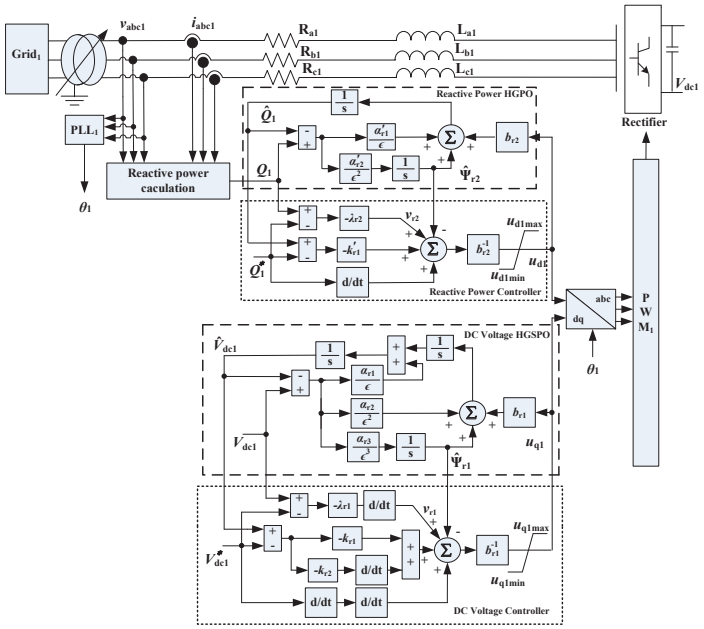

Figure 3.2: Structure of the rectifier controller in two-terminal VSC-HVDC systems.

3.4.2 Inverter controller design

Define the tracking error $e_{\mathrm{i}} = [e_{\mathrm{i}1}, e_{\mathrm{i}2}]^{\mathrm{T}} = [P_2 - P_2^*, Q_2 - Q_2^*]^{\mathrm{T}}$, differentiate e_{i} until the control inputs $u_{\mathrm{q}2}$ and $u_{\mathrm{d}2}$ appear explicitly, yields

$$\begin{cases} \dot{e}_{\mathrm{i}1} = \frac{3u_{\mathrm{sq}2}}{2}\left(-\frac{R_2}{L_2}i_{\mathrm{q}2} - \omega i_{\mathrm{d}2}\right) - \dot{P}_2^* + \frac{3u_{\mathrm{sq}2}}{2L_2}u_{\mathrm{q}2} \\ \dot{e}_{\mathrm{i}2} = \frac{3u_{\mathrm{sq}2}}{2}\left(-\frac{R_2}{L_2}i_{\mathrm{d}2} + \omega i_{\mathrm{q}2}\right) - \dot{Q}_2^* + \frac{3u_{\mathrm{sq}2}}{2L_2}u_{\mathrm{d}2} \end{cases} \tag{3.4.10}$$

The perturbations of system (3.4.10) are defined as

$$\Psi_{\mathrm{i}1}(\cdot) = \frac{3u_{\mathrm{sq}2}}{2}\left(-\frac{R_2}{L_2}i_{\mathrm{q}2} - \omega i_{\mathrm{d}2}\right) + (\frac{3u_{\mathrm{sq}2}}{2L_2} - b_{\mathrm{i}1})u_{\mathrm{q}2} \tag{3.4.11}$$

$$\Psi_{\mathrm{i}2}(\cdot) = \frac{3u_{\mathrm{sq}2}}{2}\left(-\frac{R_2}{L_2}i_{\mathrm{d}2} + \omega i_{\mathrm{q}2}\right) + (\frac{3u_{\mathrm{sq}2}}{2L_2} - b_{\mathrm{i}2})u_{\mathrm{d}2} \tag{3.4.12}$$

And system (3.4.10) can be expressed by

$$\begin{cases} \dot{e}_{\mathrm{i}1} = \Psi_{\mathrm{i}1}(\cdot) + b_{\mathrm{i}1}u_{\mathrm{q}2} - \dot{P}_2^* \\ \dot{e}_{\mathrm{i}2} = \Psi_{\mathrm{i}2}(\cdot) + b_{\mathrm{i}2}u_{\mathrm{d}2} - \dot{Q}_2^* \end{cases} \tag{3.4.13}$$

where $b_{\mathrm{i}1}$ and $b_{\mathrm{i}2}$ are constant control gains.

Similarly, define $z_{21} = P_2$ and $z'_{21} = Q_2$, two second-order HGPOs are designed as

$$\begin{cases} \dot{\hat{z}}_{21} = \hat{\Psi}_{\mathrm{i}1}(\cdot) + \frac{\alpha_{\mathrm{i}1}}{\epsilon}(z_{21} - \hat{z}_{21}) + b_{\mathrm{i}1}u_{\mathrm{q}2} \\ \dot{\hat{\Psi}}_{\mathrm{i}1}(\cdot) = \frac{\alpha_{\mathrm{i}2}}{\epsilon^2}(z_{21} - \hat{z}_{21}) \end{cases} \tag{3.4.14}$$

where $\alpha_{\mathrm{i}1}$ and $\alpha_{\mathrm{i}2}$ are positive observer gains.

$$\begin{cases} \dot{\hat{z}}'_{21} = \hat{\Psi}_{\mathrm{i}2}(\cdot) + \frac{\alpha'_{\mathrm{i}1}}{\epsilon}(z'_{21} - \hat{z}'_{21}) + b_{\mathrm{i}2}u_{\mathrm{d}2} \\ \dot{\hat{\Psi}}_{\mathrm{i}2}(\cdot) = \frac{\alpha'_{\mathrm{i}2}}{\epsilon^2}(z'_{21} - \hat{z}'_{21}) \end{cases} \tag{3.4.15}$$

where $\alpha'_{\mathrm{i}1}$ and $\alpha'_{\mathrm{i}2}$ are positive observer gains.

The POAPC for system (3.4.10) using the estimates of state and perturbation is designed as

$$\begin{cases} u_{\mathrm{q}2} = b_{\mathrm{i}1}^{-1}(-\hat{\Psi}_{\mathrm{i}1}(\cdot) - k_{\mathrm{i}1}(\hat{z}_{21} - P_2^*) + \dot{P}_2^* + \nu_{\mathrm{i}1}) \\ u_{\mathrm{d}2} = b_{\mathrm{i}2}^{-1}(-\hat{\Psi}_{\mathrm{i}2}(\cdot) - k'_{\mathrm{i}1}(\hat{z}'_{21} - Q_2^*) + \dot{Q}_2^* + \nu_{\mathrm{i}2}) \end{cases} \tag{3.4.16}$$

where $k_{\mathrm{i}1}$ and $k'_{\mathrm{i}1}$ are the feedback control gains; $V_{\mathrm{i}} = [\nu_{\mathrm{i}1}, \nu_{\mathrm{i}2}]^{\mathrm{T}}$ is the additional input.

Choose the output of system (3.4.10) as $Y_{\mathrm{i}} = [Y_{\mathrm{i}1}, Y_{\mathrm{i}2}]^{\mathrm{T}} = [P_2 - P_2^*, Q_2 - Q_2^*]^{\mathrm{T}}$. Let $V_{\mathrm{i}} = [-\lambda_{\mathrm{i}1}Y_{\mathrm{i}1}, -\lambda_{\mathrm{i}2}Y_{\mathrm{i}2}]^{\mathrm{T}}$, where $\lambda_{\mathrm{i}1}$ and $\lambda_{\mathrm{i}2}$ are some positive constants to inject an extra system damping into system (3.4.10). Similarly, the closed-loop system is output strictly passive from output Y_{i} to input V_{i}.

Similarly, constants $b_{\mathrm{i}1}$ and $b_{\mathrm{i}2}$ are chosen to satisfy:

$$3u_{\mathrm{sq}2}/[2L_2(1-\theta_{\mathrm{i}1})] \geq b_{\mathrm{i}1} \geq 3u_{\mathrm{sq}2}/[2L_2(1+\theta_{\mathrm{i}1})] \tag{3.4.17}$$

$$3u_{\mathrm{sq}2}/[2L_2(1-\theta_{\mathrm{i}2})] \geq b_{\mathrm{i}2} \geq 3u_{\mathrm{sq}2}/[2L_2(1+\theta_{\mathrm{i}2})] \tag{3.4.18}$$

where $\theta_{\mathrm{i}1} < 1$ and $\theta_{\mathrm{i}2} < 1$ are positive constants. Again, the boundary values of the state and perturbation estimates are obtained as $|\hat{z}_{21}| \leq |P_2^*|$, $|\hat{\Psi}_{\mathrm{i}1}(\cdot)| \leq |P_2^*|/\Delta$, $|\hat{z}'_{21}| \leq |Q_2^*|$, and $|\hat{\Psi}_{\mathrm{i}2}(\cdot)| \leq |Q_2^*|/\Delta$, respectively.

The structure of inverter controller is illustrated by Fig. 3.3, in which only active power P_2 and reactive power Q_2 need to be measured.

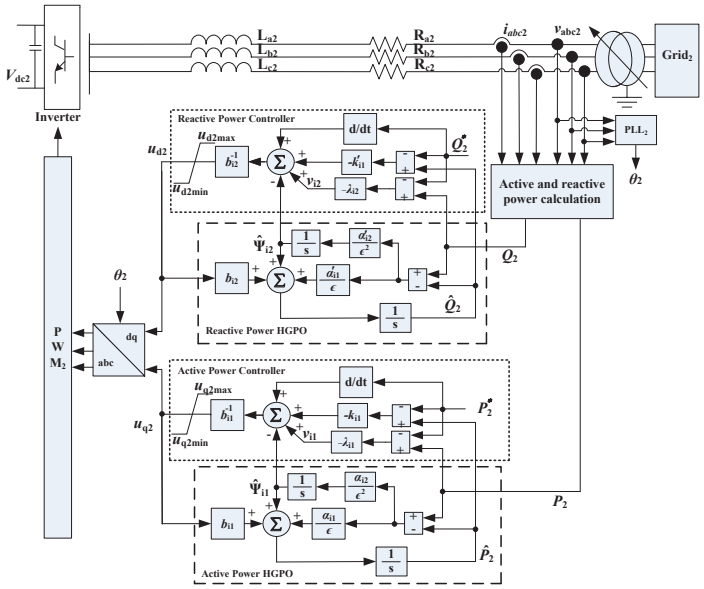

Figure 3.3: Structure of the inverter controller in two-terminal VSC-HVDC systems.

3.5 Simulation Results for Two-terminal VSC-HVDC System

The proposed approach is applied on the two-terminal VSC-HVDC system illustrated by Fig. 3.1, in which the rectifier regulates DC voltage and reactive power, while the inverter regulates the active and reactive power. The control performance of POAPC is compared with that of conventional proportional-integral (PI) control used in [39], note that parameters of PI control is not optimally tuned as our interests focus on the feature of one-point linearization, in other words, its control performance will be degraded when operating points vary. Passive control (PC) has also been used for comparison, note that parameters of PC are the same of that of POAPC, however its control performance will be degraded when any system uncertainties exist as it requires an accurate system model.

The system parameters used in the simulation are listed in Table 3.1. The POAPC parameters are given in Table 3.2. The control inputs are bounded as $|u_{\mathrm{d1}}| \leq 1$ p.u., $|u_{\mathrm{q1}}| \leq 1$ p.u., $|u_{\mathrm{d2}}| \leq 1$ p.u., and $|u_{\mathrm{q2}}| \leq 1$ p.u..

The simulation is undertaken in Matlab/Simulink 2013a by a personal computer

Table 3.1: System parameters used in the two-terminal VSC-HVDC system.

System frequency of both AC grids	f	50 Hz
Base voltage of both AC grids	$V_{\mathrm{AC}_{\mathrm{base}}}$	100 kV
DC cable base voltage	$V_{\mathrm{DC}_{\mathrm{base}}}$	200 kV
System base power	S_{base}	100 MVA
AC system resistance (25 km)	R_1, R_2	0.05 Ω/km
AC system inductance (25 km)	L_1, L_2	0.026 mH/km
DC cable resistance (50 km)	R_0	0.21 Ω/km
DC capacitance	C_1, C_2	11.94 μF

Table 3.2: Control parameters in the two-terminal VSC-HVDC systems.

Rectifier controller			
Control gains	$k'_{\mathrm{r1}} = 64$	$k_{\mathrm{r1}} = 16$	$k_{\mathrm{r2}} = 60$
	$b_{\mathrm{r1}} = 200$	$b_{\mathrm{r2}} = 150$	$\lambda_{\mathrm{r1}} = 5$
	$\lambda_{\mathrm{r2}} = 5$		
Observer gains	$\alpha'_{\mathrm{r1}} = 400$	$\alpha'_{\mathrm{r2}} = 4 \times 10^4$	$\alpha_{\mathrm{r1}} = 1200$
	$\alpha_{\mathrm{r2}} = 4.8 \times 10^5$	$\alpha_{\mathrm{r3}} = 6.4 \times 10^7$	$\epsilon = 0.1$
Inverter controller			
Control gains	$k_{\mathrm{i1}} = 70$	$k'_{\mathrm{i1}} = 70$	$b_{\mathrm{i1}} = 100$
	$b_{\mathrm{i2}} = 100$	$\lambda_{\mathrm{i1}} = 10$	$\lambda_{\mathrm{i2}} = 10$
Observer gains	$\alpha_{\mathrm{i1}} = 400$	$\alpha_{\mathrm{i2}} = 4 \times 10^4$	$\alpha'_{\mathrm{i1}} = 400$
	$\alpha'_{\mathrm{i2}} = 4 \times 10^4$	$\epsilon = 0.1$	

with an Intel(R) Core TM i7-2600 CPU at 3.4 GHz and 8GB of RAM. The solver used is the Ode4 (Fourth-order Runge-Kutta) with a fixed-step size of 10^{-4} s.

1) Case 1: Active and reactive power tracking. An active and reactive power tracking started at $t = 0.5$ s and restored to the original value at $t = 1$ s has been tested, while DC voltage is regulated at its rated value. The system responses are illustrated by Fig. 3.4. One can find that the overshoot of active and reactive power is completely eliminated by PC and POAPC compared to PI control, which is resulted from the cancelation of system nonlinearities. Moreover, DC voltage can be effectively regulated to its rated value by the POAPC, which enhances the system stability. Note that POAPC can achieve as good control performance as that of PC due to the fast online estimation, the tiny difference between them is caused by the estimation error when the power tracking starts.

2) Case 2: 10-cycle voltage drop at AC grids. A 60% voltage drop of both AC grids occurs at $t = 0.5$ s and restored at $t = 0.7$ s, the system transient responses are illustrated by Fig. 3.5. It can be found that POAPC and PC can effectively stabilize the system with a faster rate than PI control. This is due to the extra system damping which has been injected via passivation.

3) Case 3: Uncertainties in the system resistances and inductances. In order to test the robustness of POAPC, a 20% increase of system resistances and inductances from their nominal values is tested. The corresponding system responses and control efforts are shown are by Fig. 3.6 and Fig. 3.7, respectively. It can be seen that the control performance of PC degrades dramatically as it requires an accurate system model. In fact, if there exists any parameter uncertainties, PC cannot maintain its control performance. In contrast, PI control and POAPC are not sensitive to the parameter uncertainties as their design do not need the system parameters. Therefore, POAPC can provide a great robustness to the VSC-HVDC systems in the presence of parameter uncertainties.

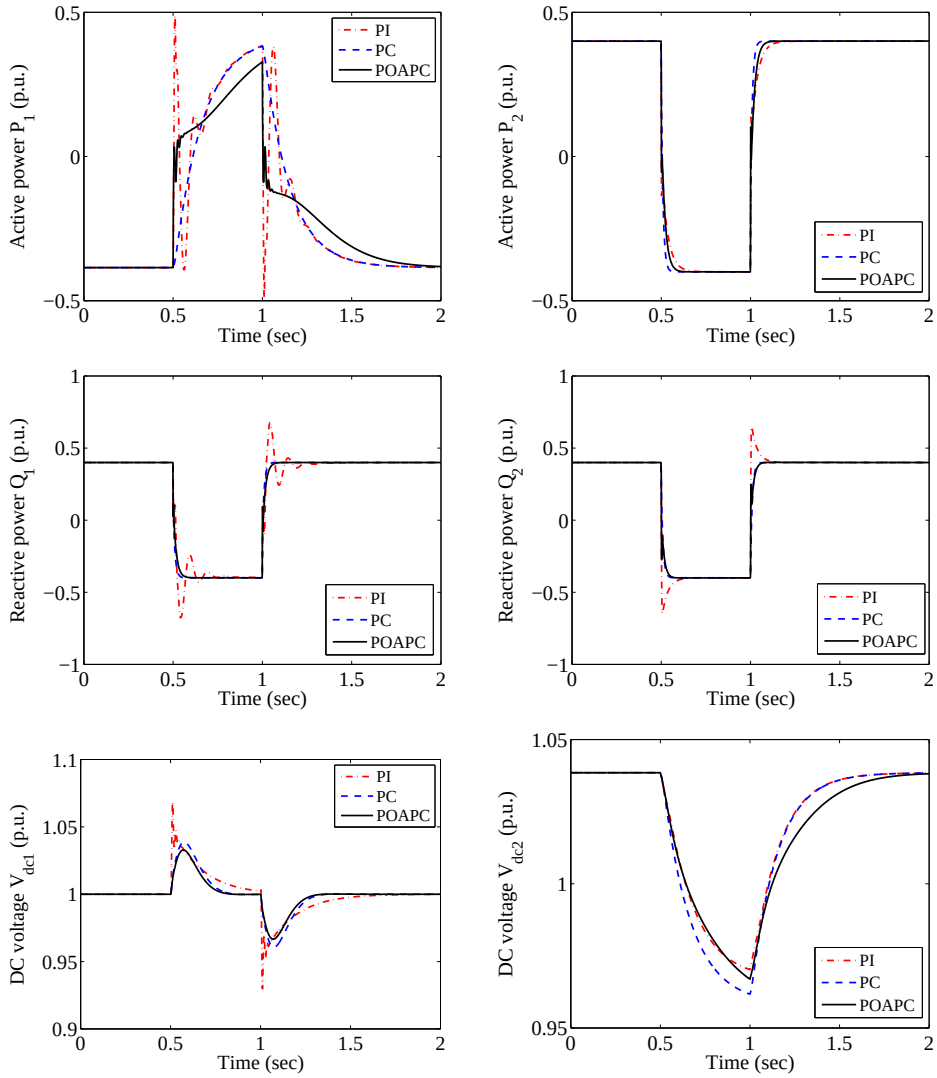

Figure 3.4: System responses obtained in an active and reactive power tracking.

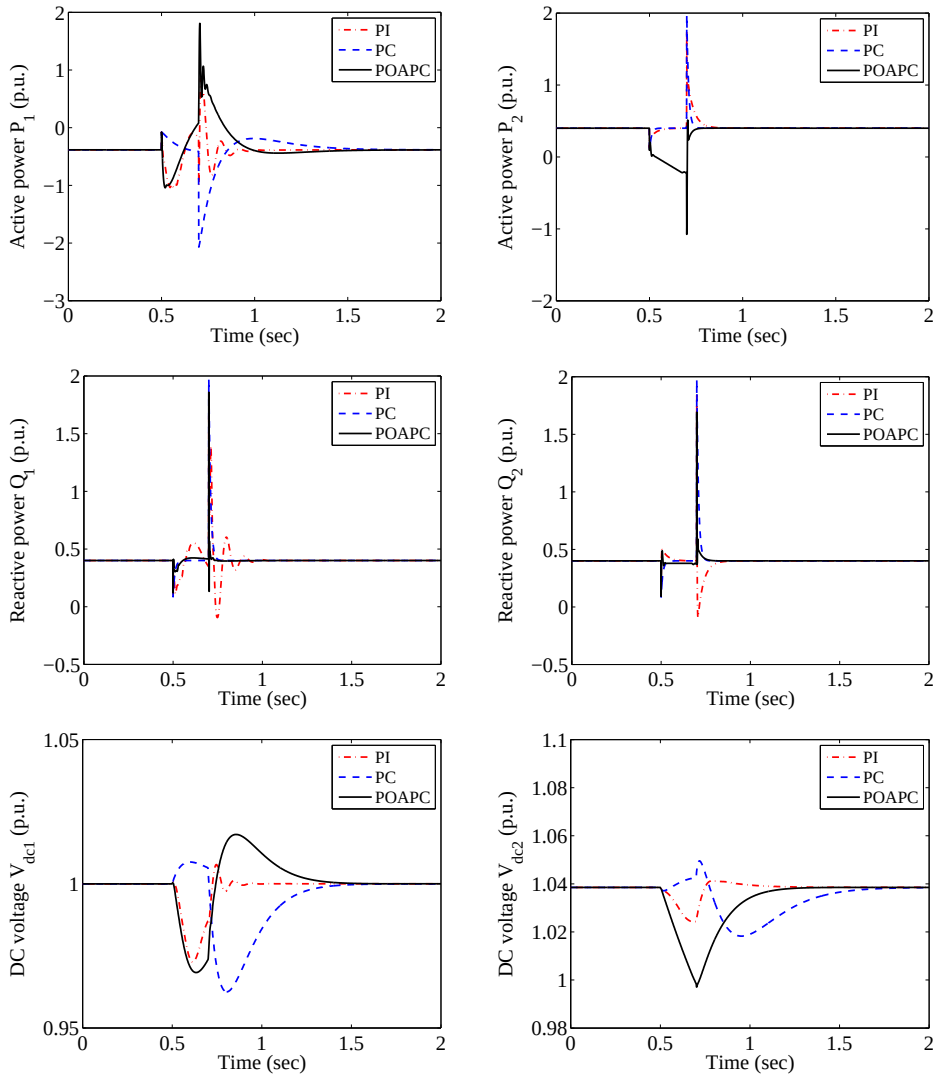

Figure 3.5: System responses obtained in the voltage drop of AC grids.

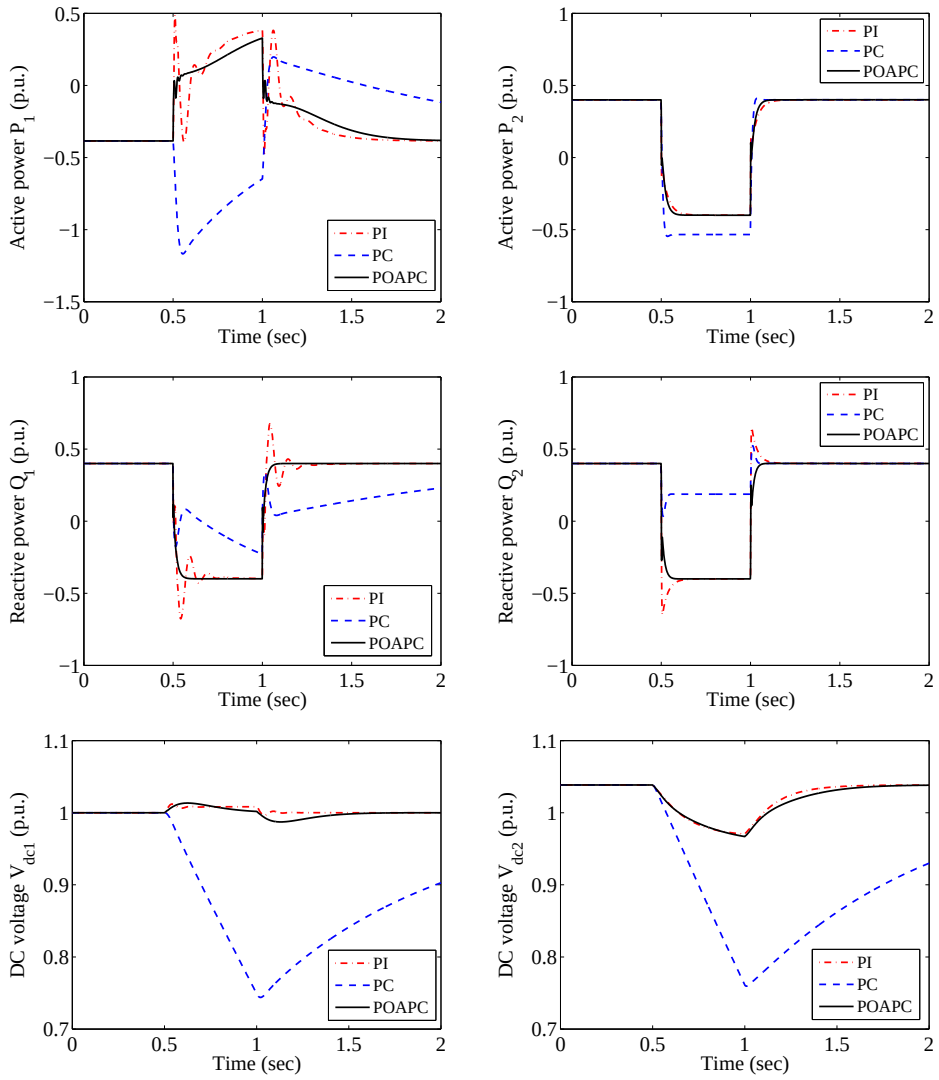

Figure 3.6: System responses obtained under a 20% increase of system resistances and inductances.

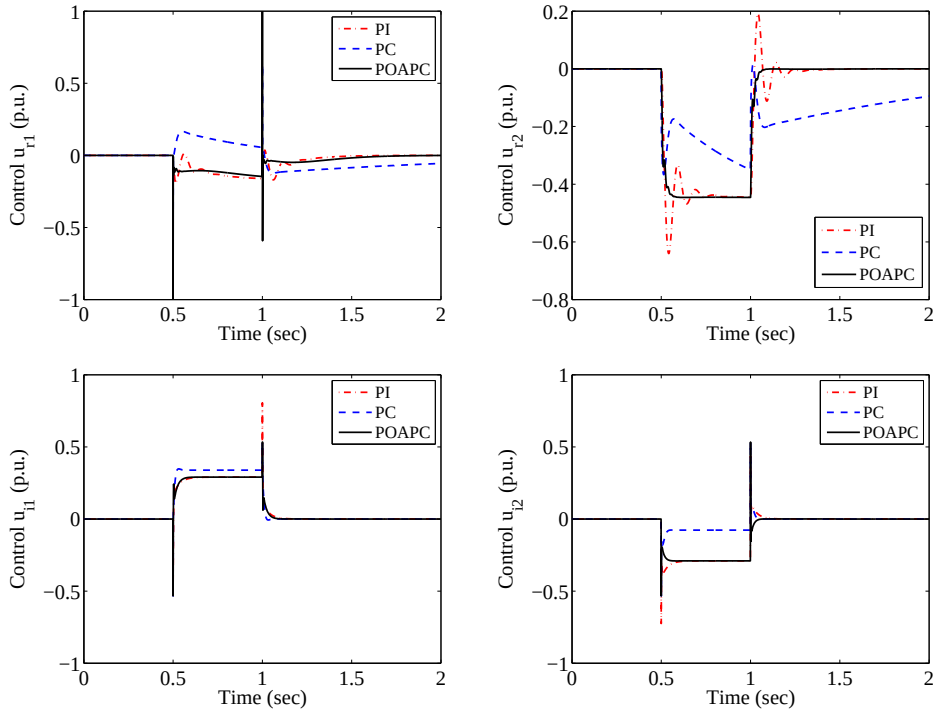

Figure 3.7: Control efforts obtained under a 20% increase of system resistances and inductances.

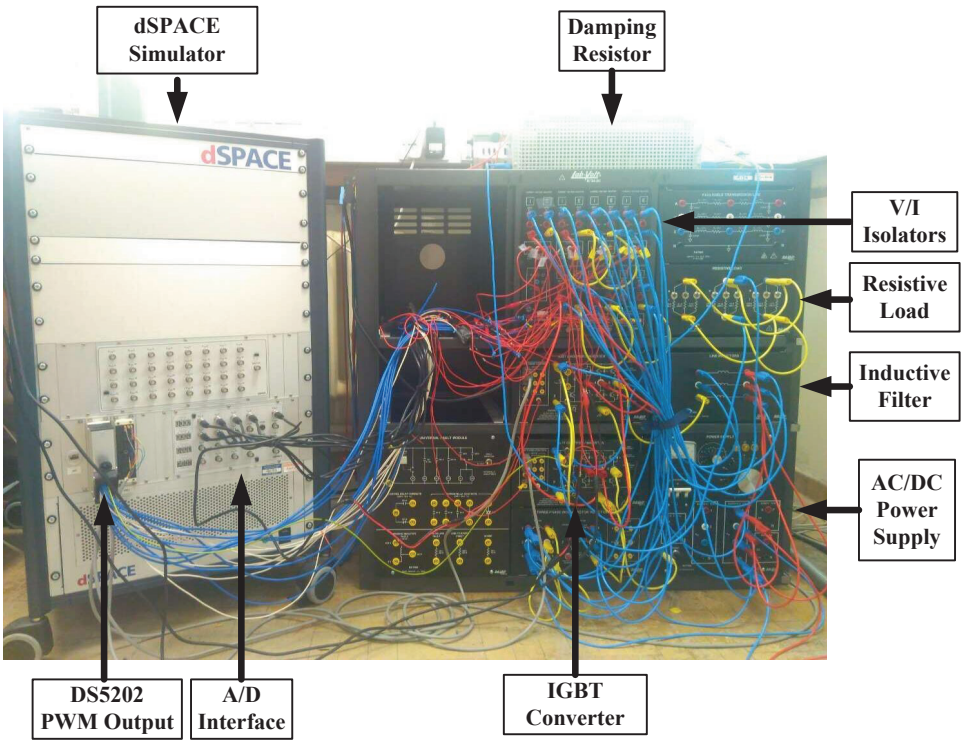

Figure 3.8: Overall hardware platform.

3.6 Experiment Results for Rectifier Controller and Inverter Controller

The implementation feasibility of the proposed controller is tested by the hardware experiment. Due to the limit of experimental facilities, the controller is implemented to the rectifier and inverter separately. Two case studies are carried out, Case I studies the rectifier controller with an equivalent resistor representing the DC cable connected to the rectifier, while Case II studies the inverter controller with a constant DC voltage source representing the regulated DC voltage. As the control of rectifier and inverter is independent, such experiments could capture the main features of the controller performance in the complete VSC-HVDC system.

3.6.1 Experiment platform

The control of rectifier and inverter has been tested on an experiment platform shown in Fig. 3.8. A strong power supply is able to supply stable three-phase AC and DC voltages, thus it is used as the AC grid in Case I and Case II, which also provides a stable DC voltage source in Case II. An IGBT converter is used with an inductive filter between the power supply and converter. The voltage/current isolators measure the currents and voltages, which are then sent to the dSPACE simulator through analogue/digital (A/D) blocks.

The dSPACE simulator has quad-core AMD processors (DS1006) and operates with DS5202 ACMC board, which is capable of generating high-frequency PWM signals and providing high-speed A/D interfaces. The IGBT converter, inductive filter, measurement units, and power supply, etc. all are from the Lab-Volt company, which provides various equipments with the user-friendly interfaces, accurate system parameters, and reliable hardware protections. The DC bus of the IGBT converter is protected by using a 100 Ω damping resistor with 1000 W rated power, which is connected to the damping circuit built in Lab-Volt IGBT converter to avoid potential damages caused by over-voltage or over-current in the DC bus.

The control algorithm is compiled and downloaded into the dSPCAE simulator shown in Fig. 3.8 by using the measured active and reactive power, and DC voltage as inputs from the equipment, such that the I/O interface of dSPACE simulator enables the real-time sampling of inputs from measurements and output control signals. Then the PWM signals are generated with various duty cycles as controller outputs to the IGBT converter. Furthermore, the sampling frequency f_{s} and the PWM frequency f_{PWM} with the space vector PWM (SVPWM) implemented in the dSPACE simulator are given in Table 3.3. The proposed controller is embedded into the dSPACE simulator and connected to the VSC with IGBT converter, which is compatible with Matlab/Simulink.

Two separate experiments are carried out on this platform to implement POAPC on the rectifier and inverter, respectively. The experiment configuration of Case I is illustrated in Fig. 3.9, a resistive load is connected to DC side to test the control performance when the active power flows from the AC grid to the DC bus. The

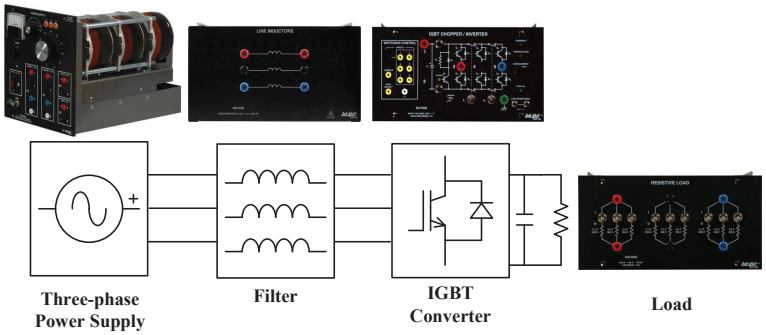

Figure 3.9: Experiment configuration of Case I.

Table 3.3: System parameters used in Case I.

Rated active power	P_0 =300 W	Rated rms voltage	$V_0 = 30$ V
Rated rms current	$I_0 = 10$ A	Rated frequency	$f_0 = 50$ Hz
DC line voltage	$V_{\mathrm{dc1}} = 100$ V	Filter inductance	$L_1 = 60$ mH
PWM frequency	$f_{\mathrm{PWM}} = 2$ kHz	Sampling frequency	$f_{\mathrm{s}} = 10$ kHz
DC capacitance	$C_1 = 1320$ μF	Load resistance	$R_{\mathrm{L}} = 1200$ Ω

Table 3.4: System parameters used in Case II.

Rated active power	$P_0 = 300$ W	Rated rms voltage	$V_0 = 30$ V
Rated rms current	$I_0 = 10$ A	Rated frequency	$f_0 = 50$ Hz
DC line voltage	$V_{\mathrm{dc2}} = 60$ V	Filter inductance	$L_2 = 60$ mH
PWM frequency	$f_{\mathrm{PWM}} = 2$ kHz	Sampling frequency	$f_{\mathrm{s}} = 10$ kHz
DC capacitance	$C_2 = 1320$ μF		

hardware parameters are listed in Table 3.3. The experiment configuration of Case II is shown in Fig. 3.10, a DC power supply is used to provide the regulated DC voltage to ensure the IGBT converter can operate properly. The hardware parameters are listed in Table 3.4.

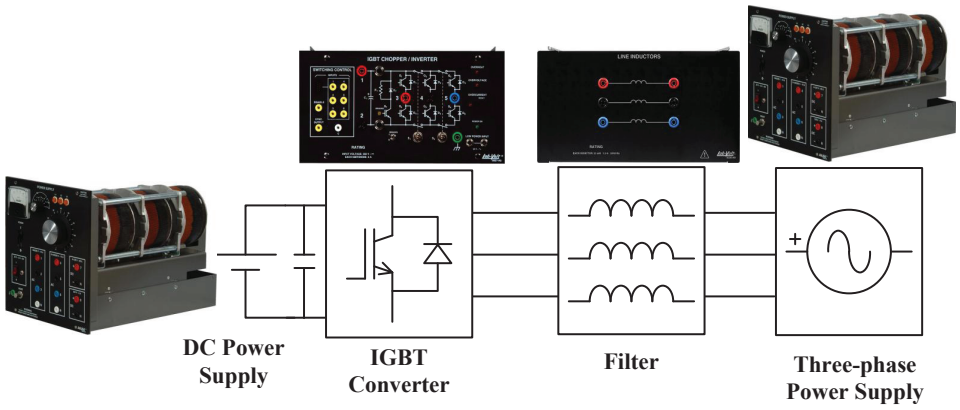

Figure 3.10: Experiment configuration of Case II.

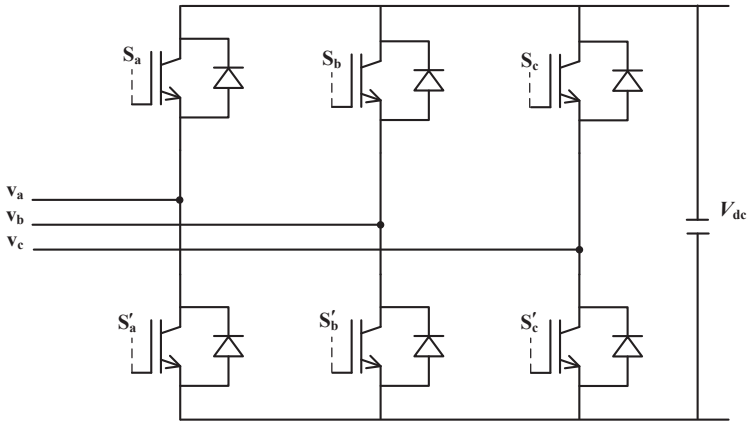

Figure 3.11: The structure of an IGBT converter.

The structure of an IGBT converter is shown in Fig. 3.11, which can be modelled as

$$\begin{cases} v_{\mathrm{a}} = V_{\mathrm{dc}}\left(S_{\mathrm{a}} - \frac{1}{3}(S_{\mathrm{a}} + S_{\mathrm{b}} + S_{\mathrm{c}})\right) \\ v_{\mathrm{b}} = V_{\mathrm{dc}}\left(S_{\mathrm{b}} - \frac{1}{3}(S_{\mathrm{a}} + S_{\mathrm{b}} + S_{\mathrm{c}})\right) \\ v_{\mathrm{c}} = V_{\mathrm{dc}}\left(S_{\mathrm{c}} - \frac{1}{3}(S_{\mathrm{a}} + S_{\mathrm{b}} + S_{\mathrm{c}})\right) \\ i_{\mathrm{DC}} = i_{\mathrm{a}}S_{\mathrm{a}} + i_{\mathrm{b}}S_{\mathrm{b}} + i_{\mathrm{c}}S_{\mathrm{c}} \end{cases} \tag{3.6.1}$$

where v_{a}, v_{b} and v_{c} are the three-phase voltages, i_{a}, i_{b} and i_{c} are the three-phase currents, respectively. i_{DC} is the current through the DC capacitor. S_{a}, S_{b}, and S_{c} are the switch signals (1 is on and 0 is off) [137].

IGBT converters can be driven by PWM signals. Compared with the conven-

tional PWM or sinusoidal pulse width modulation (SPWM) techniques, the space vector modulation (SVM) can increase 15% more of the maximum output voltage and reduce the switching times.

Based on SVM and ignoring the resistances in the steady-state, the minimum DC voltage must satisfy the following inequality to ensure the IGBT converter is controllable and can work properly as [137]

$$V_{\mathrm{dc}i} \geq \sqrt{3}\sqrt{(u_{\mathrm{sd}i} + \omega L_i i_{\mathrm{q}i})^2 + (u_{\mathrm{sq}i} - \omega L_i i_{\mathrm{d}i})^2},\ i = 1, 2 \tag{3.6.2}$$

At last, the IGBT converter is used as the DC/AC converter, the anti-parallel diodes are combined with the IGBT converters such that it can be operated as either a rectifier or an inverter.

3.6.2 Case studies

The implementation feasibility of rectifier controller and inverter controller is tested separately by two cases. The control parameters used in the experiment are provided in Table 3.5, the control inputs are bounded as $|u_{\mathrm{d}i}| \leq 50$ V and $|u_{\mathrm{q}i}| \leq 50$ V, respectively. The time period Δ is chosen to be 0.05 s for the calculation of boundary values of state and perturbation estimates. Simulation is firstly undertaken with the standard Matlab/Simulink IGBT converter model to evaluate the effectiveness of the rectifier controller and inverter controller, then the controller is implemented into the dSPACE simulator and connected to the IGBT converter.

1) Case I: Rectifier controller experiment. The POAPC for rectifier is firstly tested, in which the initial DC voltage V_{dc1} and reactive power Q_1 will be regulated to be 100 V and 0 Var, respectively. DC voltage is regulated to be 100 V for the whole period of the experiment. The reference value of reactive power is set to be 15 Var, then drops to 5 Var and restores to 15 Var. After reactive power is stabilized at 15 Var, a resistive load R_{L} is connected to the DC side shown in Fig. 3.9 to simulate the DC cable used in complete VSC-HVDC systems. Then a 50% AC grid voltage drop is applied to test the system transient performance.

The experiment results are given in Fig. 3.12, in which the controller is activated at 10 s and the whole experiment lasts for 150 s. It presents that the reactive power

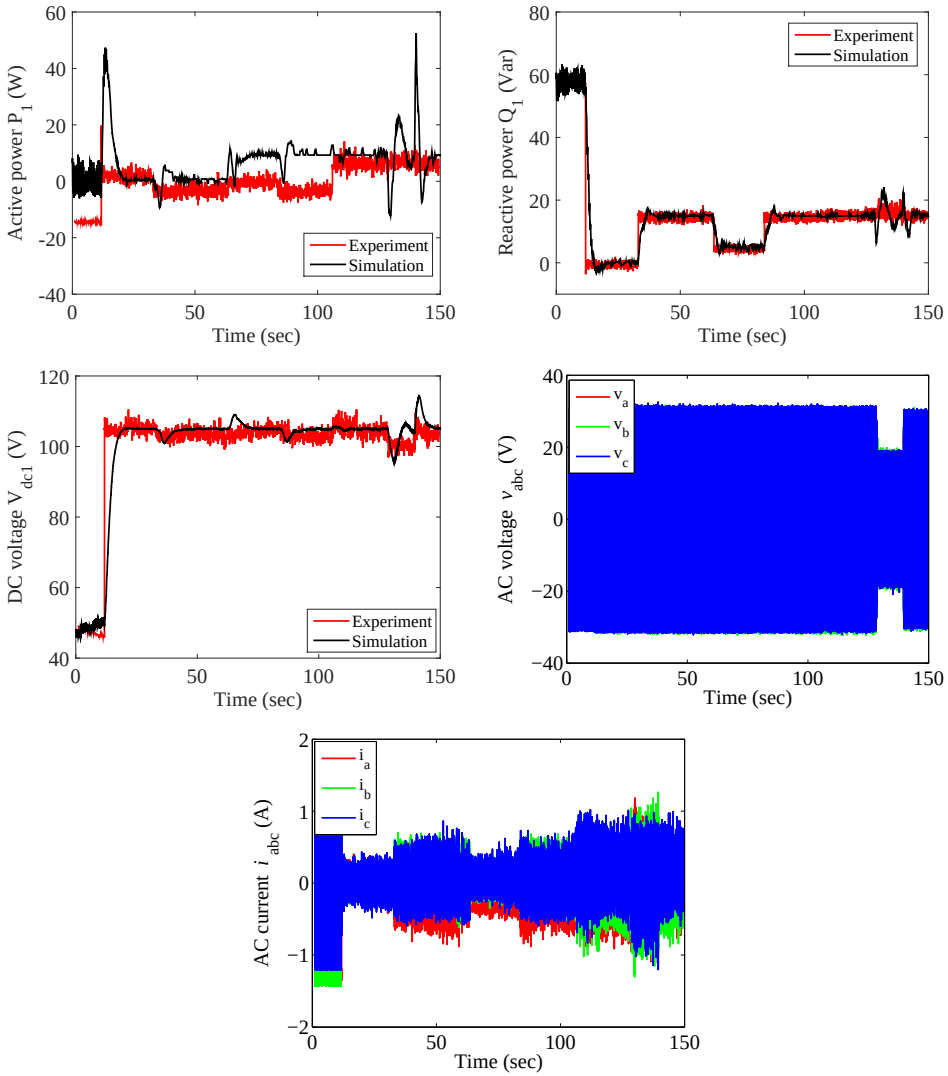

Figure 3.12: Experiment results obtained in case I.

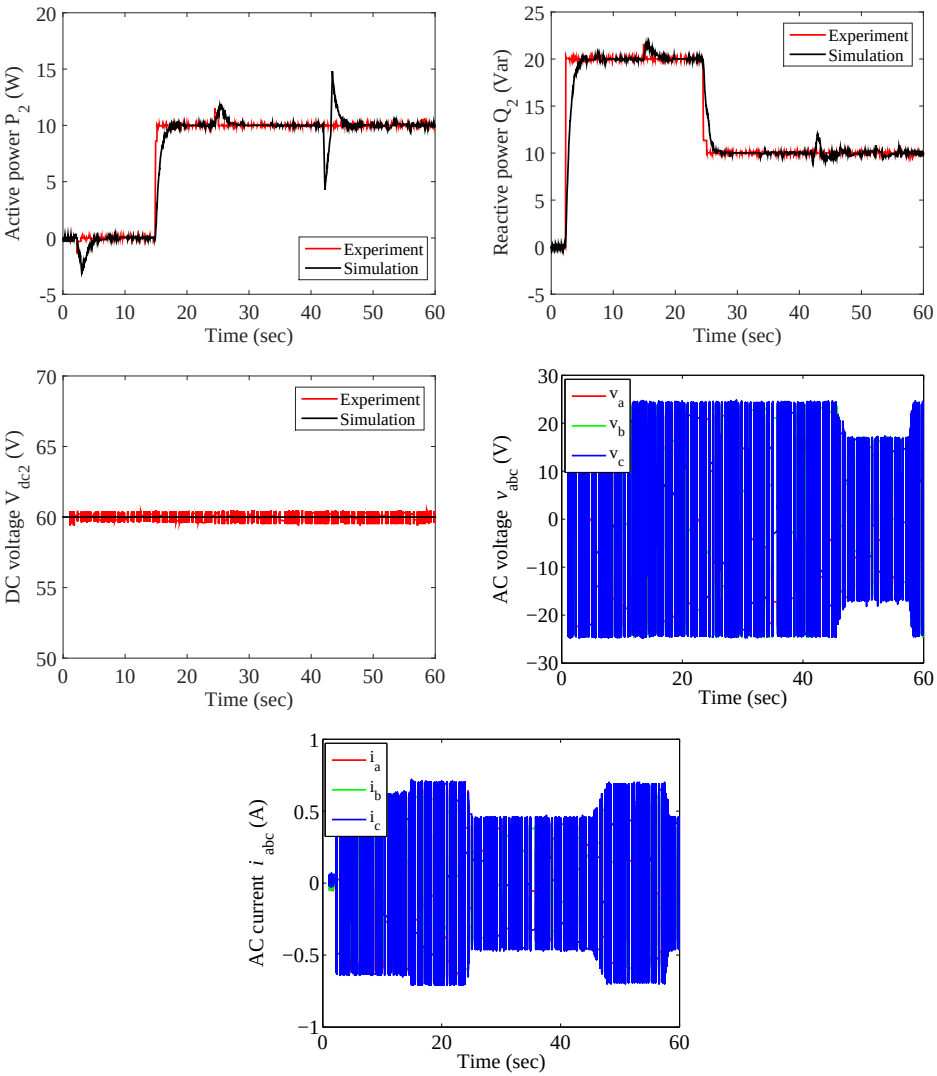

Figure 3.13: Experiment results obtained in case II.

Table 3.5: Control parameters used in the experiment.

Rectifier controller			
Control gains	$k'_{\mathrm{r}1} = 40$	$k_{\mathrm{r}1} = 300$	$k_{\mathrm{r}2} = 30$
	$b_{\mathrm{r}1} = 105$	$b_{\mathrm{r}2} = -3000$	$\lambda_{\mathrm{r}1} = 100$
	$\lambda_{\mathrm{r}2} = 10$		
Observer gains	$\alpha'_{\mathrm{r}1} = 80$	$\alpha'_{\mathrm{r}2} = 1600$	$\alpha_{\mathrm{r}1} = 120$
	$\alpha_{\mathrm{r}2} = 4800$	$\alpha_{\mathrm{r}3} = 6.4 \times 10^4$	$\epsilon = 0.1$
Inverter controller			
Control gains	$k_{\mathrm{i}1} = 15$	$k'_{\mathrm{i}1} = 15$	$b_{\mathrm{i}1} = 100$
	$b_{\mathrm{i}2} = -100$	$\lambda_{\mathrm{i}1} = 5$	$\lambda_{\mathrm{i}2} = 5$
Observer gains	$\alpha_{\mathrm{i}1} = 60$	$\alpha_{\mathrm{i}2} = 900$	$\alpha'_{\mathrm{i}1} = 60$
	$\alpha'_{\mathrm{i}2} = 900$	$\epsilon = 0.1$	

and DC voltage can be rapidly regulated. Note that the initial reactive power Q_1 of the experiment is different from that of the simulation, this is because the initial conditions of the hardware are difficult to acquire, however it is not important as the same initial operating conditions of the simulation and hardware experiment will be achieved after the controller is activated. Compared to the simulation, a relatively small system transient response is found during the AC grid voltage drop, this is due to the slow manual tuning of the AC grid voltage drop compared to the step change used in the simulation. Moreover, the consistent oscillation of system variables in the steady-state is due to the large observer gains (one third-order HGSPO for $V_{\mathrm{dc}1}$ and one second-order HGPO for Q_1), which will amplify the environment noises or measurement errors. However, these oscillations are insignificant (around 5% from the reference value) and are acceptable in real system operation and control.

2) Case II: Inverter controller experiment. The POAPC for inverter is then tested, the initial active and reactive power are set to be zero. In this case DC voltage

V_{dc2} is regulated to be 60 V for the whole period of the experiment by a constant DC power supply. The controller is activated to increase reactive power Q_2 to be 20 Var at first, after reactive power Q_2 is stabilized, active power P_2 is increased to be 10 W, then reactive power Q_2 is decreased to be 10 Var. At last a 33.3% AC grid voltage drop occurs to test the system transient performance.

The experiment results are given in Fig. 3.13, in which the controller is activated at 2 s and the whole experiment lasts for 60 s. Note that the oscillation of system variables is insignificant compared to those of Case I as relatively small observer gains are used (two second-order HGPO for Q_2 and P_2, respectively). It is obvious that P_2 and Q_2 can be independently controlled. Similar to the Case I, a much smaller system transient response can be found when the AC grid voltage drop is applied due to the slow manual tuning.

3.7 Conclusion

This chapter has extended POAPC into general canonical systems, such that it can be applied for two-terminal VSC-HVDC systems. POAPC can provide significant robustness and does not require an accurate system model. Based on the online estimation, only active power P_2, reactive powers Q_1 and Q_2, and DC voltage V_{dc1} need to be measured. Simulation has been carried out based on the complete two-terminal VSC-HVDC system, which demonstrates the effectiveness and robustness of POAPC compared to those of PI control and PC. In order to test the implementation feasibility of POAPC, two separate hardware experiments are undertaken for rectifier controller and inverter controller due to the limit of the experimental facilities. The simulation including the IGBT converter model was firstly carried out to evaluate the effectiveness of the controller, then it is implemented into the dSPACE simulator. Both the active and reactive power tracking, and AC grid voltage drop are tested. The hardware experiment results validate the implementation feasibility.

Chapter 4

Passive Control Design for VSC-MTDC Systems via Energy Shaping

4.1 Introduction

VSC-HVDC system is able to control the active and reactive power independently and supply a passive network. Furthermore, power flow reversal can be realized by reversing DC current direction without reversing DC voltage polarity. There is no need for communications between the converters at each node, and this is an important advantage that can facilitate the creation of VSC-MTDC systems [4, 145], which have the superiority over two-terminal VSC-HVDC systems, in that they can facilitate gradual expansion of distributed networks. Hence the input and output power can be controlled flexibly to increase the total power transmission capacity [18, 21]. The VSC-MTDC system can easily achieve power exchanges among multi-points, connection between multiple asynchronous networks, and integration of scattered power plants like offshore renewable energy sources [27], urban subtransmission [28], oil and gas platforms [29], and premium quality power parks [30]. Recently, the world's first MTDC system employing VSC technology called Nanao's VSC-MTDC project has been built in China [32].

So far, several controllers have been designed for the VSC-MTDC system, such as adaptive parallel multi-PI controller [49], adaptive droop controller [47], and wide area measurement system (WAMS) based controller [146]. However, the stability of the internal dynamics related to DC cable current and common DC voltage remains undiscussed during its design, which may cause an instability issue for the closed-loop system.

PC has been applied to VSC-HVDC systems. In terms of passivity, the power flow of AC networks into VSC-HVDC systems must be greater than or equal to the rate of change of the overall energies in VSC-HVDC systems, which are stored and exchangeable in the energy storage components such as capacitors and inductors [147]. The IDA-PB control has been applied based on the port-controlled Hamiltonian with dissipation (PCHD) model in [42] for a two-terminal VSC-HVDC system, which can provide more system damping than that of FLC [40] as the beneficial system nonlinearities are remained. However, it cannot be extended into VSC-MTDC systems as the internal dynamics cannot be represented and analyzed through the PCHD model.

In this chapter, PC has been developed for an N-terminal VSC-MTDC system. It reshapes the storage function into an output strictly passive form of three controlled states: active power, reactive power, and DC cable voltage, via feedback passivation with an extra system damping. The proposed control partially cancels the system nonlinearities and keeps the beneficial parts, which improves the system damping compared to the exact system nonlinearities cancelation based FLC [40]. Moreover, considering system nonlinearities can provide a consistent control performance under various operating points, compared with PI control [39]. Considering zero-dynamics of the active power, reactive power, and DC cable voltage, the remained internal dynamics related to DC cable current and common DC voltage is proved to be asymptotically stable in the context of Lyapunov criterion. The control performance of PC is evaluated on a four-terminal VSC-MTDC system, in which the tracking performance of active and reactive power is tested at first. Then the enhancement of system transient responses is investigated under faults at AC buses and DC cable, transmission line disconnection and system frequency modulation,

respectively. At last, the robustness to parameter uncertainties, weak AC networks connection, and DC voltage measurement noises is discussed. Simulation results are provided to demonstrate a better control performance of PC over that of FLC and PI control.

4.2 N-terminal VSC-MTDC System Modelling

The mathematical model of an N-terminal VSC-MTDC system is established in the synchronous *dq* frame. A lumped parameter model is assumed and AC network is represented through the series connection of AC network and transmission line, which is interfaced to a VSC at the point of common coupling (PCC) through the transformer. A more detailed VSC model featuring the related switches can be employed but this would only add a slight ripple in the voltage waveforms due to the associated switching action, which does not significantly affect the fundamental dynamics, thus the VSCs are represented by their averaged model [47].

The *dq* frame is placed on AC network terminals. The same PLL used in Chapter 3 is applied during the transformation of the *abc* frame to the *dq* frame. The d-axis is locked with the voltage V_{si} on AC side of the VSCs to ensure a decoupled control of the active and reactive power. Only the balanced condition is considered, i.e., the three phases have identical parameters and their voltages and currents have the same amplitude while each phase shifts 120° between themselves. In addition, it is assumed that the VSC-MTDC system is connected to sufficiently strong AC networks, such that the AC voltage remains as a constant.

One terminal of an N-terminal VSC-MTDC system is illustrated in Fig. 4.1. On AC side of the VSC, the system dynamics can be expressed at the angular frequency ω_i as [47]

$$\begin{cases} \dot{I}_{\mathrm{d}i} = -\frac{R_i}{L_i} I_{\mathrm{d}i} + \omega_i I_{\mathrm{q}i} + \frac{V_{\mathrm{sq}i}}{L_i} + \frac{u_{\mathrm{d}i}}{L_i} \\ \dot{I}_{\mathrm{q}i} = -\frac{R_i}{L_i} I_{\mathrm{q}i} + \omega_i I_{\mathrm{d}i} + \frac{V_{\mathrm{sd}i}}{L_i} + \frac{u_{\mathrm{q}i}}{L_i} \end{cases} \tag{4.2.1}$$

where $I_{\mathrm{d}i}$ and $I_{\mathrm{q}i}$ are the *i*th d-axis and q-axis AC current; $V_{\mathrm{sd}i}$ and $V_{\mathrm{sq}i}$ are the *i*th d-axis and q-axis AC voltage, in the synchronous frame $V_{\mathrm{sd}i} = 0$ and $V_{\mathrm{sq}i} = V_{\mathrm{s}}$; $u_{\mathrm{d}i}$ and $u_{\mathrm{q}i}$ are the *i*th d-axis and q-axis control inputs; R_i and L_i are the *i*th resistance

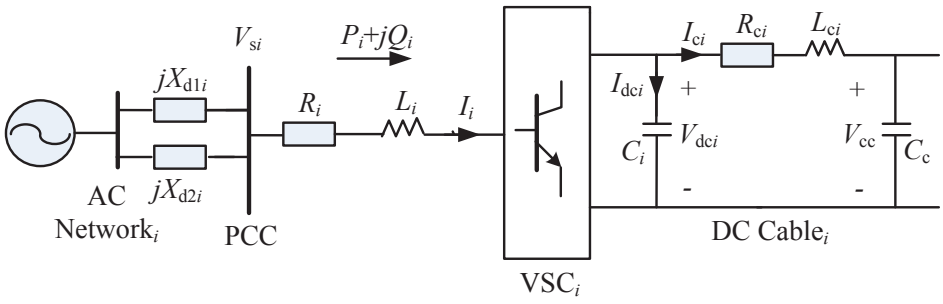

Figure 4.1: One terminal in an N-terminal VSC-MTDC system.

and inductance of the VSC transformer and phase reactor.

By neglecting the resistance of the VSC reactor and switching losses (which is around 2% of the overall power [56]), the active power P_i and reactive power Q_i on the *i*th AC side of the VSC can be calculated as follows [47]

$$\begin{cases} P_i = \frac{3}{2}(V_{\mathrm{sq}i}I_{\mathrm{q}i} + V_{\mathrm{sd}i}I_{\mathrm{d}i}) = \frac{3}{2}V_{\mathrm{sq}i}I_{\mathrm{q}i} \\ Q_i = \frac{3}{2}(V_{\mathrm{sq}i}I_{\mathrm{d}i} - V_{\mathrm{sd}i}I_{\mathrm{q}i}) = \frac{3}{2}V_{\mathrm{sq}i}I_{\mathrm{d}i} \end{cases} \tag{4.2.2}$$

DC cable dynamics can be expressed by [47]

$$\begin{cases} \dot{V}_{\mathrm{dc}i} = \frac{1}{V_{\mathrm{dc}i}C_i}P_i - \frac{1}{C_i}I_{\mathrm{c}i} \\ \dot{I}_{\mathrm{c}i} = \frac{1}{L_{\mathrm{c}i}}V_{\mathrm{dc}i} - \frac{R_{\mathrm{c}i}}{L_{\mathrm{c}i}}I_{\mathrm{c}i} - \frac{1}{L_{\mathrm{c}i}}V_{\mathrm{cc}} \end{cases} \tag{4.2.3}$$

where C_i and C_{c} are the *i*th and common DC capacitance which voltages are denoted by $V_{\mathrm{dc}i}$ and V_{cc}, respectively; $R_{\mathrm{c}i}$ and $L_{\mathrm{c}i}$ are the resistance and inductance of the *i*th DC cable; and $I_{\mathrm{c}i}$ is the current through the *i*th DC cable. The featured DC cable model corresponds to a simplified equivalent of a cable connection, because an inductive element could be presented for an overhead line. This is a reasonable approximation for the purpose of control systems analysis [47].

The topology of an N-terminal VSC-MTDC system is illustrated by Fig. 4.2 [49], the dynamics of the common DC capacitor can be obtained according to the Kirchhoff's current law as

$$\dot{V}_{\mathrm{cc}} = \frac{1}{C_{\mathrm{c}}}\sum_{i=1}^{N} I_{\mathrm{c}i} \tag{4.2.4}$$

To this end, the global model of the N-terminal VSC-MTDC system is written as

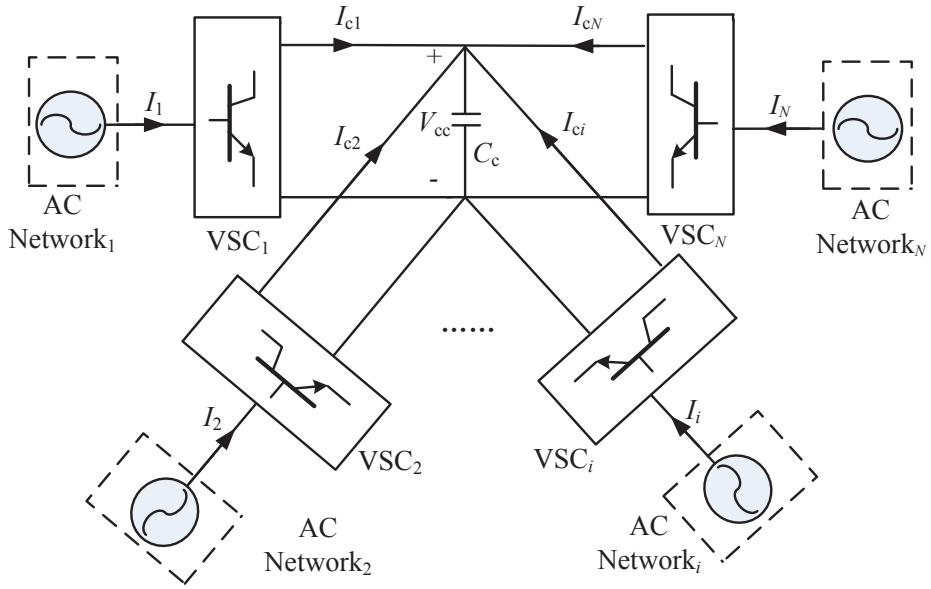

Figure 4.2: The topology of an N-terminal VSC-MTDC system.

follows

$$\begin{cases} \dot{I}_{\mathrm{d}i} = -\frac{R_i}{L_i} I_{\mathrm{d}i} + \omega_i I_{\mathrm{q}i} + \frac{V_{\mathrm{sq}i}}{L_i} + \frac{u_{\mathrm{d}i}}{L_i} \\ \dot{I}_{\mathrm{q}i} = -\frac{R_i}{L_i} I_{\mathrm{q}i} + \omega_i I_{\mathrm{d}i} + \frac{u_{\mathrm{q}i}}{L_i} \\ \dot{V}_{\mathrm{dc}i} = \frac{3V_{\mathrm{sq}i} I_{\mathrm{q}i}}{2V_{\mathrm{dc}i} C_i} - \frac{1}{C_i} I_{\mathrm{c}i} \qquad , i = 1, \ldots, N \\ \dot{I}_{\mathrm{c}i} = \frac{1}{L_{\mathrm{c}i}} V_{\mathrm{dc}i} - \frac{R_{\mathrm{c}i}}{L_{\mathrm{c}i}} I_{\mathrm{c}i} - \frac{1}{L_{\mathrm{c}i}} V_{\mathrm{cc}} \\ \dot{V}_{\mathrm{cc}} = \frac{1}{C_{\mathrm{c}}} \sum_{i=1}^{N} I_{\mathrm{c}i} \end{cases} \tag{4.2.5}$$

The dimension of system (4.2.5) is $4N + 1$ and the equations are not changed in the transient process. In general, each VSC has a local controller to independently control its reactive power injection in AC networks, and the whole system is coordinated by a master controller, which aims to generate the current for system loads, and coordinates the overall current during the abnormal situations such as AC or DC faults [49]. In this control mode, one VSC connected to AC networks operates with DC voltage control, namely single-point DC voltage control, such that DC voltage can be regulated at its reference level. All other VSCs control the active power so as to ensure a proper power sharing [47].

4.3 PC Design for N-terminal VSC-MTDC System

The basic concepts and theorems of PC are given in Appendix. The control objectives are to send the required active and reactive power through DC cable and maintain DC voltages at their reference values. Furthermore, the control scheme should be implemented as independent controllers for each VSC.

4.3.1 Rectifier controller design

For system (4.2.5), denote the jth VSC as the rectifier such that DC voltage $V_{\mathrm{dc}j}$ and reactive power Q_j can be regulated to their reference values $V^*_{\mathrm{dc}j}$ and Q^*_j, respectively. Define the tracking error $e_j = [e_{j1}, e_{j2}]^{\mathrm{T}} = [V_{\mathrm{dc}j} - V^*_{\mathrm{dc}j}, Q_j - Q^*_j]^{\mathrm{T}}$, and differentiate e_j until control inputs $u_{\mathrm{q}j}$ and $u_{\mathrm{d}j}$ appear explicitly, gives

$$\begin{cases} \ddot{e}_{j1} = \frac{3V_{\mathrm{sq}j}}{2C_jV_{\mathrm{dc}j}}\Big[-\frac{R_j}{L_j}I_{\mathrm{q}j} + \omega_j I_{\mathrm{d}j} - \frac{I_{\mathrm{q}j}}{C_jV_{\mathrm{dc}j}}\Big(\frac{3V_{\mathrm{sq}j}I_{\mathrm{q}j}}{2V_{\mathrm{dc}j}} - I_{\mathrm{c}j}\Big)\Big] \\ \quad -\frac{1}{C_jL_{\mathrm{c}j}}(V_{\mathrm{dc}j} - R_{\mathrm{c}j}I_{\mathrm{c}j} - V_{\mathrm{cc}}) + \frac{3V_{\mathrm{sq}j}}{2C_jL_jV_{\mathrm{dc}j}}u_{\mathrm{q}j} - \ddot{V}^*_{\mathrm{dc}j} \\ \dot{e}_{j2} = \frac{3V_{\mathrm{sq}j}}{2}\Big(-\frac{R_j}{L_j}I_{\mathrm{d}j} + \omega_j I_{\mathrm{q}j} + \frac{V_{\mathrm{sq}j}}{L_j}\Big) + \frac{3V_{\mathrm{sq}j}}{2L_j}u_{\mathrm{d}j} - \dot{Q}^*_j \end{cases} \tag{4.3.1}$$

Construct a storage function of system (4.3.1) as follows

$$H_j(V_{\mathrm{dc}j}, I_{\mathrm{dc}j}, Q_j) = \frac{1}{2}(V_{\mathrm{dc}j} - V^*_{\mathrm{dc}j})^2 + \frac{1}{2C_j^2}(I_{\mathrm{dc}j} - I^*_{\mathrm{dc}j})^2 + \frac{1}{2}(Q_j - Q^*_j)^2 \tag{4.3.2}$$

where $I_{\mathrm{dc}j}$ and $I^*_{\mathrm{dc}j}$ are the current through capacitor C_j and its reference value, respectively, with $I^*_{\mathrm{dc}j} = C_j\frac{\mathrm{d}V_{\mathrm{dc}j}}{\mathrm{d}t}|_{V_{\mathrm{dc}j}=V^*_{\mathrm{dc}j}}$.

H_j includes the quadratic sum of the voltage and current of the jth DC capacitor and the reactive power in the jth AC network. Differentiate H_j with respect to the

time, yields

$$\begin{aligned}\dot{H}_j &= \frac{1}{C_j}(V_{\mathrm{dc}j}-V^*_{\mathrm{dc}j})(I_{\mathrm{dc}j}-I^*_{\mathrm{dc}j})+\frac{1}{C_j}(I_{\mathrm{dc}j}-I^*_{\mathrm{dc}j})(\ddot{V}_{\mathrm{dc}j}-\ddot{V}^*_{\mathrm{dc}j})\\ &\quad+(Q_j-Q^*_j)(\dot{Q}_j-\dot{Q}^*_j)\\ &= \frac{1}{C_j}(I_{\mathrm{dc}j}-I^*_{\mathrm{dc}j})\Big\{(V_{\mathrm{dc}j}-V^*_{\mathrm{dc}j})+\frac{3V_{\mathrm{sq}j}}{2C_jV_{\mathrm{dc}j}}\Big[-\frac{R_j}{L_j}I_{\mathrm{q}j}+\omega_jI_{\mathrm{d}j}\\ &\quad-\frac{I_{\mathrm{q}j}}{C_jV_{\mathrm{dc}j}}\Big(\frac{3V_{\mathrm{sq}j}I_{\mathrm{q}j}}{2V_{\mathrm{dc}j}}-I_{\mathrm{c}j}\Big)\Big]-\frac{1}{C_jL_{\mathrm{c}j}}(V_{\mathrm{dc}j}-R_{\mathrm{c}j}I_{\mathrm{c}j}-V_{\mathrm{cc}})\\ &\quad+\frac{3V_{\mathrm{sq}j}}{2C_jL_jV_{\mathrm{dc}j}}u_{\mathrm{q}j}-\ddot{V}^*_{\mathrm{dc}j}\Big\}+(Q_j-Q^*_j)\\ &\quad\times\Big[\frac{3V_{\mathrm{sq}j}}{2}\left(-\frac{R_j}{L_j}I_{\mathrm{d}j}+\omega_jI_{\mathrm{q}j}+\frac{V_{\mathrm{sq}j}}{L_j}\right)+\frac{3V_{\mathrm{sq}j}}{2L_j}u_{\mathrm{d}j}-\dot{Q}^*_j\Big]\end{aligned}\tag{4.3.3}$$

Design the rectifier controller for system (4.3.1) as

$$\begin{cases}u_{\mathrm{q}j}=\frac{2C_jL_jV_{\mathrm{dc}j}}{3V_{\mathrm{sq}j}}\Big\{-(V_{\mathrm{dc}j}-V^*_{\mathrm{dc}j})+\frac{1}{C_jV_{\mathrm{dc}j}}\Big[\frac{R_j}{L_j}P_j-\omega_jQ_j+\frac{P_j}{C_jV_{\mathrm{dc}j}}\Big(\frac{P_j}{V_{\mathrm{dc}j}}-I_{\mathrm{c}j}\Big)\Big]\\ \quad+\frac{1}{C_jL_{\mathrm{c}j}}(V_{\mathrm{dc}j}-R_{\mathrm{c}j}I_{\mathrm{c}j}-V_{\mathrm{cc}})+\ddot{V}^*_{\mathrm{dc}j}+\nu_{j1}\Big\}\\ u_{\mathrm{d}j}=\frac{2L_j}{3V_{\mathrm{sq}j}}\Big[-\omega_jP_j-\frac{3V^2_{\mathrm{sq}j}}{2L_j}+\frac{R_j}{L_j}Q^*_j+\dot{Q}^*_j+\nu_{j2}\Big]\end{cases}\tag{4.3.4}$$

where $V_j=[\nu_{j1},\nu_{j2}]^{\mathrm{T}}$ is the additional input.

Choose the output of system (4.3.1) as $Y_j=[Y_{j1},Y_{j2}]^{\mathrm{T}}=[(I_{\mathrm{dc}j}-I^*_{\mathrm{dc}j})/C_j,Q_j-Q^*_j]^{\mathrm{T}}$. Let $V_j=[-\lambda_{j1}Y_{j1},-\lambda_{j2}Y_{j2}]^{\mathrm{T}}$, where λ_{j1} and λ_{j2} are some positive constants for the feedback passivation to inject an extra system damping in $I_{\mathrm{dc}j}$ and Q_j. Substitute control (4.3.4) into (4.3.3) and use (4.2.2), obtains

$$\begin{aligned}\dot{H}_j &= \frac{1}{C_j}(I_{\mathrm{dc}j}-I^*_{\mathrm{dc}j})\nu_{j1}+(Q_j-Q^*_j)\Big(-\frac{R_j}{L_j}(Q_j-Q^*_j)+\nu_{j2}\Big)\\ &= \nu_{j1}Y_{j1}+\nu_{j2}Y_{j2}-\frac{R_j}{L_j}Y^2_{j2}\\ &= -\lambda_{j1}Y^2_{j1}-(\lambda_{j2}+\frac{R_j}{L_j})Y^2_{j2}\le 0\end{aligned}\tag{4.3.5}$$

It can be easily verified that the uncontrolled system is zero-state detectable. According to the passivity theory, system (4.3.1) is output strictly passive from output Y_j to input V_j. From power-current relationship (4.2.2) and DC dynamics (4.2.3), $I_{\mathrm{d}j}$, $I_{\mathrm{q}j}$, and $V_{\mathrm{dc}j}$ can be asymptotically stabilized to their reference values $I^*_{\mathrm{d}j}$, $I^*_{\mathrm{q}j}$, and $V^*_{\mathrm{dc}j}$. According to system (4.2.5), once DC voltage $V_{\mathrm{dc}j}$ is regulated to its refer-

ence value, all DC voltages $V_{\mathrm{dc}i}$ will be simultaneously regulated to their reference values.

4.3.2 Inverter controller design

The kth VSC is chosen as the inverter to regulate active power P_k and reactive power Q_k to their reference values P_k^* and Q_k^*, respectively, where $k = 1, \cdots, N$ and $k \neq j$. Define the tracking error $e_k = [e_{k1}, e_{k2}]^{\mathrm{T}} = [P_k - P_k^*, Q_k - Q_k^*]^{\mathrm{T}}$, and differentiate e_k until control inputs $u_{\mathrm{q}k}$ and $u_{\mathrm{d}k}$ appear explicitly, gives

$$\begin{cases} \dot{e}_{k1} = \frac{3V_{\mathrm{sq}k}}{2}\left(-\frac{R_k}{L_k}I_{\mathrm{q}k} - \omega_k I_{\mathrm{d}k}\right) + \frac{3V_{\mathrm{sq}k}}{2L_k}u_{\mathrm{q}k} - \dot{P}_k^* \\ \dot{e}_{k2} = \frac{3V_{\mathrm{sq}k}}{2}\left(-\frac{R_k}{L_k}I_{\mathrm{d}k} + \omega_k I_{\mathrm{q}k} + \frac{V_{\mathrm{sq}k}}{L_k}\right) + \frac{3V_{\mathrm{sq}k}}{2L_k}u_{\mathrm{d}k} - \dot{Q}_k^* \end{cases} \tag{4.3.6}$$

Construct a storage function of system (4.3.6) as follows

$$H_k(P_k, Q_k) = \frac{1}{2}(P_k - P_k^*)^2 + \frac{1}{2}(Q_k - Q_k^*)^2 \tag{4.3.7}$$

H_k includes the quadratic sum of the active and reactive power in the kth AC network. Differentiate H_k with respect to the time, yields

$$\begin{aligned} \dot{H}_k &= (P_k - P_k^*)(\dot{P}_k - \dot{P}_k^*) + (Q_k - Q_k^*)(\dot{Q}_k - \dot{Q}_k^*) \\ &= (P_k - P_k^*)\Big[\frac{3V_{\mathrm{sq}k}}{2}\left(-\frac{R_k}{L_k}I_{\mathrm{q}k} - \omega_k I_{\mathrm{d}k}\right) + \frac{3V_{\mathrm{sq}k}}{2L_k}u_{\mathrm{q}k} - \dot{P}_k^*\Big] \\ &+ (Q_k - Q_k^*)\Big[\frac{3V_{\mathrm{sq}k}}{2}\left(-\frac{R_k}{L_k}I_{\mathrm{d}k} + \omega_k I_{\mathrm{q}k} + \frac{V_{\mathrm{sq}k}}{L_k}\right) + \frac{3V_{\mathrm{sq}k}}{2L_k}u_{\mathrm{d}k} - \dot{Q}_k^*\Big] \end{aligned} \tag{4.3.8}$$

Design the inverter controller for system (4.3.6) as

$$\begin{cases} u_{\mathrm{q}k} = \frac{2L_k}{3V_{\mathrm{sq}k}}\left(\omega_k Q_k + \frac{R_k}{L_k}P_k^* + \dot{P}_k^* + \nu_{k1}\right) \\ u_{\mathrm{d}k} = \frac{2L_k}{3V_{\mathrm{sq}k}}\left(-\omega_k P_k - \frac{3V_{\mathrm{sq}k}^2}{2L_k} + \frac{R_k}{L_k}Q_k^* + \dot{Q}_k^* + \nu_{k2}\right) \end{cases} \tag{4.3.9}$$

where $V_k = [\nu_{k1}, \nu_{k2}]^{\mathrm{T}}$ is the additional input. Choose the output of system (4.3.6) as $Y_k = [Y_{k1}, Y_{k2}]^{\mathrm{T}} = [P_k - P_k^*, Q_k - Q_k^*]^{\mathrm{T}}$. Let $V_k = [-\lambda_{k1}Y_{k1}, -\lambda_{k2}Y_{k2}]^{\mathrm{T}}$, where λ_{k1} and λ_{k2} are some positive constants for the feedback passivation to inject an extra system damping in P_k and Q_k. Substitute control (4.3.9) into (4.3.8) and use

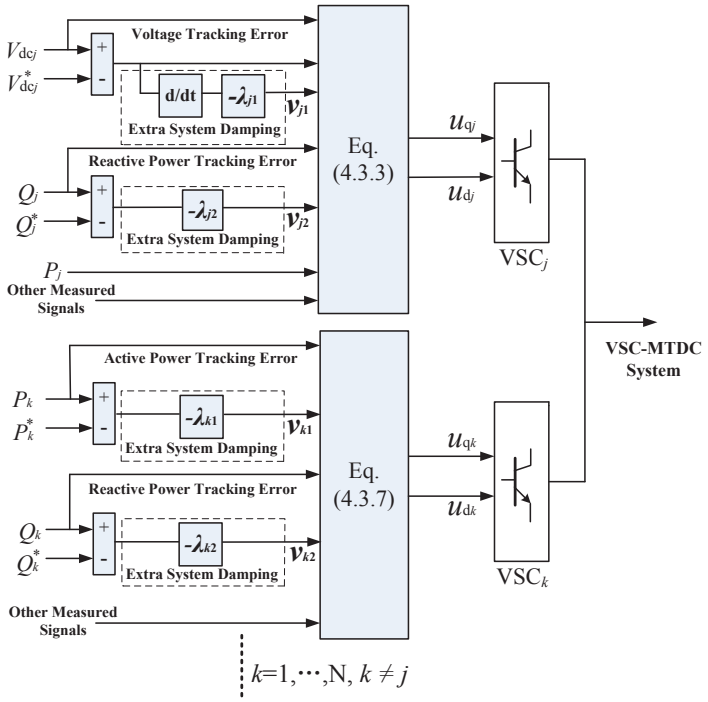

Figure 4.3: Structure of PC for the VSC-MTDC system.

(4.2.2), yields

$$\begin{aligned}\dot{H}_k &= (P_k - P_k^*)\left(-\frac{R_k}{L_k}(P_k - P_k^*) + \nu_{k1}\right) + (Q_k - Q_k^*)\left(-\frac{R_k}{L_k}(Q_k - Q_k^*) + \nu_{k2}\right) \\ &= \nu_{k1}Y_{k1} + \nu_{k2}Y_{k2} - \frac{R_k}{L_k}Y_{k1}^2 - \frac{R_k}{L_k}Y_{k2}^2 \\ &= -(\lambda_{k1} + \frac{R_k}{L_k})Y_{k1}^2 - (\lambda_{k2} + \frac{R_k}{L_k})Y_{k2}^2 \leq 0 \end{aligned} \tag{4.3.10}$$

Similarly, system (4.3.6) is output strictly passive from output Y_k to input V_k. Thus $I_{\mathrm{d}k}$, $I_{\mathrm{q}k}$, and $V_{\mathrm{dc}k}$ can be asymptotically stabilized to their reference values $I^*_{\mathrm{d}k}$, $I^*_{\mathrm{q}k}$, and $V^*_{\mathrm{dc}k}$.

To this end, inequalities (4.3.5) and (4.3.10) indicate that systems (4.3.1) and (4.3.6) can be asymptotically stabilized to the desired equilibrium point as the energy fluctuations converge to zero. The overall storage function H_{t} of the N-terminal VSC-MTDC system (4.2.5) can be expressed in the following form

$$H_{\mathrm{t}} = H_j(V_{\mathrm{dc}j}, I_{\mathrm{dc}j}, Q_j) + \sum_{k=1, k\neq j}^{N} H_k(P_k, Q_k) \tag{4.3.11}$$

The structure of PC can be illustrated by Fig. 4.3. DC cable voltage $V_{\mathrm{dc}j}$ and reactive power Q_j are regulated by rectifier controller (4.3.4), while active power P_k and reactive power Q_k are regulated by inverter controller (4.3.9).

4.3.3 Internal dynamics stability

Under controllers (4.3.4) and (4.3.9), the dynamics of the active power P_i, reactive power Q_i, and DC cable voltage $V_{\mathrm{dc}i}$ can be asymptotically stabilized, which has a dimension of $3N$. Now the remained internal dynamics is related to DC cable current I_{ci} and common DC voltage V_{cc}, which has a dimension of $N+1$. The effectiveness of the proposed control cannot be guaranteed unless the asymptotic stability of the internal dynamics is proved.

The zero-dynamics describes those internal dynamics which are consistent with the external constraints equal to zero, it is a powerful technique to analyze the stability of internal dynamics. To simplify the analysis, shift the reference values of the overall system to the origin and the following new state vector is introduced as $\tilde{x} = [\tilde{I}_{\mathrm{d}i}, \tilde{I}_{\mathrm{q}i}, \tilde{V}_{\mathrm{dc}i}, \tilde{I}_{ci}, \tilde{V}_{\mathrm{cc}}]^{\mathrm{T}}$. where $\tilde{x}_i = x_i - x_i^*$ is denoted as the estimation error of x_i and x_i^* is its reference value, respectively.

Theorem 4.1. *Under controllers (4.3.4) and (4.3.9), the internal dynamics of VSC-MTDC system (4.2.5) is asymptotically stable.*

Proof. System (4.2.5) can be expressed in terms of the new states as

$$\begin{cases} \dot{\tilde{I}}_{\mathrm{d}i} = -\frac{R_i}{L_i}\tilde{I}_{\mathrm{d}i} + \omega_i \tilde{I}_{\mathrm{q}i} + \frac{\tilde{u}_{\mathrm{d}i}}{L_i} \\ \dot{\tilde{I}}_{\mathrm{q}i} = -\frac{R_i}{L_i}\tilde{I}_{\mathrm{q}i} + \omega_i \tilde{I}_{\mathrm{d}i} + \frac{\tilde{u}_{\mathrm{q}i}}{L_i} \\ \dot{\tilde{V}}_{\mathrm{dc}i} = \frac{3V_{\mathrm{sq}i}I_{\mathrm{q}i}}{2V_{\mathrm{dc}i}C_i} - \frac{3V_{\mathrm{sq}i}I^*_{\mathrm{q}i}}{2V^*_{\mathrm{dc}i}C_i} - \frac{1}{C_i}\tilde{I}_{ci} \quad , i = 1, \ldots, N \\ \dot{\tilde{I}}_{ci} = \frac{1}{L_{ci}}\tilde{V}_{\mathrm{dc}i} - \frac{R_{ci}}{L_{ci}}\tilde{I}_{ci} - \frac{1}{L_{ci}}\tilde{V}_{\mathrm{cc}} \\ \dot{\tilde{V}}_{\mathrm{cc}} = \frac{1}{C_{\mathrm{c}}}\sum_{i=1}^{N}\tilde{I}_{ci} \end{cases} \tag{4.3.12}$$

Divide the state vector $\tilde{x}$ into two parts as the output $\eta = [\tilde{I}_{\mathrm{d}i}, \tilde{I}_{\mathrm{q}i}, \tilde{V}_{\mathrm{dc}i}]^{\mathrm{T}}$ and internal state $\xi = [\tilde{I}_{ci}, \tilde{V}_{\mathrm{cc}}]^{\mathrm{T}}$. Now system (4.3.12) can be considered as the normal form [73]

$$\begin{cases} \dot{\eta} = f_1(\eta, \xi, u) \\ \dot{\xi} = f_2(\eta, \xi) \end{cases} \tag{4.3.13}$$

with

$$u = f_3(\eta, \xi) \tag{4.3.14}$$

When output η is identically zero, the behaviour of system (4.3.13) is governed by the differential equation

$$\dot{\xi} = f_2(0, \xi) \tag{4.3.15}$$

which is the zero-dynamics of system (4.3.13).

Based on the previous analysis and power-current relationship (4.2.2), it has been proved that $\tilde{V}_{\mathrm{dc}i}$, $\tilde{I}_{\mathrm{d}i}$, and $\tilde{I}_{\mathrm{q}i}$ are asymptotically stable by controllers (4.3.4) and (4.3.9). It remains now to investigate the behaviour of internal state ξ when η converges to zero. Substitute $\eta = 0$, ξ is governed by the following differential equation

$$[\dot{\tilde{I}}_{\mathrm{c}1}, \dot{\tilde{I}}_{\mathrm{c}2}, \ldots, \dot{\tilde{I}}_{\mathrm{c}N}, \dot{\tilde{V}}_{\mathrm{cc}}]^{\mathrm{T}} = A[\tilde{I}_{\mathrm{c}1}, \tilde{I}_{\mathrm{c}2}, \ldots, \tilde{I}_{\mathrm{c}N}, \tilde{V}_{\mathrm{cc}}]^{\mathrm{T}} \tag{4.3.16}$$

where

$$A = \begin{bmatrix} -\frac{R_{\mathrm{c}1}}{L_{\mathrm{c}1}} & 0 & \cdots & 0 & -\frac{1}{L_{\mathrm{c}1}} \\ 0 & -\frac{R_{\mathrm{c}2}}{L_{\mathrm{c}2}} & \cdots & 0 & -\frac{1}{L_{\mathrm{c}2}} \\ \vdots & \vdots & \ddots & \vdots & \vdots \\ 0 & 0 & \cdots & -\frac{R_{\mathrm{c}N}}{L_{\mathrm{c}N}} & -\frac{1}{L_{\mathrm{c}N}} \\ \frac{1}{C_{\mathrm{c}}} & \frac{1}{C_{\mathrm{c}}} & \cdots & \frac{1}{C_{\mathrm{c}}} & 0 \end{bmatrix}_{(N+1)\times(N+1)} \tag{4.3.17}$$

Thus, the zero-dynamics of system (4.3.12) becomes

$$\dot{\xi} = A\xi \tag{4.3.18}$$

To study the stability of zero-dynamics (4.3.18), choose a Lyapunov function as

$$V(\tilde{I}_{\mathrm{c}i}, \tilde{V}_{\mathrm{cc}}) = \sum_{i=1}^{N} \frac{L_{\mathrm{c}i}}{2C_{\mathrm{c}}} \tilde{I}_{\mathrm{c}i}^2 + \frac{1}{2}\tilde{V}_{\mathrm{cc}}^2 \tag{4.3.19}$$

The derivative of V along system (4.3.18) is given by

$$\begin{aligned}\dot{V} &= \sum_{i=1}^{N} \frac{L_{ci}}{C_{\rm c}} \tilde{I}_{ci} \dot{\tilde{I}}_{ci} + \tilde{V}_{\rm cc} \dot{\tilde{V}}_{\rm cc} \\ &= \sum_{i=1}^{N} \frac{L_{ci}}{C_{\rm c}} \tilde{I}_{ci} \left(-\frac{R_{ci}}{L_{ci}} \tilde{I}_{ci} - \frac{1}{L_{ci}} \tilde{V}_{\rm cc} \right) + \frac{\tilde{V}_{\rm cc}}{C_{\rm c}} \sum_{i=1}^{N} \tilde{I}_{ci} \\ &= -\sum_{i=1}^{N} \frac{R_{ci}}{C_{\rm c}} \tilde{I}_{ci}^2 \leq 0 \end{aligned} \tag{4.3.20}$$

It is obvious that $\dot{V}$ is negative semi-definite as $R_{ci} > 0$ and $C_{\rm c} > 0$. To find the neighbourhood of origin $\mathcal{S} = \{\xi \in \mathbb{R}^{N+1} | \dot{V}(\xi) = 0\}$, note that

$$\dot{V}(\xi) = 0 \Rightarrow \tilde{I}_{ci} = 0, i = 1, \ldots, N \tag{4.3.21}$$

Thus $\mathcal{S} = \{\xi \in \mathbb{R}^{N+1} | \tilde{I}_{ci} = 0, i = 1, \ldots, N\}$. Let ξ be a solution that belongs identically to $\mathcal{S}$ as

$$\tilde{I}_{ci} \equiv 0 \Rightarrow \dot{\tilde{I}}_{ci} \equiv 0 \Rightarrow \tilde{V}_{\rm cc} \equiv 0 \tag{4.3.22}$$

Obviously, the only solution that can stay identically in $\mathcal{S}$ is the trivial solution $\xi \equiv 0$. According to LaSalle's theorem and its corollary [73], the zero-dynamics of system (4.3.12) is asymptotically stable.

Therefore, under controllers (4.3.4) and (4.3.9), the internal dynamics of VSC-MTDC system (4.2.5) is asymptotically stable. □

4.4 Case Studies

Passive control (PC) is applied on a four-terminal VSC-MTDC system illustrated by Fig. 4.4, in which VSC_1 is chosen as the rectifier to regulate DC voltage and reactive power, while the other three VSCs are chosen as the inverters to independently control their active and reactive power. The system frequency of AC network_4 is 60 Hz, and the others are 50 Hz. The system parameters are given in Table 4.1. The control performance of PC is evaluated under various operating conditions in a wide neighbourhood of the initial operating points, that is, a power reversal

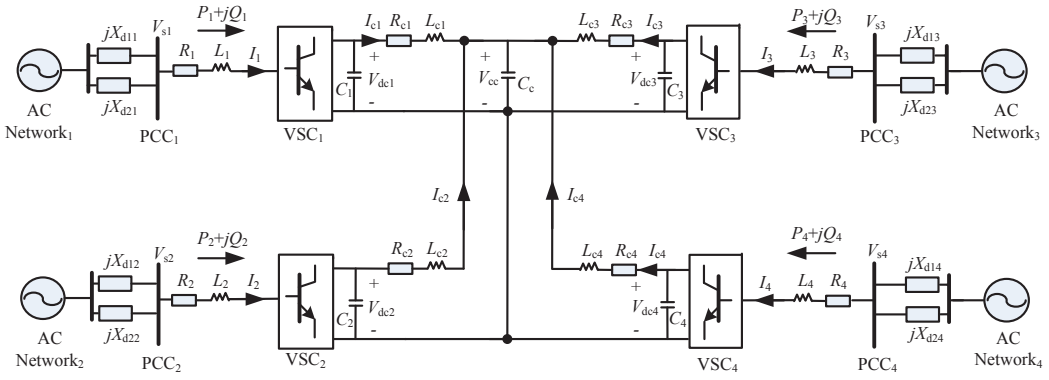

Figure 4.4: A four-terminal VSC-MTDC system.

ranging from -0.4 p.u. to 0.4 p.u., and compared to that of proportional-integral (PI) [39] and feedback linearization control (FLC) [40]. Note that the full cancelation of system nonlinearities of FLC may cancel some beneficial system nonlinearites, which decrease the system damping.

Table 4.1: System parameters used in the four-terminal VSC-MTDC system.

Base power	S_{base}=100 MVA
AC base voltage	V_{ACbase}=100 kV
DC base voltage	V_{DCbase}=200 kV
AC system resistance (25 km)	$R_i = 0.05$ Ω/km
AC system inductance (25 km)	$L_i = 0.026$ mH/km
DC cable resistance (50 km)	$R_{ci} = 0.16$ Ω/km
DC cable inductance (50 km)	$L_{\text{c}i} = 0.076$ mH/km
DC link capacitance	$C_i = 7.96$ μF
Common DC capacitance	$C_{\text{c}} = 19.95$ μF

PC parameters are chosen as: For VSC_1 rectifier controller: $\lambda_{11} = 105$, $\lambda_{12} = 75$; For VSC_k inverter controller: $\lambda_{k1} = \lambda_{k2} = 75$, where $k = 2, 3, 4$; The control

inputs are bounded as $|u_{\mathrm{q}i}| \leq 1$ p.u., $|u_{\mathrm{d}i}| \leq 1$ p.u., where $i = 1, \ldots, 4$.

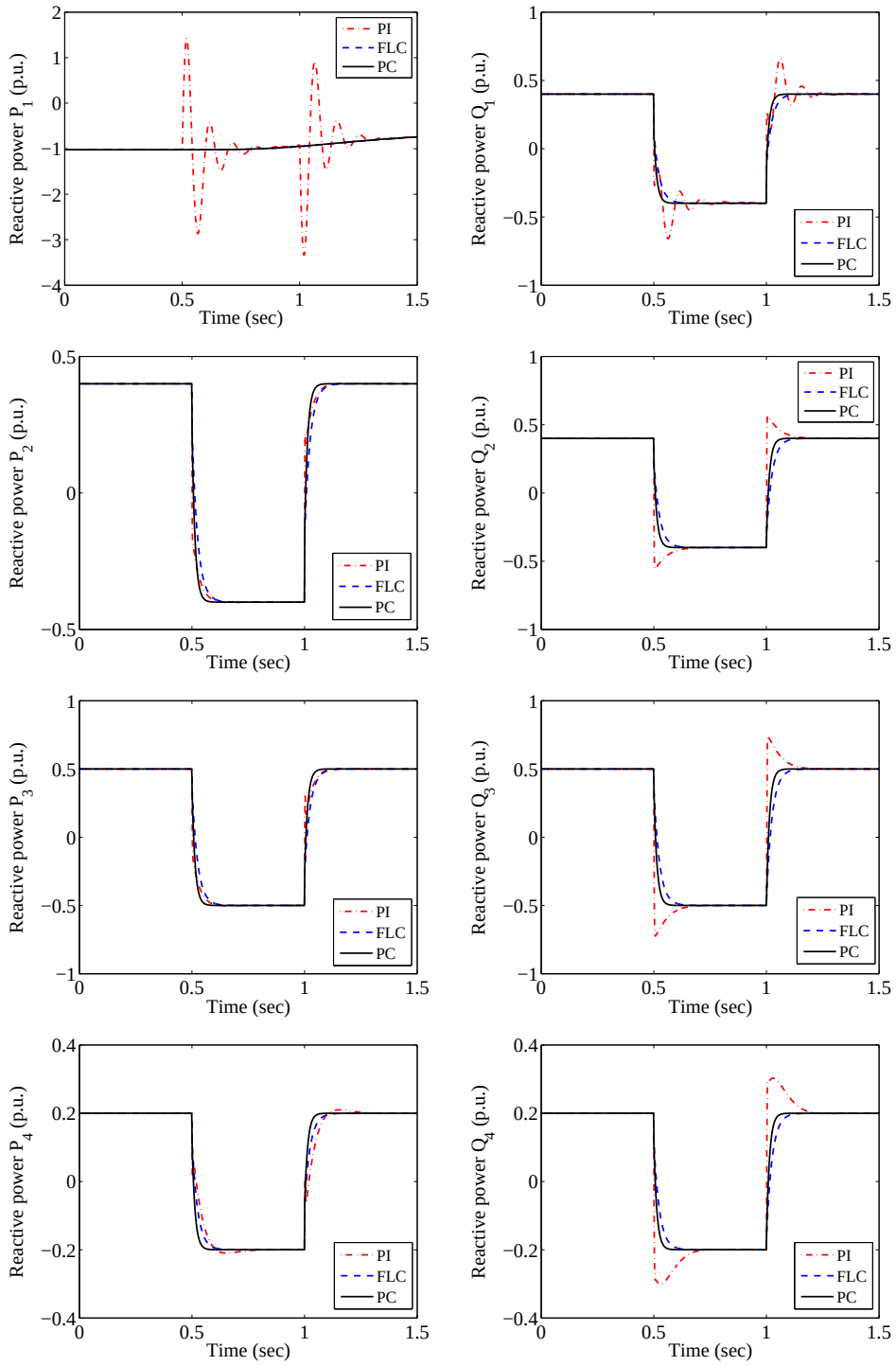

Figure 4.5: System responses obtained in active and reactive power tracking.

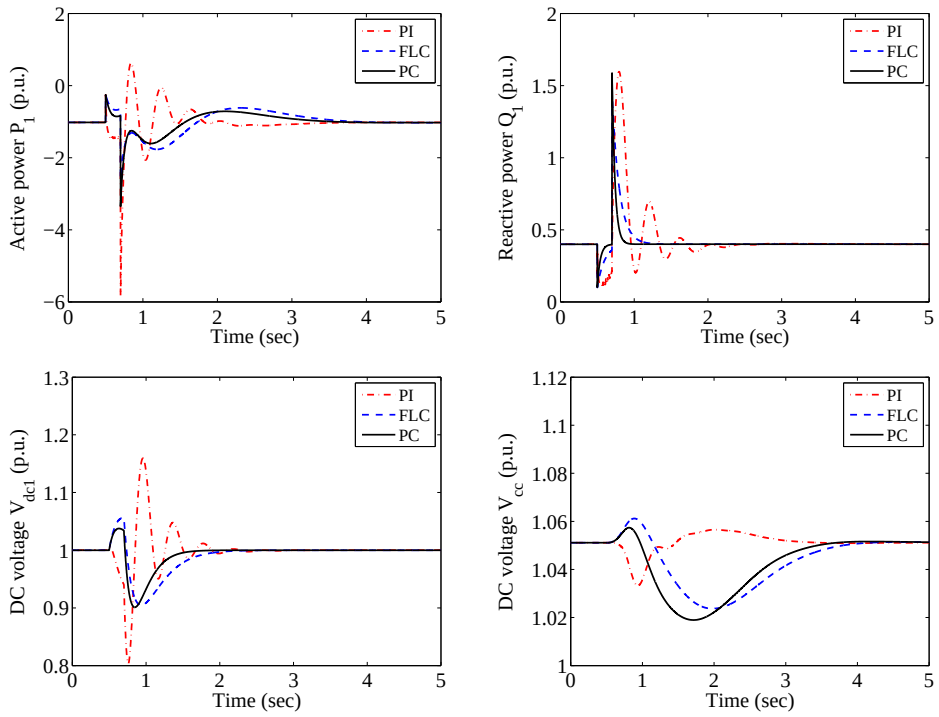

Figure 4.6: System responses obtained under a 10-cycle LLLG fault at bus 1.

1) Case 1: Active and reactive power tracking. An active and reactive power tracking started at $t = 0.5$ s and restored to the original value at $t = 1$ s has been tested, while DC voltage is regulated at its rated value. The system responses are provided by Fig. 4.5. One can find that the overshoot of active and reactive power is completely eliminated by PC and FLC compared to PI control. In addition, PC tracks the reference values more rapidly than that of FLC as it remains the beneficial system nonlinearities instead of the full system nonlinearities cancelation. Note that PI control performance is degraded dramatically under varied operating points as its control parameters are tuned based on one operating point.

2) Case 2: 10-cycle line-line-line-ground (LLLG) fault at AC buses. A 10-cycle LLLG fault occurs at bus 1 from 0.5 s to 0.7 s. Due to the fault, AC voltage at the corresponding bus is decreased to a critical level. Fig. 4.6 shows that PC can effectively restore the system with less active power oscillations. Note that the system damping marginally improves along with the reduction in overshoot and settling time, less overshoot is very important as it avoids the saturation of the VSC currents.

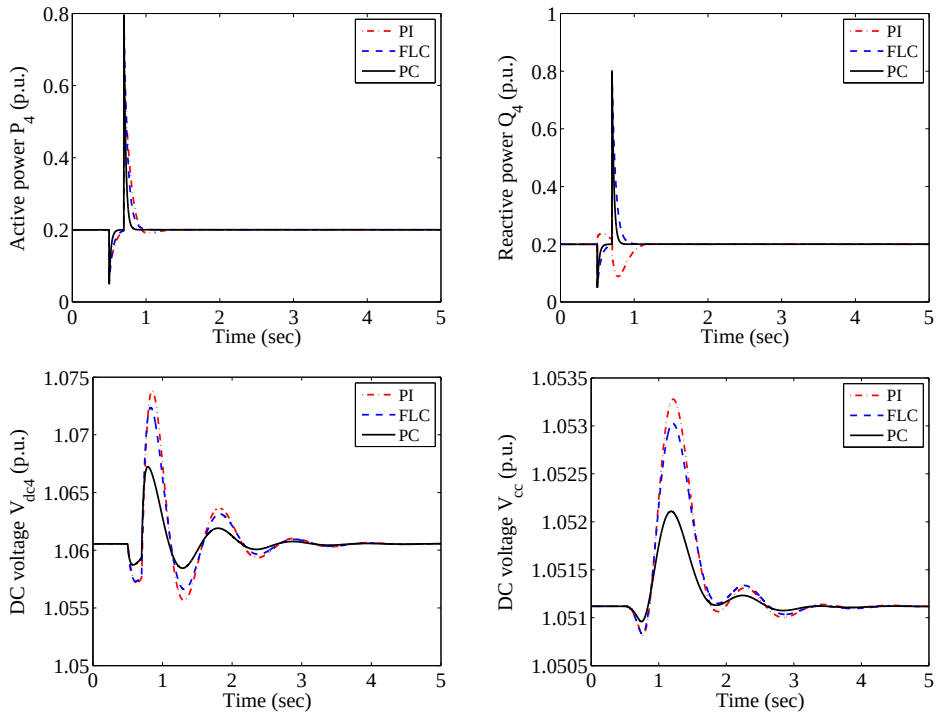

Figure 4.7: System responses obtained under a 10-cycle LLLG fault at bus 4.

Due to the large undershoot of AC voltage, instantaneous demand of reactive power Q_1 increases and a spike appears expectedly. To reduce the spike, the control gain of PC needs to be readjusted but the settling time of DC voltage V_{dc1} will be increased, thus a compromise between the overshoot of the reactive power and the settling time of DC voltage must be made. With the same operating condition, the same fault is simulated at bus 4, where the system frequency is 60 Hz thus the fault lasts from 0.5 s to 0.667 s. Similarly, Fig. 4.7 demonstrates PC can improve the system damping and restore the system more effectively than PI control and FLC.

The overall storage function during the LLLG fault at AC buses is illustrated in Fig. 4.8. A dramatic system energy increase can be found, which is resulted from the immediate AC bus voltage variation at the instant when the fault occurs. As the system has been reshaped into the output strictly passive form, the overall storage function will asymptotically converge to zero after the fault.

3) Case 3: Transmission line disconnection on AC networks. One of the two parallel transmission lines connected to AC network$_1$ and AC network$_4$ is removed

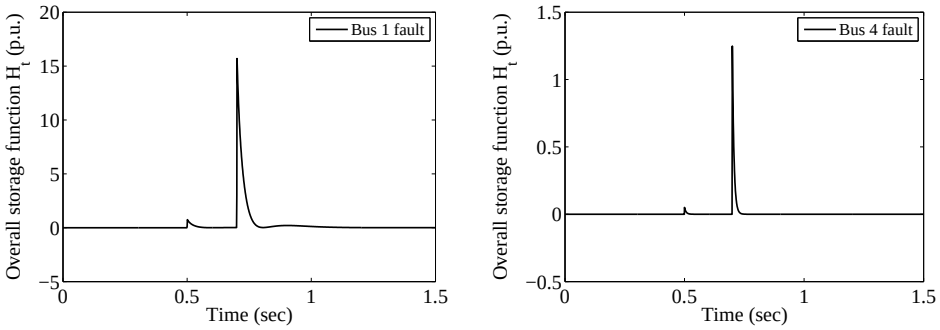

Figure 4.8: The overall storage function obtained under a 10-cycle LLLG fault at bus 1 and bus 4.

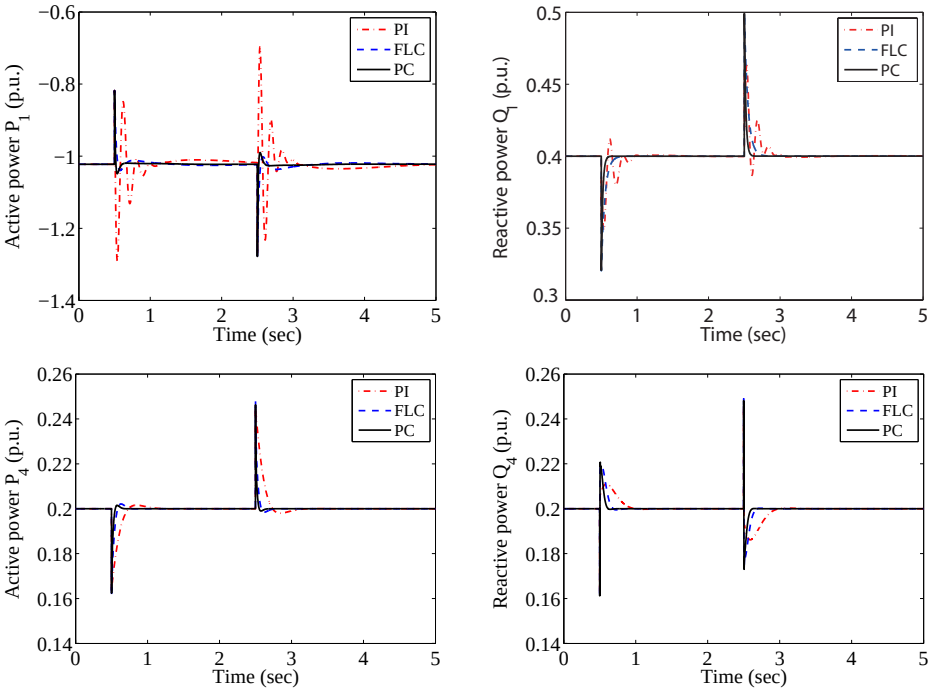

Figure 4.9: System responses obtained under a transmission line disconnection of AC network$_1$ and AC network$_4$.

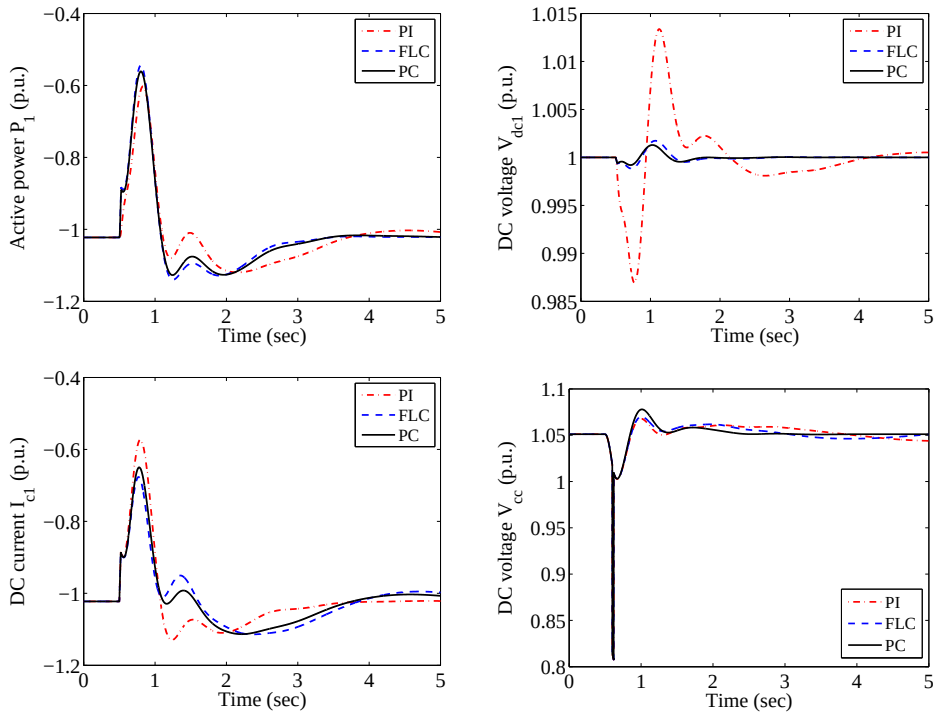

Figure 4.10: System responses obtained in a temporary DC cable$_1$ fault.

from the operation at 0.5 s and again reconnected at 2.5 s. The control performance of the three approaches is presented by Fig. 4.9, which shows that PC can stabilize the system with the fastest rate.

4) Case 4: Temporary fault at DC cable. A 2 ms temporary short-circuit fault occurs at the midpoint of DC cable$_1$ at $t = 0.5$ s and removed automatically thereafter, in which every terminal maintains operating. The DC fault will cause a voltage drop in DC cable and generate a significant transient fault current which may exceed the VSC rated power [152]. Fig. 4.10 illustrates the corresponding system responses, it can be found that active power P_1 and DC voltage V_{dc1} can be restored more rapidly and smoothly by PC. Moreover, it can reduce the possibility of VSC overloading when DC fault occurs as less fault current I_{c1} is produced in comparison to that of FLC and PI control, thus the system stability can be enhanced.

5) Case 5: Modulated change in the angular frequency. Fig. 4.11 depicts the system responses when a 2% change occurs in the angular frequency for 2 s at AC network$_1$ and AC network$_4$, respectively. Due to the change in the system frequency,

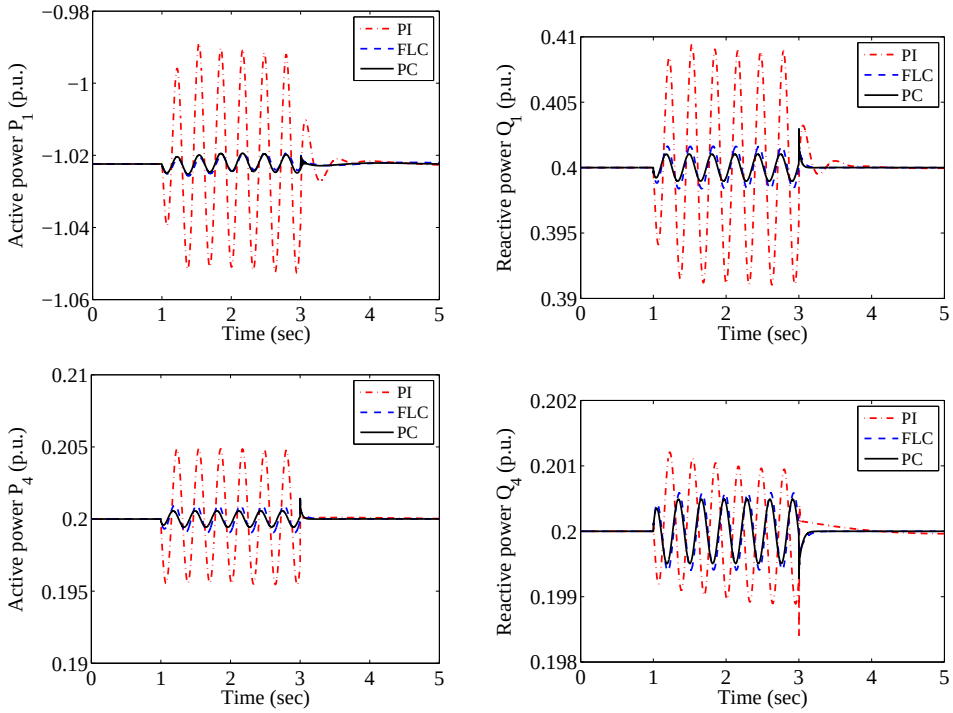

Figure 4.11: System responses obtained when a modulated change occurs in the angular frequency.

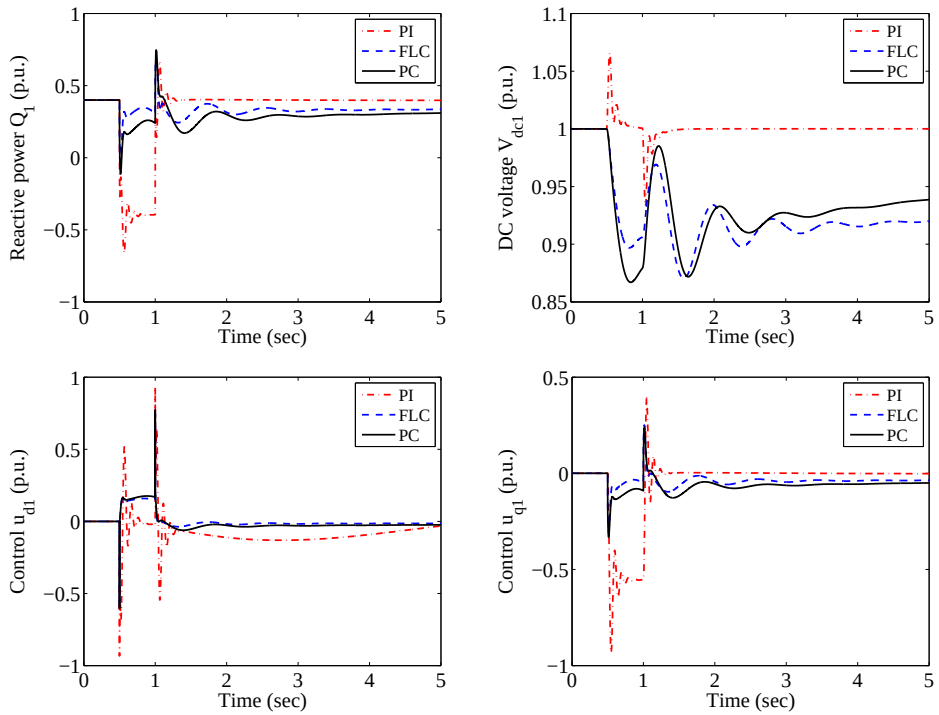

Figure 4.12: System responses obtained under a 20% decrease of the system resistances and inductances.

both active and reactive power are disturbed, which can be stabilized by PC more effectively in comparison to that of FLC and PI control.

6) Case 6: Uncertainties in the system resistances and inductances. The robustness of the three approaches are evaluated by reducing AC network resistance R_i and inductance L_i, DC cable resistance $R_{\mathrm{c}i}$ and inductance $L_{\mathrm{c}i}$ by 20% from their nominal values. The same reactive power tracking used in Case 1 is tested with DC voltage regulated to its rate value. System responses are provided in Fig. 4.12, it can be seen that the control performance of FLC and PC degrades dramatically as they need an accurate system model. In contrast, PI control remains a satisfactory control performance as its control parameters do not depend on system parameters.

7) Case 7: Weak AC networks connection. The AC networks are assumed to be sufficiently strong such that voltage $V_{\mathrm{s}i}$ is an ideal constant. It is worth considering a weak AC network connected to the VSC-MTDC system, e.g., offshore wind farms, where voltage $V_{\mathrm{s}i}$ becomes a time-varying function. AC network$_1$ and AC network$_4$

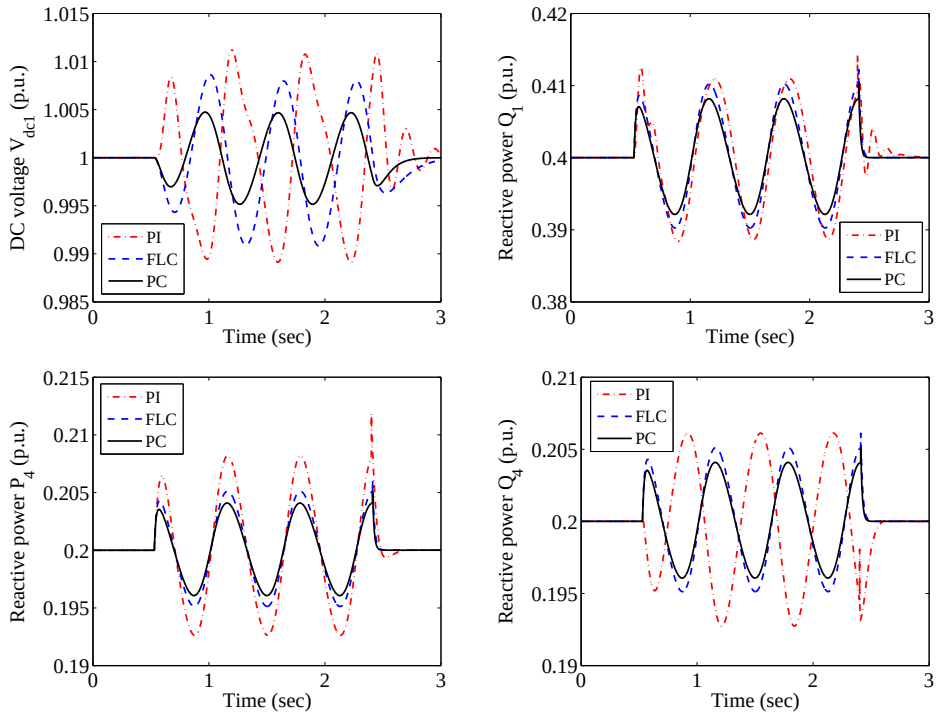

Figure 4.13: System responses obtained when weak AC networks are connected.

are modelled as offshore wind farms to investigate the control performance to weak AC networks connection, a voltage disturbance occurs from 0.5 s to 2.5 s caused by the wind speed variation is simulated, with $V_{s1} = V_{s4} = 1 + 0.15\sin(0.2\pi t)$. System responses are illustrated in Fig. 4.13, it shows that both active and reactive power are oscillatory, in which PC has the smallest oscillation magnitude of the system variables.

8) Case 8: Robustness to DC voltage measurement noises. A 1% white noise of the rated DC voltage $V^*_{dc1} = 1$ p.u. is applied to mimic the effect of measurement noises or exogenous unmeasured disturbances. A second-order low-pass filter with a cut-off frequency $f_c = 20$ Hz is used to filter out such noise. A reactive power tracking starts at 0.2 s and ends at 0.7 s are applied. The system responses are shown by Fig. 4.14, a significant chattering of Q_1 and V_{dc1} of FLC and PC, with and without the filter, can be observed which control performance is degraded dramatically resulted from the requirement of exact DC voltage measurement. The low-pass filter can effectively attenuate such chattering such that a reliable control performance

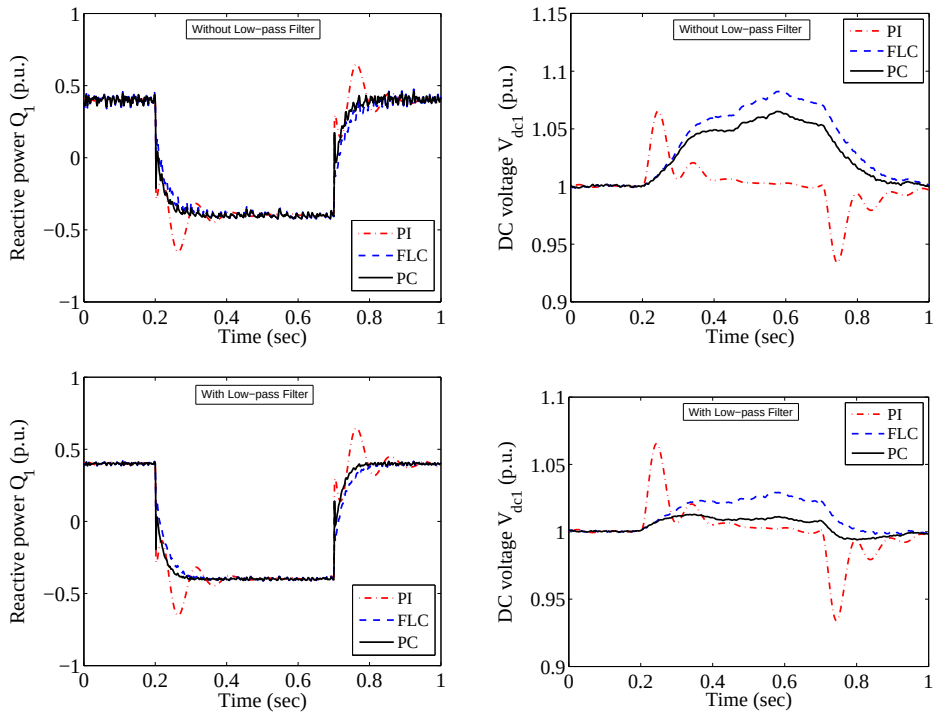

Figure 4.14: System responses obtained with DC voltage measurement noises.

can be maintained.

4.5 Conclusion

In this chapter, PC has been developed for an N-terminal VSC-MTDC system. The storage function is reshaped into an output strictly passive form, in which the beneficial system nonlinearities are remained to provide a better transient performance of active power, reactive power, and DC voltage. Then the closed-loop system stability has been proved to be asymptotically stable by the zero-dynamics technique.

Case studies have been carried out on a four-terminal VSC-MTDC system, a comparison has been done with PI control and FLC. The tracking performance of active and reactive power is tested at first, where a typical power tracking is used, which demonstrates that PC can achieve a rapid power tracking and eliminate the overshoot. Then the system transient responses are evaluated under AC buses fault,

transmission line disconnection, temporary DC cable fault, and system frequency modulation. Finally, robustness is discussed in the presence of parameter uncertainties, weak AC networks connection, and DC voltage measurement noises. Simulation results show that PC can restore the disturbed system more effectively than FLC as it remains the beneficial system nonlinearites, it can also maintain a consistent control performance under different system operating points. In addition, the fault current of PC is minimal, thus it can reduce the possibility of VSC overloading. One obvious drawback of PC is that it requires the accurate measurements of many system variables and parameters, which is not robust to any parameter uncertainties. Hence, the POAPC will be applied to tackle this issue in the next chapter.

Chapter 5

Perturbation Observer based Adaptive Passive Control for VSC-MTDC Systems

5.1 Introduction

The VSC-HVDC systems are highly nonlinear resulted from the converters and also operate in power systems with various system uncertainties, which make it difficult to accurately model the power system equipped with VSC-HVDC systems. Thus, adaptive control design for the VSC-HVDC systems is desperately needed. One particular issue of the VSC-HVDC control design is how to effectively handle system uncertainties. Parameter estimation based approaches are developed to estimate uncertain system parameters, such as adaptive backstepping [40] and multivariable optimal control [155]. However, their control performance will be degraded when other modelling uncertainties exist. A robust FLSMC is developed by [46], which is insensitive to both parameter uncertainties and time-varying external disturbances. However, the above methods are only designed for two-terminal VSC-HVDC systems.

In this chapter, POAPC scheme is designed for the same VSC-MTDC system used in Chapter 4, in which the combinatorial effect of system nonlinearities, pa-

rameter uncertainties, unmodelled dynamics and time-varying external disturbances is aggregated into a perturbation, which is estimated online by the HGSPO and HGPO. POAPC does not require an accurate system model and only the DC voltage, active and reactive power need to be measured. Once it is set up for the VSC-MTDC system within a predetermined range of variation in system variables, no tuning is needed for start-up or compensation of changes in the system dynamics and disturbance. Moreover, the proposed controller can improve the system damping via passivation [101, 103, 104], hence it is able to reduce the overshoot of active and reactive power for different operating conditions as the system nonlinearities are partially removed (the beneficial ones are remained only). The control performance of POAPC is evaluated on a four-terminal VSC-MTDC system, in which the tracking performance of active and reactive power is evaluated at first. Then the enhancement of system transient responses is discussed under faults at AC buses and DC cable, transmission line disconnection and system frequency modulation, respectively. Finally, the robustness to parameter uncertainties, weak AC networks connection, and DC voltage measurement noises will be studied. Simulation results are provided to demonstrate its superiority over PI control and PC, note that the parameters used in PI control is not optimized thus the conclusion may not be universal.

5.2 POAPC Design for N-terminal VSC-MTDC System

5.2.1 Rectifier controller design

Denote the jth VSC as the rectifier such that DC voltage $V_{\mathrm{dc}j}$ and reactive power Q_j can be regulated to their reference values $V_{\mathrm{dc}j}^*$ and Q_j^*, respectively. Define the tracking error $e_j = [e_{j1}, e_{j2}]^{\mathrm{T}} = [V_{\mathrm{dc}j} - V_{\mathrm{dc}j}^*, Q_j - Q_j^*]^{\mathrm{T}}$, and differentiate e_j until

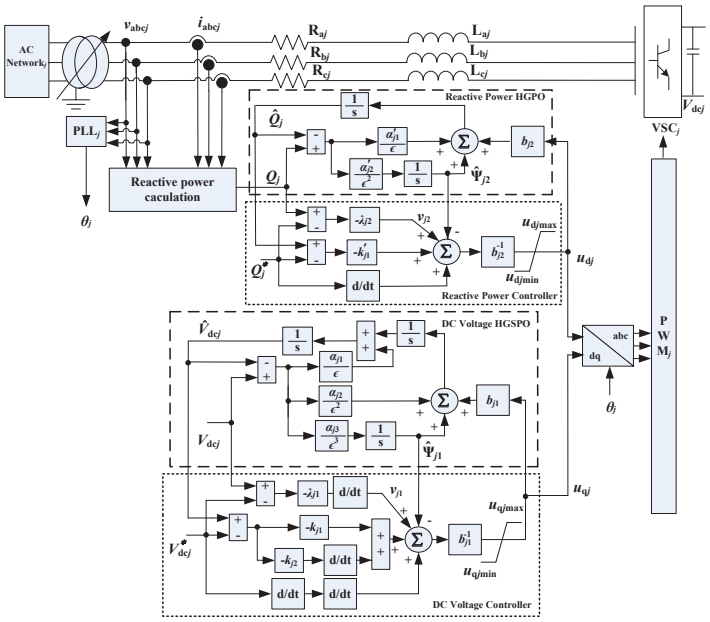

Figure 5.1: Structure of the rectifier controller in VSC-MTDC systems.

control inputs $u_{\mathrm{q}j}$ and $u_{\mathrm{d}j}$ appear explicitly as

$$\begin{cases} \ddot{e}_{j1} = \frac{3V_{\mathrm{sq}j}}{2C_jV_{\mathrm{dc}j}}\Big[-\frac{R_j}{L_j}I_{\mathrm{q}j}+\omega_jI_{\mathrm{d}j}-\frac{I_{\mathrm{q}j}}{C_jV_{\mathrm{dc}j}}\Big(\frac{3V_{\mathrm{sq}j}I_{\mathrm{q}j}}{2V_{\mathrm{dc}j}}-I_{\mathrm{c}j}\Big)\Big] \\ \quad -\frac{1}{C_jL_{\mathrm{c}j}}(V_{\mathrm{dc}j}-R_{\mathrm{c}j}I_{\mathrm{c}j}-V_{\mathrm{cc}})+\frac{3V_{\mathrm{sq}j}}{2C_jL_jV_{\mathrm{dc}j}}u_{\mathrm{q}j}-\ddot{V}_{\mathrm{dc}j}^* \\ \dot{e}_{j2} = \frac{3V_{\mathrm{sq}j}}{2}\left(-\frac{R_j}{L_j}I_{\mathrm{d}j}+\omega_jI_{\mathrm{q}j}+\frac{V_{\mathrm{sq}j}}{L_j}\right)+\frac{3V_{\mathrm{sq}j}}{2L_j}u_{\mathrm{d}j}-\dot{Q}_j^* \end{cases} \tag{5.2.1}$$

The perturbations of system (5.2.1) are defined as

$$\begin{aligned} \Psi_{j1}(\cdot) &= \frac{3V_{\mathrm{sq}j}}{2C_jV_{\mathrm{dc}j}}\Big[-\frac{R_j}{L_j}I_{\mathrm{q}j}+\omega_jI_{\mathrm{d}j}-\frac{I_{\mathrm{q}j}}{C_jV_{\mathrm{dc}j}}\Big(\frac{3V_{\mathrm{sq}j}I_{\mathrm{q}j}}{2V_{\mathrm{dc}j}}-I_{\mathrm{c}j}\Big)\Big] \\ &\quad -\frac{1}{C_jL_{\mathrm{c}j}}(V_{\mathrm{dc}j}-R_{\mathrm{c}j}I_{\mathrm{c}j}-V_{\mathrm{cc}})+(\frac{3V_{\mathrm{sq}j}}{2C_jL_jV_{\mathrm{dc}j}}-b_{j1})u_{\mathrm{q}j} \qquad (5.2.2) \\ \Psi_{j2}(\cdot) &= \frac{3V_{\mathrm{sq}j}}{2}\left(-\frac{R_j}{L_j}I_{\mathrm{d}j}+\omega_jI_{\mathrm{q}j}+\frac{V_{\mathrm{sq}j}}{L_j}\right)+(\frac{3V_{\mathrm{sq}j}}{2L_j}-b_{j2})u_{\mathrm{d}j} \qquad (5.2.3) \end{aligned}$$

And system (5.2.1) can be expressed by

$$\begin{cases} \ddot{e}_{j1} = \Psi_{j1}(\cdot)+b_{j1}u_{\mathrm{q}j}-\ddot{V}_{\mathrm{dc}j}^* \\ \dot{e}_{j2} = \Psi_{j2}(\cdot)+b_{j2}u_{\mathrm{d}j}-\dot{Q}_j^* \end{cases} \tag{5.2.4}$$

where b_{j1} and b_{j2} are constant control gains.

Define $z_{j1} = V_{\mathrm{dc}j}$ and $z_{j2} = \dot{z}_{j1}$, a third-order HGSPO is designed as

$$\begin{cases} \dot{\hat{z}}_{j1} = \hat{z}_{j2} + \frac{\alpha_{j1}}{\epsilon}(z_{j1} - \hat{z}_{j1}) \\ \dot{\hat{z}}_{j2} = \hat{\Psi}_{j1}(\cdot) + \frac{\alpha_{j2}}{\epsilon^2}(z_{j1} - \hat{z}_{j1}) + b_{j1}u_{\mathrm{q}j} \\ \dot{\hat{\Psi}}_{j1}(\cdot) = \frac{\alpha_{j3}}{\epsilon^3}(z_{j1} - \hat{z}_{j1}) \end{cases} \tag{5.2.5}$$

where α_{j1}, α_{j2}, and α_{j3} are positive observer gains, with $0 < \epsilon \ll 1$.

Define $z'_{j1} = Q_j$, a second-order HGPO is designed as

$$\begin{cases} \dot{\hat{z}}'_{j1} = \hat{\Psi}_{j2}(\cdot) + \frac{\alpha'_{j1}}{\epsilon}(z'_{j1} - \hat{z}'_{j1}) + b_{j2}u_{\mathrm{d}j} \\ \dot{\hat{\Psi}}_{j2}(\cdot) = \frac{\alpha'_{j2}}{\epsilon^2}(z'_{j1} - \hat{z}'_{j1}) \end{cases} \tag{5.2.6}$$

where α'_{j1} and α'_{j2} are positive observer gains.

The POAPC for system (5.2.1) using the estimates of perturbation is designed as

$$\begin{cases} u_{\mathrm{q}j} &= b_{j1}^{-1}[-\hat{\Psi}_{j1}(\cdot) - k_{j1}(\hat{z}_{j1} - V^*_{\mathrm{dc}j}) - k_{j2}(\hat{z}_{j2} - \dot{V}^*_{\mathrm{dc}j}) + \ddot{V}^*_{\mathrm{dc}j} + \nu_{j1}] \\ u_{\mathrm{d}j} &= b_{j2}^{-1}(-\hat{\Psi}_{j2}(\cdot) - k'_{j1}(\hat{z}'_{j1} - Q^*_j) + \dot{Q}^*_j + \nu_{j2}) \end{cases} \tag{5.2.7}$$

where k_{j1}, k_{j2} and k'_{j1} are the feedback control gains; $V_j = [\nu_{j1}, \nu_{j2}]^{\mathrm{T}}$ is the additional input.

Note that $\dot{V}_{\mathrm{dc}j} = I_{\mathrm{dc}j}/C_j$, choose the output of system (5.2.1) as $Y_j = [Y_{j1}, Y_{j2}]^{\mathrm{T}} = [\dot{V}_{\mathrm{dc}j} - \dot{V}^*_{\mathrm{dc}j}, Q_j - Q^*_j]^{\mathrm{T}}$. Then let $V_j = [-\lambda_{j1}Y_{j1}, -\lambda_{j2}Y_{j2}]^{\mathrm{T}}$, where λ_{j1} and λ_{j2} are some positive constants to inject an extra system damping into system (5.2.1). Hence the closed-loop system is output strictly passive from output Y_j to input V_j.

Constants b_{j1} and b_{j2} are chosen to satisfy following inequalities when the rectifier operates within its normal region:

$$3V_{\mathrm{sq}j}/[2C_jL_jV_{\mathrm{dc}j}(1-\theta_{j1})] \geq b_{j1} \geq 3V_{\mathrm{sq}j}/[2C_jL_jV_{\mathrm{dc}j}(1+\theta_{j1})] \tag{5.2.8}$$

$$3V_{\mathrm{sq}j}/[2L_j(1-\theta_{j2})] \geq b_{j2} \geq 3V_{\mathrm{sq}j}/[2L_j(1+\theta_{j2})] \tag{5.2.9}$$

where $\theta_{j1} < 1$ and $\theta_{j2} < 1$ are positive constants. In addition, during the most severe disturbance, both the DC voltage and reactive power reduce from their initial values to around zero within a short period of time Δ. Thus the boundary values of the estimated states can be obtained as $|\hat{z}_{j1}| \leq |V^*_{\mathrm{dc}j}|$, $|\hat{z}_{j2}| \leq |V^*_{\mathrm{dc}j}|/\Delta$, $|\hat{\Psi}_{j1}(\cdot)| \leq |V^*_{\mathrm{dc}j}|/\Delta^2$, $|\hat{z}'_{j1}| \leq |Q^*_j|$, and $|\hat{\Psi}_{j2}(\cdot)| \leq |Q^*_j|/\Delta$, respectively.

The structure of rectifier controller is illustrated by Fig. 5.1, in which only the measurement of DC voltage $V_{\mathrm{dc}j}$ and reactive power Q_j is needed for the controller and observer design.

5.2.2 Inverter controller design

The kth VSC is chosen as the inverter to regulate active power P_k and reactive power Q_k to their reference values P_k^* and Q_k^*, respectively, where $k = 1, \cdots, N$ and $k \neq j$. Define the tracking error $e_k = [e_{k1}, e_{k2}]^{\mathrm{T}} = [P_k - P_k^*, Q_k - Q_k^*]^{\mathrm{T}}$, and differentiate e_k until control inputs $u_{\mathrm{q}k}$ and $u_{\mathrm{d}k}$ appear explicitly as

$$\begin{cases} \dot{e}_{k1} = \frac{3V_{\mathrm{sq}k}}{2}\left(-\frac{R_k}{L_k}I_{\mathrm{q}k} - \omega_k I_{\mathrm{d}k}\right) + \frac{3V_{\mathrm{sq}k}}{2L_k}u_{\mathrm{q}k} - \dot{P}_k^* \\ \dot{e}_{k2} = \frac{3V_{\mathrm{sq}k}}{2}\left(-\frac{R_k}{L_k}I_{\mathrm{d}k} + \omega_k I_{\mathrm{q}k} + \frac{V_{\mathrm{sq}k}}{L_k}\right) + \frac{3V_{\mathrm{sq}k}}{2L_k}u_{\mathrm{d}k} - \dot{Q}_k^* \end{cases} \tag{5.2.10}$$

The perturbations of system (5.2.10) are defined as

$$\Psi_{k1}(\cdot) = \frac{3V_{\mathrm{sq}k}}{2}\left(-\frac{R_k}{L_k}I_{\mathrm{q}k} - \omega_k I_{\mathrm{d}k}\right) + (\frac{3V_{\mathrm{sq}k}}{2L_k} - b_{k1})u_{\mathrm{q}k} \tag{5.2.11}$$

$$\Psi_{k2}(\cdot) = \frac{3V_{\mathrm{sq}k}}{2}\left(-\frac{R_k}{L_k}I_{\mathrm{d}k} + \omega_k I_{\mathrm{q}k} + \frac{V_{\mathrm{sq}k}}{L_k}\right) + (\frac{3V_{\mathrm{sq}k}}{2L_k} - b_{k2})u_{\mathrm{d}k} \tag{5.2.12}$$

And system (5.2.10) can be expressed by

$$\begin{cases} \dot{e}_{k1} = \Psi_{k1}(\cdot) + b_{k1}u_{\mathrm{q}k} - \dot{P}_k^* \\ \dot{e}_{k2} = \Psi_{k2}(\cdot) + b_{k2}u_{\mathrm{d}k} - \dot{Q}_k^* \end{cases} \tag{5.2.13}$$

where b_{k1} and b_{k2} are constant control gains.

Define $z_{k1} = P_k$, a second-order HGPO is designed as

$$\begin{cases} \dot{\hat{z}}_{k1} = \hat{\Psi}_{k1}(\cdot) + \frac{\alpha_{k1}}{\epsilon}(z_{k1} - \hat{z}_{k1}) + b_{k1}u_{\mathrm{q}k} \\ \dot{\hat{\Psi}}_{k1}(\cdot) = \frac{\alpha_{k2}}{\epsilon^2}(z_{k1} - \hat{z}_{k1}) \end{cases} \tag{5.2.14}$$

where α_{k1} and α_{k2} are positive observer gains.

Define $z'_{k1} = Q_k$, a second-order HGPO is designed as

$$\begin{cases} \dot{\hat{z}}'_{k1} = \hat{\Psi}_{k2}(\cdot) + \frac{\alpha'_{k1}}{\epsilon}(z'_{k1} - \hat{z}'_{k1}) + b_{k2}u_{\mathrm{d}k} \\ \dot{\hat{\Psi}}_{k2}(\cdot) = \frac{\alpha'_{k2}}{\epsilon^2}(z'_{k1} - \hat{z}'_{k1}) \end{cases} \tag{5.2.15}$$

where α'_{k1} and α'_{k2} are positive observer gains.

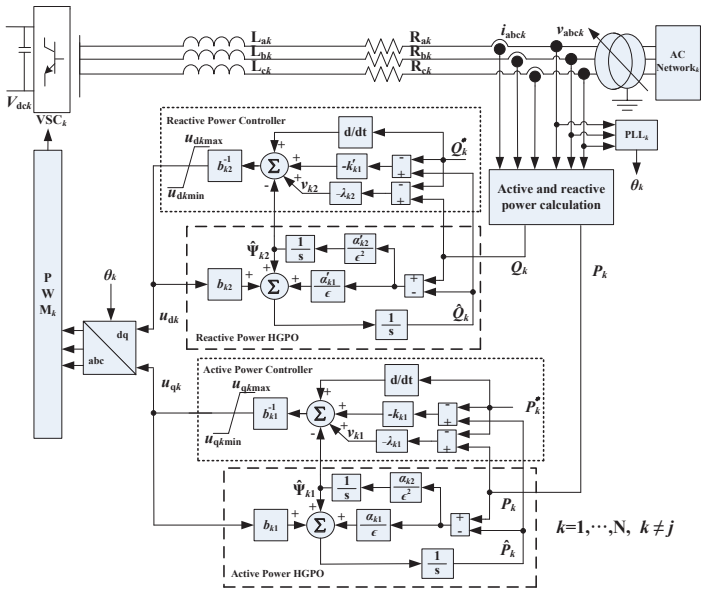

Figure 5.2: Structure of the inverter controller in VSC-MTDC systems.

The POAPC for system (5.2.10) using the estimates of perturbation is designed as

$$\begin{cases} u_{\mathrm{q}k} = b_{k1}^{-1}(-\hat{\Psi}_{k1}(\cdot) - k_{k1}(\hat{z}_{k1} - P_k^*) + \dot{P}_k^* + \nu_{k1}) \\ u_{\mathrm{d}k} = b_{k2}^{-1}(-\hat{\Psi}_{k2}(\cdot) - k'_{k1}(\hat{z}'_{k1} - Q_k^*) + \dot{Q}_k^* + \nu_{k2}) \end{cases} \tag{5.2.16}$$

where k_{k1} and k'_{k1} are the feedback control gains; $V_k = [\nu_{k1}, \nu_{k2}]^{\mathrm{T}}$ is the additional input.

Choose the output of system (5.2.10) as $Y_k = [Y_{k1}, Y_{k2}]^{\mathrm{T}} = [P_k - P_k^*, Q_k - Q_k^*]^{\mathrm{T}}$. Let $V_k = [-\lambda_{k1}Y_{k1}, -\lambda_{k2}Y_{k2}]^{\mathrm{T}}$, where λ_{k1} and λ_{k2} are some positive constants to inject an extra system damping into system (5.2.10). Similarly, the closed-loop system is output strictly passive from output Y_k to input V_k.

Constants b_{k1} and b_{k2} are chosen to satisfy:

$$3V_{\mathrm{sq}k}/[2L_k(1-\theta_{k1})] \geq b_{k1} \geq 3V_{\mathrm{sq}k}/[2L_k(1+\theta_{k1})] \tag{5.2.17}$$

$$3V_{\mathrm{sq}k}/[2L_k(1-\theta_{k2})] \geq b_{k2} \geq 3V_{\mathrm{sq}k}/[2L_k(1+\theta_{k2})] \tag{5.2.18}$$

where $\theta_{k1} < 1$ and $\theta_{k2} < 1$ are positive constants. Again, the boundary values of the estimated states are calculated by $|\hat{z}_{k1}| \leq |P_k^*|$, $|\hat{\Psi}_{k1}(\cdot)| \leq |P_k^*|/\Delta$, $|\hat{z}'_{k1}| \leq |Q_k^*|$, and $|\hat{\Psi}_{k2}(\cdot)| \leq |Q_k^*|/\Delta$, respectively.

The structure of inverter controller is illustrated by Fig. 5.2, in which only the measurement of active power P_k and reactive power Q_k is needed for the controller and observer design.

At last, once the control parameters of controllers (5.2.7) and (5.2.16) are chosen, no further tuning is needed. The internal dynamics stability has been proved in Chapter 4.

5.3 Case Studies

The POAPC is applied on the same four-terminal VSC-MTDC system used in Chapter 4. The control performance of POAPC is evaluated under various operating conditions in a wide neighbourhood of the initial operating points and compared to that of PI control used in [39] and PC used in Chapter 4.

The POAPC parameters used are given in Table 5.1, the control inputs are bounded as $|u_{\mathrm{q}i}| \leq 1$ p.u., $|u_{\mathrm{d}i}| \leq 1$ p.u., where $i = 1, \ldots, 4$. The time period Δ is chosen to be 0.05 s for the calculation of boundary values of state and perturbation estimates.

Table 5.1: Control parameters used in the four-terminal VSC-MTDC system.

Rectifier controller			
Control gains	$k_{11} = 100$	$k_{12} = 20$	$\lambda_{11} = 5$
	$b_{11} = 300$	$k'_{11} = 70$	$\lambda_{12} = 5$
	$b_{12} = 150$		
Observer gains	$\alpha_{11} = 1200$	$\alpha_{12} = 4.8 \times 10^5$	$\alpha_{13} = 6.4 \times 10^7$
	$\alpha'_{11} = 400$	$\alpha'_{12} = 4 \times 10^4$	$\epsilon = 0.1$
Inverter controller, $k = 2, 3, 4$			
Control gains	$k_{\mathrm{k1}} = 70$	$k'_{\mathrm{k1}} = 70$	$b_{\mathrm{k1}} = 150$
	$b_{\mathrm{k2}} = 150$	$\lambda_{\mathrm{k1}} = 5$	$\lambda_{\mathrm{k2}} = 5$
Observer gains	$\alpha_{\mathrm{k1}} = 400$	$\alpha'_{\mathrm{k1}} = 400$	$\alpha_{\mathrm{k2}} = 4 \times 10^4$
	$\alpha'_{\mathrm{k2}} = 4 \times 10^4$	$\epsilon = 0.1$	

1) Case 1: Active and reactive power tracking. An active and reactive power tracking started at $t = 0.5$ s and restored to the original value at $t = 1$ s have been tested, while DC voltage is regulated at the rated value $V^*_{\mathrm{dc1}} = 1.0$ p.u.. The system responses are illustrated by Fig. 5.3. One can find POAPC is able to achieve as satisfactory tracking performance as that of PC, the tiny difference is due to the estimation error.

2) Case 2: 10-cycle LLLG fault at AC buses. A 10-cycle LLLG fault occurs at bus 1 from 0.5 s to 0.7 s. Due to the fault, AC voltage at bus 1 is decreased to a critical level. Fig. 5.4 shows that POAPC can effectively restore the system with less active power oscillations than that of PI control, which can also stabilize the disturbed system faster than PC. With the same operating condition, the same fault is simulated at bus 4. Fig. 5.5 demonstrates that POAPC and PC can improve the system damping and restore the system more rapidly than PI control. Note that V_{cc} of POAPC is worse than that of PI control and PC, however they all converge to the

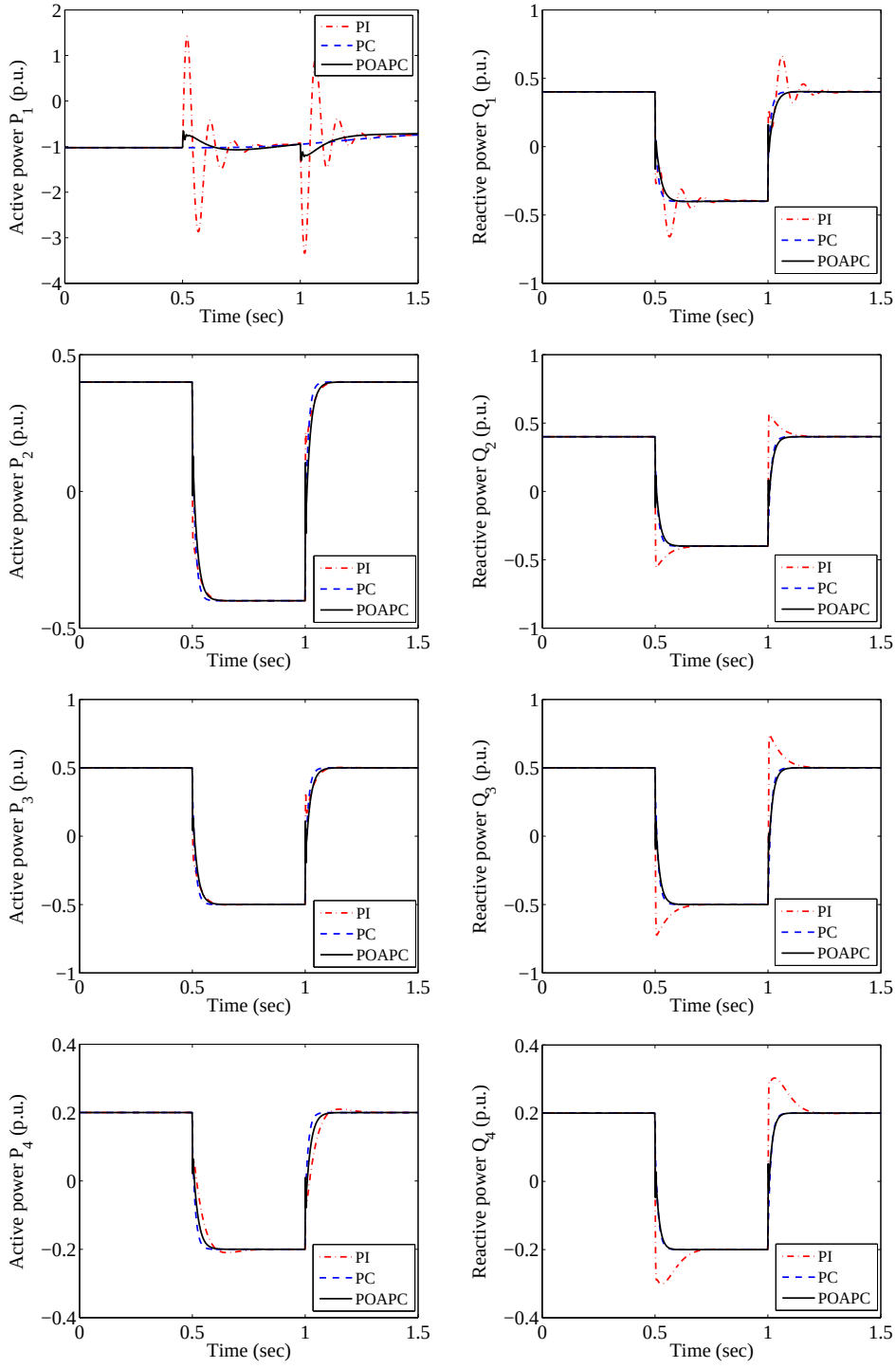

Figure 5.3: System responses obtained in active and reactive power tracking.

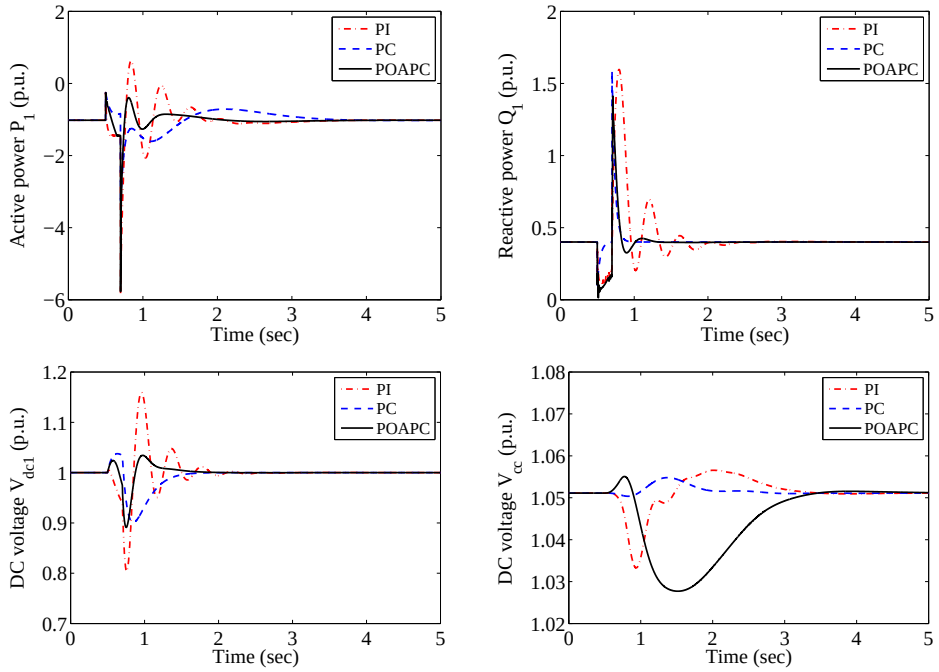

Figure 5.4: System responses obtained under a 10-cycle LLLG fault at bus 1.

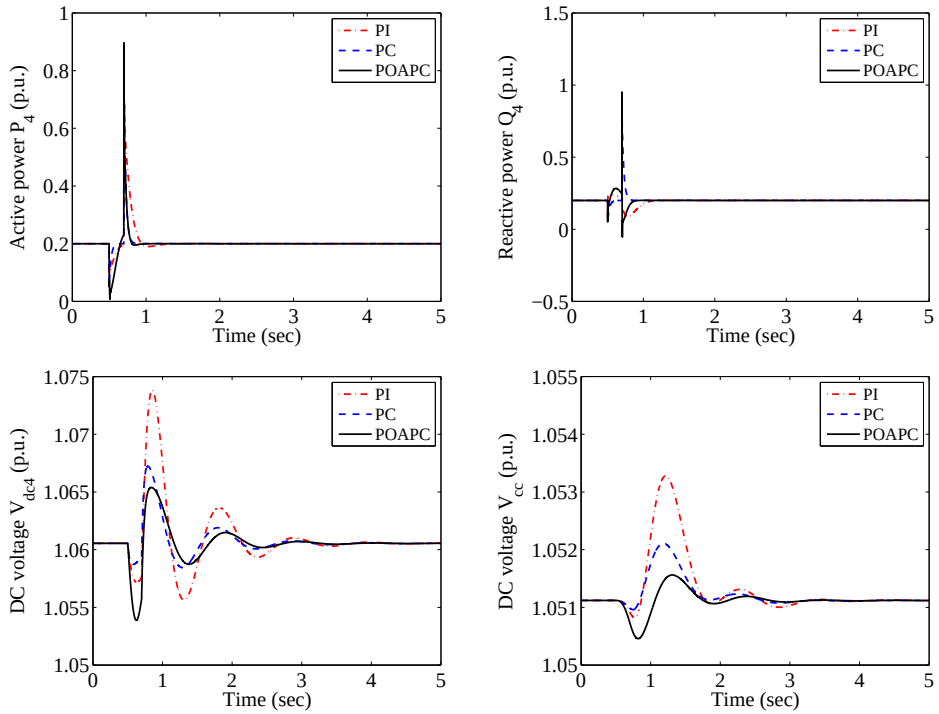

Figure 5.5: System responses obtained under a 10-cycle LLLG fault at bus 4.

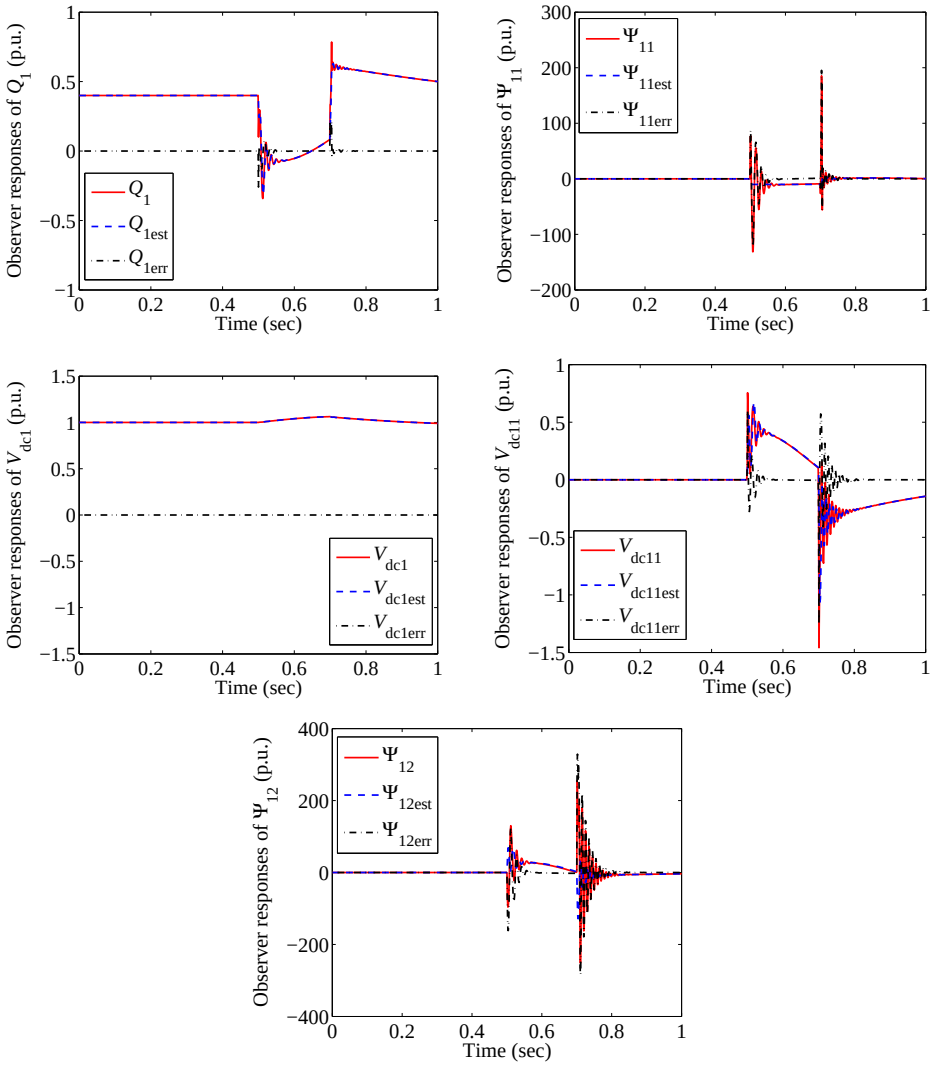

Figure 5.6: Estimation errors of $HGSPO_1$ and $HGPO_1$ obtained under a 10-cycle LLLG fault at bus 1.

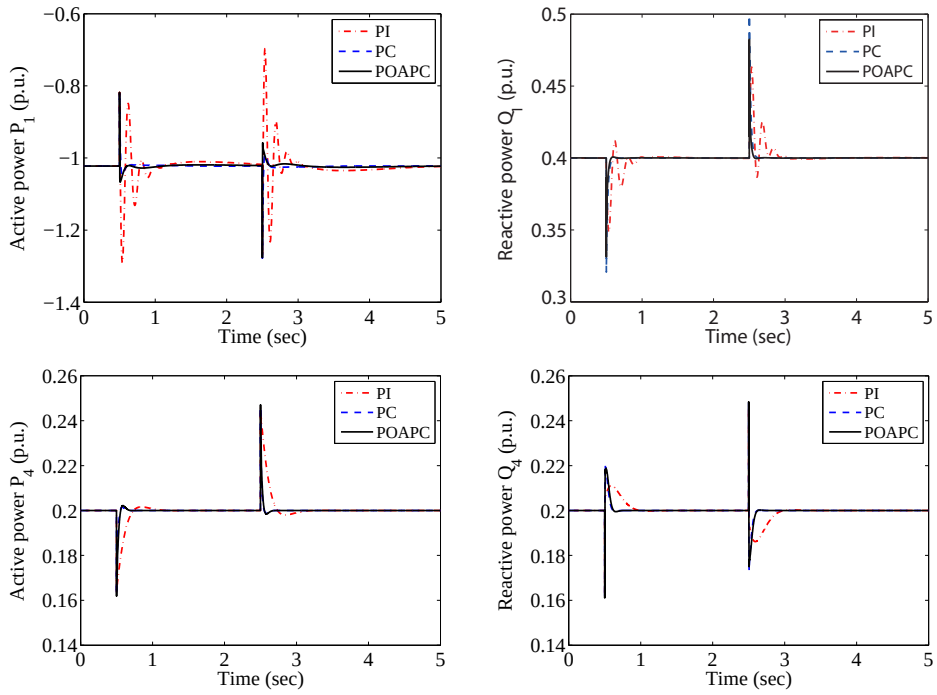

Figure 5.7: System responses obtained under a transmission line disconnection of AC network$_1$ and AC network$_4$.

equilibrium point within the same time.

The observer performance obtained during the 10-cycle LLLG fault at bus 1 is also monitored. The estimation errors of HGSPO$_1$ and HGPO$_1$ are illustrated by Fig. 5.6, which shows the observers can estimate the states with a fast tracking rate. However, there exists relatively larger errors in the estimate of perturbations at the instant of $t = 0.5$ s and $t = 0.7$ s when the fault occurs, this is due to the discontinuity in the AC bus voltage at the instant when the fault occurs. Note that the boundary limit of the estimates can partially lessen this malignant effect.

3) Case 3: Transmission line disconnection on AC networks. One of the two parallel transmission lines connected to AC network$_1$ and AC network$_4$ is removed from the operation at 0.5 s and again reconnected at 2.5 s. The control performance of the three approaches is presented by Fig. 5.7, which shows that POAPC and PC can stabilize the system with a faster rate and smaller overshoot of active and reactive power than that of PI control.

4) Case 4: Temporary fault at DC cable. A 2 ms temporary short-circuit fault

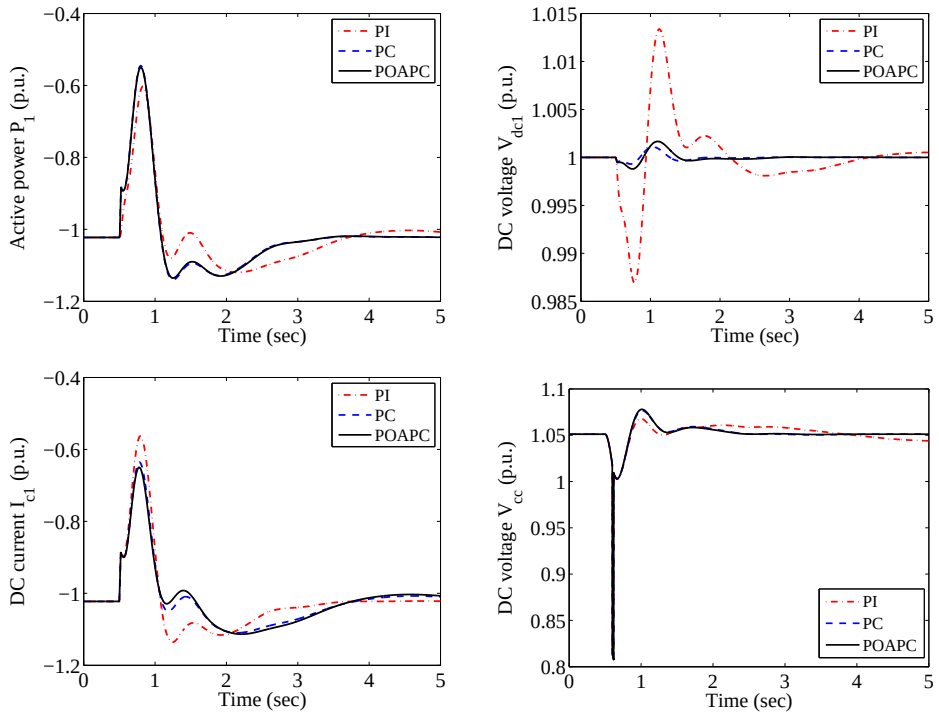

Figure 5.8: System responses obtained in a temporary DC cable$_1$ fault.

occurs at the midpoint of DC cable$_1$ at $t = 0.5$ s and removed automatically thereafter, in which each terminal of the VSC-MTDC system maintains operating. Fig. 5.8 illustrates the obtained system responses, it is found that active power and DC voltage can be restored more rapidly and smoothly by POAPC and PC than that of PI control.

5) Case 5: Modulated change in the angular frequency. Fig. 5.9 depicts the system responses obtained when a 2% change occurs in the angular frequency for 2 s on AC network$_1$ and AC network$_4$. Due to the change in the system frequency, both active and reactive power are disturbed, which can be stabilized by PC and POAPC more effectively in comparison to PI control.

6) Case 6: Uncertainties in the system resistances and inductances. The robustness of the three approaches is tested by reducing AC network resistance R_i, inductance L_i, DC cable resistance R_{ci}, and inductance L_{ci} by 20% from their nominal values. The same reactive power tracking used in Case 1 is tested with DC voltage regulated to its rate value. System responses are demonstrated in Fig. 5.10,

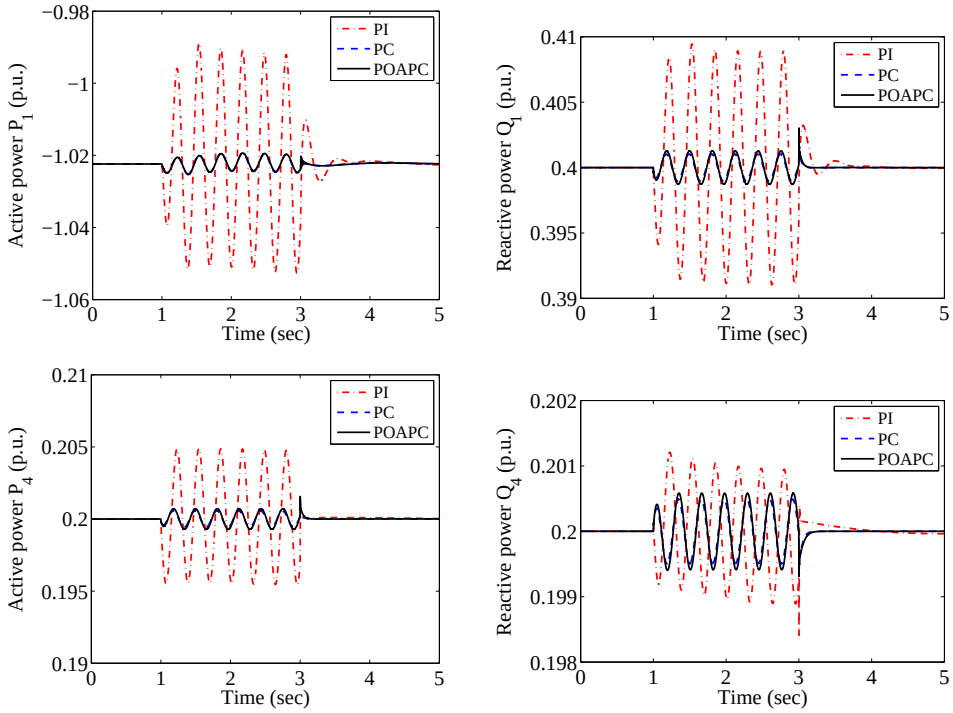

Figure 5.9: System responses obtained when a modulated change occurs in the angular frequency.

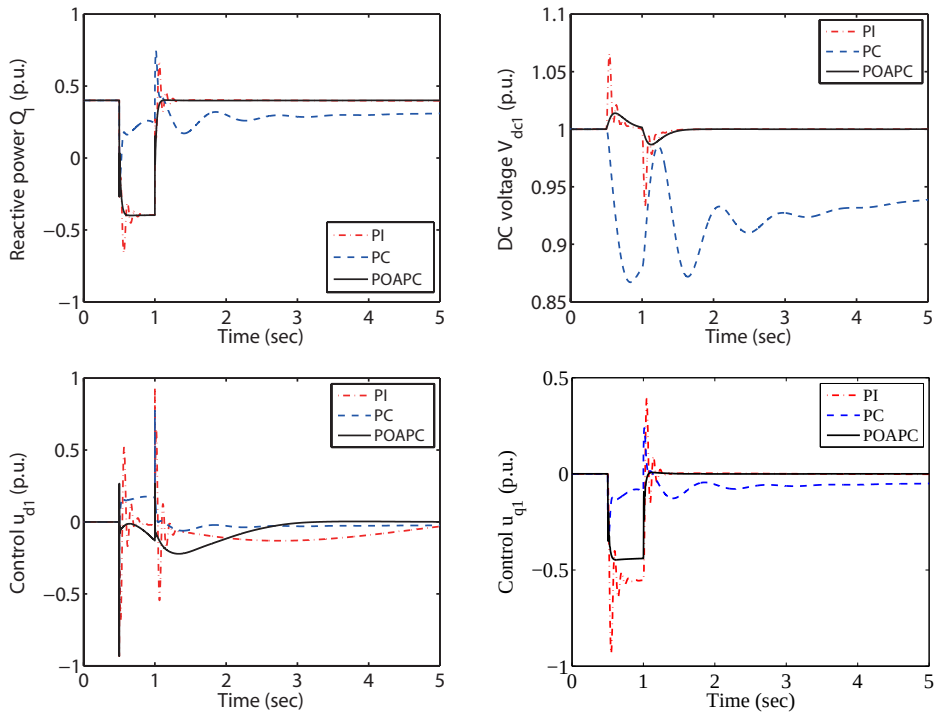

Figure 5.10: System responses obtained under a 20% decrease of the system resistances and inductances.

from which a big difference of PC has been identified, with and without accurate system parameters. PC is not robust to any modelling uncertainties as it requires an accurate system model. In contrast, PI control and POAPC remain a satisfactory control performance as their control design do not depend on system parameters.

7) Case 7: Weak AC networks connection. AC network$_1$ and AC network$_4$ are modelled as offshore wind farms to investigate the control performance to weak AC networks connection, a voltage disturbance occurs from 0.5 s to 2.5 s caused by the wind speed variation is simulated, with $V_{\mathrm{s1}} = V_{\mathrm{s4}} = 1 + 0.15\sin(0.2\pi t)$. System responses are illustrated in Fig. 5.11, it shows that POAPC can effectively regulate the active and reactive power as its design does not need an accurate system model.

8) Case 8: Robustness to DC voltage measurement noises. A 1% white noise of the rated DC voltage $V^*_{\mathrm{dc1}} = 1$ p.u. is applied and a second-order low-pass filter with a cut-off frequency $f_{\mathrm{c}} = 20$ Hz is used to filter out such noise. The system responses are shown by Fig. 5.12, a significant chattering of Q_1 and V_{dc1} of PC and POAPC,

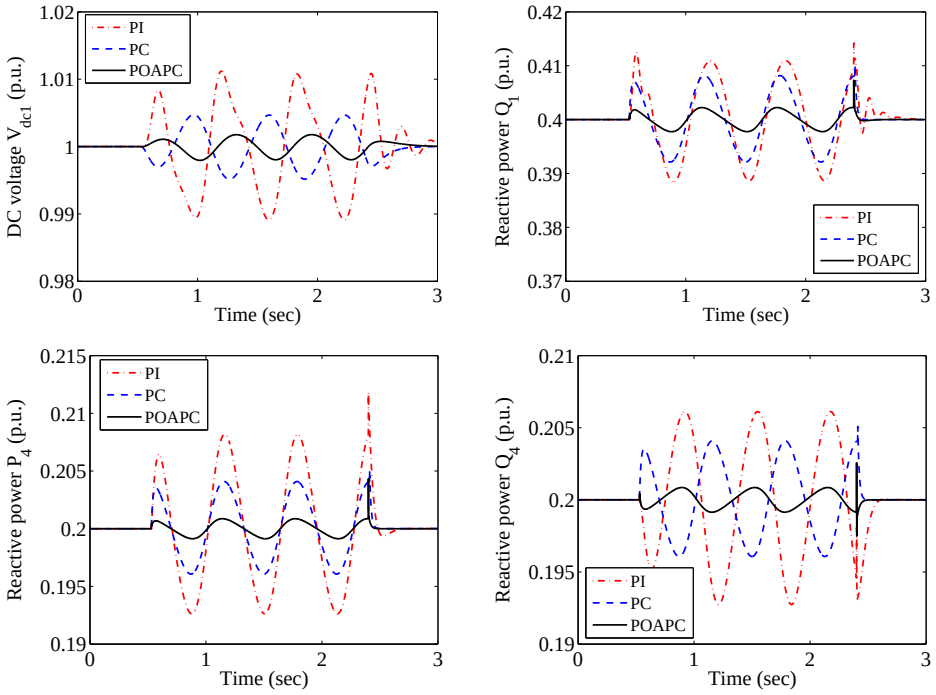

Figure 5.11: System responses obtained when weak AC networks are connected.

with and without the filter, can be found which control performance is degraded dramatically resulted from the requirement of exact DC voltage measurement. Note that in this particular case POAPC performs a little bit worse than PC, which is resulted from the estimation errors. The low-pass filter can effectively attenuate such chattering such that a reliable control performance can be maintained.

Remark 5.1. It is worth mentioning that a spike appeared from Fig. 5.4 to Fig. 5.8. This is resulted from the discontinuity of the system variables and parameters when system operating points suddenly varies. The estimation error therefore increases significantly as it is amplified by the large observer gain values used in the high gain observer, known as the 'peaking phenomenon'. Note that the spike decays very rapidly as the high gain observer will respond quickly and track the new system operating points.

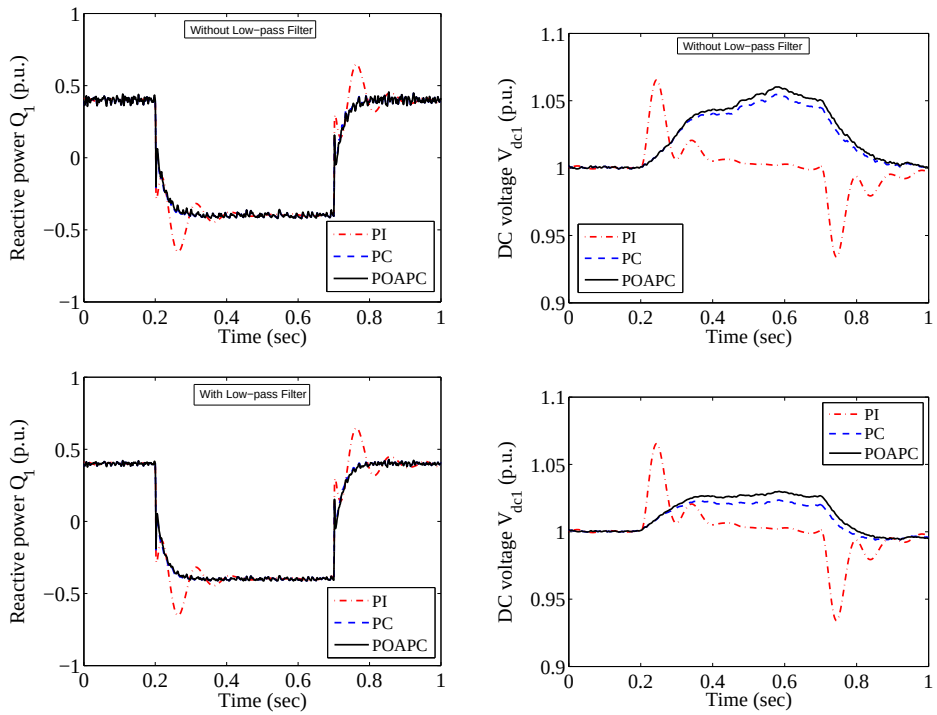

Figure 5.12: System responses obtained with DC voltage measurement noises.

5.4 Conclusion

In this chapter, POAPC has been applied on an N-terminal VSC-MTDC system. It does not require an accurate system model and only the measurement of DC voltage, active and reactive power is needed. Case studies have been undertaken on a four-terminal VSC-MTDC system, which verify that the proposed controller can provide a significant system damping. Hence it can reduce the overshoot of active and reactive power under various operating conditions, such as active and reactive power tracking, faults at AC buses and DC cable, transmission line disconnection, and system frequency modulation. Moreover, the robustness to parameter uncertainties, weak AC networks connection, and DC voltage measurement noises has been studied, which demonstrates that POAPC can effectively handle the parameter uncertainties, together with other unmodelled dynamics and time-varying external disturbances. Simulation results show that the system stability margin can be increased hence the possibility of VSC overloading is diminished. In comparison, PI

control cannot maintain a consistent control performance when system operating condition varies, while the control performance of PC is degraded dramatically in the presence of parameter uncertainties and weak AC networks connection.

Chapter 6

Perturbation Observer based Coordinated Adaptive Passive Control for Multi-machine Power Systems with FACTS Devices

6.1 Introduction

Power system stability has become a crucial issue as the size and complexity of power systems increase [56]. Conventional linear control methods have been widely used, however, they cannot maintain consistent control performance as power systems are highly nonlinear, which operate under a wide range of operating conditions and various modelling uncertainties [113]. Synchronous generator excitation control is one of the most popular methods to enhance the power system stability. On one hand, many nonlinear control approaches have been used for the EC, such as adaptive H_∞ control [114], L-2 disturbance attenuation control [115], nonlinear adaptive control [94], adaptive dynamic programming [116], and optimal predictive control [117]. On the other hand, proper controllers of FACTS devices can also improve the power system stability. Many studies have been undertaken on the development of nonlinear controllers for TCSC [118], SVC [119], and STATCOM [120]. However,

uncoordinated EC and FACTS controller may deteriorate each other or even lead to instability under large disturbances [56].

To resolve the above issues, several nonlinear coordinated control approaches of EC and FACTS controller have been applied to achieve an optimal control performance of the whole system, such as optimal-variable-aim strategies [121], global control [122], zero-dynamics method [123], pole-assignment technique [124], and parameter-constrained nonlinear optimization algorithm [125]. However, these methods require an accurate system model during the controller design, which are difficult to guarantee a reliable control performance when implemented in a real multi-machine power system. Hence several adaptive and robust coordinated control methods are investigated in [86, 126, 127], which design is complicated and cancels possible beneficial system nonlinearities. Besides, the optimal control performance may not be obtained as the physical property of a power system is ignored. Several adaptive tuning based approaches have also been developed to obtain the optimal control parameters, such as particle swarm optimization [128] and probabilistic eigenvalue-based objective function method [129].

It is well known that the nature of a power system is to produce, transmit and consume energy, and the power flow into the power system must be greater than or equal to the rate of change of the energy stored in the power system [130]. CPC [83, 84] is an extended passivity-based method [78, 82], which requires an accurate system model. Therefore, CAPC has been developed for the control of EC and TCSC controller by [92, 93]. However, it is based on the linearly parametric adaption, which updating law can only deal with an uncertain damping coefficient and a nonlinear TCSC unmodelled dynamics satisfying a linear growth condition. These assumptions restrict its application in real multi-machine power system operations as the modelling uncertainty consists of the inertial constant, time constant, general unmodelled TCSC dynamics and inter-area type disturbance. Moreover, an explicit CLF needs to be constructed, which is difficult to achieve in multi-machine power systems.

This chapter develops the POCAPC scheme at first, via designing a PO to estimate and compensate the perturbation which is a lumped term including system

nonlinearities, parameter uncertainties, unmodelled dynamics and time-varying external disturbances. POCAPC can partially release the dependence of an accurate system model needed by PC. Moreover, it can handle fast varying unknown dynamics, comparing with the parameter estimation based APC which can only estimate unknown constant or slow varying parameters. PO has been used in [94] for large-scale power system, however, it did not take the system physical property and the unmodelled TCSC dynamics into account, which control performance is not optimal compared to that of POCAPC. Moreover, POCAPC can be effectively applied on real multi-machine power system operations as modelling uncertainties can be compensated online via the functional estimation, hence the strict assumption of linearly parametric uncertainties made on system structures in [92] can be avoided. In addition, only the range of CLF is needed for controller design, which can be easily applied to the multi-machine power systems. Analysis begins with decomposing the original power system into several subsystems, in which the TCSC reactance and its modulated input are chosen as the output and control input, respectively, such that the relative degree is one. A decentralized stabilizing EC for each generator is designed and a coordinated TCSC controller is developed via passivation, which ensures the whole system stability. Two case studies are undertaken on an SMIB system and a three-machine power system under different operating conditions, respectively. Both simulation and HIL test are carried out to verify the effectiveness and implementation feasibility of POCAPC.

6.2 Problem Formulation

Consider a two-input system in the formal form of passive system as follows [73, 83]

$$\dot{z} = Az + B(a(z, y) + b(z, y)u_2 + \xi(t)) \tag{6.2.1}$$

$$\dot{y} = \alpha(z, y) + \beta_1(z, y)u_1 + \beta_2(z, y)u_2 + \zeta(t) \tag{6.2.2}$$

where $y \in \mathbb{R}$ is the output, $u_1 \in \mathbb{R}$ and $u_2 \in \mathbb{R}$ are the control inputs, while the relative degree from u_1 to y is one, which is the basic form in the standard

CPC design [83]. $z \in \mathbb{R}^{n-1}$ is the state vector of the internal dynamics; $a(z,y)$: $\mathbb{R}^{n-1} \times \mathbb{R} \mapsto \mathbb{R}$ and $b(z,y) : \mathbb{R}^{n-1} \times \mathbb{R} \mapsto \mathbb{R}$ are C^∞ unknown smooth functions, $\xi(t) \in \mathbb{R}$ and $\zeta(t) \in \mathbb{R}$ are time-varying external disturbances. $\alpha(z,y)$, $\beta_1(z,y)$ and $\beta_2(z,y)$ are all unknown functions defined on $\mathbb{R}^{n-1} \times \mathbb{R}$. Matrices A and B are

$$A = \begin{bmatrix} 0 & 1 & 0 & \cdots & 0 \\ 0 & 0 & 1 & \cdots & 0 \\ \vdots & & & & \vdots \\ 0 & 0 & 0 & \cdots & 1 \\ 0 & 0 & 0 & \cdots & 0 \end{bmatrix}_{(n-1)\times(n-1)}, \quad B = \begin{bmatrix} 0 \\ 0 \\ \vdots \\ 0 \\ 1 \end{bmatrix}_{(n-1)\times 1} \tag{6.2.3}$$

The zero-dynamics of system (6.2.1) is assumed to be stabilizable by u_2 and can be written as

$$\dot{z} = Az + B(a(z,0) + b(z,0)u_2 + \xi(t)) \tag{6.2.4}$$

6.2.1 Design of HGSPO and HGPO

The perturbation of system (6.2.4) is defined as

$$\Psi_1(z,y,u,t) = a(z,0) + (b(z,0) - b_{10})u_2 + \xi(t) \tag{6.2.5}$$

Define a fictitious state to represent the perturbation, that is, $z_n = \Psi_1(\cdot)$. System (6.2.4) can be rewritten into

$$\dot{z}_{\mathrm{e}} = A_1 z_{\mathrm{e}} + B_1 u_2 + B_2 \dot{\Psi}_1(\cdot) \tag{6.2.6}$$

where $z_{\mathrm{e}} = [z_1, z_2, \cdots, z_{n-1}, z_n]^{\mathrm{T}}$. $B_1 = [0, 0, \ldots, b_{10}, 0]^{\mathrm{T}} \in \mathbb{R}^n$ and $B_2 = [0, 0, \ldots, 1]^{\mathrm{T}} \in \mathbb{R}^n$. Matrix A_1 is

$$A_1 = \begin{bmatrix} 0 & 1 & \cdots & \cdots & 0 \\ 0 & 0 & 1 & \cdots & 0 \\ \vdots & & & & \vdots \\ 0 & 0 & 0 & \cdots & 1 \\ 0 & 0 & 0 & \cdots & 0 \end{bmatrix}_{n\times n} \tag{6.2.7}$$

An nth-order HGSPO is used to estimate $\hat{z}_{\mathrm{e}}$ for system (6.2.6) as

$$\dot{\hat{z}}_{\mathrm{e}} = A_1\hat{z}_{\mathrm{e}} + B_1u_2 + H(z_1 - \hat{z}_1) \tag{6.2.8}$$

where $H = [\alpha_1/\epsilon, \alpha_2/\epsilon^2, \cdots, \alpha_{n-1}/\epsilon^{n-1}, \alpha_n/\epsilon^n]^{\mathrm{T}}$ is the observer gain with $0 < \epsilon \ll 1$.

The estimation error of HGSPO (6.2.8) is calculated as

$$\dot{\tilde{z}}_{\mathrm{e}} = A_1\tilde{z}_{\mathrm{e}} + B_2\dot{\Psi}_1(\cdot) - H(z_1 - \hat{z}_1) \tag{6.2.9}$$

The design procedure of HGSPO (6.2.8) can be summarized as following steps:

Step 1: Define the perturbation of system (6.2.4) as Eq. (6.2.5);

Step 2: Define a fictitious state to represent the perturbation as $z_n = \Psi_1(\cdot)$;

Step 3: Extend the original (n-1)th-order system (6.2.4) into the extended nth-order system (6.2.6);

Step 4: Design the nth-order HGSPO (6.2.8) to estimate state z and perturbation $\Psi_1(\cdot)$ for the extended nth-order system (6.2.6);

Step 5: Choose $\alpha_i = C_n^i\lambda^i$ such that the pole of HGSPO (6.2.8) can be placed at $-\lambda$, where $i = 1, 2, \cdots, n$ and $\lambda > 0$.

Similarly, the perturbation of system (6.2.2) is defined as

$$\Psi_2(z, y, u, t) = \alpha(z, y) + \beta_2(z, y)u_2 + (\beta_1(z, y) - b_{20})u_1 + \zeta(t) \tag{6.2.10}$$

Define a fictitious state to represent the perturbation, that is, $y_2 = \Psi_2(\cdot)$. System (6.2.2) becomes

$$\begin{cases} \dot{y} = y_2 + b_{20}u_1 \\ \dot{y}_2 = \dot{\Psi}_2(\cdot) \end{cases} \tag{6.2.11}$$

A second-order HGPO is used to obtain estimates $\hat{y}$ and $\hat{\Psi}_2$ for system (6.2.11) as

$$\begin{cases} \dot{\hat{y}} = \hat{\Psi}_2(\cdot) + \frac{\alpha_1'}{\epsilon'}(y - \hat{y}) + b_{20}u_1 \\ \dot{\hat{\Psi}}_2(\cdot) = \frac{\alpha_2'}{\epsilon'^2}(y - \hat{y}) \end{cases} \tag{6.2.12}$$

where $0 < \epsilon' \ll 1$.

Define the scaled estimation errors of HGPO (6.2.12) as $\eta'_1 = \tilde{y}/\epsilon'$, $\eta'_2 = \tilde{\Psi}_2(\cdot)$, and $\eta' = [\eta'_1, \eta'_2]^{\mathrm{T}}$, gives

$$\epsilon'\dot{\eta}' = A'_1\eta' + \epsilon' B'_1\dot{\Psi}_2(\cdot) \tag{6.2.13}$$

with

$$A'_1 = \begin{bmatrix} -\alpha'_1 & 1 \\ -\alpha'_2 & 0 \end{bmatrix}, \quad B'_1 = \begin{bmatrix} 0 \\ 1 \end{bmatrix} \tag{6.2.14}$$

where α'_1 and α'_2 are chosen such that A'_1 is a Hurwitz matrix.

The design procedure of HGPO (6.2.12) can be summarized as following steps:

Step 1: Define the perturbation of system (6.2.2) as Eq. (6.2.10);

Step 2: Define a fictitious state to represent the perturbation as $y_2 = \Psi_2(\cdot)$;

Step 3: Extend the original first-order system (6.2.2) into the extended second-order system (6.2.11);

Step 4: Design a second-order HGPO (6.2.12) to estimate perturbation $\Psi_2(\cdot)$ for the extended second-order system (6.2.11);

Step 5: Choose $\alpha'_1 = 2\lambda'$ and $\alpha'_2 = \lambda'^2$ such that the pole of HGPO (6.2.12) can be placed at $-\lambda'$, where $-\lambda' > 0$.

Normally the pole of HGSPO (6.2.8) and HGPO (6.2.12) is chosen to be 10 times larger than the dominant pole of the equivalent linear system of (6.2.4) and (6.2.2), respectively, which can ensure a fast estimation of perturbation $\Psi_1(\cdot)$ and $\Psi_2(\cdot)$. Note that one only needs the measurement of state z_1 and control input u_2 for the design of HGSPO (6.2.8), and the measurement of output y and control input u_1 for the design of HGPO (6.2.12).

The following assumptions are made on systems (6.2.6) and (6.2.11).

Assumption 6.1. b_{10} and b_{20} are chosen to satisfy:

$$0 < |b(z,0)/b_{10} - 1| \leq \theta_1, \;\; 0 < |\beta_1(z,y)/b_{20} - 1| \leq \theta_2 \tag{6.2.15}$$

where $\theta_1 < 1$ and $\theta_2 < 1$ are positive constants.

Assumption 6.2. The perturbation $\Psi_k(z, y, u, t) : \mathbb{R}^{n-1} \times \mathbb{R} \times \mathbb{R}^2 \times \mathbb{R}^+ \mapsto \mathbb{R}$ and its derivative $\dot{\Psi}_k(z, y, u, t) : \mathbb{R}^{n-1} \times \mathbb{R} \times \mathbb{R}^2 \times \mathbb{R}^+ \mapsto \mathbb{R}$ are Lipschitz in their arguments over the domain of interest and are globally bounded:

$$|\Psi_k(z, y, u, t)| \leq \gamma_1, \quad |\dot{\Psi}_k(z, y, u, t)| \leq \gamma_2 \tag{6.2.16}$$

where γ_1 and γ_2 are positive constants. In addition, $\Psi_k(0, 0, 0, 0) = 0$, $\dot{\Psi}_k(0, 0, 0, 0) = 0$, $k = 1, 2$, such that the origin is an equilibrium point of the open-loop system

Remark 6.1. It should be mentioned that during the design procedure, ϵ and ϵ' used in HGSPO (6.2.8) and HGPO (6.2.12) are required to be some relatively small positive constants only, and the performance of HGSPO and HGPO is not very sensitive to the observer gains, which are determined based on the upper bound of the derivative of perturbation.

6.2.2 Design of stabilizing controller and coordinated controller

Based on the standard CPC design [83], the stabilizing controller u_2 is designed at first as follows

$$u_2 = \gamma(\hat{z}_{\mathrm{e}}) = \frac{1}{b_{10}}(-K\hat{z} - \hat{z}_n) \tag{6.2.17}$$

which renders system (6.2.1) into

$$\dot{z} = Az + B(a(z, y) + b(z, y)\gamma(\hat{z}_{\mathrm{e}}) + \xi(t)) = \tilde{q}(z) + \tilde{p}(z, y)y \tag{6.2.18}$$

with

$$\tilde{q}(z) = Az + B(a(z, 0) + b(z, 0)\gamma(\hat{z}_{\mathrm{e}}) + \xi(t)) \tag{6.2.19}$$

and

$$\tilde{p}(z, y) = B(a(z, y) - a(z, 0) + (b(z, y) - b(z, 0))\gamma(\hat{z}_{\mathrm{e}}))y^{-1} \tag{6.2.20}$$

where $\tilde{q}(z)$ represents the zero-dynamics, $\tilde{p}(z, y)$ denotes the difference between the original system and zero-dynamics, which will be cancelled later by u_1. $K =$

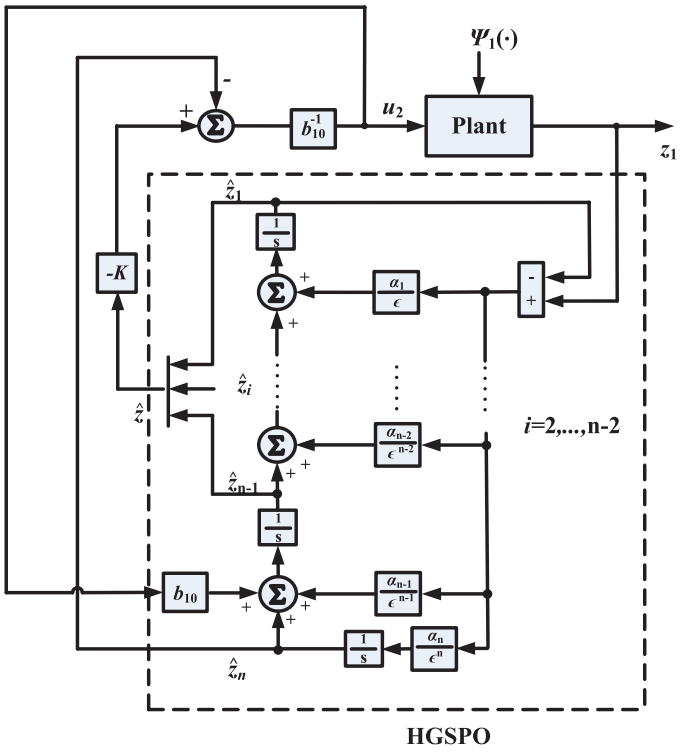

Figure 6.1: Structure of the stabilizing controller u_2.

$[k_1, k_2, \cdots, k_{n-1}]$ is the control gain which makes matrix $A - BK$ Hurwitzian, such that the following condition can be satisfied

$$\dot{W} = \frac{\partial W(z)}{\partial z^{\mathrm{T}}}\tilde{q}(z) + \frac{\partial W}{\partial \eta^{\mathrm{T}}}\dot{\eta} \leq -\alpha(\|z\|) \tag{6.2.21}$$

where α is a class-$\mathcal{K}$ function, and $\eta = [\tilde{z}_1/\epsilon^{n-1}, \tilde{z}_2/\epsilon^{n-2}, \cdots, \tilde{z}_n] \in \mathbb{R}^n$. The proof of inequality (6.2.21) is given in [94].

The structure of stabilizing controller (6.2.17) is illustrated in Fig. 6.1. The nominal plant is disturbed by the perturbation $\Psi_1(\cdot)$, the stabilizing controller u_2 can be separated as $u_2 = b_{10}^{-1}(u_{\mathrm{s}1} + u_{\mathrm{s}2})$, where $u_{\mathrm{s}1} = -K\hat{z}$ is the state feedback and choose $k_i = C_{n-1}^i \xi^i$ to place the pole of the equivalent linear system of (6.2.4) at $-\xi$, where $i = 1, ..., n-1$ and $\xi > 0$; and $u_{\mathrm{s}2} = -\hat{z}_n$ compensates the combinatorial effect of system nonlinearities, parameter uncertainties, unmodelled dynamics, and time-varying external disturbances.

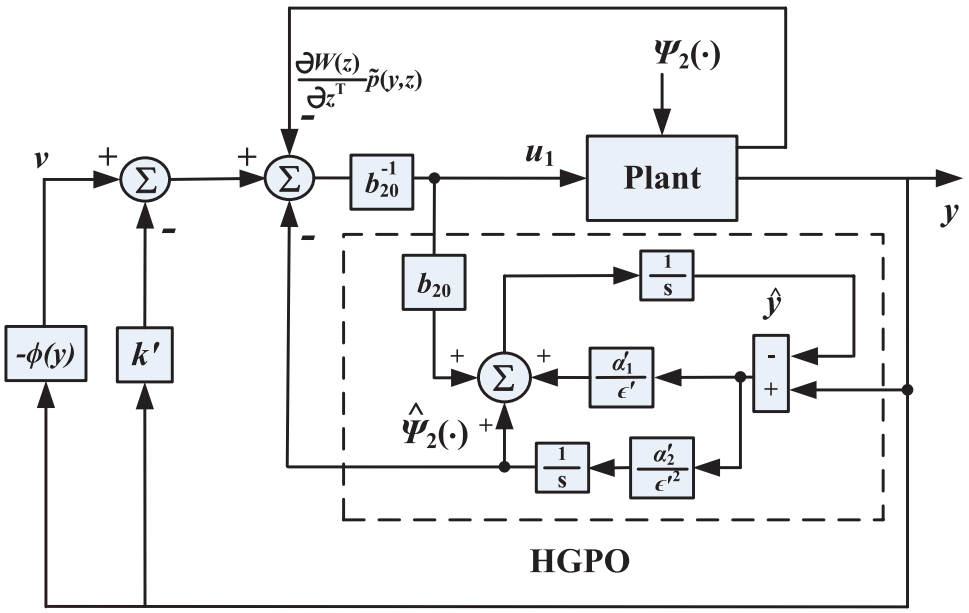

Figure 6.2: Structure of the coordinated controller u_1.

The coordinated controller u_1 is designed as

$$\begin{cases} u_1 = b_{20}^{-1}\left(-\hat{\Psi}_2(\cdot) - k'y - \frac{\partial W}{\partial z^{\mathrm{T}}}\tilde{p}(z,y) + \nu\right) \\ \nu = -\phi(y) \end{cases} \tag{6.2.22}$$

where ν is the additional input, ϕ is any smooth function such that $\phi(0) = 0$ and $y\phi(y) > 0$ for all $y \neq 0$. $k' > 1$ is the feedback control gain.

The structure of coordinated controller (6.2.22) is illustrated in Fig. 6.2. The nominal plant is disturbed by the perturbation $\Psi_2(\cdot)$, the coordinated controller u_1 can be separated as $u_1 = b_{20}^{-1}(u_{\mathrm{c}1} + u_{\mathrm{c}2} + u_{\mathrm{c}3} + u_{\mathrm{c}4})$, where $u_{\mathrm{c}1} = -\hat{\Psi}_2(\cdot)$ is the perturbation compensation; $u_{\mathrm{c}2} = -k'y$ places the pole of the equivalent linear system of (6.2.2) at $-k'$, where $k' > 0$; $u_{\mathrm{c}3} = \frac{\partial W}{\partial z^{\mathrm{T}}}\tilde{p}(y,z)$ coordinates the two controllers by cancelling the difference between the original system and zero-dynamics represented by $\tilde{p}(y,z)$; and $u_{\mathrm{c}4} = \nu$ constructs a passive system by introducing an additional input in the form of a sector-nonlinearity $\phi(y)$.

Remark 6.2. Note that $\frac{\partial W(z)}{\partial z^{\mathrm{T}}}\tilde{p}(z,y) = \frac{\partial W(z)}{\partial z_{n-1}}\tilde{p}_{n-1}(z,y)$ as $\tilde{p}_i(z,y) = 0$, $i = 1,2,\cdots,n-2$, which can be interpreted as the distributed energies in a complex system and needs to be reshaped. One can choose $\frac{\partial W(z)}{\partial z^{\mathrm{T}}}\tilde{p}(z,y) = cz_{n-1}\tilde{p}_{n-1}(z,y)$

regardless of the system order, where c is called the coordination coefficient.

To this end, POCAPC design procedure for systems (6.2.1) and (6.2.2) can be summarized as follows:

Step 1: Obtain zero-dynamics (6.2.4) of system (6.2.1) by setting $y = 0$;

Step 2: Extend the original (n-1)th-order system (6.2.4) into the extended nth-order system (6.2.6), and design HGSPO (6.2.8) to obtain estimates $\hat{z}$ and $\hat{z}_n$;

Step 3: Design stabilizing controller (6.2.17) for original system (6.2.1);

Step 4: Extend the original first-order system (6.2.2) into the extended second-order system (6.2.11), and design HGPO (6.2.12) to obtain the estimate $\hat{\Psi}_2(\cdot)$;

Step 5: Design coordinated controller (6.2.22) for original system (6.2.2).

6.2.3 The closed-loop system stability

The proof of stability of the closed-loop system with stabilizing controller u_2 and coordinated controller u_1 is given in the following Theorem 6.1.

Theorem 6.1. *Consider systems (6.2.1) and (6.2.2), with controllers (6.2.17) and (6.2.22), and let Assumptions 6.1 and 6.2 hold; then* $\exists\epsilon_1^*$, $\epsilon_1^* > 0$ *such that,* $\forall\epsilon'$, $0 < \epsilon' < \epsilon_1^*$, *then the closed-loop system is output strictly passive and the origin is stable.*

Proof. Define the scaled estimation errors of HGPO (6.2.12) as $\eta_1' = \tilde{y}/\epsilon'$, $\eta_2' = \tilde{\Psi}_2(\cdot)$, and $\eta' = [\eta_1', \eta_2']^{\mathrm{T}}$, gives

$$\epsilon'\dot{\eta}' = A_1'\eta' + \epsilon' B_1'\dot{\Psi}_2(\cdot) \tag{6.2.23}$$

with

$$A_1' = \begin{bmatrix} -\alpha_1' & 1 \\ -\alpha_2' & 0 \end{bmatrix}, \quad B_1' = \begin{bmatrix} 0 \\ 1 \end{bmatrix} \tag{6.2.24}$$

where α_1' and α_2' are chosen such that A_1' is a Hurwitz matrix.

The closed-loop system (6.2.2) using controller (6.2.22) is

$$\begin{cases} \dot{y} = \eta_2' - k'y - \frac{\partial W}{\partial z^{\mathrm{T}}}\tilde{p}(z,y) + \nu \\ \epsilon'\dot{\eta}' = A_1'\eta' + \epsilon' B_1'\dot{\Psi}_2(\cdot) \end{cases} \tag{6.2.25}$$

Define a Lyapunov function $V(\eta') = \eta'^{\mathrm{T}} P_1 \eta'$, where $P_1 \in \mathbb{R}^{2\times 2}$ is the positive definite solution of the Lyapunov equation $P_1 A_1' + A_1'^{\mathrm{T}} P_1 = -I$. This function satisfies

$$\lambda_{\min}(P_1)\|\eta'\|^2 \le V(\eta') \le \lambda_{\max}(P_1)\|\eta'\|^2 \tag{6.2.26}$$

$$\frac{\partial V(\eta')}{\partial \eta'} A_1 \eta' \le -\|\eta'\|^2 \tag{6.2.27}$$

$$\|\frac{\partial V(\eta')}{\partial \eta'}\| \le 2\lambda_{\max}(P_1)\|\eta'\| \tag{6.2.28}$$

Consider a storage function for the closed-loop system (6.2.25) as follows

$$H(z,\eta,y,\eta') = W(z,\eta) + \frac{1}{2}y^2 + \beta V(\eta') \tag{6.2.29}$$

where $\beta > 0$ is to be determined. Moreover, assume

$$\|\dot{\Psi}_2(\cdot)\| \le L_1\|y\| + L_2\|\eta'\| \tag{6.2.30}$$

where L_1 and L_2 are Lipschitz constants.

Differentiate $H(z,\eta,y,\eta')$ along system (6.2.25), use inequalities (6.2.26) to (6.2.28), (6.2.30), with Corollary 2.1 and condition (6.2.21), yields

$$\begin{aligned}
\dot{H} &= \frac{\partial W}{\partial z^{\mathrm{T}}}(\tilde{q}(z) + \tilde{p}(z,y)y) + \frac{\partial W}{\partial \eta^{\mathrm{T}}}\dot{\eta} + y\Big(\eta_2' - k'y - \frac{\partial W}{\partial z^{\mathrm{T}}}\tilde{p}(z,y) + \nu\Big) \\
&\quad + \beta\frac{\partial V}{\partial \eta'^{\mathrm{T}}}\left(\frac{A_1'\eta'}{\epsilon'} + B_1'\dot{\Psi}_2(\cdot)\right) \\
&\le -\alpha(\|z\|) + y\nu - \|y\|^2 - \frac{\beta}{\epsilon'}\|\eta'\|^2 + 2\beta L_2\|P_1\|\|\eta'\|^2 + (1 + 2\beta L_1\|P_1\|)\|y\|\|\eta'\| \\
&\le -\alpha(\|z\|) + y\nu - \|y\|^2 - \frac{\beta}{\epsilon'}\|\eta'\|^2 + 2\beta L_2\|P_1\|\|\eta'\|^2 + (1 + 2\beta L_1\|P_1\|) \\
&\quad \times \left(\frac{1}{\epsilon_0}\|y\|^2 + \epsilon_0\|\eta'\|^2\right) \\
&\le -\alpha(\|z\|) + y\nu - \frac{1}{2}\|y\|^2 - \frac{\beta}{2\epsilon'}\|\eta'\|^2 - b_1\|y\|^2 - b_2\|\eta'\|^2
\end{aligned} \tag{6.2.31}$$

where

$$b_1 = \frac{1}{2} - \frac{2}{\epsilon_0}\left(\frac{1}{2} + \beta L_1 \|P_1\|\right) \tag{6.2.32}$$

$$b_2 = \frac{\beta}{2\epsilon'} - 2\beta(\epsilon_0 L_1 + L_2)\|P_1\| - \epsilon_0 \tag{6.2.33}$$

with $\epsilon_0 > 0$. One can choose β small enough and $\epsilon_0 \geq \epsilon_0^* = 2 + 4\beta L_1 \|P_1\|$ such that $b_1 > 0$, then choose $\epsilon_1^* = \beta/(\epsilon_0^{*2} + 4\beta L_2 \|P_1\|)$, $\forall \epsilon', \epsilon' \leq \epsilon_1^*$, and choose the additional input $\nu = -\phi(y)$, where $\phi(y)$ is a sector-nonlinearity defined by (A.0.11). It can be shown that

$$\begin{aligned} \dot{H} &\leq -\alpha(\|z\|) - \min(1/2, \beta/(2\epsilon'))(\|y\|^2 + \|\eta'\|^2) + y\nu \\ &\leq -\alpha(\|z\|) - \alpha_1(\|y\|) + y\nu \leq y\nu \leq -y\phi(y) \leq 0 \end{aligned} \tag{6.2.34}$$

where α_1 is a class-$\mathcal{K}$ function. We can conclude that the closed-loop system is output strictly passive and the origin is stable. □

Proposition 6.1. POCAPC can be easily extended into multi-input systems. If there exists m subsystems for system (6.2.1) with m control inputs u_{2j}, the vector variables of states and estimation errors for each subsystem are denoted as z_j^* and η_j^*, $j = 1, 2, \cdots, m$, respectively. Controller (6.2.17) using HGSPO (6.2.8) can decouple each subsystem by rendering their interactions into the perturbation. Hence u_{2j} can stabilize the jth subsystem, which results in an equivalent CLF $W(z^*, \eta^*) = W_1 + W_2 + \cdots + W_m$, and condition (6.2.21) becomes

$$\dot{W} = \sum_{j=1}^{m}\left(\frac{\partial W}{\partial z_j^{*\mathrm{T}}}\tilde{q}_j(z_j^*) + \frac{\partial W}{\partial \eta_j^{*\mathrm{T}}}\dot{\eta}_j^*\right) \leq \sum_{j=1}^{m}\alpha_j(\|z_j^*\|) \tag{6.2.35}$$

Remark 6.3. For the closed-loop system (6.2.25), control gain k' should be designed to suppress the perturbation estimation error $\tilde{\Psi}_2(\cdot)$. Compared to the approach without perturbation compensation, in which k' should be chosen to suppress the perturbation $\Psi_2(\cdot)$. As $|\Psi_2(\cdot)|$ is normally larger than $|\tilde{\Psi}_2(\cdot)|$, a smaller k' could be resulted in due to the compensation of perturbation by POCAPC.

Remark 6.4. Denote $(z_0, y_0) \in \Gamma_{\mathrm{o}}$ and $z_0' \in \Gamma_{\mathrm{z}}$ as the equilibrium point of systems (6.2.1) and (6.2.4), respectively, where their stability region $\Gamma_{\mathrm{o}} \neq \Gamma_{\mathrm{z}}$ during transient process. However, with a proper coordination coefficient c, coordinated controller (6.2.22) will exponentially drive $\lim_{t\to\infty}(z_0, y_0) = z_0'$ and $\lim_{t\to\infty}\Gamma_{\mathrm{o}} = \Gamma_{\mathrm{z}}$

as $\lim_{t\to\infty} y = 0$.

Remark 6.5. Compared to CAPC [92, 93] which can only estimate the linearly parametric uncertainties, POCAPC can be regarded as a nonlinearly functional estimation method, as it can estimate the combinatorial effect of system nonlinearities, parameter uncertainties, unmodelled dynamics and time-varying external disturbances.

6.3 Power System Modelling

6.3.1 An SMIB system with a TCSC device

An SMIB system with a TCSC device is shown in Fig. 6.3, of which the system dynamics is described as [92]

$$\begin{cases} \dot{\delta} = \omega - \omega_0 \\ \dot{\omega} = -\frac{D}{H}(\omega - \omega_0) + \frac{\omega_0}{H}\left(P_{\rm m} - \frac{E'_{\rm q}V_{\rm s}\sin\delta}{X'_{\rm d\Sigma}+X_{\rm tcsc}}\right) \\ \dot{E}'_{\rm q} = \frac{(X_{\rm d}-X'_{\rm d})(V_{\rm s}\cos\delta - E'_{\rm q})}{T_{\rm d0}(X'_{\rm d\Sigma}+X_{\rm tcsc})} - \frac{1}{T_{\rm d0}}E'_{\rm q} + \frac{K_{\rm c}}{T_{\rm d0}}u_{\rm fd} \\ \dot{X}_{\rm tcsc} = -\frac{1}{T_{\rm c}}(X_{\rm tcsc} - X_{\rm tcsc0}) + \frac{K_{\rm T}}{T_{\rm c}}u_{\rm c} + \zeta_{\rm tcsc} \end{cases} \tag{6.3.1}$$

where δ and ω denote the angle and relative speed of the generator rotor, respectively; H the inertia constant; $P_{\rm m}$ the constant mechanical power on the generator shaft; D the damping coefficient; $E'_{\rm q}$ and $V_{\rm s}$ the inner generator voltage and infinite bus voltage; $T_{\rm d0}$ the d-axis transient short-circuit time constant; $T_{\rm c}$ the time constant of TCSC; $X'_{\rm d\Sigma} = X_{\rm t} + X'_{\rm d} + \frac{1}{2}(X_{\rm L1} + X_{\rm L2})$; $X_{\rm t}$ the transformer reactance; $X'_{\rm d}$ the d-axis generator transient reactance; $X_{\rm L1}$ and $X_{\rm L2}$ the transmission line reactance; $X_{\rm tcsc}$ the TCSC reactance and $X_{\rm tcsc0}$ the initial TCSC reactance; $K_{\rm c}$ the gain of excitation amplifier; $u_{\rm fd}$ the excitation voltage; $K_{\rm T}$ the gain of TCSC regulator and $u_{\rm c}$ the TCSC modulated input; and $\zeta_{\rm tcsc}$ the unmodelled TCSC dynamics.

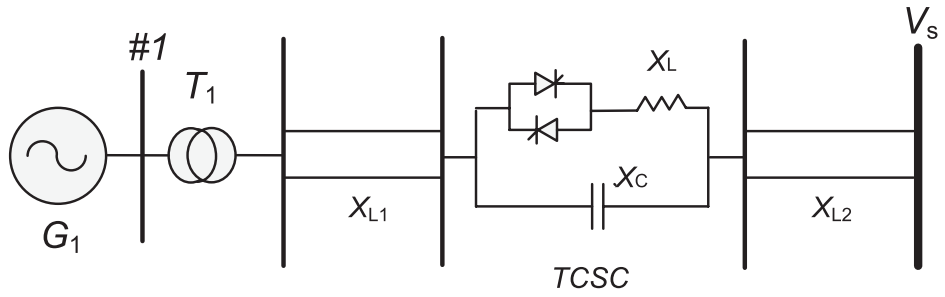

Figure 6.3: The SMIB system equipped with a TCSC device.

6.3.2 A multi-machine power system with a TCSC device

A multi-machine power system with n machines and a TCSC device, where the nth machine is the reference machine, is described by [94]

$$\begin{cases} \dot{\delta}_i = \omega_i - \omega_0 \\ \dot{\omega}_i = \frac{\omega_0}{2H_i}\left(P_{\mathrm{m}i} - \frac{D_i}{\omega_0}(\omega_i - \omega_0) - P_{\mathrm{e}i}\right) \\ \dot{E}'_{\mathrm{q}i} = \frac{1}{T_{\mathrm{d0}i}}(u_{\mathrm{fd}i} - E_{\mathrm{q}i}), \quad i = 1, 2, \cdots, n, \\ \dot{X}_{\mathrm{tcsc}} = -\frac{1}{T_{\mathrm{c}}}(X_{\mathrm{tcsc}} - X_{\mathrm{tcsc0}}) + \frac{K_{\mathrm{T}}}{T_{\mathrm{c}}}u_{\mathrm{c}} + \zeta_{\mathrm{tcsc}} \end{cases} \tag{6.3.2}$$

with

$$\begin{cases} E_{\mathrm{q}i} = E'_{\mathrm{q}i} + (x_{\mathrm{d}i} - x'_{\mathrm{d}i})I_{\mathrm{d}i} \\ P_{\mathrm{e}i} = E'_{\mathrm{q}i}I_{\mathrm{q}i} + E'^2_{\mathrm{q}i}G_{ii} \\ I_{\mathrm{d}i} = -\sum_{j=1,j\neq i}^{n} E'_{\mathrm{q}j}Y_{ij}\cos(\delta_i - \delta_j) \\ I_{\mathrm{q}i} = -\sum_{j=1,j\neq i}^{n} E'_{\mathrm{q}j}Y_{ij}\sin(\delta_i - \delta_j) \end{cases} \tag{6.3.3}$$

where subscript i denotes the variables of the ith machine; δ_i the relative rotor angle; ω_i the generator speed; $E_{\mathrm{q}i}$ and $E'_{\mathrm{q}i}$ the voltage and transient voltage on the q-axis; $P_{\mathrm{m}i}$ the constant mechanical power; $P_{\mathrm{e}i}$ the electrical power output; H_i the rotor inertia; $T_{\mathrm{d0}i}$ the d-axis transient short-circuit time constant; $I_{\mathrm{d}i}$ and $I_{\mathrm{q}i}$ the d-axis and q-axis generator current; Y_{ij} the equivalent admittance between the ith and jth nodes, which is modified as $Y'_{ij} = 1/(1/Y_{ij} + X_{\mathrm{tcsc}})$ when a TCSC is equipped between the ith and jth nodes; and G_{ii} the equivalent self conductance of the ith machine.

6.4 POCAPC Design for Generator Excitor and TCSC Device

Controllers (6.2.17) and (6.2.22) will be applied for both SMIB system (6.3.1) and multi-machine power system (6.3.2).

6.4.1 Controller design for an SMIB system

For system (6.3.1), we choose $y = X_{\rm tcsc} - X_{\rm tcsc0}$, $u_1 = u_{\rm c}$ and $u_2 = u_{\rm fd}$. By setting $y = 0$, the zero-dynamics of system (6.3.1) can be written as

$$\begin{cases} \dot{\delta} = \omega - \omega_0 \\ \dot{\omega} = -\frac{D}{H}(\omega - \omega_0) + \frac{\omega_0}{H}\left(P_{\rm m} - \frac{E'_{\rm q}V_{\rm s}\sin\delta}{X'_{\rm d\Sigma}+X_{\rm tcsc0}}\right) \\ \dot{E}'_{\rm q} = \frac{(X_{\rm d}-X'_{\rm d})(V_{\rm s}\cos\delta - E'_{\rm q})}{T_{\rm d0}(X'_{\rm d\Sigma}+X_{\rm tcsc0})} - \frac{1}{T_{\rm d0}}E'_{\rm q} + \frac{K_{\rm c}}{T_{\rm d0}}u_{\rm fd} \end{cases} \tag{6.4.1}$$

Choose $z_1 = \delta - \delta_0$ for system (6.4.1), where δ_0 is the initial generator rotor angle. Differentiate z_1 until the excitation control input $u_{\rm fd}$ appears explicitly, the perturbation $\Psi_1(\cdot)$ is obtained as

$$\begin{aligned} \Psi_1(\cdot) = &-\frac{D}{H}\left[-\frac{D}{H}(\omega-\omega_0) + \frac{\omega_0}{H}\left(P_{\rm m} - \frac{E'_{\rm q}V_{\rm s}\sin\delta}{X'_{\rm d\Sigma}+X_{\rm tcsc0}}\right)\right] - \frac{\omega_0 V_{\rm s}}{H(X'_{\rm d\Sigma}+X_{\rm tcsc0})} \\ &\times \left[E'_{\rm q}(\omega-\omega_0)\cos\delta + \frac{\sin\delta}{T_{\rm d0}}\left(\frac{(X_{\rm d}-X'_{\rm d})(V_{\rm s}\cos\delta - E'_{\rm q})}{(X'_{\rm d\Sigma}+X_{\rm tcsc0})} - E'_{\rm q}\right)\right] \\ &- \frac{\omega_0 V_{\rm s}\sin\delta}{H(X'_{\rm d\Sigma}+X_{\rm tcsc0})} \times \frac{K_{\rm c}}{T_{\rm d0}}u_{\rm fd} - b_{10}u_{\rm fd} \end{aligned} \tag{6.4.2}$$

Define a fictitious state as $z_4 = \Psi_1(\cdot)$, and the extended state is denoted as $z_{\rm e} = [z_1, z_2, z_3, z_4]^{\rm T}$, the fourth-order state equation is

$$\dot{z}_{\rm e} = A_1 z_{\rm e} + B_1 u_{\rm fd} + B_2\dot{\Psi}_1(\cdot) \tag{6.4.3}$$

where

$$A_1 = \begin{bmatrix} 0 & 1 & 0 & 0 \\ 0 & 0 & 1 & 0 \\ 0 & 0 & 0 & 1 \\ 0 & 0 & 0 & 0 \end{bmatrix}, \quad B_1 = \begin{bmatrix} 0 \\ 0 \\ b_{10} \\ 0 \end{bmatrix}, \quad B_2 = \begin{bmatrix} 0 \\ 0 \\ 0 \\ 1 \end{bmatrix} \tag{6.4.4}$$

A fourth-order HGSPO (6.2.8) is used as

$$\begin{cases} \dot{\hat{z}}_1 = \hat{z}_2 + \frac{\alpha_1}{\epsilon}(z_1 - \hat{z}_1) \\ \dot{\hat{z}}_2 = \hat{z}_3 + \frac{\alpha_2}{\epsilon^2}(z_1 - \hat{z}_1) \\ \dot{\hat{z}}_3 = \hat{\Psi}_1(\cdot) + \frac{\alpha_3}{\epsilon^3}(z_1 - \hat{z}_1) + b_{10}u_{\mathrm{fd}} \\ \dot{\hat{\Psi}}_1(\cdot) = \frac{\alpha_4}{\epsilon^4}(z_1 - \hat{z}_1) \end{cases} \tag{6.4.5}$$

Extend the TCSC dynamics, yields

$$\begin{cases} \dot{y} = \Psi_{\mathrm{tcsc}}(\cdot) + b_{20}u_{\mathrm{c}} \\ \dot{y}_2 = \dot{\Psi}_{\mathrm{tcsc}}(\cdot) \end{cases} \tag{6.4.6}$$

where

$$\Psi_{\mathrm{tcsc}}(\cdot) = -\frac{1}{T_{\mathrm{c}}}y + \frac{K_{\mathrm{T}}}{T_{\mathrm{c}}}u_{\mathrm{c}} - b_{20}u_{\mathrm{c}} + \zeta_{\mathrm{tcsc}} \tag{6.4.7}$$

A second-order HGPO (6.2.12) is used as

$$\begin{cases} \dot{\hat{y}} = \hat{\Psi}_{\mathrm{tcsc}}(\cdot) + \frac{\alpha_1'}{\epsilon}(y - \hat{y}) + b_{20}u_{\mathrm{c}} \\ \dot{\hat{\Psi}}_{\mathrm{tcsc}}(\cdot) = \frac{\alpha_2'}{\epsilon^2}(y - \hat{y}) \end{cases} \tag{6.4.8}$$

For system (6.3.1), one can obtain $\tilde{p}(z, y)$ from perturbation (6.4.2) according to Eq. (6.2.20) as

$$\begin{aligned} \tilde{p}(z, y) = \frac{\omega_0 V_{\mathrm{s}}}{H}\Big[\frac{1}{X_\Delta}\Big(\frac{-DE_{\mathrm{q}}'\sin\delta}{H} + E_{\mathrm{q}}'(\omega - \omega_0)\cos\delta + \frac{\sin\delta}{T_{\mathrm{d0}}}(-E_{\mathrm{q}}' + K_{\mathrm{c}}u_{\mathrm{fd}})\Big) \\ + \frac{X_\Delta'}{X_\Delta^2}\frac{(X_{\mathrm{d}} - X_{\mathrm{d}}')(V_{\mathrm{s}}\cos\delta - E_{\mathrm{q}}')\sin\delta}{T_{\mathrm{d0}}}\Big] \end{aligned} \tag{6.4.9}$$

where $X_\Delta = (X_{\mathrm{d}\Sigma}' + X_{\mathrm{tcsc0}} + y)(X_{\mathrm{d}\Sigma}' + X_{\mathrm{tcsc0}})$ and $X_\Delta' = (2X_{\mathrm{d}\Sigma}' + 2X_{\mathrm{tcsc0}} + y)$.

The POCAPC of EC and TCSC controller for system (6.3.1) is designed as

$$\begin{cases} u_{\mathrm{fd}} = \frac{1}{b_{10}}(-\hat{\Psi}_1(\cdot) - k_1\hat{z}_3 - k_2\hat{z}_2 - k_3\hat{z}_1) \\ u_{\mathrm{c}} = \frac{1}{b_{20}}(-\hat{\Psi}_{\mathrm{tcsc}}(\cdot) - c\hat{z}_3\tilde{p}(z, y) - k'y + \nu) \\ \nu = -\beta y \end{cases} \tag{6.4.10}$$

A known $\tilde{p}(z, y)$ is a fundamental assumption in the standard CPC design [83], which contains the states and parameters and needs to be cancelled for passivation. In real power system operations, the damping coefficient D is much smaller than the

system inertia H thus $|DE'_{\rm q}\sin\delta/H| \approx 0$, and $|\frac{X'_\Delta}{X^2_\Delta}(X_{\rm d}-X'_{\rm d})(V_{\rm s}\cos\delta - E'_{\rm q})| \ll |-E'_{\rm q}+K_{\rm c}u_{\rm fd}|$ during the transient process due to the large excitation control input $u_{\rm fd}$, thus one can approximate $\tilde{p}(z,y)$ by ignoring the relatively small components. Denote $\tilde{p}^*(z,y)$ as its approximation, obtains

$$\tilde{p}^*(z,y) = \frac{\omega_0 V_{\rm s}}{HX_\Delta}\Big(E'_{\rm q}(\omega-\omega_0)\cos\delta + \frac{\sin\delta}{T_{\rm d0}}(-E'_{\rm q}+K_{\rm c}u_{\rm fd})\Big) \tag{6.4.11}$$

Thus, we replace $\tilde{p}(z,y)$ by its approximation $\tilde{p}^*(z,y)$, controller (6.4.10) becomes

$$\begin{cases} u_{\rm fd} = \frac{1}{b_{10}}(-\hat{\Psi}_1(\cdot) - k_1\hat{z}_3 - k_2\hat{z}_2 - k_3\hat{z}_1) \\ u^*_{\rm c} = \frac{1}{b_{20}}(-\hat{\Psi}_{\rm tcsc}(\cdot) - c\hat{z}_3\tilde{p}^*(z,y) - k'y + \nu) \\ \nu = -\beta y \end{cases} \tag{6.4.12}$$

Based on Assumption 6.1, constants b_{10} and b_{20} must satisfy following inequalities when the generator operates within its normal region:

$$b_{10} < -\omega_0 V_{\rm s}K_{\rm c}\sin\delta/[2HT_{\rm d0}(X'_{\rm d\Sigma}+X_{\rm tcsc0})] \tag{6.4.13}$$

$$b_{20} > K_{\rm T}/(2T_{\rm c}) \tag{6.4.14}$$

During the most severe disturbance, the electrical power will reduce from its initial value to around zero within a short period of time, Δ. Thus the boundary values of the estimated states and perturbation can be obtained as $|\hat{z}_3| \le \omega_0 P_{\rm m}/H$, $|\hat{\Psi}_1(\cdot)| \le \omega_0 P_{\rm m}/(H\Delta)$, and $|\dot{\hat{\Psi}}_1(\cdot)| \le \omega_0 P_{\rm m}/(H\Delta^2)$, respectively.

6.4.2 Controller design for a multi-machine power system

For system (6.3.2), we choose $y = X_{\rm tcsc} - X_{\rm tcsc0}$, $u_1 = u_{\rm c}$ and $u_{2i} = u_{{\rm fd}i}$. Set $y = 0$ in the equivalent admittance matrix Y, the zero-dynamics can be obtained. Choose $z_{i1} = \delta_i - \delta_{i0}$, $i = 1, 2, \ldots, n$, where δ_{i0} is the initial rotor angle of the *i*th generator. Differentiate z_{i1} until the excitation control input $u_{{\rm fd}i}$ appears explicitly, the perturbation $\Psi_i(\cdot)$ is obtained as

$$\begin{aligned}\Psi_i(\cdot) = &-\frac{\omega_0}{2H_i}\Big[\frac{D_i}{\omega_0}\frac{{\rm d}\omega_i}{{\rm d}t} + E'_{{\rm q}i}\frac{{\rm d}I_{{\rm q}i}}{{\rm d}t} + \frac{I_{{\rm q}i}+2G_{ii}E'_{{\rm q}i}}{T_{{\rm d}0i}}(-E'_{{\rm q}i} - (x_{{\rm d}i}-x'_{{\rm d}i})I_{{\rm d}i})\Big] \\ &- \frac{\omega_0(I_{{\rm q}i}+2G_{ii}E'_{{\rm q}i})}{2H_iT_{{\rm d}0i}}u_{{\rm fd}i} - b_{10i}u_{{\rm fd}i}\end{aligned} \tag{6.4.15}$$

Define a fictitious state as $z_{i4} = \Psi_i(\cdot)$, and the extended state is denoted as $z_{i\mathrm{e}} = [z_{i1}, z_{i2}, z_{i3}, z_{i4}]^{\mathrm{T}}$, the fourth-order state equation is

$$\dot{z}_{i\mathrm{e}} = A_{i1} z_{i\mathrm{e}} + B_{i1} u_{\mathrm{fd}i} + B_{i2} \dot{\Psi}_i(\cdot) \tag{6.4.16}$$

where

$$A_{i1} = \begin{bmatrix} 0 & 1 & 0 & 0 \\ 0 & 0 & 1 & 0 \\ 0 & 0 & 0 & 1 \\ 0 & 0 & 0 & 0 \end{bmatrix}, \quad B_{i1} = \begin{bmatrix} 0 \\ 0 \\ b_{10i} \\ 0 \end{bmatrix}, \quad B_{i2} = \begin{bmatrix} 0 \\ 0 \\ 0 \\ 1 \end{bmatrix} \tag{6.4.17}$$

A fourth-order HGSPO (6.2.8) is used for the *i*th generator as

$$\begin{cases} \dot{\hat{z}}_{i1} = \hat{z}_{i2} + \frac{\alpha_{i1}}{\epsilon}(z_{i1} - \hat{z}_{i1}) \\ \dot{\hat{z}}_{i2} = \hat{z}_{i3} + \frac{\alpha_{i2}}{\epsilon^2}(z_{i1} - \hat{z}_{i1}) \\ \dot{\hat{z}}_{i3} = \hat{\Psi}_i(\cdot) + \frac{\alpha_{i3}}{\epsilon^3}(z_{i1} - \hat{z}_{i1}) + b_{10i} u_{\mathrm{fd}i} \\ \dot{\hat{\Psi}}_i(\cdot) = \frac{\alpha_{i4}}{\epsilon^4}(z_{i1} - \hat{z}_{i1}) \end{cases} \tag{6.4.18}$$

Let us consider the equivalent two-machine subsystem involving a TCSC device and denote them as the jth and kth machine, namely, the TCSC device is installed between the jth and kth machine. Furthermore, each machine denoted by the ith machine is equipped with its own EC. The extended TCSC dynamics is the same as system (6.4.6), and the same HGPO (6.4.8) is used to obtain $\hat{\Psi}_{\mathrm{tcsc}}(\cdot)$.

The POCAPC of EC and TCSC controller for system (6.3.2) is designed as

$$\begin{cases} u_{\mathrm{fd}i} = \frac{1}{b_{10i}}(-\hat{\Psi}_i(\cdot) - k_{i1}\hat{z}_{i3} - k_{i2}\hat{z}_{i2} - k_{i3}\hat{z}_{i1}) \\ u_{\mathrm{c}} = \frac{1}{b_{20}}(-\hat{\Psi}_{\mathrm{tcsc}}(\cdot) - c_j \hat{z}_{j3}\tilde{p}_j(z,y) - c_k \hat{z}_{k3}\tilde{p}_k(z,y) + \nu) \\ \nu = -\beta y, \qquad\qquad i = 1, 2, \cdots, n \end{cases} \tag{6.4.19}$$

where $\tilde{p}_j(z,y)$ and $\tilde{p}_k(z,y)$ are calculated from perturbation (6.4.15) according to Eq. (6.2.20), where $i = j$ and $i = k$, and the TCSC device is installed between the

jth and kth machine, gives

$$\tilde{p}_j(z,y) = \frac{\omega_0}{2H_j}\Big[\Big(\frac{-D_j E'_{\mathrm{q}j}E'_{\mathrm{q}k}\sin\delta_{jk}}{2H_j} + E'_{\mathrm{q}j}E'_{\mathrm{q}k}\omega_{jk}\cos\delta_{jk} + \frac{E'_{\mathrm{q}k}}{T_{\mathrm{d}0j}}(u_{\mathrm{fd}j} - E'_{\mathrm{q}j})$$
$$\times \sin\delta_{jk} + \frac{2E'_{\mathrm{q}k}}{T_{\mathrm{d}0j}}G_{jj}E'_{\mathrm{q}j}(x_{\mathrm{d}j} - x'_{\mathrm{d}j})\cos\delta_{jk} + E'_{\mathrm{q}j}\frac{\sin\delta_{jk}}{T_{\mathrm{d}0k}}\Big(u_{\mathrm{fd}k} - E'_{\mathrm{q}k} + (x_{\mathrm{d}k} - x'_{\mathrm{d}k})$$
$$\times \sum_{i=1,i\neq k,j}^{n} E'_{\mathrm{q}i}Y_{ki}\cos\delta_{ki}\Big) + \frac{E'_{\mathrm{q}k}\sin\delta_{jk}}{T_{\mathrm{d}0j}}(x_{\mathrm{d}j} - x'_{\mathrm{d}j})\sum_{i=1,i\neq k,j}^{n} E'_{\mathrm{q}i}Y_{ji}\cos\delta_{ji}\Big)X^*_\Delta$$
$$+ X^{*'}_\Delta\Big(\frac{E'^2_{\mathrm{q}j}\sin(2\delta_{jk})}{2T_{\mathrm{d}0k}}(x_{\mathrm{d}k} - x'_{\mathrm{d}k}) + \frac{E'^2_{\mathrm{q}k}\sin(2\delta_{jk})}{2T_{\mathrm{d}0j}}(x_{\mathrm{d}j} - x'_{\mathrm{d}j})\Big)\Big] \tag{6.4.20}$$

$$\tilde{p}_k(z,y) = \frac{\omega_0}{2H_k}\Big[\Big(\frac{-D_k E'_{\mathrm{q}k}E'_{\mathrm{q}j}\sin\delta_{kj}}{2H_k} + E'_{\mathrm{q}k}E'_{\mathrm{q}j}\omega_{kj}\cos\delta_{kj} + \frac{E'_{\mathrm{q}j}}{T_{\mathrm{d}0k}}(u_{\mathrm{fd}k} - E'_{\mathrm{q}k})$$
$$\times \sin\delta_{kj} + \frac{2E'_{\mathrm{q}j}}{T_{\mathrm{d}0k}}G_{kk}E'_{\mathrm{q}k}(x_{\mathrm{d}k} - x'_{\mathrm{d}k})\cos\delta_{kj} + E'_{\mathrm{q}k}\frac{\sin\delta_{kj}}{T_{\mathrm{d}0j}}\Big(u_{\mathrm{fd}j} - E'_{\mathrm{q}j} + (x_{\mathrm{d}j} - x'_{\mathrm{d}j})$$
$$\times \sum_{i=1,i\neq j,k}^{n} E'_{\mathrm{q}i}Y_{ji}\cos\delta_{ji}\Big) + \frac{E'_{\mathrm{q}j}\sin\delta_{kj}}{T_{\mathrm{d}0k}}(x_{\mathrm{d}k} - x'_{\mathrm{d}k})\sum_{i=1,i\neq j,k}^{n} E'_{\mathrm{q}i}Y_{ki}\cos\delta_{ki}\Big)X^*_\Delta$$
$$+ X^{*'}_\Delta\Big(\frac{E'^2_{\mathrm{q}k}\sin(2\delta_{kj})}{2T_{\mathrm{d}0j}}(x_{\mathrm{d}j} - x'_{\mathrm{d}j}) + \frac{E'^2_{\mathrm{q}j}\sin(2\delta_{kj})}{2T_{\mathrm{d}0k}}(x_{\mathrm{d}k} - x'_{\mathrm{d}k})\Big)\Big] \tag{6.4.21}$$

where $X_{jk} = Y_{jk}^{-1}$, $X^*_\Delta = 1/[(X_{jk} + y + X_{\mathrm{tcsc}0})X_{jk}]$, and $X^{*'}_\Delta = (y + X_{\mathrm{tcsc}0} + 2X_{jk})/[(X_{jk} + y + X_{\mathrm{tcsc}0})X_{jk}]^2$.

Similarly, in real power system operations, one has the following approximation

$$|D_j E'_{\mathrm{q}j}E'_{\mathrm{q}k}\sin\delta_{jk}/(2H_j)| \approx 0 \tag{6.4.22}$$

As damping coefficient $D_j \ll H_j$ and $|\frac{2G_{jj}}{T_{\mathrm{d}0j}}(x_{\mathrm{d}j} - x'_{\mathrm{d}j})| \ll |\omega_{jk}|$ due to the self conductance G_{jj} is much smaller than time constant $T_{\mathrm{d}0j}$. The following approximations can be made during the transient process due to the large excitation control inputs $u_{\mathrm{fd}k}$ and $u_{\mathrm{fd}j}$ as

$$|(x_{\mathrm{d}k} - x'_{\mathrm{d}k})(\sum_{i=1,i\neq k,j}^{n} E'_{\mathrm{q}i}Y_{ki}\cos\delta_{ki} + \frac{X^{*'}_\Delta}{X^*_\Delta}E'_{\mathrm{q}j}\cos\delta_{jk})| \ll |u_{\mathrm{fd}k} - E'_{\mathrm{q}k}| \tag{6.4.23}$$

$$|(x_{\mathrm{d}j} - x'_{\mathrm{d}j})(\sum_{i=1,i\neq j,k}^{n} E'_{\mathrm{q}i}Y_{ji}\cos\delta_{ji} + \frac{X^{*'}_\Delta}{X^*_\Delta}E'_{\mathrm{q}k}\cos\delta_{kj})| \ll |u_{\mathrm{fd}j} - E'_{\mathrm{q}j}| \tag{6.4.24}$$

Thus one can approximate $\tilde{p}_j(z,y)$ and $\tilde{p}_k(z,y)$ by ignoring the relatively small components. Denote their approximation as $\tilde{p}_j^*(z,y)$ and $\tilde{p}_j^*(z,y)$, respectively, gives

$$\tilde{p}_j^*(z,y) = \frac{\omega_0 X_\Delta^*}{2H_j}\Big(\frac{E'_{\mathrm{q}k}}{T_{\mathrm{d}0j}}(u_{\mathrm{fd}j} - E'_{\mathrm{q}j})\sin\delta_{jk} + \frac{E'_{\mathrm{q}j}}{T_{\mathrm{d}0k}}(u_{\mathrm{fd}k} - E'_{\mathrm{q}k})\sin\delta_{jk} + E'_{\mathrm{q}j}E'_{\mathrm{q}k}\omega_{jk}\cos\delta_{jk}\Big) \tag{6.4.25}$$

$$\tilde{p}_k^*(z,y) = \frac{\omega_0 X_\Delta^*}{2H_k}\Big(\frac{E'_{\mathrm{q}j}}{T_{\mathrm{d}0k}}(u_{\mathrm{fd}k} - E'_{\mathrm{q}k})\sin\delta_{kj} + \frac{E'_{\mathrm{q}k}}{T_{\mathrm{d}0j}}(u_{\mathrm{fd}j} - E'_{\mathrm{q}j})\sin\delta_{kj} + E'_{\mathrm{q}k}E'_{\mathrm{q}j}\omega_{kj}\cos\delta_{kj}\Big) \tag{6.4.26}$$

Then we replace $\tilde{p}_j(z,y)$ and $\tilde{p}_k(z,y)$ by their approximation $\tilde{p}_j^*(z,y)$ and $\tilde{p}_k^*(z,y)$, respectively. Controller (6.4.19) becomes

$$\begin{cases} u_{\mathrm{fd}i} = \frac{1}{b_{10i}}(-\hat{\Psi}_i(\cdot) - k_{i1}\hat{z}_{i3} - k_{i2}\hat{z}_{i2} - k_{i3}\hat{z}_{i1}) \\ u_{\mathrm{c}}^* = \frac{1}{b_{20}}(-\hat{\Psi}_{\mathrm{tcsc}}(\cdot) - c_j\hat{z}_{j3}\tilde{p}_j^*(z,y) - c_k\hat{z}_{k3}\tilde{p}_k^*(z,y) + \nu) \\ \nu = -\beta y, \qquad i = 1,2,\cdots,n \end{cases} \tag{6.4.27}$$

Similar to the SMIB system, we choose:

$$b_{10i} < -\omega_0(I_{\mathrm{q}i} + 2G_{ii}E'_{\mathrm{q}i})/(2H_iT_{\mathrm{d}0i}) \tag{6.4.28}$$

$$b_{20} > K_{\mathrm{T}}/(2T_{\mathrm{c}}) \tag{6.4.29}$$

Moreover, estimates of state and perturbation are bounded as $|\hat{z}_{i3}| \le \omega_0 P_{\mathrm{m}i}/(2H_i)$, $|\hat{\Psi}_i(\cdot)| \le \omega_0 P_{\mathrm{m}i}/(2H_i\Delta)$, and $|\dot{\hat{\Psi}}_i(\cdot)| \le \omega_0 P_{\mathrm{m}i}/(2H_i\Delta^2)$.

To this end, a decentralized stabilizing EC has been designed for the ith machine as only the measurement of its rotor angle δ_i is required, which can effectively handle the modelling uncertainties. The TCSC controller measures the rotor angle δ_j and δ_k, excitation control inputs $u_{\mathrm{fd}j}$ and $u_{\mathrm{fd}k}$, transient voltage $E'_{\mathrm{q}j}$ and $E'_{\mathrm{q}j}$. The nominal value of time constant $T_{\mathrm{d}0j}$ and $T_{\mathrm{d}0k}$, inertial constant H_j and H_k of the jth and kth machine, and transmission line reactance X_{jk} are used for coordination. Note that the difference between the nominal values and the real values of the system parameters are aggregated into the perturbation, which is estimated by the HGSPO and HGPO.

Remark 6.6. Note that the rotor angle cannot be directly measured in practice,

which needs to be calculated indirectly by other system variables, such as zero sequence harmonic components of machine terminal voltage [131], in which there is no fundamental frequency component of zero sequence voltage under normal conditions, while the effect of loading (i.e. effect of stator fundamental frequency currents) on zero sequence harmonic voltages is minor. Alternatively, [132] develops a system that would directly measure the internal angle of the generator using a rotary encoder on the shaft of the machine, which effectiveness has been verified by the experiment.

6.5 Case Studies

6.5.1 The SMIB system

A proportional-integral-derivative (PID) based TCSC controller and automatic voltage regulator (AVR) equipped with lead-lag (LL) based power system stabilizer (PSS) is used as the conventional PID+LL controller, which structure and parameters are presented by Fig. 6.4 and Table 6.1, linearly parametric estimation based coordinated adaptive passive control (CAPC) used in [92] is also adopted and described by Eq. (6.5.1), and the POCAPC parameters are given in Table 6.2. The SMIB system parameters and initial operating conditions are provided in Table 6.3, and $\omega_0 = 100\pi$.

Table 6.1: PID+LL control parameters of the SMIB system.

$T_{\mathrm{R}} = 0.01$	$K_{\mathrm{pss}} = 40$	$T_{\mathrm{w}} = 10$	$T_1 = 0.3$
$T_2 = 0.1$	$T_3 = 0.3$	$T_4 = 0.1$	$K_{\mathrm{I}} = -1$
$K_{\mathrm{D}} = -0.1$	$K_{\mathrm{e}} = 25$	$K_{\mathrm{P}} = -1$	

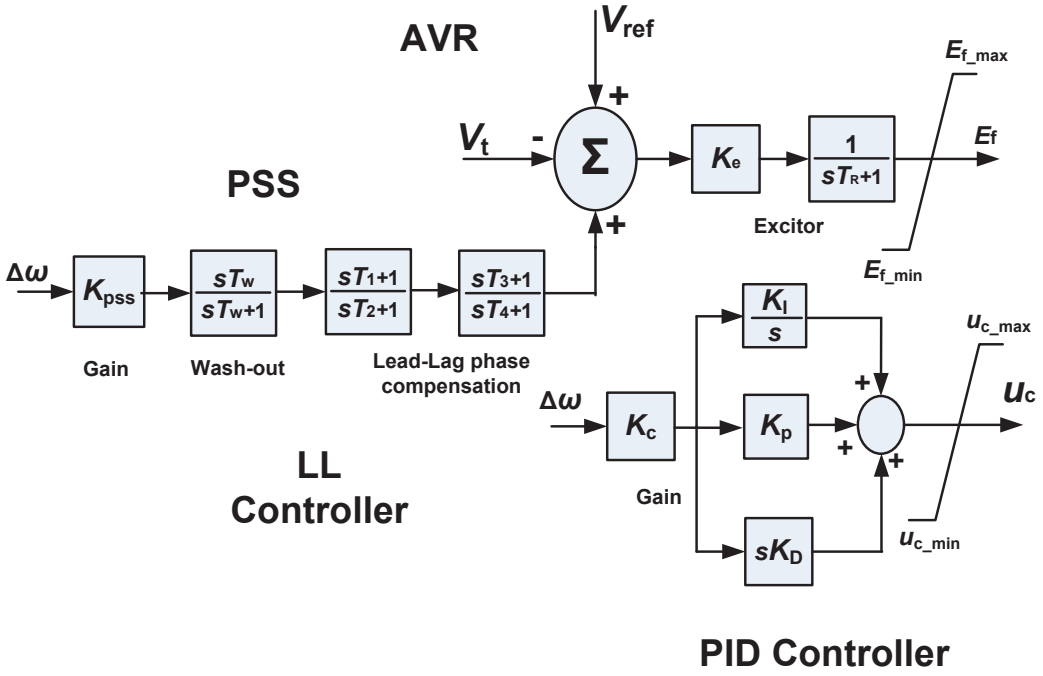

Figure 6.4: Structure of conventional PID+LL controller.

$$
\begin{cases}
u_{\mathrm{fd}} = \frac{T_{\mathrm{d0}}}{K_{\mathrm{c}}}\Big\{ z_2 \frac{\omega_0 V_{\mathrm{s}} \sin\delta}{H(X'_{\mathrm{d}\Sigma}+X_{\mathrm{tcsc0}})} - \frac{(X_{\mathrm{d}}-X'_{\mathrm{d}})(V_{\mathrm{s}}\cos\delta - E'_{\mathrm{q}})}{T_{\mathrm{d0}}(X'_{\mathrm{d}\Sigma}+X_{\mathrm{tcsc0}})} + \frac{E'_{\mathrm{q}}}{T_{\mathrm{d0}}} - c_3 z_3 \\
-x_2(x_3^* + E'_{\mathrm{q0}})\cot\delta + \frac{H(X'_{\mathrm{d}\Sigma}+X_{\mathrm{tcsc0}})}{\omega_0 V_{\mathrm{s}}\sin\delta}\Big[x_2(1+c_1c_2+\hat{\theta}) + (c_1+c_2+\hat{\theta}) \\
\times(\frac{\omega_0}{H}P_{\mathrm{m}} + \hat{\theta}x_2 - \frac{\omega_0 E'_{\mathrm{q}} V_{\mathrm{s}}\sin\delta}{H(X'_{\mathrm{d}\Sigma}+X_{\mathrm{tcsc0}})})\Big]\Big\} \\
u_{\mathrm{c}} = \frac{T_{\mathrm{c}}}{K_{\mathrm{T}}}\left(\frac{-\omega_0 E'_{\mathrm{q}} V_{\mathrm{s}}\sin\delta}{HX_\Delta} z_2 + \frac{(X_{\mathrm{d}}-X'_{\mathrm{d}})(V_{\mathrm{s}}\cos\delta - E'_{\mathrm{q}})}{T_{\mathrm{d0}}X_\Delta} z_3 - \hat{\psi}y + \nu \right) \\
\dot{\hat{\theta}} = \gamma\left(z_2 - z_3 \frac{H(X'_{\mathrm{d}\Sigma}+X_{\mathrm{tcsc0}})(\hat{\theta}+c_1+c_2)}{\omega_0 V_{\mathrm{s}}\sin\delta}\right) x_2 \\
\dot{\hat{\psi}} = \rho y^2 \\
\nu = -\beta y
\end{cases}
\tag{6.5.1}
$$

where $x_1 = \delta - \delta_0$, $x_2 = \omega - \omega_0$, $x_3 = E'_{\mathrm{q}} - E'_{\mathrm{q0}}$, $x_2^* = -c_1 x_1$, $z_2 = x_2 - x_2^*$, $z_3 = x_3 - x_3^*$, $x_3^* = [H(X'_{\mathrm{d}\Sigma} + X_{\mathrm{tcsc0}})/(\omega_0 V_{\mathrm{s}}\sin\delta)][x_1 + (\omega_0/H)P_{\mathrm{m}} + (\hat{\theta}+c_1)x_2 + c_2 z_2] - E'_{\mathrm{q0}}$.

1) Case 1: Three-phase short-circuit fault under the nominal model. A three-phase short-circuit fault occurs at $t = 1.0$ s and cleared at $t = 1.1$ s, where $|u_{\mathrm{fd}}| \leq 7$ p.u., and $|X_{\mathrm{tcsc}}| \leq 0.1$ p.u. such that a maximum 10% compensation ratio is imple-

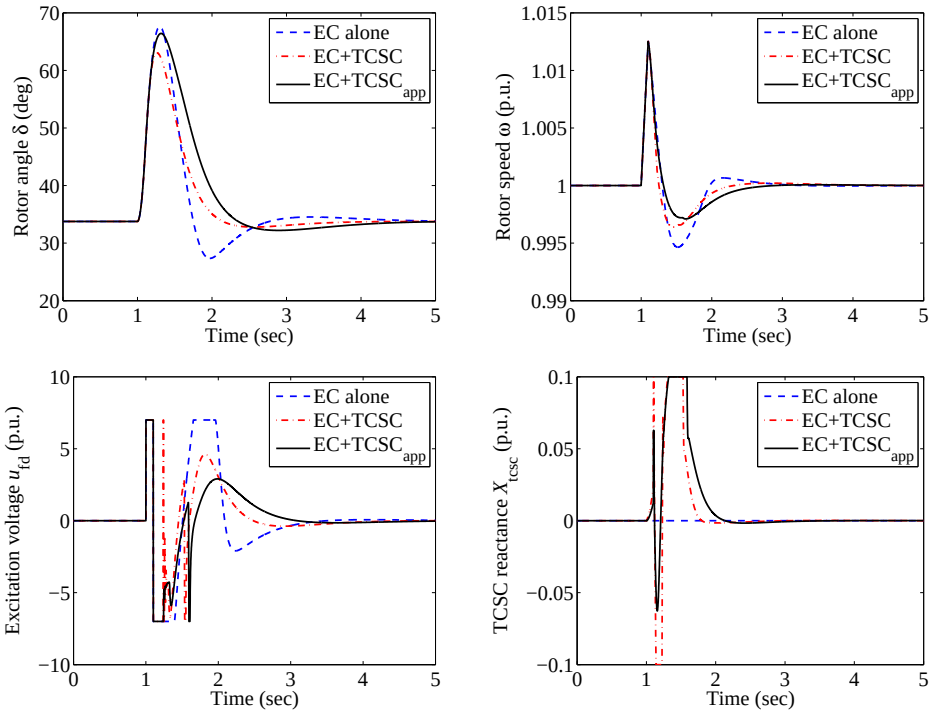

Figure 6.5: System responses obtained with the EC alone, coordinated EC and TCSC controller, and approximated EC and TCSC controller in the SMIB system.

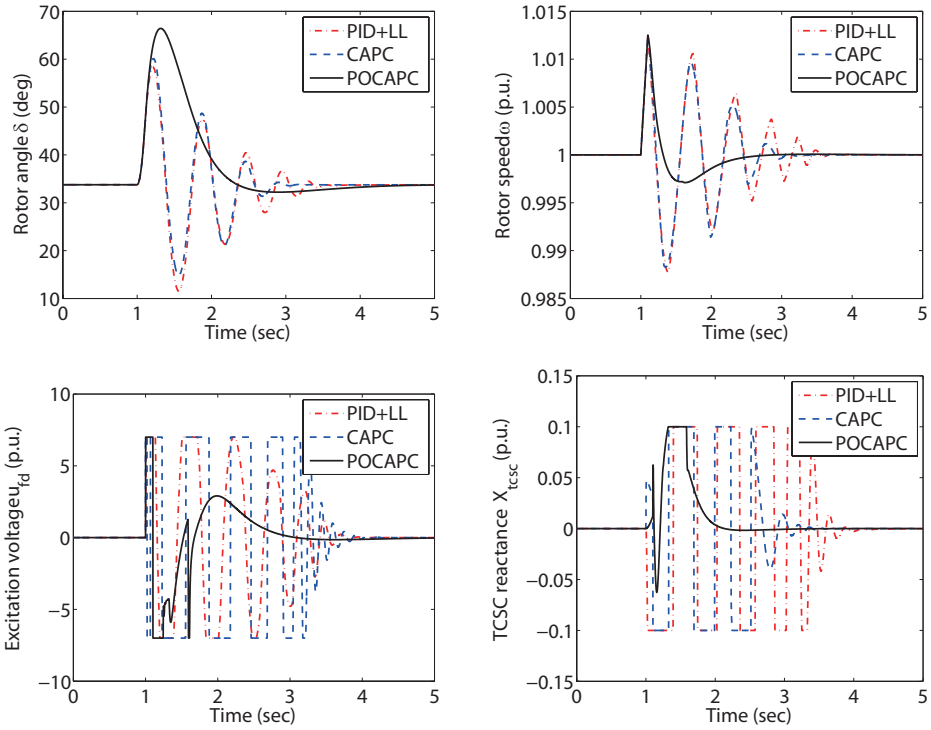

Figure 6.6: System responses obtained under the nominal model in the SMIB system.

Table 6.2: POCAPC parameters of the SMIB system.

$k_1 = 9$	$k_2 = 27$	$k_3 = 27$	$b_{10} = -15$
$b_{20} = 100$	$k' = 5$	$\beta = 15$	$c = 0.001$
$\alpha_1 = 160$	$\alpha_2 = 9.6 \times 10^3$	$\alpha_3 = 2.56 \times 10^5$	$\alpha_4 = 2.56 \times 10^6$
$\alpha'_1 = 30$	$\alpha'_2 = 225$	$\epsilon = 0.1$	$\Delta = 0.05$ s

Table 6.3: SMIB system parameters (in p.u.). [56]

$V_{\mathrm{t}} = 0.9669$	$H = 7$	$D = 0.5$	$P_{\mathrm{m}} = 0.9$
$X_{\mathrm{t}} = 0.127$	$X_{\mathrm{L1}} = 0.173$	$X_{\mathrm{L2}} = 0.3122$	$X_{\mathrm{d}} = 1.863$
$X'_{\mathrm{d}} = 0.257$	$T_{\mathrm{d0}} = 6.9$	$T_{\mathrm{c}} = 0.06$	$K_{\mathrm{T}} = 20$
$K_{\mathrm{c}} = 1$	$V_{\mathrm{s}} = 1.0$	$\delta_0 = 0.5892$	$X_{\mathrm{tcsc0}} = 0$

mented. Figure 6.5 shows the system responses obtained with the EC alone, coordinated EC and TCSC controller (6.4.10) and its approximated controller (6.4.12), respectively. From which the effectiveness of coordination is verified as an extra system damping is injected, and the excitation control effort is reduced. Moreover, the approximation is valid as it can capture the main feature of the exact coordination, hence we apply the approximated controllers for the rest of our studies.

System responses obtained under the nominal model is illustrated by Fig. 6.6. It is found that POCAPC can effectively stabilize the system. Figure 6.7 presents system responses obtained under a TCSC dynamics $\zeta_{\mathrm{tcsc}} = 10\sin(X_{\mathrm{tcsc}} - X_{\mathrm{tcsc0}})$ to represent a nonlinear unmodelled dynamics, which is the same as that used in [92] for a clear comparison of their control performance. In practice, this unmodelled dynamics describes an oscillatory disturbance in TCSC reactance which degrade the control performance thus needs to be suppressed. However, POCAPC does not require the unmodelled TCSC dynamics to satisfy this linear growth condition required by CAPC [92]. In fact, a general unmodelled TCSC dynamics can be estimated online by PO. Additionally, PID+LL control performance degrades dramatically as it is not robust to the TCSC modelling uncertainty. In contrast, both CAPC and POCAPC can maintain a consistent control performance as this uncertainty is

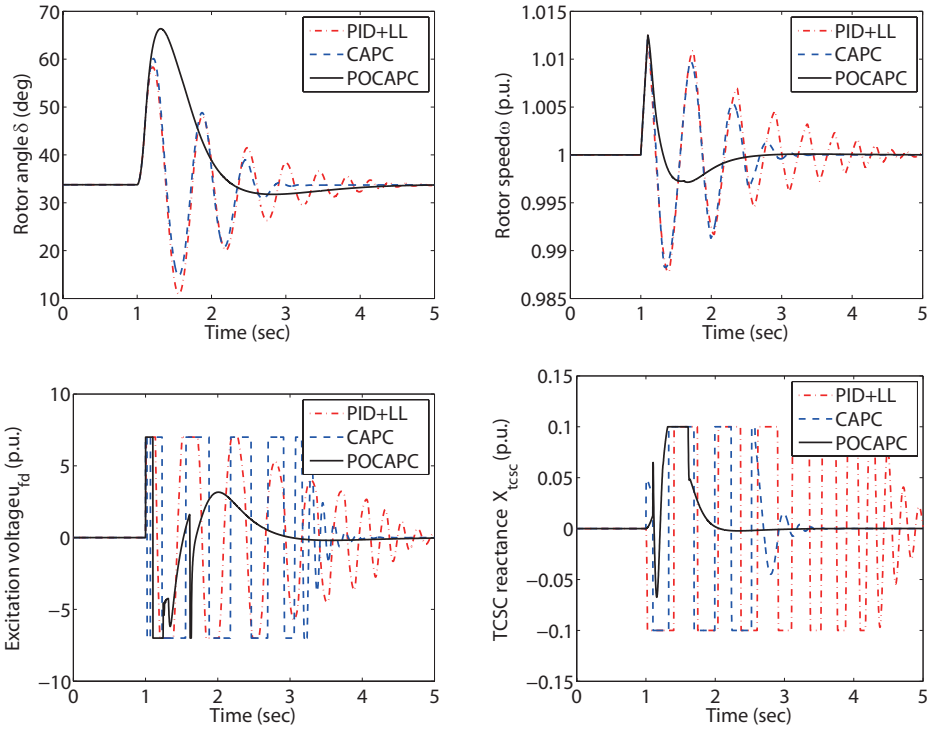

Figure 6.7: System responses obtained under an unmodelled TCSC dynamics in the SMIB system.

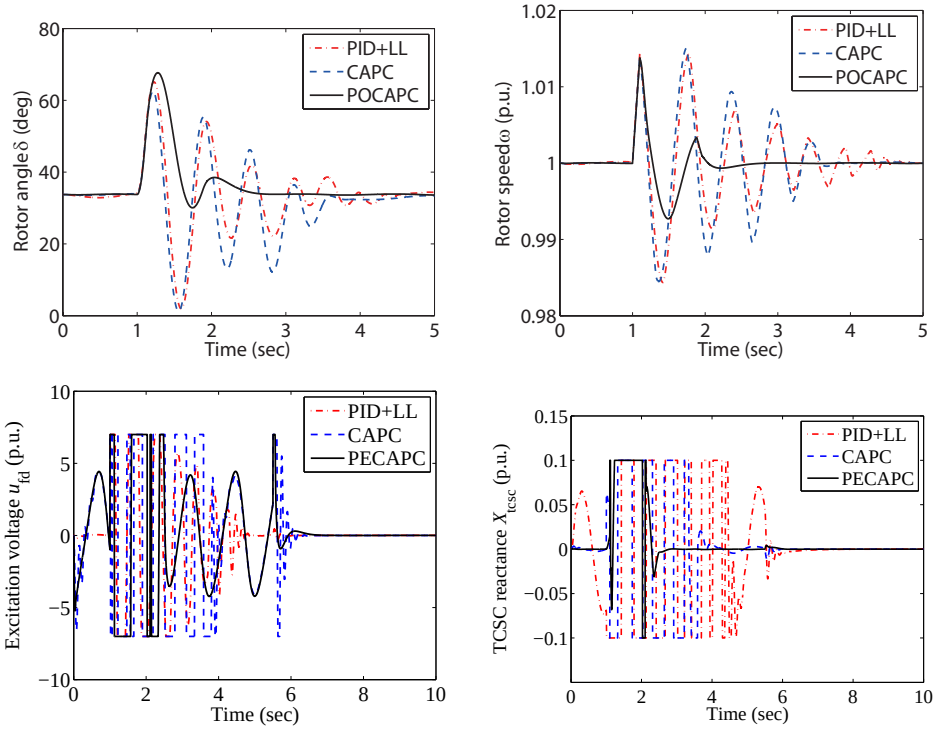

Figure 6.8: System responses obtained under an inter-area type disturbance in the SMIB system.

considered during the control design.

2) Case 2: Inter-area type disturbance. The low frequency inter-area modes oscillation has been well defined in the power system research, which is caused by the dynamic interactions, in a low frequency, between multiple groups of generators. It results in a degrade of power system stability and must be suppressed. It is concerned that the SMIB-designed controller may not perform well in the presence of inter-area modes oscillation. Thus it will be necessary to evaluate the SMIB-designed POCAPC on a more realistic multi-machine power system model with different oscillation frequencies. One approach named single machine quasi-infinite bus, where the infinite bus is modulated in magnitude by inter-area type disturbances. A typical inter-area type disturbance $V_{\rm s} = 1 + 0.1\sin(5t)$ is chosen to an corresponding low frequency oscillation (which normally ranges from 0.2 Hz to 2 Hz) of $(2.5/\pi)$ Hz as used in [59]. System responses are given in Fig. 6.8, the control performance of both PID+LL control and CAPC degrades significantly

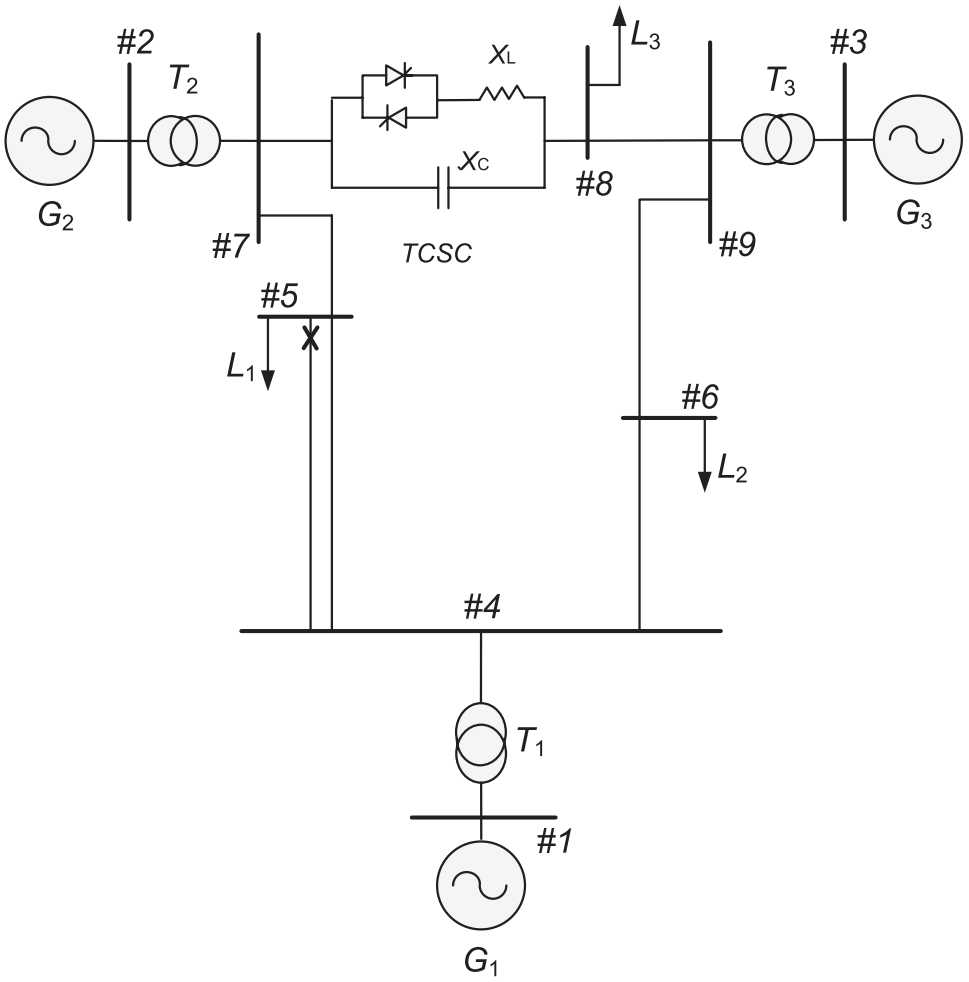

Figure 6.9: The three-machine power system equipped with a TCSC device.

due to the time-varying external disturbance. In contrast, POCAPC can effectively attenuate the inter-area type disturbance.

6.5.2 The three-machine power system

The PID+LL control, CPC, where the real value of the states and perturbation is used in the controllers, and POCAPC (6.4.27) are then applied on a three-machine nine-bus power system as shown in Fig. 6.9, where a TCSC device is installed between bus #7 and bus #8. The PID+LL control parameters and POCAPC parameters are given in Table 6.4 and Table 6.5, respectively. The transmission line parameters and initial operating condition (Type I) are given in Table 6.6 and Table

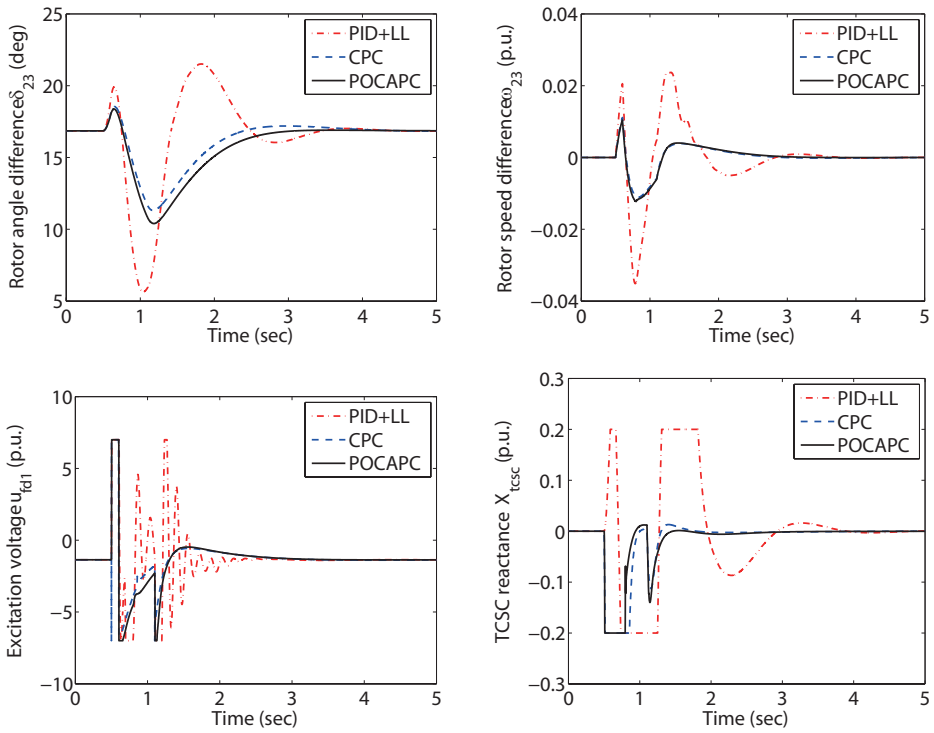

Figure 6.10: System responses obtained under operation Type I and the nominal model in the three-machine power system.

6.7, respectively.

Table 6.4: PID+LL control parameters of the three-machine power system.

$T_{\rm R} = 0.01$	$K_{\rm pss} = 30$	$T_{\rm w} = 10$	$T_1 = 0.2$
$T_2 = 0.1$	$T_3 = 0.3$	$T_4 = 0.1$	$K_{\rm I} = -5$
$K_{\rm D} = -0.5$	$K_{\rm e} = 100$	$K_{\rm P} = -10$	

A three-phase short-circuit fault occurs on one transmission line between bus $\#4$ and bus $\#5$ marked as point $'\times'$ at $t = 0.5$ s, the faulty transmission line is switched off at $t = 0.6$ s, and switched on again at $t = 1.1$ s when the fault is cleared, where $|u_{{\rm fd}i}| \leq 7$ p.u., and $|X_{\rm tcsc}| \leq 0.2$ p.u. such that a maximum 20% compensation ratio is implemented. Each generator is equipped with a decentralized stabilizing EC.

1) Case 1: Three-phase short-circuit fault under operation Type I and the nominal model. System responses obtained under operation Type I are given by Fig. 6.10, which shows POCAPC can achieve as satisfactory control performance as that

Table 6.5: POCAPC parameters of the three-machine power system.

$b_{10i} = -30$	$k_{i1} = 15$	$k_{i2} = 75$	$k_{i3} = 125$
$b_{20} = 20$	$k' = 10$	$\beta = 1$	$c_2 = 0.25$
$c_3 = 0.25$	$\alpha_{i1} = 200$	$\alpha_{i2} = 1.5 \times 10^4$	$\alpha_{i3} = 5 \times 10^5$
$\alpha_{i4} = 6.25 \times 10^6$	$\alpha'_1 = 60$	$\alpha'_2 = 900$	$\epsilon = 0.1$
$\Delta = 0.05$ s			

Table 6.6: Three-machine power system transmission line parameters (in p.u.). [56]

Line No.	Impedance
5-7	0.405
4-5(1)	0.23
4-5(2)	0.23
4-6	0.205
6-9	0.185
7-8	0.325
8-9	0.255
$P_{\mathrm{L1}} = 3.45$	$P_{\mathrm{L2}} = 2.55$
$P_{\mathrm{L3}} = 1.5$	

of CPC when an accurate system model is completely known, their tiny difference is caused by the estimation error. The observer performance during the fault is also monitored, the estimation errors of HGSPO_1 and HGPO are given in Fig. 6.11 and Fig. 6.12, respectively, which show the observers can provide accurate estimates of states with a fast tracking rate. However, there exists relatively larger errors in the estimate of perturbation at the instant of $t = 0.5$ s, $t = 0.6$ s, and $t = 1.1$ s, this is due to the discontinuity in the equivalent admittance Y_{12} caused by the disconnection and reconnection of the transmission line 4-5(2) at the instant when the fault occurs.

2) Case 2: The effect of parameter uncertainties on the system responses with the perturbation estimation. A 50% increase of the generator inertia H_i, time constant

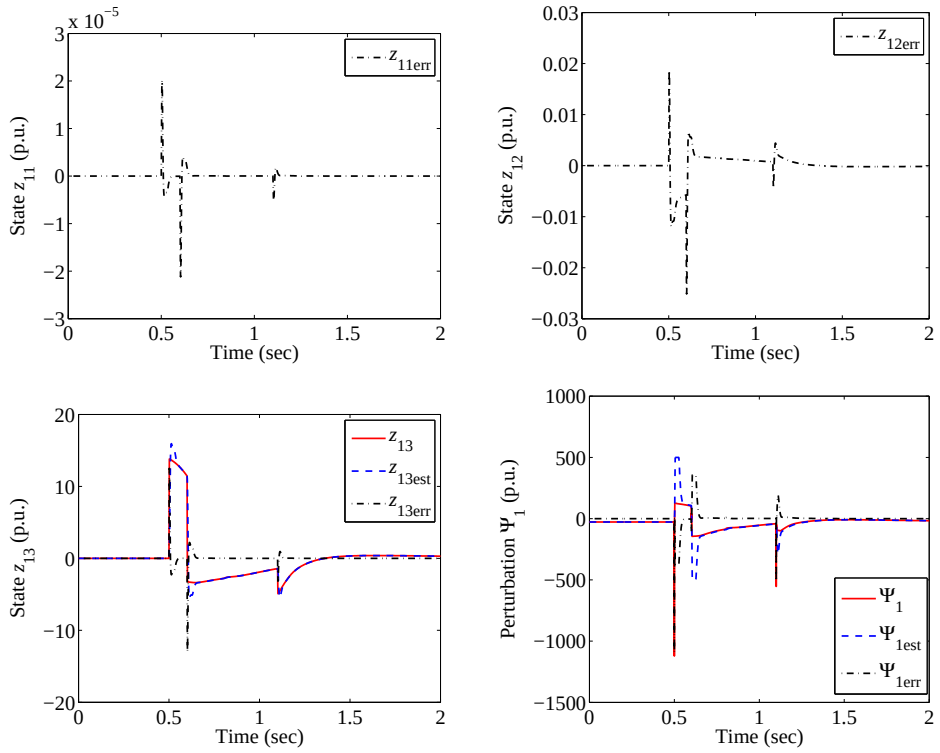

Figure 6.11: Estimation errors of $HGSPO_1$ for G_1 obtained under operation Type I and the nominal model in the three-machine power system.

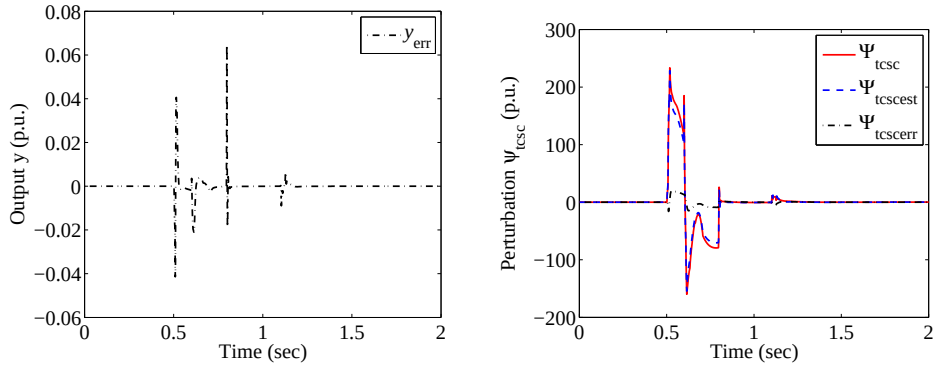

Figure 6.12: Estimation errors of HGPO for TCSC obtained under operation Type I and the nominal model in the three-machine power system.

Table 6.7: Three-machine power system operation Type I.

Generator	P(p.u.)	Q(p.u.)	V(p.u.)$\angle\theta$(deg.)
G_1	0.5821	0.9124	$1.1295\angle 0.0$
G_2	0.3577	0.8036	$1.034\angle 8.9$
G_3	0.1486	0.3040	$1.1372\angle -7.9$

$T_{\mathrm{d}0i}$ and TCSC time constant T_{c} used in controller (6.4.27) has been tested. Note that we use this dramatic parameter variation as an extreme case to evaluate the effect of parameter uncertainties, which main purpose is for the system robustness test rather than a real application. Fig. 6.13 shows that the control performance degrades dramatically in the presence of parameter uncertainties without the PO, in contrast the same control performance can be achieved with the PO shown by Fig. 6.14. This is because the parameter uncertainties of the generator inertia H_i and time constant $T_{\mathrm{d}0i}$ are lumped into the perturbation $\Psi_i(\cdot)$, which is estimated by the HGSPO and compensated by the controller. While the parameter uncertainties of the TCSC time constant T_{c} are lumped into the perturbation $\Psi_{\mathrm{tcsc}}(\cdot)$, which is estimated by the HGPO and compensated by the controller.

Table 6.8: Three-machine power system operation Type II.

Generator	P(p.u.)	Q(p.u.)	V(p.u.)$\angle\theta$(deg.)
G_1	0.5356	0.7052	$1.1488\angle 0.0$
G_2	0.6132	0.8533	$1.1171\angle 17.8$
G_3	0.1103	0.2965	$1.1524\angle -11.9$

3) Case 3: Parameter uncertainties under operation Type I. The robustness of PID+LL control, CPC and POCAPC has been evaluated by reducing the inertia constant H_i, time constant $T_{\mathrm{d}0i}$ of all generators and TCSC time constant T_{c} by 30% from their nominal values. System responses are provided in Fig. 6.15, in which a big difference in CPC has been identified, with and without accurate system parameters. In contrast, PID+LL control and POCAPC can maintain satisfactory control performance as their controller design does not require accurate system parameters.

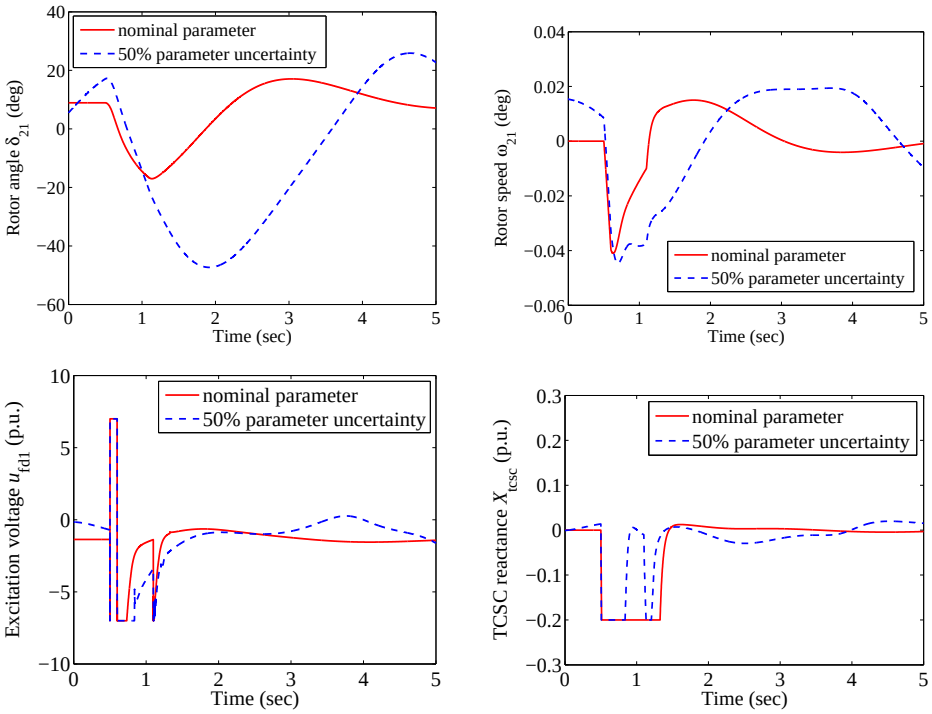

Figure 6.13: The effect of a 50% parameter increase on the dynamic response of proposed controller without perturbation compensation obtained in the three-machine power system.

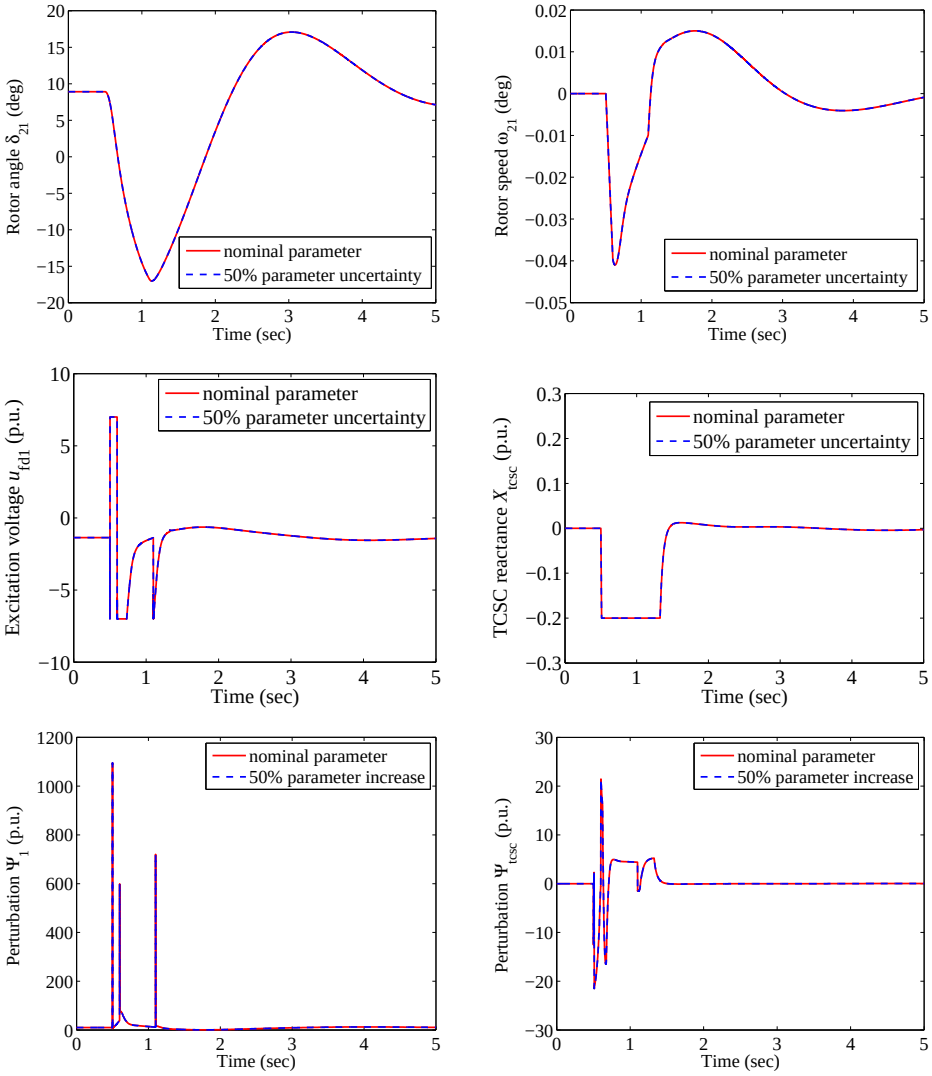

Figure 6.14: The effect of a 50% parameter increase on the dynamic response of proposed controller with perturbation estimation obtained in the three-machine power system.

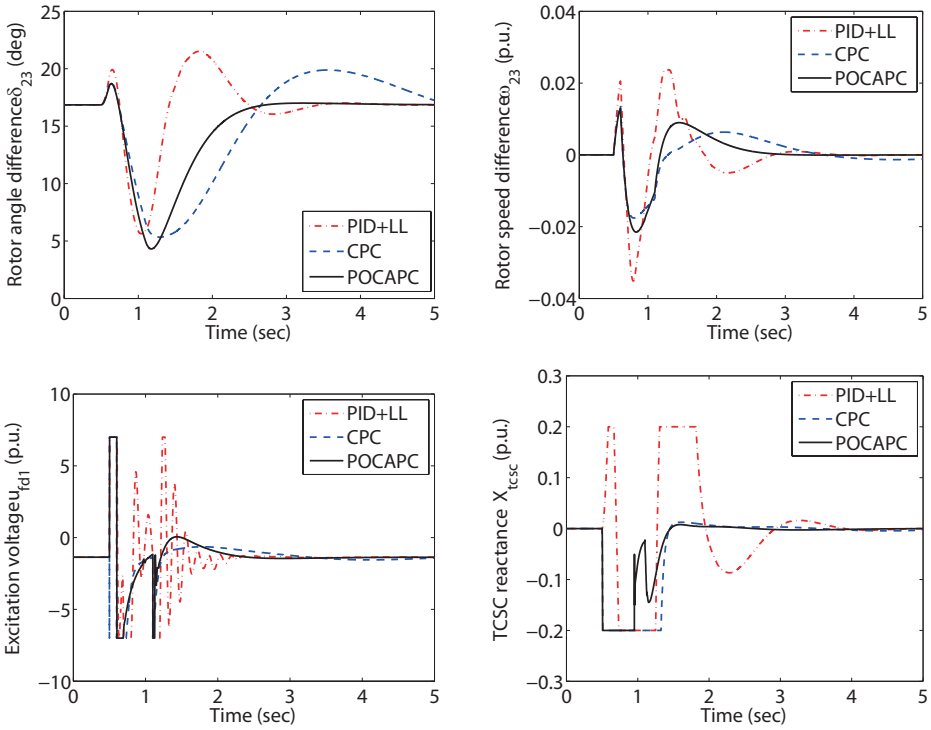

Figure 6.15: System responses obtained under operation Type I and the parameter uncertainties in the three-machine power system.

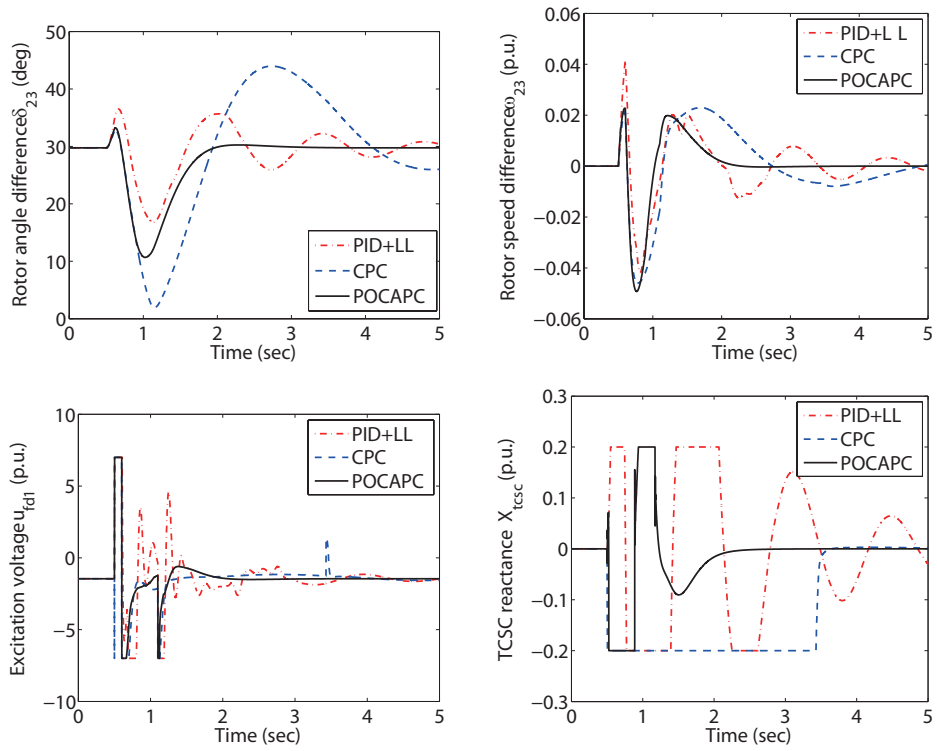

Figure 6.16: System responses obtained under operation Type II and the parameter uncertainties in the three-machine power system.

4) Case 4: Parameter uncertainties under operation Type II. In order to test the general effectiveness of POCAPC, Figure 6.16 presents system responses obtained under operation Type II given in Table 6.8 with the same parameter uncertainties. In this case a larger active power is transmitted, and the system suffers more severe oscillation when the fault occurs. One can find PID+LL control performance degrades dramatically as its control parameters are based on local system linearization. On the other hand, a severe oscillation in CPC can be seen due to the parameter uncertainties. In contrast, POCAPC can maintain a consistent control performance and provide significant robustness.

At last, the integral of absolute error (IAE) index is used to compare the control performance of each control schemes in all studied cases. Here $\text{IAE}_\delta = \int_0^T |\delta - \delta_0| \mathrm{d}t$ and $\text{IAE}_\omega = \int_0^T |\omega - \omega_0| \mathrm{d}t$, the units of rotor angle δ and speed ω are deg. and rad/s, respectively, the simulation time $T = 5$ s. The results are presented in Table 6.9. Note that POCAPC has a little bit higher IAE than that of CAPC and CPC under

nominal model, which is due to the estimation error of PO. Moreover, POCAPC provides much better robustness as it has the lowest IAE in the presence of various modelling uncertainties. In particular, its IAE_δ and IAE_ω are only 44.5% and 28.6% of those of CAPC, 50.9% and 31.5% of those of PID+LL control to the inter-area type disturbance in the SMIB system, while 27.4% and 47.7% of those of CPC, 53.1% and 56.7% of those of PID+LL control to the parameter uncertainties (Type II) in the three-machine power system.

Table 6.9: IAE index of different control schemes

The SMIB System Case						
Method \ Case	Nominal Model		Unmodelled TCSC Dynamics		Inter-area Type Disturbance	
	IAE_δ	IAE_ω	IAE_δ	IAE_ω	IAE_δ	IAE_ω
PID+LL	18.500	3.221	21.480	3.890	29.300	4.760
CAPC	16.370	2.830	17.710	2.875	33.480	5.248
POCAPC	18.030	1.193	17.500	1.207	14.900	1.500
The Three-machine Power System Case						
Method \ Case	Nominal Model		Parameter Uncertainties (Type I)		Parameter Uncertainties (Type II)	
	IAE_δ	IAE_ω	IAE_δ	IAE_ω	IAE_δ	IAE_ω
PID+LL	8.082	6.293	8.606	6.871	22.540	12.200
CPC	4.817	2.617	18.650	5.849	43.650	16.790
POCAPC	5.942	2.756	6.273	3.015	11.980	8.016

6.6 Hardware-in-the-loop Test

The HIL test is a technique used to develop and test complex, real-time embedded systems and includes the electrical emulation of sensors and actuators. These electrical emulations act as the interface between the plant simulation and the embedded system under test. The HIL technique has merits such as test environment, build-up time, and development cost for developing and testing an embedded system [170].

An HIL test has been undertaken based on dSPACE simulators to verify the implementation feasibility of POCAPC. The configuration and experiment platform of HIL test are shown in Fig. 6.17 and Fig. 6.18, respectively. The EC and TCSC controller are implemented on one dSPACE simulator (DS1104 board) with a sampling frequency $f_{\mathrm{c}} = 500$ Hz, and the SMIB system is simulated on another dSPACE simulator (DS1006 board) with the limit sampling frequency $f_{\mathrm{s}} = 50$ kHz to make HIL simulator as close to the real one as possible. A time delay $\tau = 2$ ms is used between the controller and SMIB system in the simulation to take the computational delay of the real-time controller into account. The measurements of the rotor angle δ, rotor speed ω, inner generator voltage E'_{q}, infinite bus voltage V_{s} and TCSC reactance X_{tcsc} are obtained from the real-time simulation of SMIB system on the DS1006 board, which are sent to two controllers implemented on the DS1104 board for the control outputs calculation, i.e., excitation voltage u_{fd} and TCSC modulated input u_{c}, respectively.

The disturbance is set up as: A 0.1 s three-phase short-circuit fault occurs at 1.9 s. The total experiment time is 60 s and only the response of the first 8 s is presented for a clear illustration of the transient responses. The following three tests are carried out: Test 1: Same observer parameters used in the previous simulation, original poles $\lambda = 40$, $\lambda' = 15$ with $b_{10} = -150$ and $b_{20} = 100$; Test 2: Reduced observer poles $\lambda = 15$ and $\lambda' = 15$; Test 3: Further reduced observer poles $\lambda = 5$ and $\lambda' = 5$.

It has been found from the Test 1 that an unexpected high-frequency chattering occurs in u_{fd} and X_{tcsc}, which does not appear in the simulation. This is due to the large observer poles result in high gains, which lead to highly sensitive observer

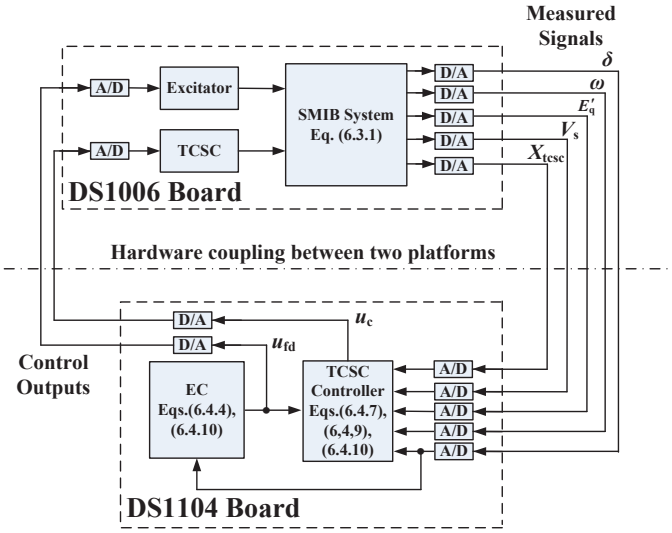

Figure 6.17: The configuration of the HIL test.

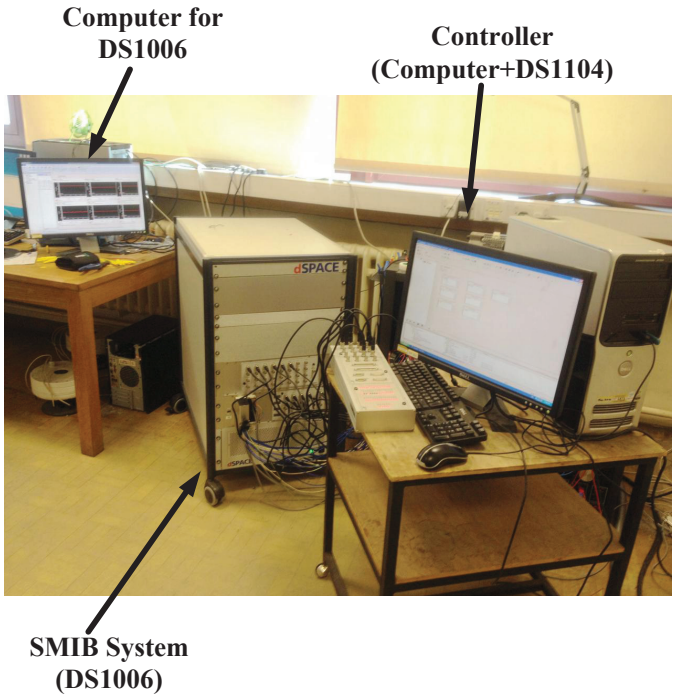

Figure 6.18: The experiment platform of the HIL test.

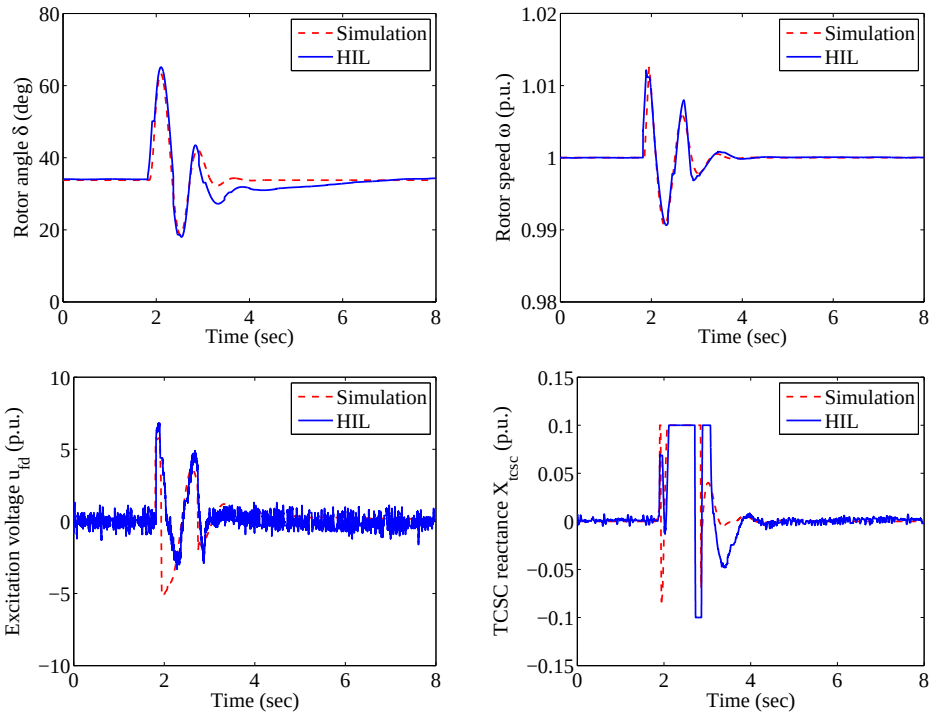

Figure 6.19: System responses obtained in the HIL test with large observer poles $\lambda = \lambda' = 15$ ($f_{\mathrm{s}} = 50$ kHz, $f_{\mathrm{c}} = 500$ Hz and $\tau = 2$ ms).

dynamics to the measurement noises. Hence in Test 2 reduced observer poles are chosen. Fig. 6.19 shows that the rotor angle and speed can be effectively stabilized, but a consistent high-frequency chattering still exists in both u_{fd} and X_{tcsc}. Through the trial-and-error it finds that an observer pole in the range of 3-10 can avoid the high-frequency chattering but with almost similar transient responses, therefore in Test 3 the observer poles are further reduced. The control performance of simulation and HIL test is given in Fig. 6.20, one can find that the high-frequency chattering disappears and the rotor angle and speed are still effectively stabilized.

The difference of the obtained results between the simulation and HIL test is possibly caused by the following three reasons: (a) There exists measurement noises in the HIL test which are not considered in the simulation, a filter could be used to remove the measurement noises and improve the control performance; (b) The discretization of the HIL test and sampling holding may introduce an additional amount of error compared to continuous control used in the simulation; and (c)

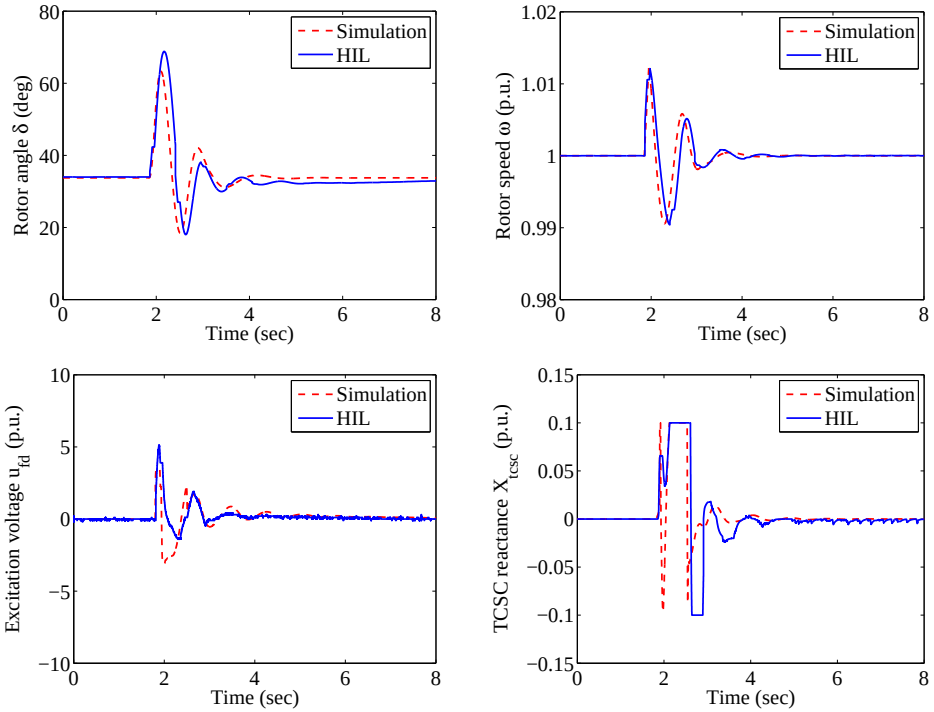

Figure 6.20: System responses obtained in the HIL test with proper observer poles $\lambda = \lambda' = 5$ ($f_s = 50$ kHz, $f_c = 500$ Hz and $\tau = 2$ ms).

The computational delay of the real-time controller, which exact value is difficult to obtain. A time delay $\tau = 2$ ms has been assumed in the simulation to consider the effect of this computational delay.

6.7 Discussion

It is necessary to study the computational cost of POCAPC as the high performance systems often have high computational cost. As POCAPC needs to calculate a fourth-order HGSPO (6.4.5) and a second-order HGPO (6.4.8) together with a nonlinear function (6.4.11), it has the highest computational cost. The computational cost of CAPC is higher than that of CPC, as CAPC requires solving a second-order parameter estimator (6.5.1). For CPC and PID+LL control, it's difficult to compare the computational cost as CPC has to calculate three complex functions (6.4.2), (6.4.7) and (6.4.11), while PID+LL control has to calculate a first-order integral used in PID loop, and a second-order LL plus a first-order washout loop. For the multi-machine power systems, the computational cost of CPC, CAPC (nonlinear functions (6.4.2), (6.4.7) and (6.4.11) become more complex) and POCAPC (nonlinear function (6.4.11) becomes more complex) will be higher than that of the SMIB system, while the computational cost of PID+LL control does not change. As POCAPC is a decentralized controller, it can be easily extended into multi-machine power systems as each generator will be equipped with a decentralized stabilizing EC, and the TCSC controller is separately implemented in the TCSC device.

Finally, the majority of studies related to power system control and operation is so far based on the simulation or HIL test. It is difficult to undertake a physical experiment for the multi-machine power system due to its significant scale and complexity.

6.8 Conclusion

In this chapter, POCAPC has been developed via designing the PO to estimate the perturbation, which is a lumped term including system nonlinearities, parame-

ter uncertainties, unmodelled dynamics and time-varying external disturbances. In addition, only the range of CLF is needed by the POCAPC, while an explicit CLF is required by CAPC which is difficult to find in complex nonlinear systems. The POCAPC has been applied to SMIB systems and multi-machine power systems. The simulation results show that it can provide similar control performance under the nominal model, but much better robustness in the presence of unmodelled dynamics and parameter uncertainties, comparing to that of PID+LL control, CPC and CAPC. Finally, an HIL test has been undertaken to verify the implementation feasibility of the proposed approach.

Chapter 7

Conclusions and Future Work

A summary of the results obtained in this thesis is provided below, and by this means its contributions are highlighted. Suggestions for future research are listed at the end.

7.1 Summary

Perturbation observer based adaptive passive control and its applications for VSC-HVDC systems and FACTS devices have been studied in this thesis. After defining the combinatorial effect of system nonlinearities, parameter uncertainties, unmodelled dynamics, and time-varying external disturbances as a perturbation, a high-gain perturbation observer is designed and the perturbation observer based adaptive passive control scheme is developed. The following results have been presented:

- The real-time estimation of perturbation, which includes system nonlinearities, parameter uncertainties, unmodelled dynamics and time-varying external disturbances, is a functional estimation rather than the parametric estimation. The controller does not require an accurate system model and only one state measurement is needed.

- The upper bounds of perturbation are only required in the design of observer, not the controller loop directly. In addition, as the upper bound of perturbation

is replaced by the smaller bound of its estimation error, an over-conservative control input is avoided such that the tracking accuracy can be improved.

- The proposed approach can be applied for general canonical systems, thus the strict requirement of a vector relative degree of one used in PC can be released. In addition, the assumptions made by APC or RPC for system uncertainties and structure can be avoided. These merits make POAPC applicable in practice.

- Perturbation observers have been used to develop a coordinated adaptive passive control, in which only the range of CLF is needed rather than its explicit form. It partially releases the dependence of an accurate system model and can handle various system uncertainties.

- The stability analysis of the closed-loop system including the controller and observer for both POAPC and POCAPC scheme has been undertaken in the context of Lyapunov criterion, and corresponding simulation results of example systems have been given.

The proposed control schemes have been applied to design adaptive passive controller for VSC-HVDC systems and FACTS devices in power systems, respectively.

- Perturbation observer based adaptive passive controller for the two-terminal VSC-HVDC system has been developed. The proposed controller is based on local measurements, which control performance is evaluated by simulation and compared with PI control and PC. Furthermore, hardware experiments of rectifier controller and inverter controller have been carried out.

- Passive controller has been applied for the N-terminal VSC-MTDC systems, which remains the beneficial system nonlinearities to improve the system damping. The remained internal dynamics has been proved to be asymptotically stable in the context of Lyapunov criterion. Eight case studies on a four-terminal VSC-MTDC system have been done by simulation to evaluate the control performance of PC, which is compared to that of PI control and FLC.

- Perturbation observer based adaptive passive controller has been developed for the N-terminal VSC-MTDC system, which only requires the measurement of DC voltage, active and reactive power. It can provide a significant robustness to various system uncertainties as no accurate system model is needed.

- Perturbation observer based coordinated adaptive passive controller of generator excitation system and TCSC device for SMIB systems and multi-machine power systems has been designed. It is implemented locally for each generator and can maintain a consistent control performance under different operating conditions. Simulation results have been provided to demonstrate its superiority over conventional PID+LL controller, coordinated passive controller and coordinated adaptive passive controller. An HIL test has been carried out to verify the implementation feasibility of the proposed controller.

7.2 Future Studies

We point out several related directions which deserve further investigations as follows:

- Discrete adaptive passive control design via perturbation observers. Our work has been developed mainly for continuous systems. It is desired to extend the research into discrete time systems.

- Hardware implementation of POAPC for a complete two-terminal VSC-HVDC system or VSC-MTDC systems. Due to the limit of experimental facilities, the proposed approach has been separately implemented for rectifier controller and inverter controller for the two-terminal VSC-HVDC system. It is worth developing a hardware platform for a complete two-terminal VSC-HVDC system connected to two strong AC girds, and VSC-MTDC system connected to both strong AC grids and DFIG (representing the offshore wind farm) to test the control performance of the proposed controller.

- POCAPC can lead to more applications in power systems with different FACTS devices. This thesis has designed the coordinated control of EC and TCSC controller, it is valuable to investigate the coordinated control of EC and other FACTS devices, such as SVC, STATCOM, and UPEC.

- HIL test for multi-machine power systems. We have undertaken the HIL test of POCAPC on SMIB systems, future studies can be carried out on the multi-machine power systems and VSC-MTDC systems.

- The physical meaning of Assumption 2.2 to VSC-HVDC systems and multi-machine power systems is worth further investigating, i.e., the explicit value (or range) of perturbation bounds γ_{i1} and γ_{i2} in a practical system.

Appendix A

Basic Concepts of Passive Systems

This chapter recalls some basic concepts of passive systems which lay the foundation of the developments described in this thesis. We are interested here in lumped-parameter systems interconnected to the external environment through some port power variables, which are conjugated in the sense that their product has units of power (e.g., currents and voltages in electrical circuits, or forces and velocities in mechanical systems).

Consider a nonlinear system as follows

$$\begin{cases} \dot{x} = f(x) + g(x)u \\ y = h(x) \end{cases} \tag{A.0.1}$$

where state $x \in \mathbb{R}^n$, control input $u \in \mathbb{R}^m$ and output $y \in \mathbb{R}^m$. $f(x) \in \mathbb{R}^n$, $g(x) \in \mathbb{R}^{n \times m}$, and $h(x) \in \mathbb{R}^m$ are some smooth functions. The system has the same number of inputs and outputs.

Definition A.1. *System (A.0.1) is defined to be passive if there exists a continuously differentiable positive semi-definite function $H(x)$ (called the storage function) such that*

$$u^{\mathrm{T}} y \geq \dot{H} \geq \frac{\partial H}{\partial x}(f(x) + g(x)u), \quad \forall (x, u) \in \mathbb{R}^n \times \mathbb{R}^m \tag{A.0.2}$$

Moreover, it is said to be

• *losses if $u^{\mathrm{T}} y = \dot{H}$;*

• *input-feedforward passive if* $u^{\mathrm{T}}y \geq \dot{H} + u^{\mathrm{T}}\varphi(u)$ *for some function* φ*;*

• *input strictly passive if* $u^{\mathrm{T}}y \geq \dot{H} + u^{\mathrm{T}}\varphi(u)$ *and* $u^{\mathrm{T}}\varphi(u) > 0$*,* $\forall u \neq 0$*;*

• *output-feedback passive if* $u^{\mathrm{T}}y \geq \dot{H} + y^{\mathrm{T}}\rho(u)$ *for some function* ρ*;*

• *output strictly passive if* $u^{\mathrm{T}}y \geq \dot{H} + y^{\mathrm{T}}\rho(u)$ *and* $y^{\mathrm{T}}\rho(u) > 0$*,* $\forall y \neq 0$*;*

• *strictly passive if* $u^{\mathrm{T}}y \geq \dot{H} + \psi(x)$ *for some positive definite function* ψ*.*

In all cases, the inequality should hold for all (x, u)*.*

Lemma A.1. *If system (A.0.1) is passive with a positive semi-definite storage function* $H(x)$*, then the origin of* $\dot{x} = f(x)$ *is stable.*

Proof. Take $H(x)$ as a Lyapunov function candidate for $\dot{x} = f(x)$, then $\dot{H}(x) \leq 0$. □

Definition A.2. *A system as given in (A.0.1) is zero-state observable if for any* $x \in X$

$$y(t) = h(\phi(t, t_0, x)) = 0, \quad \forall t \geq t_0 \geq 0 \qquad \Rightarrow \quad x = 0 \tag{A.0.3}$$

and the system is locally zero-state observable if there exists a neighbourhood X_n *of the origin, such that for all* $x \in X_n$*, inequality (A.0.3) holds. The system is zero-state detectable if for any* $x \in X$*,*

$$y(t) = h(\phi(t, t_0, x)) = 0, \quad \forall t \geq t_0 \geq 0 \qquad \Rightarrow \quad \lim_{t\to\infty} \phi(t, t_0, x) = 0 \tag{A.0.4}$$

and the system is locally zero-state detectable if there exists a neighbourhood X_n *of the origin, such that for all* $x \in X_n$*, inequality (A.0.4) holds.*

Lemma A.2. *Consider system (A.0.1), the origin of* $\dot{x} = f(x)$ *is asymptotically stable if the system is*

• *strictly passive or*

• *output strictly passive and zero-state observable.*

Furthermore, if the storage function is radially unbounded, the origin will be globally asymptotically stable.

Proof. Suppose that system is strictly passive and let $H(x)$ be its storage function.

Then, with $u = 0$, $\dot{H}$ satisfies the inequality $\dot{H} \leq -\psi(x)$, where $\psi(x)$ is positive definite. In particular, for any $x \in \mathbb{R}^n$, the equation $\dot{x} = f(x)$ has a solution $\phi(t, x)$, starting from x at $t = 0$ and defined on some interval $[0, \delta]$. Integrate the inequality $\dot{H} \leq -\psi(x)$, yields

$$H(\phi(\tau, x)) - H(x) \leq -\int_0^\tau \psi(\phi(t, x))\mathrm{d}t \ , \forall \tau \in [0, \delta] \tag{A.0.5}$$

Use $H(\phi(\tau, x)) \geq 0$, we obtain

$$H(x) \geq \int_0^\tau \psi(\phi(t, x))\mathrm{d}t \tag{A.0.6}$$

Suppose now that there is $\bar{x} \neq 0$ such that $H(\bar{x}) = 0$. The foregoing inequality implies

$$\begin{aligned} &\int_0^\tau \psi(\phi(t, \bar{x}))\mathrm{d}t \ = 0 \ , \forall \tau \in [0, \delta] \Rightarrow \psi(\phi(t, \bar{x})) \equiv 0 \\ &\Rightarrow \phi(t, \bar{x}) \equiv 0 \Rightarrow \bar{x} = 0 \end{aligned} \tag{A.0.7}$$

which contradicts the claim that $\bar{x} \neq 0$. Thus, $H(x) > 0$ for all $x \neq 0$. This qualifies $H(x)$ as a Lyapunov function candidate, and since $\dot{H}(x) \leq -\psi(x)$, we conclude that the origin is asymptotically stable. □

Suppose now the system is output strictly passive and let $H(x)$ be its storage function. Then, with $u = 0$, $\dot{H}$ satisfies the inequality $\dot{H} \leq -y^{\mathrm{T}}\rho(y)$, where $-y^{\mathrm{T}}\rho(y) > 0$ for all $y \neq 0$. By repeating the preceding argument, we can use the inequality to show that $H(x)$ is positive semi-definite. In particular, for any $x \in \mathbb{R}^n$, we have

$$H(x) \geq \int_0^\tau h^{\mathrm{T}}(\phi(t, x))\rho(h(\phi(t, x)))\mathrm{d}t \tag{A.0.8}$$

Suppose that there is $\bar{x} \neq 0$ such that $H(\bar{x}) = 0$ The foregoing inequality implies

$$\int_0^\tau h^{\mathrm{T}}(\phi(t, \bar{x}))\rho(h(\phi(t, \bar{x})))\mathrm{d}t = 0 \ , \forall \tau \in [0, \delta] \Rightarrow h(\phi(t, \bar{x})) \equiv 0 \tag{A.0.9}$$

which, due to zero-state observability, implies

$$\phi(t, \bar{x}) \equiv 0 \Rightarrow \bar{x} = 0 \tag{A.0.10}$$

Hence, $H(x) > 0$ for all $x \neq 0$. This qualifies $H(x)$ as a Lyapunov function candidate, and since $\dot{H}(x) \leq -y^T\rho(y)$ and $y(t) \equiv 0 \Rightarrow x(t) \equiv 0$, we conclude by

the invariance principle that the origin is asymptotically stable. Finally, if $H(x)$ is radially unbounded, the origin will be globally asymptotically stable. □

Lemma A.3. *If system (A.0.1) is not passive, but there exists a positive semi-definite storage function $H(x)$ and a feedback control $u = \beta(x) + \kappa\nu$ such that $\dot{H} \leq \nu^{\mathrm{T}} y$, then the feedback system is passive. As a result, the feedback passivation can be used as a preliminary step in a stabilization design by choosing the additional input in the following output feedback form*

$$\nu^{\mathrm{T}} = -\phi(y) \tag{A.0.11}$$

where $\phi(y)$ is a sector-nonlinearity satisfying $\phi(y)y > 0$ for $y \neq 0$ and $\phi(0) = 0$, can achieve $\dot{H} \leq -\phi(y)y \leq 0$.

Definition A.3. *Consider system (A.0.1) with the constraint $y = 0$ as follows*

$$\begin{cases} \dot{x} = f(x) + g(x)u \\ 0 = h(x) \end{cases} \tag{A.0.12}$$

The constrained system (A.0.12) is called the zero-output dynamics, or briefly, the zero-dynamics.

If the matrix $L_g h(0) \triangleq | \frac{\partial h(x)}{\partial x} g(x) |_{x=0}$ of system (A.0.1) is nonsingular and the distribution spanned by the vector fields $g_1(x), \cdots, g_m(x)$ is involutive in a neighbourhood of $x = 0$, then there exists new local coordinates (z, y) under which the system can be represented as the so-called normal form

$$\begin{cases} \dot{z} = q(z, y) \\ \dot{y} = b(z, y) + a(z, y)u \end{cases} \tag{A.0.13}$$

The zero-dynamics of system (A.0.13) are given by

$$\dot{z} = q(z, 0) \tag{A.0.14}$$

Denote $q(z, 0)$ by $f_0(z)$. Then, the function $q(z, y)$ can be expressed in the following form

$$q(z, y) = f_0(z) + p(z, y)y \tag{A.0.15}$$

where $p(z, y)$ is a smooth function.

Definition A.4. *Consider system (A.0.1). Suppose that $L_g h(0)$ is nonsingular, then the system is said to be:*

1. minimum-phase if its zero-dynamics (A.0.14) are asymptotically stable in a neighbourhood of $z = 0$;

2. weakly minimum-phase if there exists a positive differentiable function $W(z)$ with $W(0) = 0$, such that

$$\frac{\partial W(z)}{\partial z} f_0(z) \leq 0 \tag{A.0.16}$$

in a neighbourhood of $z = 0$.

Similarly, we can define globally minimum-phase and globally weakly minimum-phase if the normal form and minimum-phase are global.

Lemma A.4. *Consider system (A.0.1). Assume that rank $L_g h(x)$ is constant in a neighbourhood of $x = 0$. If system (A.0.1) is passive with a C^2 storage function $H(x)$ which is positive semi-definite, then*

1. $L_g h(0)$ is nonsingular and system (A.0.1) has a vector relative degree of one.

2. The zero-dynamics of system (A.0.1) exist locally at $x = 0$, and system (A.0.1) is weakly minimum-phase.

References

[1] G. Asplund, "Application of HVDC Light to power system enhancement," *in Proc. IEEE Power Eng. Soc. Winter Meeting*, pp. 2498-2503, 2000.

[2] U. Axelsson, A. Holm, C. Liljegren, M. Aberg, K. Eriksson, and O. Tollerz, "The Gotland HVDC Light Project-Experiences from trial and commercial operation," *in CIRED Conf.*, Amsterdam, The Netherlands, pp. 1-5, 2001.

[3] K. Eriksson, "Operational experience of HVDC LIGHT," *in Proc. AC DC Conf. Transmiss.*, London, U.K., pp. 205-210, 2001.

[4] N. Flourentzou, V. G. Agelidis, and G. D. Demetriades, "VSC-based HVDC power transmission systems: an overview," *IEEE Trans. Power Electron.*, vol. 24, no. 3, pp. 592-602, Mar. 2009.

[5] P. K. Steimer, H. E. Gruening, J. Werninger, E. Carroll, S. Klaka, and S. Linder, "IGCT-A new emerging technology for high power, low cost inverters," *IEEE Ind. Appl. Mag.*, vol. 5, no. 4, pp. 12-18, Jul./Aug. 1999.

[6] S. Gunturi and D. Schneider, "On the operation of a press pack IGBT module under short circuit conditions," *IEEE Trans. Adv. Packag.*, vol. 29, no. 3, pp. 433-440, Aug. 2006.

[7] L. Weimers, "AC or DC: Which way should China go?," *Modern Power Syst.*, vol. 25, no. 8, pp. 11-17, 2005.

[8] C. Ashmore, "Transmit the light fantastic [HVDC power transmission]," *IET Power Eng.*, vol. 20, no. 2, pp. 24-27, 2006.

[9] L. Willis and N. Stig, "HVDC transmission: Yesterday and today," *IEEE Power Energy Mag.*, vol. 5, no. 2, pp. 22-31, Mar./Apr. 2007.

[10] G. Asplund, "Ultra high voltage transmission," *ABB Rev.*, vol. 2, pp. 22-27, 2007.

[11] B. Andersen and C. Barker, "A new era in HVDC?," *Inst. Electr. Eng. Rev.*, vol. 46, no. 2, pp. 33-39, 2000.

[12] J. Varley, "HVDC: Fifty years on," *Modern Power Syst.*, vol. 24, no. 10, pp. 18-20, 2004.

[13] G. Asplund, K. Eriksson, and O. Tollerz, "HVDC light: A tool for electric power transmission to distant load," *in Proc. VI Sepope Conf.*, Salvador, Brazil, pp. 1-7, 1998.

[14] L. Carlsson, "'Classical' HVDC: Still continuing to evolve," *Modern Power Syst.*, vol. 22, no. 6, pp. 19-21, 2002.

[15] A. Ericsson, M. Jeroense, J. Miller, L. Palmgvist, B. Railing, and P. Riffon, "HVDC light cable systems-The latest projects," *in Proc. Nordic Insul. Symp.*, pp. 107-116, 2003.

[16] C. Meyer, S. Schroder, and R. W. D. Doncker, "Solid-state circuit breakers and current limiters for medium-voltage systems having distributed power systems," *IEEE Trans. Power Electron.*, vol. 19, no. 5, pp. 1333-1340, Sep. 2004.

[17] C. Meyer and R. W. D. Doncker, "Solid-state circuit breaker based on active thyristor topologies," *IEEE Trans. Power Electron.*, vol. 21, no. 2, pp. 450-458, Mar. 2006.

[18] W. Lu and B. Ooi, "DC overvoltage control during loss of converter in multiterminal voltage-source converter-based HVDC (M-VSC-HVDC)," *IEEE Trans. Power Del.*, vol. 18, no. 3, pp. 915-920, Jul. 2003.

[19] M. X. Bui, M. H. Nguyen, and T. K. Saha, "Dynamic simulation of HVDC interconnection in large power system," *Proceedings of Power and Energy Society General Meeting*, 2011.

[20] P. Fairley, "Germany jump-starts the supergird," *IEEE Spectrum*, vol. 50, no. 5, pp. 36-41, 2013.

[21] G. Asplund, "HVDC grids-possibilities and challenges," CIGRE SC B4 Bergen Colloq. Bergen, Norway, Jun. 2009.

[22] X. D. Zheng, N. L. Tai, J. S. Thorp, and G. L. Yang, "A transient harmonic current protection scheme for HVDC transmission line," *IEEE Trans. Power Del.*, vol. 27, no. 4, pp. 2278-2285, Oct. 2012.

[23] Y. Zhang, N. L. Tai, and B. Xu, "Fault analysis and traveling-wave protection scheme for bipolar HVDC lines," *IEEE Trans. Power Del.*, vol. 27, no. 3, pp. 1583-1591, Jul. 2012.

[24] X. D. Zheng, N. L. Tai, G. L. Yang, and H. Y. Ding, "A transient protection scheme for HVDC transmission line," *IEEE Trans. Power Del.*, vol. 27, no. 2, pp. 718-724, Apr. 2012.

[25] L. N. He, C. C. Liu, A. Pitto, and D. Cirio, "Distance protection of AC grid with HVDC-connected offshore wind generators," *IEEE Trans. Power Del.*, vol. 29, no. 2, pp. 493-501, Apr. 2014.

[26] G. B. Song, X. Chu, S. P. Gao, X. N. Kang, and Z. B. Jiao, "A new whole-line quick-action protection principle for HVDC transmission lines using one-end current," *IEEE Trans. Power Del.*, vol. 30, no. 2, pp. 599-607, Apr. 2015.

[27] J. Liang, T. J. Jing, O. G. Bellmunt, J. Ekanayake, and N. Jenkins, "Operation and control of multiterminal HVDC transmission for offshore wind farms," *IEEE Trans. Power Del.*, vol. 26, no. 4, pp. 2596-2604, Oct. 2011.

[28] J. Hongbo and A. Ekstrom, "Multiterminal HVDC systems in urban areas of large cities," *IEEE Trans. Power Del.*, vol. 13, pp. 1278-1284, 1998.

[29] T. M. Haileselassie, M. Molinas, and T. Undeland, "Multi-terminal VSC-HVDC system for integration of offshore wind farms and green electrification of platforms in the north sea," *Nordic Workshop on Power and Industrial Electronics*, June 9-11, 2008.

[30] L. Weixing and O. B. Teck, "Multi-terminal HVDC as enabling technology of premium quality power park," *IEEE Power Engineering Society Winter Meeting*, vol. 2, pp. 719-724, 2002.

[31] S. Gordon, "Supergrid to the rescue," *Inst. Eng. Technol. Power Eng.*, vol. 20, pp. 30-33, Oct./Nov. 2006.

[32] H. Rao "Architecture of Nan'ao multi-terminal VSC-HVDC system and its multi-functional control," *CSEE Journal of Power and Energy Systems*, vol. 1, no. 1, pp. 9-18, Mar. 2015.

[33] ABB, "BorWin1 offshore wind connections", Available: http://new.abb.com/systems/hvdc/references/borwin1, 2015.

[34] S. Cole and R. Belmans, "A proposal for standard VSC HVDC dynamic models in power system stability studies," *Electr. Power Syst. Res.*, vol. 81, pp. 967-973, 2011.

[35] L. Zhang, L. Harnefors, and P. Rey, "Power system reliability and transfer capability improvement by vsc-hvdc," *in Proc. Cigre regional meeting*, 2007.

[36] H. F. Latorre and M. Ghandhari, "Improvement of power system stability by using a VSC-HVdc," *International Journal of Electrical Power and Energy Systems*, vol. 33, pp. 332-339, 2011.

[37] S. P. Azad, R. Iravani, and J. E. Tate, "Dynamic stability enhancement of a DC-segmented AC power system via HVDC operating-point adjustment," *IEEE Trans. Power Del.*, vol. 30, no. 2, pp. 657-665, Apr. 2015.

[38] X. I. Koutiv, T. D. Vrionis, Nicholas A. Vovos, and G. B. Giannakopoulos, "Optimal integration of an offshore wind farm to a weak AC grid," *IEEE Trans. Power Del.*, vol. 21, no. 2, pp. 987-994, Apr. 2006.

[39] S. Li, T. A. Haskew, and L. Xu, "Control of HVDC light system using conventional and direct current vector control approaches," *IEEE Trans. Power Electron.*, vol. 25, no. 12, pp. 3106-3118, Dec. 2010.

[40] S. Y. Ruan, G. J. Li, L. Peng, Y. Z. Sun, and T. T. Lie, "A nonlinear control for enhancing HVDC light transmission system stability," *Electrical Power and Energy Syst.*, vol. 29, pp. 565-570, 2007.

[41] L. Zhang, L. Harnefors, and H. Nee, "Interconnection of two very weak AC systems by VSC-HVDC links using power-synchronization control," *IEEE Trans. Power Syst.*, vol. 26, no. 1, pp. 344-355, July 2011.

[42] X. M. Fan, L. Guan, C. J. Xia, and T. Y. Ji, "IDA-PB control design for VSC-HVDC transmission based on PCHD model," *Int. Trans. Electr. Energ. Syst.*, doi: 10.1002/etep.1953 June 2014.

[43] M. Durrant, H. Werner, and K. Abbott, "Synthesis of multi-objective controllers for a VSC HVDC terminal using LMIs," in *Proc. IEEE Conf. Decision and Control*, Dec. 2004, pp. 4473-4478.

[44] S. Y. Ruan, G. J. Li, X. H. Jiao, Y. Z. Sun, and T. Lie, "Adaptive control design for VSC-HVDC systems based on backstepping method," *Elect. Power Syst. Res.*, vol. 77, pp. 559-565, Apr. 2007.

[45] A. E. Leon, J. M. Mauricio, J. A. Solsona, and A. G. Exposito, "Adaptive control strategy for VSC-based systems under unbalanced network conditions," *IEEE Trans. Smart Grid*, vol. 1, no. 3, pp. 311-319, Dec. 2010.

[46] A. Moharana and P. K. Dash, "Input-output linearization and robust sliding-mode controller for the VSC-HVDC transmission link," *IEEE Trans. Power Del.*, vol. 25, no. 3, pp. 1952-1961, July 2010.

[47] N. R. Chaudhuri and B. Chaudhuri, "Adaptive droop control for effective power sharing in multi-terminal DC (MTDC) grids," *IEEE Trans. Power Syst.*, vol. 28, no. 1, pp. 21-29, Feb. 2013.

[48] X. D. Zhao and K. Li, "Adaptive backstepping droop controller design for multi-terminal high-voltage direct current systems," *IET Gener. Transm. Distrib.*, Feb. 2015.

[49] K. Meah and A. H. M. Sadrul Ula, "A new simplified adaptive control scheme for multi-terminal HVDC transmission systems," *Electrical Power and Energy Syst.*, vol. 32, pp. 243-253, 2010.

[50] K. Meah and A. H. M. Sadrul Ula, "Simple fuzzy self-tuning PI controller for multiterminal HVDC transmission systems," *Elect. Power Component and Syst.*, vol. 36, no. 3, pp. 224-238, Feb. 2008.

[51] W. Y. Wang and M. Barnes, "Power flow algorithms for multi-terminal VSC-HVDC with droop control," *IEEE Trans. Power Syst.*, vol. 29, no. 4, pp. 1721-1730, Jul. 2014.

[52] C. Dierckxsensa, K. Srivastavab, M. Rezab, S. Colec, J. Beertena, and R. Belmansa, "A distributed DC voltage control method for VSC MTDC systems," *Electr. Power Syst. Res.*, vol. 82, pp. 54-58, 2012.

[53] A. E. Alvareza, J. Beertenc, D. V. Hertemc, and O. G. Bellmunta, "Hierarchical power control of multiterminal HVDC grids," *Electr. Power Syst. Res.*, vol. 121, pp. 207-215, 2015.

[54] S. Rodrigues, R. T. Pinto, P. Bauer, and J. Pierik, "Optimal power flow control of VSC-based multiterminal DC network for offshore wind integration in the north sea," *IEEE Journal of Emerging and Selected Topics in Power Electronics*, vol. 1, no. 4, pp. 260-268, 2013.

[55] M. A. Penalbaa, A. E. Alvareza, O. G. Bellmunta, and A. Sumpera, "Optimum voltage control for loss minimization in HVDC multi-terminal transmission systems for large offshore wind farms," *Electr. Power Syst. Res.*, vol. 89, pp. 54-63, 2012.

[56] L. L. Grigsby, "Power system stability and control," CRC Press, Boca Raton, FL, USA, Third edition, 2012.

[57] N. G. Hingorani and L. Gyugyi, "Undestanding FACTS," IEEE Press, New York, 1999.

[58] A. Edris et al., "Proposed terms and definitions for flexible AC transmission system (FACTS)," *IEEE Trans. Power Del.*, vol. 12, no. 4, pp. 1848-1852, 1997.

[59] P. Kundur, "Power system stability and control," McGraw-Hill, New York, 1994.

[60] X. P. Zhang, "Flexible AC transmission systems: Modelling and control," Springer, Verlag Berlin Heidelberg, 2006

[61] M. M. Farsangi, Y. H. Song, W. F. Fang, and X. F. Wang, "Robust FACTS control design using the H_∞ loop shaping method," *IEE Proc. Genet. Transm. Distrib.*, vol. 149, no. 3, pp. 352-358, 2002.

[62] N. Mithulananthan, C. A. Canizares, J. Reeve, and G. J. Rogers, "Comparison of PSS, SVC, and STATCOM controllers for damping power system oscillations," *IEEE Trans. Power Syst.*, vol. 18, no. 2, pp. 786-792, 2003.

[63] T. T. Nguyen and R. Gianto, "Neural networks for adaptive control coordination of PSSs and FACTS devices in multimachine power system," *IET Gener. Transm. Distrib.*, vol. 2, no. 3, pp. 355-372, 2008.

[64] M. Zarghami, M. L. Crow, and S. Jagannathan, "Nonlinear control of FACTS controllers for damping interarea oscillations in power systems," *IEEE Trans. Power Del.*, vol. 25, no. 4, pp. 3113-3121, Oct. 2010.

[65] D. Menniti., A. Pinnarelli, N. Scordino, and N. Sorrentino, "Using a FACTS device controlled by a decentralised control law to damp the transient frequency deviation in a deregulated electric power system," *Electr Power Syst Res.*, vol. 72, pp. 289-298, 2004.

[66] S. Panda and N. P. Padhy, "Comparison of particle swarm optimization and genetic algorithm for FACTS-based controller design," *Appl. Soft Comput.*, vol. 8, pp. 1418-1427, 2008.

[67] A. Kazemi and M. V. Sohrforouzani, "Power system damping using fuzzy controlled facts devices," *Internation Journal of Electrical Power and Energy Systems*, vol. 28, pp. 349-357, 2006.

[68] R. Majumder, B. C. Pal, C. Dufour, and P. Korba, "Design and real-time implementation of robust FACTS controller for damping inter-area oscillation," *IEEE Trans. Power Syst.*, vol. 21, no. 2, pp. 809-816, May, 2006.

[69] W. Shao and V. Vittal, "LP-based OPF for corrective FACTS control to relieve overloads and voltage violations," *IEEE Trans. Power Syst.*, vol. 21, no. 4, pp. 1832-1839, Nov., 2006.

[70] J. J. Wang, C. Fu, and Y. Zhang, "SVC control system based on instantaneous reactive power theory and fuzzy PID," *IEEE Trans. Ind. Electron.*, vol. 55, no. 4, pp. 1658-1665, Apr., 2008.

[71] L. M. Liu, P. C. Zhu, Y. Kang, and J. Chen, "Power-flow control performance analysis of a unified power-flow controller in a novel control scheme," *IEEE Trans. Power Del.*, vol. 22, no. 3, pp. 1613-1619, Jul., 2007.

[72] N. C. Sahoo, B. K. Panigrahi, P. K. Dash, and G. Panda, "Application of a multivariable feedback linearization scheme for STATCOM control," *Electr Power Syst Res.*, vol. 62, pp. 81-91, 2002.

[73] A. Isidori, "Nonlinear control systems," Berlin: Springer, third edition, 1995.

[74] H. K. Khalil, "Nonlinear systems," Prentice-Hall, Inc., London, second edition, 1996.

[75] C. I. Byrnes, A. Isidori, and J. C. Willems, "Passivity, feedback equivalence, and the global stabilization of minimum phase nonlinear systems," *IEEE Trans. Control Syst. Technol.*, vol. 36, pp. 1228-1240, 1991.

[76] R. Ortega, A. Van der Schaft, I. Mareels, and B. Maschke, "Putting energy back in control," *IEEE Control Syst.*, vol. 21, no. 2, pp. 18-33, Apr. 2001.

[77] R. Ortega, A. Van der Schaft, B. Maschke, and E. Gerardo, "Interconnection and damping assignment passivity-based control of port-controlled Hamiltonian systems," *Automatica*, vol. 38, pp. 585-596, 2002.

[78] R. Ortega, A. Schaf, F. Castanos, and A. Astolfi, "Control by interconnection and standard passivity-based control of port-Hamiltonian systems," *IEEE Trans. Automat. Control.*, vol. 53, no. 11, pp. 2527-2542, 2008.

[79] K. Fujimoto and T. Sugie, "Trajectory tracking control of port-controlled Hamiltonian systems via generalized canonical transformations," *Automatica*, vol. 39, pp. 2059-2069, 2003.

[80] A. Loria, E. Panteley, and H. Nijmeijer, "A remark on passivity-based and discontinuous control of uncertain nonlinear systems," *Automatica*, vol. 37, pp. 1481-1487, 2001.

[81] F. Kenji, S. Satoru, and S. Toshiharu, "Passivity based control of a class of Hamiltonian systems with nonholonomic constraints," *Automatica*, vol. 48, no. 12, pp. 3054-3063, 2012.

[82] Y. Jing, Z. H. Guan, and D. J. Hill, "Passivity-based control and synchronization of general complex dynamical networks," *Automatica*, vol. 45, no. 9, pp. 2107-2113, 2009.

[83] M. Larsena, M. Jankovi, and P. V. Kokotovi, "Coordinated passivation designs," *Automatica*, vol. 39, pp. 335-341, 2003.

[84] H. Chen, H. B. Ji, B. Wang, and H. S. Xi, "Coordinated passivation techniques for the dual-excited and steam-valve control of synchronous generators," *IEE Proc. Control Theory Appl.*, vol. 153, no. 1, pp. 69-73, 2006.

[85] M. A. Mermoud, R. C. Linares, and A. C. Facuse, "Adaptive passivity of nonlinear systems using time-varying gains," *Dynamics and Control*, vol. 11, pp. 333-351, 2001.

[86] Y. Wang, D. J. Hill, R. H. Middleton, and L. Gao, "Robust nonlinear coordinated excitation and TCSC control for power systems," *IEE Proc. Gen. Tran. Dist.*, vol. 149, no. 3, pp. 367-372, 2002.

[87] A. A. Bobtsov, A. A. Pyrkin, and S. A. Kolyubin, "Simple output feedback adaptive control based on passification principle," *International Journal of Adaptive Control and Signal Processing*, vol. 28, no. (7,8), pp. 620-632, 2014.

[88] W. Lin and T. Shen, "Robust passivity and feedback design for minimum-phase nonlinear systems with structural uncertainty," *Automatica*, vol. 35, no. 1, pp. 35-47, 1999.

[89] S. M. Joshia and A. G. Kelkar, "Passivity-based robust control of systems with redundant sensors and actuators," *Int. J. Control*, vol. 74, no. 5, pp. 474-481, 2001.

[90] X. B. Zhou, Z. B. Fan, D. M. Zhou, and X. M. Cai, "Passivity-based adaptive hybrid synchronization of a new hyperchaotic system with uncertain parameters," *The Scientific World Journal*, pp. 1-6, 2012.

[91] Z. G. Wu, P. Shi, H. Y. Su, and J. Chu, "Network-based robust passive control for fuzzy systems with randomly occurring uncertainties," *IEEE Trans. Fuzzy Syst.*, vol. 21, no. 5, pp. 966-971, 2013.

[92] L. Y. Sun, J. Zhao, and G. M. Dimirovski, "Adaptive coordinated passivation control for generator excitation and thyristor controlled series compensation system," *Control Eng. Pract.*, vol. 17, pp. 766-772, 2009.

[93] S. Fang and J. Wang, "Coordinated control of generator excitation and TCSC based on Hamilton energy function," *Power System Protection Con.*, vol. 45, no. 15, pp. 24-28, 2012.

[94] L. Jiang, Q. H. Wu, and J. Y. Wen, "Decentralized nonlinear adaptive control for multi-machine power systems via high-gain perturbation observer," *IEEE Trans. Circuits Syst. I, Reg. Papers*, vol. 51, no. 10, pp. 2052-2059, 2004.

[95] Q. H. Wu, L. Jiang, and J. Y. Wen, "Decentralized adaptive control of interconnected non-linear systems using high gain observer," *Int. J. Control*, vol. 77, no. 8, pp. 703-712, 2004.

[96] L. Jiang, Q. H. Wu, and J. Y. Wen, "Nonlinear adaptive control via sliding-mode state and perturbation observer," *IEE Proc. Control Theory and Applications.*, vol. 149, no. 4, pp. 269-277, 2002.

[97] B. Yang, Q. H. Wu, L. Jiang, and J. S. Smith, "Adaptive passivity-based control of a TCSC for the power system damping improvement of a PMSG based offshore wind farm," *Proceeding of Renewable Energy Research and Applications (ICRERA)*, Madrid, Spain, 20-23 Oct., pp. 717-721, 2013.

[98] J. Chen, L. Jiang, W. Yao, and Q. H. Wu, "Perturbation estimation based nonlinear adaptive control of a full-rated converter wind turbine for fault ride-through capability enhancement," *IEEE Trans. Power Syst.*, vol. 29, no. 6, pp. 2733-2743, 2014.

[99] Y. Z. Wang, and S. S. Ge, "Augmented hamiltonian formulation and energy-based control design of uncertain mechanical systems," *IEEE Trans. Control Syst. Technol.*, vol. 16, no. 2, pp. 202-213, Mar. 2008.

[100] Y. Z. Wang, D. Z. Cheng, C. W. Li, and Y. Ge, "Dissipative hamiltonian realization and energy-based L_2-disturbance attenuation control of multimachine power systems," *IEEE Trans. Autom. Control*, vol. 48, no. 8, pp. 1428-1433, Aug. 2003.

[101] R. Ortega, M. Galaz, A. Astolfi, Y. Z. Sun, and T. L. Shen, "Transient stabilization of multimachine power systems with nontrivial transfer conductances," *IEEE Trans. Autom. Control*, vol. 50, no. 1, pp. 60-75, Jan. 2005.

[102] M. Perez, R. Ortega, and J. R. Espinoza, "Passivity-based PI control of switched power converters," *IEEE Trans. Control Syst. Technol.*, vol. 12, no. 6, pp. 881-890, Nov. 2004.

[103] D. P. Flores, J. M. A. Scherpen, M. Liserre, M. M. J. Vriesand, M. J. Kransse, and V. G. Monopoli, "Passivity-based control by series/parallel damping of single-phase PWM voltage source converter," *IEEE Trans. Control Syst. Technol.*, vol. 22, no. 4, pp. 2107-2113, July 2014.

[104] L. Harnefors, A. G. Yepes, A. Vidal, and J. Doval-Gandoy, "Passivity-based controller design of grid-connected VSCs for prevention of electrical resonance instability," *IEEE Trans. Ind. Electron.*, vol. 62, no. 2, pp. 702-710, Feb. 2015.

[105] H. Du, S. S. Ge, and J. K. Liu, "Adaptive neural network output feedback control for a class of non-affine non-linear systems with unmodelled dynamics," *IET Control Theory Appl.*, vol. 5, no. 3, pp. 465-477, 2011.

[106] C. Mou, S. G. Shu, V. E. H. Bernard, "Robust adaptive neural network control for a class of uncertain MIMO nonlinear systems with input nonlinearities," *IEEE Trans. Neural Netw.*, vol. 21, no. 5, pp. 796-812, 2010.

[107] S. S. Ge and K. P. Tee, "Approximation-based control of nonlinear MIMO time-delay systems," *Automatica*, vol. 43, pp. 31-43, 2007.

[108] J. Fu, H. He, X. Zhou, "Adaptive learning and control for MIMO system based on adaptive dynamic programming," *IEEE Trans. Neural Netw.*, vol. 22, no. 7, pp. 1133-1148, 2011.

[109] H. G. Zhang, L. L. Cui, X. Zhang, and Y. H. Luo, "Data-driven robust approximate optimal tracking control for unknown general nonlinear systems using adaptive dynamic programming method," *IEEE Trans. Neural Netw.*, vol. 22, no. 12, pp. 2226-2236, 2011.

[110] Y. Jiang, Z. P. Jiang, "Robust adaptive dynamic programming with an application to power systems," *IEEE Trans. Neural Netw.*, vol. 24, no. 7, pp. 1150-1156, 2013.

[111] A. A. Bobtsov and N. A. Nikolaev, "Fradkov theorem-based design of the control of nonlinear systems with functional and parametric uncertainties," *Autom. Remote Control*, vol. 66, no. 1, pp. 108-118, 2005.

[112] A. A. Bobtsov and M. V. Faronov, "Output control of nonlinear delay systems with unmodeled dynamics," *Journal of Computer and Systems Sciences International*, vol. 50, no. 3, pp. 429-437, 2011.

[113] G. Revel, A. E. Leön, D. M. Alonso, and J. L. Moiola, "Bifurcation analysis on a multimachine power system model," *IEEE Trans. Circuits Syst. I, Reg. Papers*, vol. 57, no. 4, pp. 937-949, 2010.

[114] Y. Wang, D. Cheng, Y. Liu, and C. Li, "Adaptive $H_{\inf}$ excitation control of multimachine power systems via the Hamiltonian function method. ," *Int. J. Control*, vol. 77, no. 4, pp. 336-350, 2004.

[115] T. L. Shen, S. W. Mei, Q. Lu, W. Hu, and K. Tamura K, "Adaptive nonlinear excitation control with L-2 disturbance attenuation for power systems," *Automatica*, vol. 39, no. 1, pp. 81-89, 2003.

[116] Y. Jiang and Z. P. Jiang, "Robust adaptive dynamic programming for large-scale systems with an application to multimachine power system," *IEEE Trans. Circuits Syst. II, Bri. Express.*, vol. 59, no. 10, pp. 693-697, 2012.

[117] W. Yao, L. Jiang, J. K. Fang, J. Y. Wen, and S. J. Cheng, "Decentralized nonlinear optimal predictive excitation control for multi-machine power systems," *Int. J. Electr. Pow. Energy Syst.*, vol. 55, pp. 620-627, 2014.

[118] N. S. Manjarekar, R. N. Banavar, and R. Ortega, "Application of interconnection and damping assignment to the stabilization of a synchronous generator with a controllable series capacitor," *Int. J. Elect. Power Energy Syst.*, vol. 32, pp. 63-70, 2010.

[119] L. Y. Sun, S. C. Tong, and Y. Liu, "Adaptive backstepping sliding mode H_∞ control of static var compensator," *IEEE Trans. Control Syst. Technol.*, vol. 19, no. 5, pp. 1178-1185, 2011.

[120] S. Panda and N. P. Padhy, "Optimal location and controller design of STATCOM for power system stability improvement using PSO," *J. Franklin Inst.*, vol. 345, no. 2, pp. 166-181, 2008.

[121] X. Lei, X. Li, and D. Povh, "A nonlinear control for coordinating TCSC and generator excitation to enhance the transient stability of long transmission systems," *Electr Power Syst Res.*, vol. 59, no. 2, pp. 103-109, 2001.

[122] J. S. K. Leung, D. J. Hill, and Y. X. Ni, "Global power system control using generator excitation, PSS, FACTS devices and capacitor switching," *Int. J. Elect. Power Energy Syst.*, vol. 27, no. 5-6, pp. 448-464, 2006.

[123] K. Amin, J. M. Mohammad, and P. Moein, "Coordinated design of STATCOM and excitation system controllers for multi-machine power systems using zero dynamics method," *Int. J. Elect. Power Energy Syst.*, vol. 49, no. 5-6, pp. 269-279, 2013.

[124] L. H. Gu and J. Wang, "Nonlinear coordinated control design of excitation and STATCOM of power systems," *Electr Power Syst Res.*, vol. 77, pp. 788-796, 2007.

[125] L. J. Cai and I. Erlich, "Simultaneous coordinated tuning of PSS and FACTS damping controllers in large power systems," *IEEE Trans. Power Syst.*, vol. 20, no. 1, pp. 294-300, Feb. 2005.

[126] Q. J. Liu, Y. Z. Sun, T. L. Shen, and Y. H. Song, "Adaptive nonlinear coordinated excitation and STATCOM controller based on Hamiltonian structure for multimachine-power-system stability enhancement," *IET Control Theory Appl.*, vol. 150, no. 3, pp. 285-294, 2003.

[127] S. W. Mei, J. Chen, Q. Lu, A. Yokoyama, and M. Goto, "Coordinated nonlinear robust control of TCSC and excitation for multi-machine systems," *Int. J. Control Theory Appl.*, vol. 2, no. 1, pp. 35-42, 2004.

[128] H. Shayeghi, A. Safari, and H. A. Shayanfar, "PSS and TCSC damping controller coordinated design using PSO in multi-machine power system," *Energy Convers. Manage.*, vol. 51, pp. 2930-2937, 2010.

[129] X. Y. Bian, C. T. Tse, J. F. Zhang, and K. W. Wang, "Coordinated design of probabilistic PSS and SVC damping controllers," *Int. J. Elect. Power Energy Syst.*, vol. 33, pp. 445-452, 2011.

[130] C. M. Verrelli and G. Damm, "Robust transient stabilization problem for a synchronous generator in a power network," *Int. J. Control.*, vol. 83, no. 4, pp. 816-828, 2010.

[131] F. P. Mello, "Measurement of synchronous machine rotor angle from analysis of zero sequence harmonic components of machine terminal voltage," *IEEE Trans. Power Del.*, vol. 9, no. 4, pp. 1770-1777, Oct. 1994.

[132] D. L. Ree, D. C. Mazur, "Synchronized rotor angle measurement of synchronous machines," *IEEE Industry Applications Society Annual Meeting (IAS)*, pp. 1-8, 7-11 Oct. 2012.

[133] U. Gnanarathna, A. Gole, and R. Jayasinghe, "Efficient modeling of modular multilevel hvdc converters (mmc) on electromagnetic transient simulation programs," *IEEE Trans. Power Del.*, vol. 26, no. 1, pp. 316-324, Jan. 2011.

[134] K. J. Ou, H. Rao, Z. X. Cai, H. P. Guo, X. H. Lin, L. Guan, T. Maguire, B. Warkentin, and Y. Chen, "MMC-HVDC simulation and testing based on real-time digital simulator and physical control system," *IEEE J. Emerging and Selected Topics in Power Electronics*, vol. 2, no. 4, pp. 1109-1116, Dec. 2014.

[135] H. I. Son, H. J. Yoo, and H. M. Kim, "Development of hardware-in-the-Loop simulation system to test HVDC controllers," *Int. J. Control Autom.*, vol. 7, no. 9, pp. 451-462, 2014.

[136] A. Egea-Alvarez, F. Bianchi, A. Junyent-Ferre, G. Gross, and O. Gomis-Bellmunt, "Experimental implementation of a voltage control for a multi-

terminal VSC-HVDC offshore transmission system," *Innovative Smart Grid Technologies (ISGT Europe)*, pp. 1-7, 14-17 Oct. 2012.

[137] R. E. Best, *Phase Locked Loops*, 5th Edition, McGraw-Hill, 2003.

[138] S. H. Kim, M. C. Chin, and C. N. Chu, "Development of EHPS motor speed map using HILS system," *IEEE Trans. Veh. Technol.*, vol. 62, no. 4, pp. 1553-1567, 2013.

[139] D. Venkata, M. R. Iravani, and R. Bonert, "Real-time digital simulation of power electronic apparatus interfaced with digital controllers," *IEEE Trans. Power Del.*, vol. 16, no. 4, pp. 775-781, Oct. 2001.

[140] M. O. Faruque and V. Dinavahi, "Hardware-in-the-loop simulation of power electronic systems using adaptive discretization," *IEEE Trans. Ind. Electron.*, vol. 57, no. 4, pp. 1146-1158, April, 2010.

[141] J. He, C. Lu, X. Wu, P. Li, and J. Wu, "Design and experiment of wide area HVDC supplementary damping controller considering time delay in China southern power grid," *IET Gener. Transm. Distrib.*, vol. 3, no. 1, pp. 17-25, 2009.

[142] G. Parma and V. Dinavahi, "Real-time digital hardware simulation of power electronics and drives." *IEEE Trans. Power Del.*, vol. 22, pp. 1235-1246, 2007.

[143] B. Lu, X. Wu, H. Figueroa, and A. Monti, "A Low-cost real-time hardware-in-the-loop testing approach of power electronics controls," *IEEE Trans. Power Electron.*, vol. 54, no. 2, pp. 919-931, 2007.

[144] J. H. Jeon, J. Y. Kim, H. M. Kim, S. K. Kim, C. H. Cho, J. M. Kim, J. B. Ahn, and K. Y. Nam, "Development of hardware in-the-loop simulation system for testing operation and control functions of microgrid," *IEEE Trans. Power Electron.*, vol. 25, no. 12, pp. 2919-2929, 2010.

[145] D. V. Hertem and M. Ghandhari, "Multi-terminal VSC HVDC for the European supergrid: obstacles," *Renewable Sustainable Energy Rev.*, vol. 14, pp. 3156-3163, 2010.

[146] J. Machowski, P. Kacejko, L. Nogal, and M. Wancerz, "Power system stability enhancement by WAMS-based supplementary control of multi-terminal HVDC networks," *Control Eng. Pract.*, vol. 21, pp. 583-592, 2013.

[147] N. Fernandopulle and R. T. H. Alden, "Incorporation of detailed HVDC dynamics into transient energy functions," *IEEE Trans. Power Syst.*, vol. 20, no. 2, pp. 1043-1052, May 2005.

[148] D. Jovcic, "Phase locked loop system for FACTS," *IEEE Trans. Power Syst.*, vol. 18, no. 3, pp. 1116-1124, Aug. 2003.

[149] X. P. Zhang, "Multiterminal voltage-source converter-based HVDC models for power flow analysis," *IEEE Trans. Power Syst.*, vol. 19, no. 4, pp. 1877-1884, Oct. 2004.

[150] T. Haileselassie, M. Molinas, and T. Undeland, "Multi-terminal VSCHVDC system for integration of offshore wind farms and green electrification of platforms in the North Sea," *presented at the Nordic Workshop Power Ind. Electron.*, Helsinki, Finland, Jun. 2008.

[151] W. Lu and B. Ooi, "Optimal acquisition and aggregation of offshore wind power by multiterminal voltage-source HVDC," *IEEE Trans. Power Del.*, vol. 18, no. 1, pp. 201-206, Jan. 2003.

[152] L. Tang and B. T. Ooi, "Locating and isolating DC faults in multiterminal DC systems," *IEEE Trans. Power Del.*, vol. 22, no. 3, pp. 1877-1884, Jul. 2007.

[153] C. M. Franck, "HVDC circuit breakers: A review identifying future research needs," *IEEE Trans. Power Del.*, vol. 26, no. 2, pp. 998-1007, April 2011.

[154] J. Hafner and B. Jacobson, "Proactive hybrid HVDC breakers: a key innovation for reliable HVDC grids", *International Symposium on Integrating Supergrids and Microgrids*, vol. 264, Bologna, Italy, 2011, pp. 1-8.

[155] G. Beccuti, G. Papafotiou, and L. Harnefors, "Multivariable optimal control of HVDC transmission links with network parameter estimation for weak grids," *IEEE Trans. Control Syst. Technol.*, vol. 22, no. 2, pp. 676-689, Mar. 2014.

[156] J. Beerten and R. Belmans, "Modeling and control of Multi-terminal VSC HVDC systems," *Energy Procedia*, vol. 24, pp. 123-130, 2012.

[157] S. Cole, J. Beerten, and R. Belmans, "Generalized dynamic VSC MTDC model for power system stability studies," *IEEE Trans. Power Syst.*, vol. 25, no. 3, pp. 1655-1662, Aug. 2010.

[158] N. R. Chaudhuri, R. Majumder, B. Chaudhuri, and J. Pan, "Stability analysis of VSC MTDC grids connected to multi-machine AC systems," *IEEE Trans. Power Del.*, vol. 26, no. 4, pp. 2774-2784, Oct. 2011.

[159] L. Xu and L. Yao, "DC voltage control and power dispatch of a multi-terminal HVDC system for integrating large offshore wind farms," *IET Renew. Power Gener.*, vol. 5, no. 3, pp. 223-233, 2011.

[160] O. Bellmunt, J. Liang, J. Ekanayake, and N. Jenkins, "Voltage current characteristics of multiterminal HVDC-VSC for offshore wind farms," *Elect. Power Syst. Res.*, vol. 81, pp. 440-450, 2011.

[161] O. Bellmunt, J. Liang, R. King, J. Ekanayake, and N. Jenkins, "Topologies of multiterminal HVDC-VSC transmission for large offshore wind farms," *Elect. Power Syst. Res.*, vol. 81, pp. 271-281, 2011.

[162] Y. F. Tang, H. B. He, and J. Y. Wen, "Adaptive control for an HVDC transmission link with FACTS and a wind farm," *Innovative Smart Grid Technologies (ISGT), 2013 IEEE PES*, pp. 1-6, 24-27 Feb. 2013.

[163] S. J. Kwon and W. K. Chung, "Perturbation compensator based robust tracking control and state estimation of mechanical systems," *Springer*, New York, 2004.

[164] K. Youcef-Toumi and S. Reddy, "Analysis of linear time invariant systems with time delay," *ASME J. Dyn. Sys. Meas., and Contr.*, no. 114, pp. 544-555, 1992.

[165] J. Q. Han, "From PID to active disturbance rejection control," *IEEE Trans. Ind. Electron.*, vol. 56, no. 3, pp. 900-906, 2009.

[166] J. H. Ahrens and H. K. Khalil, "High-gain observers in the presence of measurement noise: A switched-gain approach," *Automatica*, vol. 45, pp. 936-943, 2009.

[167] H. K. Khalil and L. Praly, "High-gain observers in nonlinear feedback control," *Int. J. Robust. Nonlinear Control*, vol. 24, no. 6, pp. 993-1015, April 2014.

[168] F. Da, "Decentralized sliding mode adaptive controller design based on fuzzy neural networks for interconnected uncertain nonlinear system," *IEEE Trans. on Neural Networks*, vol. 11, pp. 1471-1480, 2000.

[169] V. G. Agelidis, G. D. Demetriades, and N. Flourentzou, "Recent advances in High-Voltage Direct-Current power transmission systems," in *Proc. IEEE Conf. Industrial Technology.*, pp. 206-213, 15-17 Dec. 2006.

[170] Jeon, Jin-Hong, et al., "Development of hardware in-the-loop simulation system for testing operation and control functions of microgrid," *IEEE Trans. Power Electron.*, vol. 25, no. 12, pp. 2919-2929, Dec. 2010.